Sustainable Biofuel Production via the Hydrothermal Liquefaction of Microalgae and Subsequent Bio-Oil Upgrading

Wagner, Jonathan

Award date:
2017

Awarding institution:
University of Bath

Sustainable Biofuel Production via the Hydrothermal Liquefaction of Microalgae and Subsequent Bio-Oil Upgrading

Jonathan Lothar Wagner

A thesis submitted for the degree of Doctor of Philosophy

University of Bath

Department of Chemical Engineering

Centre for Sustainable Chemical Technologies

September 2016

ABSTRACT

Microalgae are a promising feedstock for the production of sustainable, 3rd generation biofuels; however, current lipid-based processes are too expensive to effectively compete with existing transportation fuels. A potential solution is to convert the entire algae via hydrothermal liquefaction (HTL) instead, therefore allowing the use of faster-growing, and cheaper microalgae.

This project sought to address some of the main challenges with this technology, currently restricting its use for large-scale fuel production. Fuels are low value products and unlikely to pay for the entire fuel production process on their own. Consequently, the possibility of producing additional by-products from the conversion of polymer-containing algae, or combining HTL with a more conventional lipid-extraction process, was explored. In addition, the project studied the conversion of microalgae produced during the bioremediation of domestic wastewater, in order to help to offset the overall biomass production costs.

The majority of research into algal HTL has been confined to batch systems, which are not fully representative of the continuous flow processes used for large-scale fuel production. Consequently, an inexpensive laboratory-scale system was designed to study the continuous HTL of algae under a range of operating conditions. Using this system, it was found that, compared to a batch reactor, significantly enhanced oil yields could be obtained from the system, as a result of increased heating rates, together with prolonged reaction times.

Finally, the poor quality of the bio-oils produced by the HTL of microalgae is a major challenge. Particularly their high nitrogen content restricts their conversion within conventional petrochemical refineries. Therefore, significant upgrading is required before the oil can be fractionated into fuels. In order to achieve this, a range of zeolite-supported nickel phosphide catalysts were synthesised in this project, and tested for the denitrogenation of the model compound quinoline, before they were

applied to the upgrading of bio-oil obtained from the continuous liquefaction of the wastewater-derived algae. Although the synthesised catalysts showed only low activity towards the denitrogenation of the bio-oil, they were more active for the hydrogenation of quinoline, compared to two conventional sulphided transition metal catalysts, and following further optimization, could therefore represent a viable class of oil upgrading catalysts.

ACKNOWLEDGMENTS

Firstly, I would like to thank my two lead supervisors Dr Valeska Ting and Dr Chris Chuck, for all their support and enthusiasm throughout my PhD. I am very grateful for the freedom that they have given me in pursuing my own research ideas, our many interesting discussions, and for going out of their way to help make things happen.

Thanks must also go to my two co-supervisors Dr Asel Sartbaeva and Prof Mark Weller, who have provided valuable input on the material synthesis.

Over my PhD I have had the pleasure of working with a number of collaborators. Special thanks must go Drs Tracey Beacham, Rachel Bransgrove and Katharina Meixner, for providing me with the PHB containing algae and helping me with some of the biomass characterization. I'd also like to acknowledge Dr Phillippe Mozzanega for providing me with large amounts of his lovely, smelly wastewater algae.

Thanks must go to Dr. Sean Davis at the University of Bristol for helping me with all the SEM and TEM analysis and Dr Laura Torrente at the University of Cambridge for conducting the TPR analysis on my catalyst samples. I'd also like to mention Emyr Jones for providing me with the base-treated catalysts.

During my PhD I had the opportunity to spend three months at the Universidade Estadual de Campinas in São Paulo State in Brazil, and I would like to thank the Global Research Scholarship Scheme of the University of Bath for providing the funding to make this happen. Thanks must also go to Prof Telma Franco and Dr Júlio Perin for hosting me.

My research wouldn't have been possible without the help of our departmental team of technicians, particularly Robert Brain, John Bishop, Fernando Acosta and Dr Daniel Lou-Hing. However I'd like to specifically mention Dr Alex Ciupa, who has not only been particularly helpful, but has always provided his help with a smile on his face.

I couldn’t have done my PhD without the generous funding provided by the EPSRC. Additional funding was also received from the Airbus Group, which was essential to conducting all the research I wanted.

I really enjoyed being part of the Centre for Sustainable Chemical Technologies, and believe that the programme structure and training provided have really contributed to the value of my time in Bath. In addition, it has provided me with a great social circle, which made it much easier to start making friends in Bath.

My time in Bath wouldn’t have been the same without my friends and colleagues. I’d like to specifically mention Joseph Donnelly, Stephen Bradley and Marcus Johns, however, there are many others that have made my time here in Bath very enjoyable.

I am very proud to have been part of the Chuck group as a whole, which has done exceedingly well over the time I was at Bath. I must apologise for my occasional bad moods and the sufferings received by my iron fist as washing up dictator.

A huge thanks needs to go to my parents, for encouraging me to do a PhD, long before I ever thought about research, and taking an active interest in my work. My PhD would never have been possible without all the opportunities that they provided me throughout my life, and for this I will be eternally grateful.

Finally, I must mention Dayanne, for supporting me throughout my PhD and all the patience she’s had to show. I hope that now I will finally be able to pay her back and give her the time that she deserves.

DISSEMINATIONS

Journal Articles

As an outcome of this thesis:

Wagner, J.L., Bransgrove, R., Beacham, T.A., Allen, M.J., Meixner, K., Drosg, B., Ting, V.P. and Chuck, C.J., *Co-production of bio-oil and propylene through the hydrothermal liquefaction of polyhydroxybutyrate producing cyanobacteria.* Bioresource Technology, 2016. **207**: p. 166-74.

Further articles co-authored:

Raikova, S., Smith-Baedorf, H., Bransgrove, R., Barlow, O., Santomauro, F., Wagner, J.L., Allen, M.J., Bryan, C.G., Sapsford, D. and Chuck, C. J., *Assessing hydrothermal liquefaction for the production of bio-oil and enhanced metal recovery from microalgae cultivated on acid mine drainage.* Fuel Processing Technology, 2016. **142**: p. 219-227

Book chapters

Raikova, S., Le, C.D., Wagner, J.L., Ting, V.P. and Chuck, C.J., *Towards an Aviation Fuel Through the Hydrothermal Liquefaction of Algae*, in *Biofuels for Aviation - Feedstocks, Technology and Implementation*. Edited by C.J. Chuck. Elsevier: London, **2016**.

Chuck, C.J., Wagner, J.L., and Jenkins, R.W., *Biofuels from Microalgae*, in *Chemical Processes for a Sustainable Future*. Edited by T.M. Letcher, J.L. Scott, and D.A. Patterson. The Royal Society of Chemistry: Cambridge, **2015**.

Conferences

12th International Conference on Renewable Resources and Biorefineries, Ghent, Belgium. May 30 – June 1, 2016. Oral Presentation, “Maximising value recovery from the hydrothermal liquefaction of microalgae”

ChemEngDayUK 2016, Bath, UK. March 31 to April 1, 2016. Poster presentation, “Continuous hydrothermal liquefaction of wastewater algae”

Winter Process Chemistry Conference, Bath, UK. December 14-16, 2015. Poster presentation, “Advanced biofuels from the hydrothermal liquefaction of waste water algae”

ISACS 17: Challenges in Chemical Renewable Energy, Rio de Janeiro, Brazil. September 8-11, 2015. Flash poster presentation, “Advanced biofuels from the hydrothermal liquefaction of waste water algae”

International Bioenergy Conference, Manchester, UK. March 11-13, 2014. Poster presentation, “Upgrading of crude oils from microalgae liquefaction towards fuel range hydrocarbons”

Prizes

Finalist for University of Bath Ede and Ravenscroft Prize 2016, for the best postgraduate research student.

University finalist for Three Minute Thesis Competition (3MT®)

Part of winning team of Energy Young Entrepreneurs Scheme Competition 2014 (Energy YES)

LIST OF ABBREVIATIONS

1234THQ	1,2,3,4-tetrahydroquinoline
5678THQ	5,6,7,8-tetrahydroquinoline
bdl	below detection limit
CSTR	Continous stirred tank reactor
DHQ	Decahydroquinoline
EAFS	Electric-arc furnace slag
EDX	Energy-dispersive X-ray spectroscopy
FTIR	Fourier-transform infrared spectroscopy
FWHM	Full-width at half maximum
GC-MS	Gas chromatography – mass spectrometry
HDN	Hydrodenitrogenation
HDO	Hydrodeoxygenation
HDS	Hydrodesulphurisation
HHV	Higher heating value
HPLC	High performance liquid chromatography
HT	Harsh treatment
HTL	Hydrothermal liquefaction
ID	Internal diameter
IPA	Isopropanol
LFR	Ladle furnace residue
MT	Mild treatment
MW	Molecular weight
nd	not determined
NT	No treatment
OPA	Orthopropylaniline (2-Propylaniline)

PB	Propylbenzene
PCH	Propylcyclohexane
PCHA	Propylcyclohexylamine
PHA	Polyhydroxyalkanoate
PHB	Polyhydroxybutyrate
PML	Plymouth Marine Laboratory
SEM	Scanning electron microscopy
TEM	Transmission electron microscopy
TGA	Thermogravimetric analysis
TPABr	Tetrapropylammonium bromide
TPR	Temperature programmed reduction
XRD	X-ray diffraction

TABLE OF CONTENTS

LIST OF FIGURES

LIST OF TABLES

CHAPTER 1

INTRODUCTION

1.1 CONTEXT

One of the main challenges of the 21st century is the development of technologies that are able to sustain an ever-increasing demand of energy, without dramatically impacting on the environment. Current technologies are heavily based around fossil fuels, which not only represent a limited resource and are increasingly difficult to extract, but are also heavily contributing to anthropogenic carbon dioxide emissions, threatening to result in excessive changes in global climate with potentially disastrous consequences.

Just over a quarter of total global energy consumption is attributed to the transport sector, which has been almost exclusively based around liquid transportation fuels.[1] Emerging technologies such as battery or hydrogen-powered vehicles are expected to play an increasing role in the future, but are still unable to compete with the high energy densities of liquid fuels. Furthermore, the current infrastructure, particularly within the aviation sector, is firmly embedded,[2] and consequently sustainable liquid drop-in fuels are required that can meet the near- to mid-term demand.

One promising source of liquid fuels are biofuels, which have the potential to address the environmental and sustainability concerns associated with fossil fuels, without requiring a complete revamp of the transportation infrastructure. Indeed, 1st generation biofuels such as bioethanol from sugarcane or corn and biodiesel from rapeseed or oil palm are already widely used within Europe, Brazil and the US, however, as these fuels stand in direct competition to food production, they carry heavy ethical and environmental burdens, which restrict their overall application.[3]

In contrast, 2nd generation biofuels, produced from lignocellulosic biomass, woody crops, agricultural residues and wastes, and 3rd generation biofuels, produced from non-terrestrial organisms such as algae or yeast, have the potential to provide the same benefits as 1st generation biofuels, without their disadvantages.

Microalgae in particular, have long been seen as one of the most promising feedstocks for the production of bio-fuels. They can display

much higher solar to biomass efficiencies than land based plants,[4] they do not require agricultural land and therefore are in no direct competition with food production, they display higher water efficiencies than plants, and can provide secondary functions such as wastewater treatment, carbon sequestration or the expression of valuable by-products, which may help to subsidise the overall fuel production process.[5]

Microalgae fuels have already been successfully tested for aviation,[6] marine[7] and road applications[8] and the large-scale production of algal biofuels has been demonstrated in a number of commercial projects.[9] However, current algal fuel costs are significantly above those of petroleum-derived fuel. The U.S. Navy, for example, has agreed to pay $12 million for 1.7 million litres of biofuel, corresponding to a cost of over $7 per litre.[10]

These high costs can be predominantly attributed to the high costs of algae cultivation and harvesting. Almost all commercial facilities are based around the production of algae lipids, which are subsequently converted via transesterification to produce biodiesel, or hydrotreatment to yield 'renewable' or 'green' fuels,[11, 12] fully compatible with the existing transportation infrastructure. Although lipid conversion technology is relatively well established, it requires algae with a lipid content of at least 40 % at a biomass cost of no more than $0.25 kg^{-1} in order to be economically viable.[4] Very high lipid yields of over 85 % have been achieved under nitrogen starved conditions,[13] but the lipid content is generally inversely proportional to the biomass productivity, as the synthesis of lipids has a higher metabolic cost than proteins or carbohydrates.[14] This leads to a significant reduction in algae growth rates, eliminating one of the major advantages of using algae in the first place. Furthermore, the cultivation of pure, lipid-producing algae species requires carefully controlled growth conditions, resulting in significant increases to the cultivation costs.[15]

A potential solution to this dilemma is the application of thermochemical processing methods, which convert the entire algae, not just lipids, and can therefore utilise much faster growing algae. Furthermore, as the

biomass composition is less important, the algae can be grown in open-ponds, under non-sterile conditions, and be optimized to fulfil secondary functions such as wastewater treatment or carbon sequestration.

Particularly hydrothermal liquefaction, conducted in near-critical liquid water, is seen as a promising method of converting algae. The required biomass loading of 5 to 25 %, can be easily obtained via primary and secondary harvesting techniques such as flocculation or centrifugation,[16] whereas alternative techniques such as pyrolysis require almost completely dry biomass. An energy balance analysis comparing the two processes estimated that full biomass drying consumed more than 8 times the energy compared to pure mechanical dewatering to a biomass concentration of 16 wt%.[17]

A further advantage of HTL is the formation of distinct oil and water phases, whereas pyrolysis oil can contain a substantial quantity of water, accounting for up to 20 to 25 % of the total oil weight.[18] Finally, HTL allows a significant proportion of the nitrogen and phosphorus initially present in the algae to partition into the water phase, facilitating the recovery and recycling of these valuable resources.

Despite this, a number of significant challenges remain with this technology. The vast majority of research to date has been conducted in batch reactors. Although these provide a good indication of the factors affecting product yields and quality, they cannot be directly applied to large-scale fuel processing, heavily based around continuous flow processes. Secondly, the biocrude oil produced by the HTL of algae is much more difficult to convert than lipids. It contains high concentrations of heteroatoms, particularly nitrogen, which restrict its processing within conventional petrochemical refineries. Consequently, significant oil upgrading is required, before the oil can be processed into a fuel. Finally, despite the reduction in cultivation costs, fuel production is unlikely to pay for the entire process on its own and additional value streams must be established, which are able to subsidise the process.

1.2 AIMS AND OBJECTIVES

The overall aim of this PhD is to aid the development of commercially feasible conversion technologies for the production of sustainable transportation fuels from microalgae. Specifically, the project focused on two areas: the hydrothermal liquefaction of microalgae to form a crude bio-oil, and the catalytic upgrading of this oil into fuel precursors that can be readily processed within existing fossil fuel refineries. To be industrially relevant, the project sought to incorporate additional value streams, which could help to subsidise the overall fuel production process.

In order to achieve these aims, the following objectives were set:

- Study the liquefaction of model compounds to obtain a better understanding of the impact of biochemical composition on the overall product distribution.
- Evaluate the potential of converting PHB accumulating cyanobacteria for the production of high-value by-products during the HTL of algae
- Assess the effect of adding solvents and industrial wastes as potential catalysts for the conversion of lipid-extracted algae
- Design, commission and characterize a continuous system for the HTL of microalgae produced during wastewater treatment. Compare the results from the continuous HTL of this algae with batch data to evaluate the effect of reaction temperature, heating rates and reaction time
- Synthesize and characterise zeolite-supported nickel phosphide catalysts. Study the effect of preparation methods and zeolite structure on the formation of the active phase.
- Test the catalysts for the denitrogenation of model compounds, before applying them to the upgrading of crude bio-oil produced from the continuous HTL of wastewater algae.

CHAPTER 2

LITERATURE REVIEW

This chapter provides a review of the literature relevant to the production of sustainable biofuels via the hydrothermal liquefaction of algae. It starts with a review of the HTL process itself, covering the effect of processing conditions, algae composition and the addition of organic solvents, as well as the work done on continuous processing. This is followed by a description of the studies conducted on the upgrading of the resulting bio-oil so far and a review of the denitrogenation catalysts applied to petroleum processing. Finally, a number of strategies for establishing additional value streams and reducing the fuel production costs are presented.

This work has directly contributed to the following two book chapters:

1) Chuck, C.J., J.L. Wagner, and R.W. Jenkins, *Biofuels from Microalgae*, in *Chemical Processes for a Sustainable Future*, T.M. Letcher, J.L. Scott, and D.A. Patterson, Editors. 2015, Royal Society of Chemistry: Cambridge. p. 425-442.

2) Raikova, S., J. L. Wagner *et al.*, *Towards an Aviation Fuel Through the Hydrothermal Liquefaction of Algae*, in *Biofuels for Aviation - Feedstocks, Technology and Implementation*, C.J. Chuck, Editor. 2016, Elsevier: London.

2.1 HYDROTHERMAL LIQUEFACTION OF MICROALGAE

Although the first publications on the HTL of microalgae were published in the mid-nineties,[19, 20] the technology has only started to attract widespread research interest over the last 6 years (Figure 2.1).

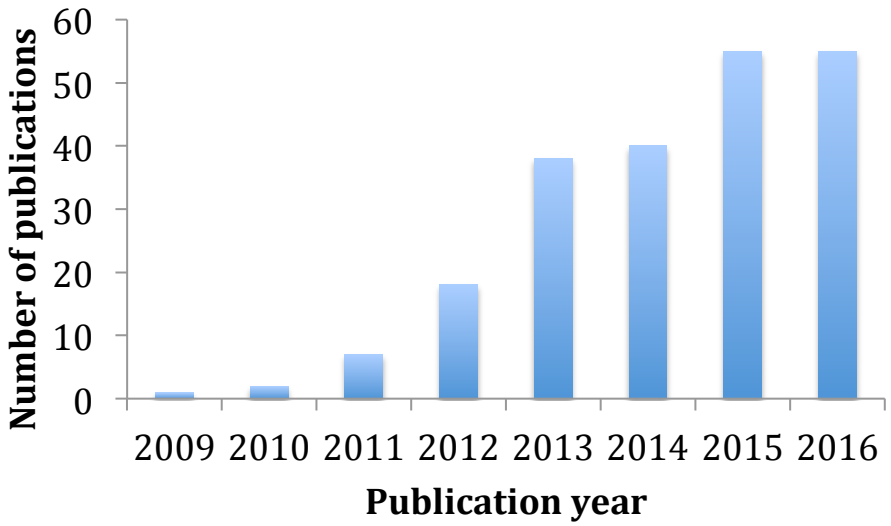

Figure 2.1: Frequency of publications on the 'hydrothermal liquefaction' of 'algae', based on Web of Science™ search

Despite this, various reviews by Peterson,[21] Toor *et al.*,[22] Yeh *et al.*,[23] Barriero *et al.*,[14] Chuck *et al.*,[24] and Raikova *et al.*[25] have already been published.

2.1.1 PRINCIPLE OF OPERATION

HTL is conducted in the presence of subcritical water close to its critical point. At these conditions, hydrogen bonding within the water phase is significantly reduced, transforming it from a polar, highly H-bonded solvent to a non-polar solvent capable of extracting and dissolving organic components from the biomass.[21, 22] Furthermore, close to its critical point, the dissociation constant of water, $K_{w,}$ is about three orders of magnitude higher than at ambient conditions, significantly increasing the number of H^+ and OH^- ions, which may help to promote base- and acid catalysed reactions.[26]

However, as shown from the phase diagram of water (Figure 2.2), HTL also requires high reaction pressures to maintain water in the liquid phase and minimise steam formation, in order to prevent the latent heat losses associated with vaporisation.[25]

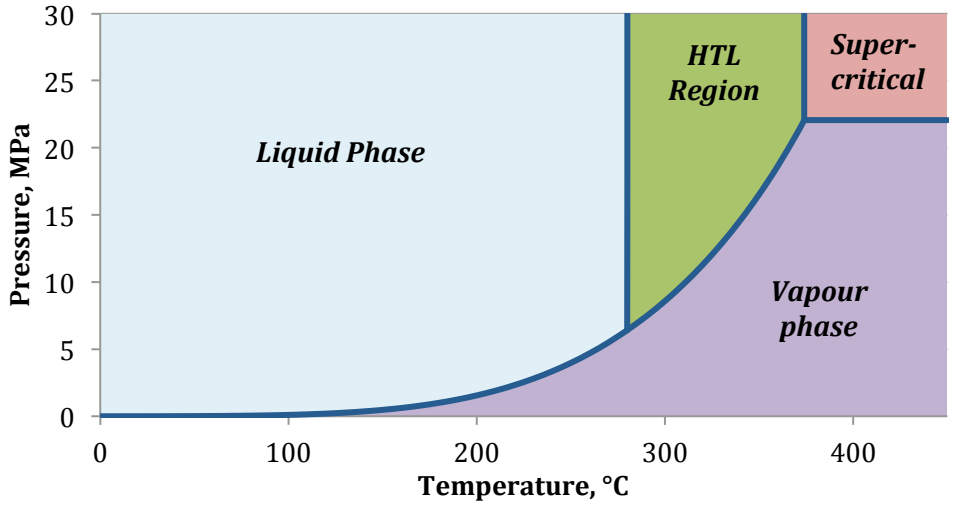

Figure 2.2: Phase diagram for hydrothermal liquefaction reaction

HTL is comprised of hundreds of simultaneous and competitive reactions,[25] resulting in the formation of four different product phases: solid ash, bio-crude oil, water-soluble compounds and reaction gases. These reactions can generally be divided into three different stages: (1) hydrolysis of the biomass macromolecules (lipids, proteins and carbohydrates) into smaller, water-soluble fragments; (2) rearrangement of the fragments through decarboxylation, deamination and dehydration reactions; (3) combination of reactive fragments through dehydration, condensation, cyclisation and polymerization reactions to form the desired bio-oil.[22, 27, 28]

The relative reaction rates are strongly dependent on processing conditions, such as reaction temperature, residence time and biomass loadings, influencing the ultimate product distribution and composition that is obtained from any one feedstock.

However, the bio-oil typically contains around 50-65 % of the initial carbon and hydrogen and 20 wt% of the nitrogen originally present within the algae feedstock.[29] The gas product is predominantly composed of

carbon dioxide, although high temperatures and the presence of catalysts can result in the formation of short hydrocarbons as well.[27] Nitrogen is removed as water-soluble ammonia, accounting for around 50 % of the total nitrogen, whereas minerals such as phosphorus, potassium and calcium either partition into the water or the solid phase.[30]

2.1.2 EFFECT OF ALGAE COMPOSITION

Microalgae are predominantly composed of three main biochemical compounds, namely proteins, lipids and carbohydrates, and their relative contributions are strongly dependent on the algae species itself and its growth conditions. Fast-growing algae, for example, mostly contain proteins, whereas lipid production has a higher metabolic cost, requiring longer cultivation times and harsher growth conditions.[13, 14] Microalgae can also contain a large number of other constituents, such as chlorophyll,[31] algaenans[32] and polyhydroxyalkanoates,[33] which may contribute to, or influence the liquefaction yields.

Initial studies often compared the bio-crude yields obtained from HTL with the lipid content of the algae to prove an enhancement in oil production compared to conventional lipid-extraction techniques.[19, 34] Oil yields from lipid-rich algae were found to be much higher than from protein-producers, suggesting that lipids are more readily converted into bio-oil than proteins or carbohydrates.[28, 35]

To investigate this in more detail, Biller and Ross converted a number of model compounds, representing the three main classes of biochemical components, and compared the resulting yields with the conversion results of four different species of microalgae and cyanobacteria.[36] As expected, the highest oil yields were obtained from lipids (55 – 80%), followed by proteins (11 – 18 %) and carbohydrates (6 – 15 %). Scaling these yields to the compositions of the four algae species, they obtained a good match to the actual yields from the two microalgae *Chlorella* and *Nannochloropsis*, whereas a poor fit was obtained for *Porphyridium* and the cyanobacteria *Spirulina*.

Subsequent model compound studies revealed that binary protein-carbohydrate mixtures yielded higher amounts of oil than expected from the yields from each model compound on its own.[37-39] This enhancing effect was attributed to Maillard type reactions between amino acids and reducing sugars formed from the hydrolysis of proteins and carbohydrates, respectively. In contrast, during the co-liquefaction of *Spirulina* and *Nannochloropsis*, the presence of high protein loadings was found to have a negative effect on the bio-oil production of lipids.[39]

2.1.3 Effect of operating conditions and product recovery

2.1.3.1 Reaction temperature

Microalgae HTL is typically conducted at temperatures ranging from around 280 °C to 370 °C,[24, 30] although temperatures as low as 200 °C have been tested for the conversion of lipid-rich algae. Optimal reaction temperatures appear to be highly dependent on the algae species and were found to range from 220 °C for a lipid-rich algae (*Chlorella* sp.)[28] to up to 375 °C for *Desmodesmus* sp.[27]

Low temperatures of around 225 °C to 250 °C were generally found to favour the formation of aqueous phase products,[27] resulting in the production of a bio-oil predominantly composed of lipid-derived products.[40] At these temperatures, oil yields were found to be strongly dependent on the algae species,[41] as a result of varying lipid contents as well as differences in cell wall strengths, resisting hydrothermal treatment.[42]

As temperatures were increased above 300 °C, the bio-crude phase became more dominant, as water-phase products were converted further via condensation and repolymerization reactions.[43] The oil yields also became less dependent on the initial algae composition and contained a much broader molecular weight (MW) distribution, compared to the oil produced at 250 °C.[41] At the same time, the nitrogen content in the bio-oil started to increase significantly,[27, 44] suggesting increased incorporation

of protein-derived molecules.[40] As nitrogen removal from the oil is one of the major challenges associated with algae derived fuels, it is clear that maximum bio-oil yields do not correspond to best bio-oil quality, and these two factors must be carefully balanced.[44] Another consideration is the overall energy consumption of the process, which was found to be 22 % higher at 350 °C compared to 300 °C, with bio-oil yields increasing by only 3 % over the same temperature range.[36]

2.1.3.2 Biomass loading

Research on the HTL of algae has been conducted over a wide range of biomass loadings, from around 1 wt% to 50 wt%. Jena *et al.* applied biomass loadings from 10 to 50 % and observed a slight increase in bio-oil yields from 32.5 % at a 10 wt% loading to 39.9 % at 20 wt% loading, whereas further increases had no noticeable effect.[45] Similar results were obtained by Xu and Savage, who observed a substantial increase in the yield of water-insoluble biocrude from 29.2 % to 38.1 %, as the algae loading was increased from 8.6 wt% to 11.4 wt%, but only a small additional increase to 44.0 % as the loading was raised further to 18.7 %.[46] In contrast, biomass concentrations appear to have a much larger effect at lower algae concentrations, as bio-oil yields more than doubled as the algae loading was increased from 1 to 5 wt%.[44] At the same time, the carbon recovery in the water phase reduced from 60 % at 1 wt% loading to 30 % at 10 wt% loading, whereas the nitrogen content in the oil increased.

Given that HTL is believed to proceed via the hydrolysis of macromolecules into water-soluble intermediates, which subsequently react to form less polar biomass components, the relationship between algae loading and bio-oil yields is unsurprising. At very low loadings, concentrations of intermediates are low, reducing the chances of molecular collisions. In addition, there is no clear line between which molecules partition to the water or the oil phase, but instead the final distribution is controlled by equilibrium. This means that as long as the biomass concentration is sufficient to fully saturate the water phase,

increases in biomass concentration are unlikely to have a strong impact on oil yields and operational considerations become more dominant. Whilst high algae loadings are desirable to minimise equipment and processing costs, they also require a higher extent of algae drying and may be difficult to pump under continuous flow conditions. Based on these considerations, Peterson *et al.* proposed a minimum algae loading of 15 to 20 wt%,[21] whereas Barreiro *et al.* suggested slightly lower loadings ranging from 5 to 15 %.[14]

2.1.3.3 Heating rates/Reaction time

To date, the vast majority of research into the HTL of algae has been conducted using batch reactors. Most of these are operated under isothermal conditions, where a constant reaction temperature is maintained for a prolonged period of time.

Typical reaction times have ranged from around 5 to 120 minutes,[20, 27, 45] however these values are generally reported from the point that the reaction temperature has been reached and therefore do not include heating times. Nevertheless, these times can make a significant contribution to the overall reaction times, as shown by Chen et al.[43] They employed retention times ranging from 0 to 1.5 h but reported heating times of up to 1.25 h for a reaction temperature of 320 °C. Even after a nominal reaction time of 0 minutes, their bio-crude yields exceeded 30 % for all reaction temperatures, demonstrating that a significant amount of oil is formed before the actual reaction temperature has been reached.

Even so, bio-oil yields were generally found to peak for reaction times between 30 and 60 minutes,[45] and subsequently drop-off as the holding time was increased further. Increased reaction times were also found to result in increased N/C ratios, whereas the oxygen and hydrogen concentrations in the oil dropped.[28, 45] This shows that similar to the reaction temperatures, the holding times need to be carefully adjusted to obtain an optimal balance between bio-oil yields and quality.

An alternative to isothermal liquefaction is the application of transient reaction conditions, allowing the use of much faster heating rates. Faeth

et al. achieved very fast heating rates by heating their batch reactors within a sandbath, set to a temperature significantly above the desired reaction temperature.[47] Very high oil yields of up to 66 % were obtained after a reaction time of 1 min with a sandbath temperature of 600 °C, after which the reactor temperature was estimated to have reached 300 °C. Longer reaction times of 3 or 5 minutes were required to achieve maximum oil yields at lower sandbath temperatures, but were significantly reduced compared to the highest value of 66 %.

Follow on studies employed varying algae concentrations (5 wt% and 25 wt%) and reactor loadings (11 vol% and 30 vol%) and obtained maximum oil yields after a reaction period of 45 s in a sandbath set to 600 °C, exceeding yields obtained from an isothermal reactor operated at equivalent conditions.[48, 49] Whilst the reactions with the lower reactor loading produced the highest oil yields, the oils obtained at higher reactor loadings contained lower concentrations of oxygen and nitrogen, with the highest C and N distribution to the water phase. Unlike the isothermal HTL, the bio-oils obtained from fast HTL contained several nitrogen-free oxygen compounds, suggesting that extended reaction times in the isothermal reactor resulted in increased cross-reactions between oxygen- and nitrogen-containing compounds. Unfortunately, neither of these studies employed direct temperature measurements, and as variations in reactor loading and algae concentration would be expected to have a strong effect on heating rates, their ultimate impact on product yields is difficult to assess. Nevertheless, the studies do demonstrate that high heating rates are beneficial for obtaining increased bio-oil yields from the HTL of microalgae.

2.1.3.4 Addition of catalysts

A number of studies investigated the effect of applying homogeneous catalysts, mostly inorganic bases and organic acids, to the reaction medium.

The most widely studied catalyst was sodium carbonate (Na_2CO_3), which had been previously shown to increase bio-oil yields from lignocellulosic

biomass.[23, 34, 36] However, when applied to the HTL of algae, the beneficial effect of this catalyst was much less obvious.[19, 20, 50] Dote *et al.,* for example, observed an increase in bio-oil yields from the liquefaction of *Botryococcus braunii* at 300 °C, whereas the presence of Na_2CO_3 led to reduced yields at 200 °C and 340 °C.[19] Even less favourable results were obtained during the conversion of *Dunaliella tertiolecta*, where the presence of Na_2CO_3 reduced bio-oil yields at almost all the conditions, whilst increasing its nitrogen content.[20] By selectively applying this catalyst to model compounds, representing the individual biomass components, Biller and Ross concluded that whilst sodium carbonate improves the conversion of carbohydrate, it has a detrimental effect on the liquefaction of proteins and lipids, and should therefore not be applied to lipid-rich or protein-rich algae.[36]

The addition of acetic and formic acid, in turn, appeared to result in a significant increase in bio-oil yields from the HTL of *Chlorella* and *Spirulina*, compared to base-catalysed reaction.[35] However, as the acids were consumed during the reaction, they acted as a reagent, rather than a catalyst, and on a total organic basis gave lower bio-crude yields. Furthermore, the resulting oils suffered from significantly increased oxygen and nitrogen content.

HTL of microalgae was also conducted in the presence of heterogeneous catalysts, including noble and transition metal catalysts (Pd/C, Pt/C, Ru/C, $CoMo/Al_2O_3$, Ni/SiO_2-Al_2O_3)[34, 51] solid acids (ZrO_2/SO_4^{2-}, HZSM-5)[52] and solid bases (potassium tert-butoxide, MgO/MCM-41).[52] The addition of solid acids generally caused a reduction in bio-oil yields, possibly due to inhibited carbohydrate conversion and occurrence of cracking reactions, whereas the base catalysed reactions enhanced overall yields, but produced predominantly heavier oil components.[52] The addition of metal catalysts resulted in enhanced oil yields of around 45 to 50 %, compared to 35 % for the blank, with Pd/C even producing yields of 57 %.[34] Metal catalysed oils also appeared less viscous and contained less nitrogen. However, separation of the solid product and catalysts post reaction is a challenge, and effectively rules out the use of expensive

metal catalysts. Consequently, Yang *et al.* employed a two-stage reactor, with physical separation of the catalyst (Pt/C) and the biomass (*Nannochloropsis* sp.) with a stainless steel frit.[51] Using this arrangement, significantly enhanced bio-oils were obtained compared to a single stage reactor. However, unlike the non-catalytic blank run, the reaction was conducted in the presence of hydrogen, and significant amounts of methane and ethane were detected in the reaction gas.

2.1.3.5 Product recovery

The HTL of algae produces four different product fractions: solids, bio-oil, aqueous phase and gas, which all need to be separated post reaction.

Whilst the gas product is easily vented from the reactor, separation of the other three product fractions is more complex and can have a large bearing on the reported yields.

Most researchers have employed either one of two separation methods. In the first method, the product mixture is filtered directly to separate the aqueous phase, and subsequently the retentate is washed with a solvent to recover the bio-oil from the solid product.[28] For the second method, the solvent is added to the entire product mixture, and after filtration, the solvent and water phases are separated by gravity or centrifugation.[29] Under these conditions, a significant amount of lighter, water-soluble compounds are transferred to the oil phase, accounting for around 14 % of the total organic biomass content,[53, 54] or 20 - 30 % of the organic content in the aqueous phase product.[55] At the same time, the bio-oil quality is reduced, containing higher amounts of O and N and lower levels of C and H.[53]

Another important consideration is the choice of the solvent itself. The HTL of algae produces highly viscous bio-oils, with a significant fraction of heavy, polycyclic compounds with low solubility in linear chain hydrocarbons. Consequently, most researchers have recovered the bio-oil with more polar solvents, such as acetone, chloroform or DCM.[15] In a number of studies, the oil fraction was separated further by extraction with a non-polar solvent such as hexane or ethyl ether, to form a ‘light

biocrude' with more favourable properties.[37, 51] However, its contribution to the total biocrude yield was highly variable, ranging from 8 wt% to 83 wt% in a single study alone.[47]

Solvent choice appeared to be less significant for the extraction of the water phase, although the highest aqueous-phase fractions were obtained when applying non-polar solvents such as hexane and cyclohexane.[29]

2.1.4 HTL IN PRESENCE OF ORGANIC SOLVENTS

A number of researchers conducted the algal liquefaction within organic solvents, such as ethanol, methanol and acetone.[56-59] Switching the reaction medium from water to an organic solvent was predicted to have a number of advantages, including: a lower critical temperature and pressure, allowing the use of milder reaction conditions; the ability of some solvents to donate hydrogen, thereby stabilising free radical intermediates and reducing re-polymerization reaction; the ability of alcohols to react with acidic components in the bio-oil; and a lower dielectric constant, allowing better dissolution of high-molecular weight products derived from biomass.[60]

One of the most comprehensive studies employed 11 different solvents (water, ethylene glycol, methanol, ethanol, n-propanol, isopropanol, acetone, ethyl acetate, 1,4-dioxane, tetralin and benzene) for the conversion of *Chlorella pyrenoidosa* at 350 °C, with a reaction time of 60 min and biomass concentration of 62.5 g L^{-1}.[61] The highest bio-oil yields, ranging from 51.4 % to 57.0 %, were obtained in the highly polar solvents ethylene glycol, ethanol, acetone and ethyl acetate and significantly exceeded the yields obtained in water (43 %). Further optimization of the reaction conducted in ethanol produced a bio-oil yield of 65.1 %, however the overall product recovery exceeded the organic content of the algae, indicating that ethanol was consumed during the reaction. Similar findings were made during the conversion of *Chlorella pyrenoidosa* in acetone, which achieved remarkable bio-oil yields of 78.9 % at 290 °C, but with an overall product recovery of 106.9 %.[62] It

should also be noted that contrary to water liquefaction, the resulting oil contained a higher nitrogen content than the algae. Further evidence for the cross-reaction of biomass and alcohols was obtained from the analysis of bio-oils produced from the liquefaction of *Spirulina* in ethanol, which was found to contain a high proportion of esters, probably formed through transesterification reactions with the solvent.[60]

Despite the high bio-oil yields, liquefaction of algae in solvents other than water may not be desirable, due to the high energy costs associated with complete biomass drying. A potential solution is the addition of the solvent to the aqueous algae slurry, and conducting the reaction in water/solvent mixtures. Chen *et al.* studied the conversion of *Dunaliella tertiolecta* at 320 °C in ethanol/water mixtures ranging from pure water to pure ethanol.[63] The highest bio-oil yields were obtained for an ethanol concentration of 40 vol% (64.7 %), exceeding the yields in pure water (48 %) and pure ethanol (61 %). In a different study, maximum bio-oil yields from the conversion of *Chlorella pyrenoidosa* at 280 °C were obtained with an ethanol/water mass ratio of 5/2, whilst higher ethanol concentrations were found to reduce gas formation but increase solid yields, and produce an oil with increased nitrogen content.[62] Even lower temperatures of 240 °C were applied for the liquefaction of *Nannochloropsis oceania*, and the maximum oil yields of 60 % obtained in 1:1 water/ethanol solutions (by weight) exceeded the best oil yields in pure water (54 % at 290 °C).[64] However, once again the nitrogen content of the oil was significantly increased.

The differences in optimal ethanol concentrations between the two studies could be related to the different reaction temperatures. Chen *et al.* suggested that the optimal ethanol concentration was governed by the proximity of the critical temperature of the mixture to the reaction temperature.[63]

Finally, the use of solvents may also have implications on the product separation following the reaction. For pure solvent-phase reactions, only three product phases are recovered (solid, oil and gas), and the increase in product yields could therefore be related to the recovery of products,

which normally partition to the aqueous phase. This in turn may help to explain the elevated nitrogen contents in the oil compared to water-phase reactions. However, in the case of mixed water-solvent liquefaction, product recovery may be more difficult as polar solvents could partition into the aqueous phase, requiring additional water-solvent separation steps. In contrast, the use of the polar solvent *n*-heptane resulted in the spontaneous formation of a solvent phase above the water phase, facilitating recovery of the non-polar reaction product, although polar products could only be recovered by subsequent extraction of the water phase with DCM.[54]

2.1.5 CONTINUOUS HTL

Whilst batch reactions provide valuable information about the optimal system conditions and chemical mechanisms involved with HTL, they are unlikely to be directly applicable to large-scale fuel processing, which is heavily based around continuous flow processes.[25] Furthermore, most batch processes struggle to combine high heating rates with extended reaction times and require the extensive use of solvents to recover and separate the different product fraction.

Consequently, research must be conducted in continuous bench- or pilot-scale reactors, to simulate the conditions expected during real-world application.

Despite this, only few continuous studies on the HTL of algae have been published thus far. Most of the systems are based around plug-flow reactors, supplied from high-pressure metering pumps, and maintained at reaction pressure via a back-pressure regulator at the outlet. An exception is a study by Barreiro *et al.*, who employed a continuous stirred tank reactor (CSTR) for the conversion of *Scenedesmus almeriensis* and *Nannochloropsis gaditana*.[65] Using this design, they managed to process an algae concentration of 18.2 wt%, but experienced some operational problems after a reaction time of 160 minutes, as a result of sedimentation and biomass accumulation within the pump pistons. Compared to a batch system, overall bio-oil yields were slightly reduced

and this was attributed to the cross-reaction between primary intermediates and final reaction products. At the same time, the oil contained a larger fraction of lower molecular weight compounds, which they related to the faster heating rates obtained in this system.

Most plug flow systems employed relatively low algae loadings, ranging from 1 wt% to 10 wt%, although Elliott *et al*. successfully converted an algae slurry with a biomass loading of 35 %.[66] However, they first heated the algae feed inside a CSTR, before it was introduced into the plug flow reactor, which might have helped to eliminate the formation of viscous colloids from the denaturation of proteins, previously observed at temperatures of around 225 °C and 250 °C.[67]

In contrast, Jazrawi *et al*. experienced significant pressure fluctuations as a result of transient blockages of the back-pressure control valve, limiting their maximum biomass concentration to 10 wt%.[44] However they suggested that these problems are enhanced at bench-scale, due to inverse scaling problems, and therefore might be less significant in larger scale systems, containing wider system clearances.

Even lower algae concentrations of 1.5 wt% were applied by Patel and Hellgardt due to the limitations of the HPLC (high performance liquid chromatography) pump used for the feed delivery.[68] Maximum bio-crude yields of 38 % were obtained at a reaction temperature of 380 °C and a residence time of 30 s, whilst lower temperatures favoured the formation of aqueous phase products and longer reaction times caused an increase in the bio-oil nitrogen content.

Similar findings were obtained by Biller *et al.*, who managed to increase bio-crude yields from 36.8 % to 39.7 %, when raising the system flowrate from 10 to 40 mL min^{-1}.[69]

Interesting findings were also obtained from the HTL on a microfluidic chip, containing several viewing points at 0.4 min intervals.[31] Whilst the most significant increase in the higher heating value (HHV) occurred during the 1st minute of reaction, longer reaction times increased the nitrogen content in the oil from 4.5 % to 6.5 %. Unfortunately, the overall

bio-oil yields were not determined, and consequently the balance between product yields and crude oil quality cannot be assessed. The authors also observed distinct channel-adhered droplets, which could influence the residence times for the different product phases.

2.2 BIO-OIL UPGRADING

One of the main advantages of HTL is that it converts the entire biomass, not just lipids, and can therefore utilise faster growing algae compared to conventional lipid extraction processes. At the same time, the incorporation of protein-derived material produces a bio-oil with a high amount of nitrogen-containing compounds. Typical nitrogen levels in the bio-oil range from around 4 wt% to 8 wt% and must be significantly reduced if the resulting fuels are to comply with fuel emissions standards.[20, 25] However, nitrogen compounds are not easily removed in conventional fuel refineries, as they are known to poison the commonly used sulphide-based catalysts. Because of this, maximum nitrogen levels in refinery feeds are usually limited to around 0.25 wt%.[70] Consequently, it is clear that a significant reduction in nitrogen content is required before the final fuel-processing step can be completed.[29, 71]

2.2.1 OIL COMPOSITION

Whilst bio-oils are generally characterized according to their elemental composition, a number of researchers have attempted to perform more detailed compositional analysis using techniques such as GC-MS (gas chromatography – mass spectrometry),[65] FTIR (Fourier transform infrared spectroscopy),[53, 72] simulated distillation by TGA (thermogravimetric analysis),[43, 52] or mass spectrometry.[49] Analysis by gas chromatography identified a diverse range of compounds, including lipid derived alkanes and alkenes, nitrogen containing compounds such as amines and amides, oxygen containing compounds, such as alcohols, aldehydes and ketones, and heterocyclics such as furans, indoles or pyrroles.[45] Despite this, GC-MS analysis only covered between 35 wt%[29] to 50 wt%[40] of the total bio-oil, as the remaining fraction was not volatile enough to elute

from the GC, and consequently appears to overestimate the contribution of lipid-derived products.

Using Fourier transform ion cyclotron resonance mass spectrometry (FT-ICR MS) analysis, Faeth *et al.* identified over 25,000 unique molecular formulae in the bio-oil.[49] As they were preferably ionized by positive rather than negative electrospray ionization, the authors concluded that the bio-oil contained a larger fraction of compounds with basic, rather than acidic functional groups.

2.2.2 ALGAE PRETREATMENT

As the high nitrogen content in the bio-crude oils is predominantly formed during the conversion of proteins, a number of researchers attempted to pre-treat the algae at lower temperatures, to reduce the protein content of the algae prior to liquefaction.

Biller *et al*. applied microwave treatment at temperatures ranging from 80 °C to 140 °C, which resulted in a significant reduction in ash content and facilitated lipid extraction through solvent extraction. However, the pretreatment had little beneficial impact on the yields or composition of the bio-crude obtained by HTL at 300 °C, potentially because the temperatures were insufficient to break up the algae.[73] Higher pretreatment temperatures of 200 °C allowed almost complete protein recovery from de-oiled rice bran, however considering a total weight loss of 74 %, compared to a protein content of only 21.9 %, indicates that other bran components such as carbohydrates and fibres were hydrolysed as well.[74]

Similar results were obtained from the flash hydrolysis of *Scenedesmus* sp. at temperatures ranging from 205 °C to 325 °C. Up to 66.4 % of nitrogen was extracted at 305 °C, resulting in a reduction in the nitrogen content of the solid bio-fuel intermediate from 9.6 % to 6.6 %, however this phase only accounted for 26.7 % of the initial algal mass.[75] Significant reductions in oil yields from 26.7 % to 17.4 % were also experienced by Costanzo *et al.* following the pretreament of an algae mix at 225 °C, whilst the nitrogen content of the oil appeared to remain

unaffected.[76] However, subsequent upgrading of the pre-treated oil over a Ru/C catalyst appeared to be more effective than for the oil produced by direct HTL.[77]

Jazrawi *et al.* even observed an increase in nitrogen content following pre-treatment at temperatures ranging from 100 °C to 200 °C, unless reaction times were extended, resulting in significant reductions in the overall bio-crude yields.[78]

An obvious problem with these studies is the relatively lower stability of carbohydrates at hydrolysis conditions, resulting in excessive biomass losses. Furthermore, the whole purpose of applying HTL, rather than lipid extraction, is to utilise the other biomass components, including proteins, to form the desired bio-oil phase. Consequently, alternative studies have investigated the recovery of carbohydrates, which only form small HTL bio-oil yields, as an additional by-product instead.

Chakraborty *et al.* applied pre-treatment temperatures ranging from 140 °C to 200 °C prior to conventional liquefaction at 300 °C.[71] Whilst minimum temperatures of 140 °C were required to break up the cell wall of the algae, the highest carbohydrate recovery of 26.3 % was achieved at pretreatment temperatures of 160 °C. Further liquefaction produced an overall bio-oil yield of 23.4 %, only slightly lower than the oil yields obtained from untreated algae (27.8 %). The oil also possessed a lower N content of 0.78 % (compared to 1.14 % without pre-treatment), which could be related to a reduction in Maillard reactions between the hydrolysis products from carbohydrate and proteins. Following further optimization of the liquefaction conditions in a follow-on study, equivalent bio-oil yields of 31 % were obtained from both the pre-treated and untreated algae. However, the optimal liquefaction temperature of the pre-treated algae was reduced from 300 °C to 240 °C, and the oil had a reduced nitrogen content of 0.87 %, compared to 1.50 % without pretreatment.[79]

Despite these encouraging results, these methods need to be tested on a larger number of algae containing varying levels of proteins and

carbohydrates. Furthermore, practical considerations, such as product separation and heat integration need to be taken into account to assess the applicability of pretreatment to obtain an improved bio-oil together with the co-production of a carbohydrate feedstock.

In all cases, further upgrading of the bio-oil will still be required to reduce its nitrogen content to within the acceptable refining thresholds.

2.2.3 EXISTING UPGRADING STUDIES

Despite the high interest in the HTL of microalgae, surprisingly little research has been conducted on the upgrading of the resulting bio-oil.[25, 44, 80, 81] Most of these studies were conducted under batch conditions and achieved only partial removal of nitrogen (Table 2.1). Notable exceptions are studies by Elliott *et al*., who applied a two-stage continuous hydrotreating process to the upgrading of bio-oil produced by the continuous HTL of algae,[66] and Elkasabi *et al*., who catalytically upgraded oil obtained from the fast pyrolysis of *Spirulina* in a continuous downdraft fixed bed reactor.[82]

Upgrading studies were mostly conducted at reaction temperatures ranging from around 350 °C[83] to 530 °C,[84] although temperatures as high as 600 °C were applied to the catalytic pyrolysis of bio-oils from the HTL of *Desmodesmus*.[85] Higher reaction temperatures generally resulted in upgraded bio-oils with reduced nitrogen and oxygen contents, however also caused a significant reduction in bio-oil yields, as well as decreasing its hydrogen content as a result of aromatics formation.[69, 82, 84, 86] Consequently it was concluded that a lower reaction temperature of 430 °C is more favourable for producing high treated oil yields, with high hydrogen content and heating values.[84]

Many of the studies were conducted in the presence of supercritical water,[59, 83, 84, 87, 88] in the hope that the reaction of water with hydrocarbons would generate additional hydrogen which would promote the removal of heteroatoms from the bio-crude. Even though this may have resulted in a slight increase in upgraded oil yields,[89] it also caused a significant increase in the oxygen content of the upgraded oil, questioning

Table 2.1: Summary of upgrading studies conducted on biocrude from microalgae

Feedstock (Algae)	Biocrude composition, wt%			Catalyst	Reaction Temperature	Pressure	Reaction Mode	Reaction Time	Product composition, wt%			Ref.
	N	*S*	*O*						*N*	*S*	*O*	
Biocrude from HTL of *Nannochloropsis* (350 °C, 1 h)	5.32	0.56	8.35	HZSM-5 (0 – 50 wt% loading)	400 – 500 °C	43.5 bar (hydrogen)	Batch	0.5 – 4h	1.6 – 2.71	*bdl*	0.39 – 2.81	[86]
Biocrude from HTL of *Nannochloropsis* (340°C, 4 h)	4.80	0.48	8.07	Pt/C, Mo_2C, HZSM-5 (5 – 20 wt%)	430 – 530 °C	35 bar (hydrogen)	Batch in supercritical water (water/oil mass ratio of 4:5)	2 – 6 h	1.50 – 3.61	*bdl*	0.13 – 5.31	[84]
Biocrude from HTL of duckweed (350°C, 30min)	4.7	0.38	13.6	Ru/C, Pd/C, Pt/C, Pt/γ-Al_2O_3, Pt/C, Rh/γ-Al_2O_3, activated carbon, MoS_2, Mo_2C, CoMo/γ-Al_2O_3, zeolite	350 °C	180 bar	Batch in supercritical water (water oil mass ratio of 7:3)	4 h	4.5 – 5.9	0.13 – 0.29	0.1 – 5.4	[83]
Biocrude from HTL of *Nannochloropsis* (320°C, 4 h)	4.89	0.68	6.52	Pt/C (25wt%), HCl, NaOH	400 °C	34 bar (hydrogen)	Batch in supercritical water (water/oil mass ratio of 1:1)	4 h	2.17 – 2.79	*bdl*	4.31 – 4.71	[90]
Biocrude from HTL of *Chlorella p.* (350 °C, 1h)	7.3	*nd*	7.8	Pt/γ-Al_2O_3 (0 – 40 wt%) HCOOH (0 – 88 wt%)	400 °C	60 bar (hydrogen)	Batch in supercritical water (0 – 43wt%)	1 h	2.4 – 5.8	*nd*	4.7 – 17.9	[89]
Biocrude from HTL of *Desmodesmus sp*. (200 – 375°C, 5 to 60 min)	0.2 – 6.3	*nd*	10 – 39	HZSM-5 (SiO_2/Al_2O_3 = 280) (zeolite:sample mass ratio of 20:1)	600 °C		Pyrolysis probe (heating rate: 20C/ms^{-1}, pyrolysis time: 10 s)	10 s	0.02 – 0.14	*nd*	0.08 – 0.30	[85]
Biocrude from continuous HTL of *Nannochloropsis sp*. (344-362°C)	4.0 – 4.7	0.3 – 0.5	5.3 – 8.0	Co-promoted MoS_2 on fluorinated alumina support	125-170 °C (1st quarter of reactor) 405 °C (Main reactor)	13.6 bar (hydrogen flow)	Benchscale hydroprocessing system	LHSV of 0.14 to 0.20 h^{-1}	0.05 – 0.16	<50 ppm	0.8 – 1.2	[66]

Feedstock (Algae)	Biocrude composition, wt% N	S	O	Catalyst	Reaction Temperature	Pressure	Reaction Mode	Reaction Time	Product composition, wt% N	S	O	Ref.
Isoparaffin mixture containing 13wt% biocrude from continuous HTL of *Scenedesmus* sp. (300°C)	1.23	*nd*	6.96	Activated carbon, Co/C, Ru/C, Ni/C, Pt/C, Pre-reduced	350 °C	Not provided	Batch	4 h	0 – 0.15	*nd*	0 – 5.06	91
Biocrude from HTL of *Nannochloropsis* sp.	4.46	0.56	10.97	5wt% Pd/C	400 °C	35 bar	Batch in supercritical water	1 – 8 h	1.99 – 3.98	*bdl*	3.08 – 6.72	87
Biocrude from HTL of *Nannochloropsis* (260 °C, extracted with heptane under acidified conditions)	4.2	0.6	5.7	No catalyst	350 – 450 °C	Atmo-spheric (nitrogen)	Batch	60 min	4.2 – 4.3	0.1 – 0.4	0.2 – 2.9	92
Biocrude from HTL of *Chlorella pyrenoidosa* (350 °C, pretreated in 60 bar H_2 at 350 °C for 4h)	7.7	0.76	5.5	1:1 mixtures of Ru/C with Pd/C, Pt/C, Pt/Al_2O_3, Rh/Al_2O_3, $CoMo/Al_2O_3$, MoS2, Mo2/C, Raney-Ni, activated carbon and alumina	400 °C	60 bar (hydrogen)	Batch in supercritical water (water:oil mass ratio of 0.5)	4 h	1.9 – 3.1	0.07 – 0.11	0.1 – 5.6	88
Biocrude from continuous HTL of *Chlorella* at 350 °C	6.0 – 6.1	0.8	11.1 – 16.2	$CoMo/Al_2O_3$ $NiMo/Al_2O_3$, sulphided with 2 wt % dimethyldisulfide in kerosene	350 °C or 405 °C	138 bar	Stirred batch	2 h	2.4 – 4.7	0 – 0.12	1.0 – 5.0	69
Biocrude from HTL of pretreated, mixed algae feed	5.9	*nd*	13.9	Ru/C	350 °C	51.7 bar	Stirred batch	4 h	2.4	*nd*	20.2	76
Biocrude from HTL of *Chlorella pyrenoidosa* at 350 °C	7.05	0.68	6.07	Ru/C + Mo_2C	400° C	200 – 220 bar	Batch in supercritical water (water:oil mass ratio of 2.5)	4 h	2.87	0.09	0.63	59

the benefit of this approach.[81, 89] One study even tested the addition of weak acid (0.1 M HCl) or base (0.1 M NaOH), however this had an adverse effect on the nitrogen and oxygen content of the upgraded oil.[90]

Upgrading studies have employed many different classes of catalysts, including zeolites (HZSM-5),[81, 84-86] noble metals (Pt, Pd, Ru, Rh),[76, 81, 83, 84, 87-90] transition metals (Ni, Co),[91] sulphides (CoMo, NiMo),[66, 69, 76, 88] and carbides (Mo_2C),[83, 84, 88] mostly supported on alumina or activated carbon. However, in a number of studies the addition of catalysts, including Pt/Al_2O_3,[81] HZSM-5,[81] and Pt/C[90] had no or only minor effects on the reduction in the nitrogen and oxygen content of the bio-oil, whilst increasing the formation of coke and gas by-product.

Zhang *et al.* compared a large number of catalysts (Ru/C, Pd/C, Pt/C, $Pt/\gamma\text{-}Al_2O_3$, $Rh/\gamma\text{-}Al_2O_3$, activated carbon, MoS_2, Mo_2C, $CoMo/\gamma\text{-}Al_2O_3$ and zeolite) for the upgrading of bio-oil produced by the HTL of duckweed, but with the exception of Ru/C and MoS_2 all catalysts caused an increase in nitrogen content from 4.7 wt% in the biocrude to up to 5.9 wt% over $CoMo/\gamma\text{-}Al_2O_3$.[83] However, most catalysts resulted in a significant reduction in oxygen content from 13.6 wt% in the biocrude down to 0.1 wt% for Pt/C and Mo_2S, and the increase in nitrogen can therefore be attributed to the resulting loss of oxygen and carbon. Another study tested the conversion of HTL bio-oil from *C. pyrenoidosa*, over catalyst mixtures containing Ru/C together with Pt/C, Pt/C-sulfide, Pt/Al_2O_3, Pd/C, Rh/Al_2O_3, Mo_2C, $CoMo/Al_2O_3$-sulfide, activated carbon, alumina or Raney-Ni. Almost all catalyst mixtures, except of Pt/C-sulfide and Mo_2C, led to improved nitrogen removal compared to pure Ru/C, with the lowest N content of 1.8 wt% obtained over the mix containing Pt/Al_2O_3. However, the paper contains conflicting information on the nitrogen content of oil obtained from a non-catalytic control experiment with values of either 4.0 %, equivalent to the original nitrogen content in the crude oil, or 1.4 %, better than any of the tested catalysts.

A potential reason for the poor performance of many of the studied catalysts could be the lack of pre-reduction of the catalysts.[83] Whilst this would have lesser effect on zeolites and noble metal catalysts, transition

metal catalysts could remain in their inactive oxide form, diminishing their catalytic activity. Consequently, much better results were obtained during the upgrading of a mixture containing 13 wt% algal biocrude in isoparaffin over pre-reduced Pt/C, Ru/C, Ni/C and Co/C catalysts, with virtually complete nitrogen and oxygen removal over Pt/C and Ru/C.[91] The oil produced over these two catalysts was also recovered much more easily, indicating a reduction in its viscosity.

Another problem with the batch experiments is that they could be equilibrium limited, which is not necessarily the case for continuous operation.[66] For example, the conversion of commercial medium cycle oil over a sulphided $NiMo/Al_2O_3$ catalyst was inhibited following the accumulation of NH_3 and H_2S within the reaction gas.[93]

Continuous upgrading of a bio-oil produced by the fast pyrolysis of *Spirulina* in a downdraft fixed-bed reactor, loaded with a 1 wt% Ru/C catalyst, achieved virtually full removal of nitrogen at reaction temperatures of 400 °C.[82] However, oil yields were low (26.6 %) as a result of extensive gasification reactions. Reducing the reaction temperatures to 350 °C, resulted in higher oil yields, but increased the nitrogen content to 6.6 wt%.

Probably the best results to date were achieved using a benchtop hydrotreating reactor, converting bio-oils produced by the HTL of various *Nannochloropsis* strains over a sulphided CoMo catalysts, supported on fluorinated alumina.[66] Single stage upgrading at 405 °C with a space velocity of 0.20 h^{-1} and a pressure of 140 bar produced oils with nitrogen contents ranging from 0.07 wt% to 0.25 wt%. An even lower nitrogen content could be achieved by pre-treating the oil at temperatures between 125 °C and 170 °C in the first quarter of the reactor.

Nonetheless, the use of sulphided transition metal catalysts requires the presence of sulphur compounds to maintain their active phase. As most algae oils contain only limited quantities of sulphur, transition metal sulphides may not be the most suitable choice of catalyst. Sulphur dosing is possible, but not desirable as it could contaminate the upgraded oil.[81]

Consequently, further upgrading studies with alternative catalysts are required.

2.3 DENITROGENATION OF PETROLEUM FEEDSTOCKS

Even though only limited research has been conducted on the denitrogenation of algal bio-oil so far, the denitrogenation of petroleum feedstocks and model compounds has been studied in detail in the literature. This research was initially driven by a move away from conventional petroleum feedstocks towards heavy, low quality crudes and synthetic oils with much higher nitrogen contents, causing operational problems through catalyst deactivation, and more recently by increasingly stringent NO_x emissions specification.[94]

The research area has been extensively reviewed by Furimsky and Massoth,[95] Perot,[96] and Prins,[97] amongst others. Whilst these reviews cover a wide variety of catalysts, including sulphides, carbides, nitrides, phosphides and borides, the following section is more selective, focusing on the denitrogenation mechanism itself, the state-of-the-art transition metal sulphides and finally, one of the most promising classes of emerging denitrogenation catalysts, transition metal phosphides.

2.3.1 DENITROGENATION MECHANISM

The denitrogenation of heterocyclic nitrogen compounds often involves complex reaction pathways, requiring multiple, and sequential reaction steps. Not only is it strongly dependent on the structure of the nitrogen compounds themselves (for example non-basic five-ring cycles tend to be easier to denitrogenate than the more basic six-ring structures)[98] but also on the nature of the catalytic sites[99, 100] and the presence of promoters, such as H_2S.[96, 101]

As shown for quinoline (Figure 2.3), one of the most widely studied hydrodenitrogenation (HDN) model compounds, denitrogenation pathways generally involve only three different types of reactions: (1) hydrogenation of the nitrogen ring to convert the aromatic carbon-nitrogen bonds into single, aliphatic bonds (Reactions R1 and R7), (2)

hydrogenation of any adjacent aromatic rings in heterocyclic compounds (Reactions R2 and R4), and (3) sequential hydrogenolysis of the aliphatic C-N bonds to release nitrogen as ammonia (Reactions R3, R5, R8 and R9).[96] However, additional cracking reactions may be required to facilitate the conversion of heavily substituted nitrogen rings, as present in heavier, synthetic crude oils.[102]

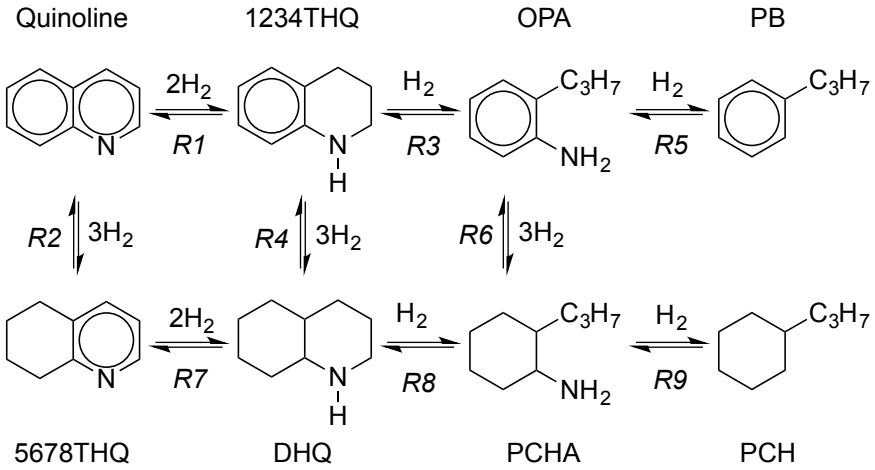

Figure 2.3: Denitrogenation pathway for quinoline, based on Laine[103]

Over conventional, sulphided transition metal catalysts, C-N bond hydrolysis reactions of primary and secondary amines mostly proceed via E_2 elimination and S_N2 substitution mechanisms.[104] Both mechanisms require initial protonation of the nitrogen atom, before a proton is extracted from a β-carbon atom, in the case of elimination, or the NH_3^+ leaving group is substituted with SH^- from the catalyst surface for substitution. Catalysts must therefore contain both acid sites, to bind the nitrogen group, and proximal base sites to carry out the β-carbon attack.[105]

However, for amines directly attached to an aromatic ring, such as orthopropylaniline (OPA), one of the reaction intermediates from the denitrogenation of quinoline, these pathways are either strongly inhibited (substitution) or cannot occur at all (elimination).[96] Consequently full hydrogenation of the secondary ring is required, resulting in the preferred formation of non-aromatic compounds such as propylcyclohexane.[106, 107]

In contrast, highly unsaturated sites with a strong electron-donating character favour S_N1 and E_1 mechanisms, allowing the direct denitrogenation of aromatically bound amines, to yield aromatics such as propylbenzene.[99, 100]

2.3.2 CONVENTIONAL SULPHIDE CATALYSTS

Conventional crude oil refining catalysts are almost exclusively based on bimetallic transition metal sulphides, and consequently a lot of the initial research into the denitrogenation of model compounds has focused on this class of materials. Even though the metal sulphides have lower hydrodesulphurisation (HDS) and HDN activities than metals, they show much higher stability during reaction, which is why they are used in industry.[108]

The activities of single metal transition metal sulphides have been found to depend strongly on their periodic position. Whilst a number of 2nd, and particularly 3rd row transition metal sulphides (Rh, Ir, Pd and Pt) display very high denitrogenation activities,[109-111] the activities of the 1st row sulphides are much lower.[112] These trends in activity have often been related to the metal-sulphur bond strength, according to the Sabatier principle.[113] In order to participate in the reaction, the catalysts need to be partially reduced under reaction conditions,[114] however, if the metal-sulphur bond strength is too low, the sulphur phase is lost completely, and the catalysts loses its activity.[115, 116]

By promoting high bond-strength sulphides such as Mo and W with metals that form very weak metal-sulphur bonds such as Ni, Co and Fe, a mixed phase sulphide is formed that possesses much more favourable bond strengths, with much higher denitrogenation activity than the individual sulphides.[110, 113] Consequently, the ratio between the two metals must be finely balanced to obtain the most active catalysts, as shown during the conversion of 1,2,3,4-tetrahydroquinoline (1234THQ) over an alumina supported NiMo catalysts.[96] A clear maximum was obtained for a Ni/(Ni+Mo) ratio of 0.2, with an activity 13 times that of the unpromoted Mo/Al_2O_3 catalyst.

Even so, the activities of these catalysts are not solely related to the metal-sulphur bond strength, as shown for the two most common bimetallic combinations, CoMo and NiMo. Whilst the Co promoted catalysts were found to display higher C-N bond cleavage activities, the NiMo catalysts were more active for the hydrogenation of aromatic rings, which is required before full denitrogenation of multi-ring nitrogen compounds can occur.[117] As this hydrogenation step is often the rate limiting step in the overall denitrogenation reaction, the NiMo catalysts were found to display higher nitrogen removal activities overall.[118]

Most upgrading studies have been conducted in the presence of sulphur, usually in the form of H_2S, in order to maintain the catalysts in the sulphided state and simulate the high concentrations of sulphur found in conventional fossil crude oils. Whilst the presence of H_2S was found to inhibit the hydrogenation of the aromatic rings, it promotes the cleavage of the C-N bonds.[101] This promotional effect is unsurprising, given the direct involvement of sulphur groups in the C-N bond hydrogenolysis reaction. Consequently, the H_2S/H_2 ratio must be carefully balanced, to obtain high rates of C-N bond hydrolysis, without inhibiting the hydrogenation reactions of the aromatic rings.[101] In the absence of sulphur, the promoting effect of Ni was lost, which suggests that the rate limiting step is switched from the hydrogenation to the C-N bond cleavage reaction.[96]

2.3.2.1 Effect of catalyst support

The choice of support was also found to have an important influence on the activity of transition metal sulphide catalysts. Commercial catalysts are usually supported on alumina, but more neutral supports, such as activated carbon, and more acidic supports, such as zeolites and aluminosilicates, have been commonly used in the literature.[119]

Zeolite and silica-alumina supported catalysts were consistently found to be more active than alumina supported catalysts despite stronger metal-support interactions. One of the main reasons for this activity improvement appears to be the improved metal dispersion on these

supports, particularly at low metal loadings.[120, 121] Alumina-supported Mo for example formed large slabs of MoS_2, whereas Y-zeolite-supported Mo formed a highly dispersed phase, which was virtually completely sulphided to MoS_2.[121] Similarly, H^+ Y and K^+ Y zeolite-supported Ru formed smaller active metal particles than Ru supported on alumina, resulting in the H^+ Y and K^+ Y catalysts being approximately two and three times more active than the alumina catalyst for the conversion of pyridine.[122]

As well as increasing the number of active sites, resulting in higher turn-over numbers, higher metal dispersion has also been linked to improved catalyst reducibility, which in turn is related to the activity of sulphide catalysts. Temperature programmed reduction studies of NiMo catalysts supported on SBA-15 showed, for example, that the incorporation of aluminium reduced the temperature of the first reduction peak maximum, as a result of improved dispersion of easily reducible Mo species.[123] The close proximity of metal and acid sites in the zeolite and silica-alumina supported catalysts may further contribute to the catalyst activity by promoting the cleavage of the C-N bond.[123, 124] Finally, these catalysts have also displayed improved activities towards the hydrogenation of aromatic rings,[120] a reaction which often represents the rate-limiting step during the denitrogenation over sulphides. This was associated with higher stacking of the MoS_2 slabs on an amorphous silica-alumina supported NiMo catalyst,[124] whereas for the zeolites this improvement may be the result of spacial constraints within the zeolite pores.

2.3.3 TRANSITION METAL PHOSPHIDE CATALYSTS

An alternative class of hydrotreating catalysts are transition metal phosphides, such as Ni_2P and MoP, which have been shown to possess significantly higher denitrogenation activities than the commercial, bimetallic transition metal sulphides.[105, 125-127] Their high activities have been generally related to more isotropic external morphologies, compared to the layered sulphide structure, exposing a greater number of

coordinatively unsaturated surface atoms and allowing high nanoparticle dispersions in the case of supported catalysts.[128-130]

It has also been suggested that the phosphidic P^{3-} sites may act as a base, assisting in the abstraction of protons from the adsorbed nitrogen-ring intermediate.[105] As these catalysts do not lose their activity in the absence of sulphur containing compounds,[127, 131, 132] they could be particularly suitable for the conversion of bio-derived oils, even though to date, they only appear to have been tested for the deoxygenation of these oils.[133, 134]

2.3.3.1 Active phase

The most widely studied phosphide phase is Ni_2P, although high denitrogenation activities have also been reported over MoP, Co_2P and WP catalysts. Some researchers have tested noble metal phosphide catalysts, such as Rh, Pd, Ru, Pt, although no comparison was made to the cheaper transition metal catalysts.[135, 136]

Varying results have been obtained regarding the relative activities of the different transition metal phosphide catalysts.[137-139] One study reported the activities for the denitrogenation of OPA to decrease in the order MoP>Ni_2P>WP>CoP,[131] whereas during the denitrogenation of a model feed containing 2000 ppm quinoline both Ni_2P and WP were found to be more active than MoP.[128] Whilst these variations could be related to the differences in the model compounds themselves, they may also depend on the basis of the activity measurement. On an active site basis, for example, an unsupported MoP catalyst was found to be six times more active for the conversion of OPA than an alumina-supported MoS_2 catalyst, whereas on a weight basis, the difference between the two catalysts was much less significant. Overall, most studies do however indicate that the most active phosphides are formed from nickel,[128, 137, 140] with the Ni_2P phase displaying higher activities than the more metal rich $Ni_{12}P_5$ or Ni_3P phases.[140]

A number of studies have also tested the activities of bimetallic phosphides, such as CoMo-P and NiMo-P. Initial results suggested that

these catalysts were much less active than single metal phosphides,[131, 139] but more recent studies found that using only trace amounts of promoters such as iron (3 %),[141] Co (7 %)[142] or Ni (7 %)[143] helped to enhance the HDS activities of these catalysts.

2.3.3.2 Catalyst supports

Most initial studies tested either bulk,[131] or silica supported transition metal catalysts,[105, 137, 144, 145] but more recently, alternative supports such as zeolites (USY,[129, 145] ZSM-5,[145] Beta Zeolite[145]), mesoporous materials (SBA-15,[125] MCM-41[127, 146-148]) and alumina (Al_2O_3)[149, 150] have also been used. A particular challenge with aluminium containing supports is the strong interaction between aluminium and phosphorus, resulting in the formation of $AlPO_4$[132] and requiring reduction temperatures significantly higher than those for silica supported or bulk phase catalysts. This in turn can lead to increased particle sizes with reduced activity,[136] although at low metal loadings, alumina was found to stabilize very small MoP particles, protecting them from sintering.[150] For H^+ MFI zeolite-supported catalysts, the interactions between aluminium and phosphates could also be modified by ion-exchange with sodium, reducing the reduction temperature to form an active Rh_2P phase by at least 100 °C.[136]

Another way of reducing crystallite sizes is the use of higher surface area supports, as found during the synthesis of silica-supported Ni_2P catalysts.[151, 152] These catalysts proved more active for the HDS of 4,6-dimethyldibenzothiophene and this was related to a larger number of Ni sites in square pyramidal co-ordinations, which appeared to catalyse the rate limiting hydrogenation step, as opposed to the flat tetrahedral sites found in the bulk phase.[152]

2.3.3.3 Catalyst synthesis

Supported transition metal phosphide catalysts are usually prepared by incipient wetness or solution based impregnation of the support with the metal and phosphorus salts, followed by drying, calcination and reduction. The most commonly used phosphorus precursors are phosphates,[105, 127, 129, 145, 149] although lower-oxidation state precursors

such as phosphites[144] and hypophosphites[146, 148] are increasingly used in an attempt to lower reduction temperatures and form more dispersed catalysts. These precursors thermally disproportionate into phosphates and phosphine,[108] which can further react with the metal to form the desired phosphide phase. Reduction temperatures for the formation of MCM-41 supported Ni_2P catalysts from a hypophosphite precursor were approximately 200 °C lower compared to the conventional phosphate method,[146] but it was found that reduction temperatures need to be carefully chosen to ensure full decomposition of the precursor, whilst preventing excessive loss of the phosphine phase, before it can react with the metal.[144]

Some researchers even supplied the phosphine gas directly, resulting in the formation of much smaller crystallite sizes compared to the phosphate method, equivalent to those of the metal precursors.[153, 154] However this approach may be unfavourable due to the high toxicity of this gas. To address this problem, one group decided to produce the phosphine gas in-situ, by placing the hypophosphite precursor in a furnace, and passing the vapours over the metal-impregnated support.[155] The resulting catalysts displayed better dispersion and higher dibenzothiophene conversion activities compared to catalysts produced by conventional co-impregnation.

2.3.3.4 P/Ni ratio

When preparing supported nickel phosphide catalysts it was found that the pure Ni_2P phase was only formed with excess phosphorus,[127, 144] as phosphorus is lost in the form of PH_3 during the reduction process.[137] The highest activities were usually reported for catalysts prepared with P/Ni ratios between 1 and 2,[105, 129, 146] as the metallic Ni and $Ni_{12}P_5$ phases were less stable, whereas higher P loadings resulted in partial blockage of the active sites.[105] However, the ideal P/Ni ratios were also found to depend on the total metal loading and the nature of the support,[137] with aluminium containing supports requiring higher phosphorus loadings due to the formation of $AlPO_4$. As the amount of surface-bound phosphorus is

more or less constant, lower P/Ni ratios were required at higher metal loadings to yield the desired Ni_2P phase.[147, 149]

2.4 PROCESS INTEGRATION

A number of lifecycle analysis and techno-economic analysis studies have been conducted on the production of algae bio-fuels. Most of these were focused on the production of lipid-based fuels, although some studies also included thermochemical processing.

For the lipid-based processes, virtually all cost predictions exceeded the current and expected near-term market prices for transportation fuels. The most positive results were obtained by Lundquist *et al.* (2010), who assessed a range of microalgal production facilities, with the cost estimates for lipid production ranging from US$ 302 to $ 417 per barrel ($∫1.9 to $∫2.6 per litre).[156] Slightly higher estimates were obtained for the production of green diesel from algae cultivated in open ponds ($ 2.6 L^{-1}) or closed tubular photobioreactors (5.4 L^{-1}) during a study by Davis *et al.* (2011).[157] Richardson *et al.* (2012) calculated lipid production costs of $∫12.73 gal^{-1} ($∫3.36 L^{-1}) for an open pond, commercial size algal biofuel facility located in Southwest USA,[158] whereas Norsker *et al.* (2011) estimated the biomass production cost in a tubular photobioreactor located in the Netherlands at €∫4.15 per kg.[159]

A lower cost estimate of $1.64 L^{-1} was obtained by Orfield (2013) for the production of bio-crude from the HTL of *Nannochloropsis* sp., however this cost is still significantly above the current fuel market price.[160]

Based on these predictions, it is unlikely that the fuel product on its own is able to pay for the entire liquefaction process. It is therefore necessary to identify and develop additional value streams, which can help to subsidise the fuel production costs.

Additional barriers are the requirements of pure sources of CO_2 and large amounts of fertilizers, which significantly add to the algae production costs.[161] Better integration of the conversion processes is therefore required to allow the efficient recycling of nutrients.

2.4.1 ADDITIONAL VALUE STREAMS

One of the main advantages of using microalgae is their high versatility, allowing them to be grown in a wide range of environments, and their ability to express a large number of high-value molecules, such as proteins, vitamins, pigments or pharmaceuticals.[162]

This opens up the possibility of combining algae fuel production with secondary objectives, such as carbon sequestration, wastewater treatment or chemicals production, which could help to partially offset the overall fuel production costs. Particularly the cultivation of algae on carbon dioxide waste streams from conventional fossil energy production has attracted a lot of interest,[163] however the high energy requirements of these system threaten to outweigh the potential carbon savings, resulting in net positive green house gas emissions.[164, 165]

In contrast, the large disparity between the market sizes for biofuels and high-value by-products could discourage the development of these products, as their large scale-production could result in a collapse of their market price.[33, 163] By-product recovery should therefore focus on lower value commodities with larger market shares, such as animal feeds, protein supplements, fertilizers or bio-plastics.[25]

2.4.1.1 Waste water treatment

The combination of algae biomass production with wastewater treatment has the potential to result in substantial cost savings as well as significantly reducing the overall environmental impact of the two processes.[166]

One of the main objectives of wastewater treatment is the removal of nutrients, particularly P and N, which is commonly achieved via physical and chemical treatment processes.[167] However, these processes can be inefficient and form waste products which are often disposed of by landfill, whereas algae-based treatment could represent a cheaper and ecologically safer alternative.[168, 169]

At the same time, fertilizer production represents one of the major contributors to total energy use and green house gas emissions associated with algae cultivation.[170] Domestic wastewater and agricultural wastes could therefore provide most of the nutrients required for the algae production.[171]

Global municipal waste water production amounts to approximately 300 billion m^3, of which just over 50 % are currently treated.[172] Consequently there is huge potential, particularly in less-developed economies, to apply algae cultivation to improve water quality whilst producing a sustainable fuel by-product.

2.4.1.2 Polymer production

Certain species of cyanobacteria have been found to accumulate significant quantities of polyhydroxyalkanoates (PHAs), particularly polyhydroxybutyrate (PHB), when grown in the presence of acetate and under nitrogen and phosphorus depleted conditions.[33] These compounds are a highly promising class of bio-polymers as they have equivalent properties to many currently available petroleum-derived plastics, with the additional benefit of being biodegradable.[173]

However, as PHB is used for energy and carbon storage within the cell, it usually only starts to accumulate at conditions where the cells cannot obtain enough nutrients to synthesize protein, but the photosynthetic activity is persevered to allow fixation of CO_2.[174] For example, the PHB concentration in *Synechocystis* sp. PCC 6803 during the lag and exponential growth phases accounted for only 1.8 wt% and 2.9 wt% respectively, but increased to 4.5 wt% during stationary growth.[175] Alternatively, the accumulation of PHB appears to be enhanced in the presence of organic carbon, particularly acetate,[176, 177] although the addition of these substrates would be expected to lead to a significant increase in production costs.

Until now, the low concentrations in fast-growing microalgae have prevented the commercial production of PHB from this feedstock.

However, these challenges could be addressed by combining the polymer recovery with the biofuel production via HTL.

2.4.2 NUTRIENT RECOVERY

The high consumption of phosphorus and nitrogen can have a significant impact on the overall sustainability of microalgae plants. Whilst phosphorus is a non-renewable resource with limited global reserves,[178] the production of nitrogen compounds is very energy intensive and can contribute more than 25 % to the total energy consumption for the fuel production from microalgae.[179] Consequently, high recovery and recycling of these nutrients is essential.[180]

A major advantage of the hydrothermal liquefaction process is that a substantial proportion of the nitrogen and phosphorus present in the biomass partitions to the aqueous phase and can therefore be recovered relatively easily. At the same time, the process water can contain up to 40 % of the carbon initially present in the biomass, and organic molecules such as phenols are known growth inhibitors.[181] Consequently it was found that the process water had to be diluted up to 100-fold with deionized water for biomass growth to occur.[182] At the same time it was found, that mixotrophic growth, utilizing the carbon present in the recycled stream could enhance the growth rates compared to pure growth medium.[181] *Desmodesmus* sp., in turn, could be grown at process water concentrations of up to 5 %, but was much less active in the absence of growth medium.[183] This was attributed to a lack of essential nutrients other than phosphorus and nitrogen, such as S, Ca, Mg, Na, K and Cl, which are present in the growth medium but not recovered in the process water stream.

Pre-treatment of the algae prior to liquefaction may also help the recovery of phosphorus and nitrogen from the algae, with the additional benefit of reducing the nitrogen content of the crude bio-oil.[36] Microwave pre-treatment of three algae species at temperatures between 80 °C and 140 °C resulted in the recovery of up to 50 % of the phosphorus into the water phase, but had no noticeable impact on the overall nitrogen

recovery following liquefaction at 300 °C.[73] In contrast, pre-treatment of a *Nannochloropsis occulata* slurry at temperatures above 200 °C produced an algal residue with a reduced nitrogen content, albeit with a significant loss of carbon, between 40 and 50 %.[184]

Yet another strategy to improve the recovery of nitrogen to the water phase, whilst maximising the crude bio-oil yields, could be the step-wise liquefaction of the algae to exploit the differences in devolatilization temperatures for lipids, proteins and carbohydrates. Thermal degradation studies showed that lipids decompose at temperatures between 150 °C and 230 °C, proteins at temperatures between 230 °C and 400 °C and carbohydrates in the temperature range from 400 °C to 500 °C.[185] Indeed it was found that bio-crude produced from the hydrothermal liquefaction of *Desmodesmus* sp. at temperatures below 250 °C produced oils with a significantly reduced nitrogen content, however with low yields.[27] In contrast, a constant nitrogen level of around 6 wt% was obtained at temperatures above 300 °C, whilst biocrude yields continued to increase up to a temperature of 375 °C.

CHAPTER 3

HTL OF PHB CONTAINING MICROALGAE

The work in this chapter was published in Bioresource Technology in May 2016, in collaboration with the Plymouth Marine Laboratory and the University of Natural Resources and Life Science Vienna:

> Wagner, J., et al., *Co-production of bio-oil and propylene through the hydrothermal liquefaction of polyhydroxybutyrate producing cyanobacteria.* Bioresour Technol, 2016. **207**: p. 166-74.

3.1 CONTEXT

As reviewed in the previous two chapters, the HTL of microalgae represents a promising pathway for the production of sustainable, 3rd generation bio-fuels. By converting all organic biomass components, it can utilize faster growing, and cheaper algae than conventional lipid-based processes, and opens up the possibility of combining algae cultivation with additional value streams such as carbon sequestration or bioremediation.

Despite this, a number of challenges remain, limiting the commercial applicability of this technology. HTL of algae tends to produce bio-oils with high concentrations of heteroatoms, particularly nitrogen, owing to the incorporation of protein- and carbohydrate-derived material. Consequently, the oils require significant upgrading before they can be processed in conventional petrochemical refineries. Bio-oil yields and composition were previously found to strongly depend on the biochemical composition of the algae. Careful selection and optimization of the feedstock could therefore be beneficial to obtaining higher bio-oil yields with reduced heteroatom content.

Another challenge is the low value of the resulting biofuel product. For example, a techno-economic analysis from 2013 estimated a bio-crude production cost of \$1.64 L^{-1} from the HTL of *Nannochloropsis* sp., significantly above the current fuel market price.[160]

Consequently, it is necessary to identify and develop additional value streams, which are able to partially offset the biofuel production costs. A potential solution is the production of higher value by-products, however their market size needs to be large enough to prevent oversaturation and collapse of their market price.[33, 163] One market that fulfils this requirement is the polymer industry. Certain species of cyanobacteria have been found to accumulate significant quantities of the polyhydroxyalkanoate PHB, which represents a promising feedstock for sustainable and biodegradable plastics.[33, 173] Even though the concentrations of this compound in fast-growing microalgae remain below

commercial extractable levels, direct HTL of these algae could represent an alternative polymer recovery method.

In this chapter, the effect of biomass composition on the product distribution obtained from the HTL of *Spirulina* was evaluated, using rapeseed oil, corn flour and soy protein as models to represent the lipid, carbohydrate and protein fractions, respectively. Subsequently, the effect of adding PHB to the liquefaction of *Spirulina* was investigated, to assess the potential of recovering additional by-products from the liquefaction of polymer-containing microalgae. Finally, these experiments were repeated with PHB-containing microalgae, obtained from collaborations with the Plymouth Marine Laboratory and the University of Natural Resources and Life Science Vienna.

This chapter is submitted in an alternative format, in line with Appendix 6A of the University of Bath 'Specifications for Higher Degree Theses and Portfolios' using a paper published in Bioresource Technology in May 2016.

All the work described in the paper was conducted by the thesis author, with exception of the following:

- The cultivation of the microalgae *Anabaena* sp. and Synechococcus sp., and general biomass characterization was carried out by Rachel Bransgrove, Tracey A. Beacham and Michael J. Allen from the Plymouth Marine Laboratory.
- The cultivation and analysis of the PHB containing algae *Synechocystis* cf. *salina* was conducted by Katharina Meixner and Bernhard Drosg at the University of Natural Resources and Life Science Vienna.

3.2 PUBLICATION

Co-production of bio-oil and propylene through the hydrothermal liquefaction of polyhydroxybutyrate producing cyanobacteria

*Jonathan Wagner,[a] Rachel Bransgrove,[b] Tracey A. Beacham,[b] Michael J. Allen,[b] Katharina Meixner,[c] Bernhard Drosg,[c] Valeska P. Ting[d] and Christopher J. Chuck[d]**

[a] Centre for Doctoral Training in Sustainable Chemical Technologies, Department of Chemical Engineering, University of Bath, Claverton Down, Bath, United Kingdom, BA2 7AY.

[b] Plymouth Marine Laboratory, Prospect Place, The Hoe, Plymouth, PL1 3DH

[c] University of Natural Resources and Life Science Vienna, Department of Agrobiotechnology IFA-Tulln, Institute for Environmental Biotechnology, Konrad Lorenz Straße 20, A-3430 Tulln, Austria

[d] Department of Chemical Engineering, University of Bath, Claverton Down, Bath, United Kingdom, BA2 7AY.

Email: C.chuck@bath.ac.uk, Tel: +44(0)1225 383537

Keywords: Polyhydroxybutyrate, advanced biofuel, microalgae, hydrothermal liquefaction, biorefinery, biopolymers

Abstract

A polyhydroxybutyrate (PHB) producing cyanobacteria was converted through hydrothermal liquefaction (HTL) into propylene and a bio-oil suitable for advanced biofuel production. HTL of model compounds demonstrated that in contrast to proteins and carbohydrates, no synergistic effects were detected when converting PHB in the presence of algae. Subsequently, Synechocystis cf. salina, which had accumulated 7.5 wt% PHB was converted via HTL (15 % dry weight loading, 340 °C). The reaction gave an overall propylene yield of 2.6 %, higher than that

obtained from the model compounds, in addition to a bio-oil with a low nitrogen content of 4.6 %. No propylene was recovered from the alternative non-PHB producing cyanobacterial strains screened, suggesting that PHB is the source of propylene. PHB producing microorganisms could therefore be used as a feedstock for a biorefinery to produce polypropylene and advanced biofuels, with the level of propylene being proportional to the accumulated amount of PHB.

1 Introduction

Over the last five years, research on the direct hydrothermal liquefaction (HTL) of microalgae into fuel range compounds has gained significant momentum (Jazrawi et al., 2013; López Barreiro et al., 2013; Tian et al., 2014). Compared to the alternative process for the production of fuels from microalgae, the extraction of lipids followed by the transesterification into biodiesel, direct HTL offers a number of significant advantages: it is capable of converting the entire biomass fraction, not just lipids, and can therefore be used for the conversion of fast growing protein producing eukaryotic algae and cyanobacteria (hereafter collectively referred to as microalgae); it is conducted in the presence of high water loadings, and therefore only partial drying of the biomass is required; and it produces a wide variety of compounds which may be further upgraded into a range of fuels and chemicals (Lopez Barreiro et al., 2014; Tian et al., 2014). Despite this, a number of challenges remain: most notably, the upgrading of the resulting crude oils (which cannot be treated in conventional refineries due to their high nitrogen contents) and the utilisation of additional product streams to help subsidise fuel costs (Biller et al., 2013; Chuck et al., 2015).

Previous studies have investigated the relationship between bio-oil yields and the biochemical make-up of the algae (Li et al., 2014; Vardon et al., 2011). The three most important biochemical constituents of microalgae are proteins, lipids and carbohydrates, and their relative compositions depend both on the individual species and the selected growth conditions. These studies identified a strong relationship between lipid

content and bio-oil yields, with lipid-rich algae producing the highest bio-crude yields. Using data from the conversion of model compounds and various microalgae species, Biller et al. estimated that the bio-crude yields from the different biochemical fractions range from 55 % to 80 % for lipids, 11 % to 18 % for proteins and 6 % to 15 % for carbohydrates (Biller & Ross, 2011). Similar yields were obtained by Teri et al. for pure model compounds, however, when converting mixtures of polysaccharides and proteins, enhanced oil yields were obtained at a reaction temperature of 350 °C (Teri et al., 2014). The authors suggested that this could be the result of Maillard reactions between sugars and amino acids formed from the carbohydrate and protein fractions respectively. Yang et al. experienced a similar behaviour using algae extracted crude polysaccharides and crude proteins (Yang et al., 2015). Yields obtained during the co-liquefaction of both compounds were enhanced compared to the yields of single compound liquefaction, also resulting in the highest energy recovery.

Besides these three main classes of biochemical compounds, some species of microalgae have been found to accumulate significant quantities of other types of compounds, such as algaenans, a series of acid and base-resistant aliphatic biomacromolecules (Versteegh & Blokker, 2004). During the HTL of these species, algaenans and algaenan derivatives were almost fully extracted into the biocrude phase at temperatures exceeding 300 °C, and can therefore help to increase potential yields of a low-nitrogen fuel precursor (Torri et al., 2012).

Some cyanobacteria (prokaryotic microalgae) also accumulate polyhydroxyalkanoates (PHAs), such as polyhydroxybutyrate (PHB), particularly in the presence of excess carbon and under nutrient (nitrogen, phosphorus) limited conditions (Markou & Nerantzis, 2013). The PHA content in the biomass can range from below 1% to over 50% and depends on the strain, the carbon and nutrient source and composition as well as on the cultivation conditions (Drosg et al., 2015; Panda et al., 2006; Wu et al., 2002; Wu et al., 2001). Fast growing thermophilic cyanobacteria such as *Chlorogleopsis fritischii* PCC 6912

and *Synechococcus* sp. MA19 have been shown to accumulate PHB in excess of 6% w/w (dry weight) when grown at 50 °C (Hai et. al. 2001).

PHAs are seen as a promising class of bio-polymers as they have equivalent properties to many currently available petroleum-derived plastics, with the added benefit of being biodegradable (Somleva et al., 2013). Despite this, PHA concentrations in fast-growing microalgae are usually too low to enable economic extraction. HTL could therefore represent a more effective method for utilising these compounds.

In this paper we investigate the potential of biopolymer-containing species of microalgae for conversion by HTL. To this end, models representing the four classes of biochemical compounds present in these species (lipids, proteins, carbohydrates and PHAs) were first converted in isolation and their product distribution determined. The results from the conversion of the model compounds were then compared to the yields obtained from the most extensively cultured and readily available cyanobacteria *Spirulina*, before liquefying *Spirulina* in the presence of varying concentrations of PHB (to compensate for its lack of natural PHB production, as a proxy for other potential cyanobacterial based PHB production platforms) to investigate if there is any interaction between the algal and the biopolymer compounds. Finally, three different species of cyanobacteria, both PHB and non-PHB producing, were liquefied and their product distribution analysed.

2 Materials and Methods

2.1 Materials

General lab solvents were purchased from Sigma–Aldrich and used without further purification. Deuterated chloroform ($CDCl_3$) for ^1H NMR analysis was purchased from Fluorochem. Rapeseed oil (*Co-operative Vegetable Oil)* was purchased from the Co-operative Food Supermarket, UK and contained 62% mono-unsaturates, 30% polyunsaturates and 8% saturated esters.

Dried Spirulina powder (*Organic Spirulina powder*) and protein (*soy protein isolate 90*) were purchased from Bulk Powders, Sports Supplements Ltd. UK. Corn flour (*Corn Flour by Sainsbury*) was obtained from Sainsbury's Supermarket Ltd. UK. Values for their biochemical composition were obtained from their packaging information. Polyhydroxybutyrate biopolymer granules were purchased from Goodfellow Cambridge Ltd.

2.2 Cultivation of microalgae

Stock cultures of *Anabaena sp.* (**CCAP 1403/4A)**, *Synechococcus sp.* (WH7803) and *Synechocystis cf. salina* Wislouch (No. 192) were maintained under batch culture conditions and sub-cultured on a weekly basis. *Anabaena* cultures were maintained in BG11 media in 10 L bubble columns under 100 µmols photons m^2 sec^{-1} irradiance on a 16 h: 8 h light: dark cycle at 20 °C (±1 °C), according to literature precedent (Stanier et al., 1971).

Synechococcus sp. was grown in a saline version of BG11 (3.5 % sea salt). Shear stresses prevented the growth of *Synechococcus sp*. in bubble columns and as such were grown in multiple 500 mL batches under the same irradiance measures and cycles and aerated by manual daily shaking. Strains were grown to mid log phase, and then sub cultured in to either fresh medium, or medium lacking the nitrogen component ($NaNO_3$). Culture density was monitored spectrophotometrically.

Synechocystis cf. salina Wislouch (No. 192) – from the culture collection of autotrophic organisms (CCALA) – was cultivated in nutrient limited (nitrogen and phosphorous) mineral medium based on BG11 (Rippka et al., 1979) in a tubular photobioreactor with a working volume of 200 L for 21 days. The biomass was harvested with a nozzle separator (GEA Westfalia, Typ NA 7-06-067/-576) (disc outer diameter 162 mm), stored at -20 °C and lyophilised.

As the quantities of the individual samples were insufficient for separate HTL analysis, harvested *Synechococcus* and *Anabaena* biomass was

combined into one sample grown under normal growth conditions (*Synechococcus* to *Anabaena* ratio of 3.53:1), and one grown under nitrogen starved conditions (*Synechococcus* to *Anabaena* ratio of 5.38:1), which will be referred to as *Synechococcus/Anabaena* and *Synechococcus/Anabaena-N*, respectively.

2.3 Biomass characterization

The CHN content of all feedstocks (except PHB) was determined on a Carlo Erba Flash 2000 elemental analyser. The ash and moisture contents were determined by thermogravimetric analysis (TGA), under air flow, ramp rate of 10 °C min^{-1} to 500 °C and 20 °C min^{-1} to 900 °C.

Sugar (carbohydrate) content was determined according to literature precedent (Rao & Pattabiraman, 1989). Briefly, 3 mL conc. sulfuric acid is added to 1 mL algae sample (1 mg rehydrated in distilled water) (n=5) and the reaction allowed to reach maximum temperature for 5 minutes before cooling to 25 °C. 1 mL 5 % (w/v) phenol solution was added and the tubes stood at 25 °C for 30 minutes. The absorbance at λ = 480 nm was determined and glucose was used for standard curve.

Protein content was determined according to the biuret method (Bellou & Aggelis, 2012). Briefly, 1 mL culture (up to 8 mg dried algae rehydrated in distilled water) (n=5) added to 0.75 mL KH_2PO4, (0.067M pH4.5) and 3 mL NaOH (20 % w/v) and incubated for 5 minutes. Thereafter 0.125 mL $CuSO_4.5H_2O$ solution (25 % w/v) was added and samples periodically shaken for 10 minutes then centrifuged. The absorbance at λ = 540 nm of the supernatant was determined. Bovine serum albumin was used for standard curve.

Lipid content was determined post conversion to fatty acid methyl esters (FAMEs) using GC-MS (Agilent 7890A GC and 5975C inert MSD, Agilent Technologies Ltd., Edinburgh, UK). Nonadecanoic acid (C19:0) was added as an internal standard to each sample (up to 9.5 mg lyophilised algae) (n=5) and cellular fatty acids were converted directly to FAMEs by adding 1 mL of transesterification mix (95:5 v/v 3 N methanolic HCl; 2,2-dimethoxypropane) followed by incubation at 90 °C for 1 h. After cooling,

FAMEs were recovered by addition of 1 % w/v NaCl solution (1 mL) and *n*-hexane (1 mL) followed by vortexing. The upper hexane layer was injected directly onto the GC-MS system as previously described (Beacham et al., 2015). FAMEs were identified using retention times and qualifier ion response and quantified using respective target ion responses. All parameters were derived from calibration curves generated from a FAME standard mix (Supelco, Sigma-Aldrich, Gillingham, Dorset, UK).

The PHB concentration was determined using a modified literature method (Karr et al., 1983), where the dried algae / cyanobacteria biomass was digested with concentrated H_2SO_4 at 90 °C for 30 minutes – in this step PHB degrades to crotonic acid. The sample was diluted for high performance liquid chromatography (HPLC) analysis. HPLC analysis was carried out with an Agilent 1100 system, equipped with an ion-exclusion column ION 300 (Transgenomic CARBOSep COREGEL 87H, part no. CHO-99-9861) heated at 65 °C and a refractive index detector (Agilent 1100/1200 – 55 °C). The flow rate of the mobile phase – 0.005 M H_2SO_4 – was 0.9 mL min^{-1}; the method lasted 25 minutes.

2.4 Reactions

Hydrothermal liquefaction reactions were conducted in a batch reactor according to literature precedent (Biller & Ross, 2011). The reactors had an approximate internal volume of 50 mL, were constructed of Swagelok tubing and fitted with a pressure gauge, vent valve and a thermocouple connected to data logging software (Raikova et al., 2016). Each reaction was conducted with 3 g (*Synechococcus/Anabaena and Synechococcus/Anabaena-N*) or 4 g of biomass and 15 mL or 20 mL, respectively, of D.O. water, giving a solid loading of approximately 16.7 %. The reactor was placed inside a tube furnace, which had been preheated to a temperature significantly above the desired reaction temperature. As soon as the desired reaction temperature was reached, the reactor was removed from the furnace. Pressure was generated internally through the partial vaporisation of water and monitored using a

pressure gauge. Total heating times varied from 26 to 71 min, depending on the desired reaction temperature, external temperature and exact position of the reactor within the furnace. The reaction system was thoroughly cleaned between reaction runs, by heating 20 mL of D.O. water to approximately 200 °C and venting the produced steam through the reactor vent valve.

Selected reactions for each model compound were conducted in triplicate, to estimate the standard deviations of the reaction results. Triplicate reactions were conducted for *Synechocystis*, but due to insufficient amounts of biomass for the *Synechococcus/Anabaena and Synechococcus/Anabaena-N* samples, these were only converted in a single HTL run.

2.5 Sample workup

Following hydrothermal liquefaction, the reactor was allowed to cool back to room temperature, before the reaction gases were vented into an inverted, water-filled measuring cylinder to determine the volume of gas produced. Selected gas samples were separated on a gas chromatograph (Agilent 7890A) containing a HP-Plot-Q capillary column using helium as carrier gas and analysed with an external Agilent 5975C MSD detector. The samples were loaded at 35 °C, hold time 7 min, ramped to 150 °C at 20 °C min^{-1}, hold time 0 min, ramped to 250 °C at 15 °C min^{-1}, hold time 16 min. Gas compositions were normalized to exclude nitrogen and chloroform, which were not formed during the reactions, but introduced during the reactor loading and cleaning procedures.

The water phase was recovered by decanting the reactor contents through filter paper, leaving behind the crude oil and solid product phases. The yield of non-volatile water residue was determined by drying water phase aliquots of approximately 5 mL in an oven overnight, and the weight of the recovered residue was scaled to the total recovered water phase volume (by weight). The oil phase was recovered by repeatedly washing the reactor and solid residue with chloroform until the solvent

remained clear, before filtering the solvent-oil mixture and evaporating the chloroform in a rotary evaporator. The solid yield was determined from the mass of retentate collected on the filter paper during the filtration of the water and oil product phases. To minimize errors associated with absorbed atmospheric moisture, the filter paper was dried overnight and weighted immediately after removal from the drying oven before and after use.

All product phase yields were calculated on a dry, ash-free basis (daf).

2.6 Product analysis

The CHN contents of the oil and residue phases produced from the HTL of proteins and algae were determined by elemental analysis. Ash and moisture contents were determined by TGA, under air flow, ramp rate of 10 °C min^{-1} to 500 °C and 20 °C min^{-1} to 900 °C. The energy densities of the oils and feedstocks were determined on an IKA® C1 bomb calorimeter. For samples which could not be combusted, the energy density was calculated using the Dulong formula,(Faeth et al., 2013) using the results from CHN and TGA analysis:

$$HHV\ (MJ\ kg^{-1}) = 0.338 \times C + 1.428 \times (H - O/8) + 0.095 \times S \quad \textbf{(1)}$$

The oxygen content was calculated by difference, subtracting the carbon, hydrogen, nitrogen and ash weights from 100. Sulphur content was assumed to be negligible.

The ammonia concentration of the water phase was determined using a Randox Urea analysis test kit. Due to the high concentration of ammonium ions in the produced water, the samples were diluted with distilled water to a concentration of 1 or 2 % v/v. Subsequently, 10 µL of sample was reacted for 5 min with 1000 µL of a urease reactant, followed by the addition of 200 µL of sodium hypochlorite solution to induce the colour change. Finally the sample absorbance was measured at 600 nm and calibrated using a reagent blank and standard solution.

NMR spectra were obtained on a 300 MHz Bruker Avance spectrometer.

3 Results and Discussion

3.1 Biomass characterization

A total of four different microalgae samples and four different model compounds were tested in this work as HTL feedstocks (Table 1). *Spirulina* was selected for this study as it is amongst the most well studied species of microalgae for HTL. Some strains of *Synechocystis* and *Synechococcus* in turn have been reported to accumulate high levels of PHB of up to 55 % (daf) when cultivated under nitrogen and phosphorus depleted conditions (Drosg et al., 2015; Miyake et al., 1996; Nishioka et al., 2001; Panda et al., 2006; Wu et al., 2002; Wu et al., 2001).

Soy protein, rapeseed oil, corn flour and PHB were selected to represent the expected four main biochemical compound fractions found in the biopolymer producing cyanobacteria, namely protein, lipid, carbohydrates and PHAs. The proximate analysis of the models shows high purity in the desired compound group, and therefore the selected models are an adequate representation of the biochemical composition of microalgae.

As a result of its high carbon and hydrogen content, rapeseed oil possesses by far the highest energy density of all the four model compounds. Consequently, much research has focused on increasing the lipid content in microalgae. Unfortunately, this can reduce microalgae growth rates to an uneconomic level and therefore the focus has shifted towards faster growing protein producers. The energy densities of PHB and soy protein are quite similar, despite displaying large differences in elemental composition. PHB contains more carbon and oxygen, but less hydrogen and no nitrogen. Corn flour possesses the lowest energy density of all model compounds, as a result of its high oxygen and low carbon and hydrogen content.

All four model compounds had much lower ash contents than the microalgae samples, especially rapeseed oil, corn flour and PHB. Amongst the microalgae samples the highest ash content was observed

for the two mixed *Synechococcus/Anabaena* samples, particularly those grown in normal growth medium (38.1 %), compared to ash contents for *Spirulina* and *Synechocystis* of 9.3 % and 11.2 %, respectively. A potential explanation for the high ash content of the *Synechococcus/Anabaena* samples is that *Synechococcus* was cultured in a saline growth medium, containing 3.5 % sea salt, resulting in the carry-over of high levels of inorganic solids to the resulting biomass. The differences in ash content will not only impact the overall product yields, but could also have important catalytic effects during the HTL of these compound (Biller & Ross, 2011).

The composition of *Spirulina* is typical for fast-growing microalgae, with a low lipid and high protein concentration. Consequently, it has a high nitrogen content of 12.51 % (daf), a carbon content, nitrogen content and energy density similar to those of soy protein. The *Synechocystis* and mixed *Synechococcus/Anabaena* samples all have significantly lower nitrogen concentrations (3.52 to 7.91 %), linked to a reduced protein content (53.7 to 54.9 %). For HTL, the high nitrogen content of the protein fraction is one of the major challenges, as it results in the formation of nitrogen rich oils which require significant further upgrading. Consequently the reduced nitrogen content in the PHA producers is desirable for increased bio-oil quality. The three *Synechocystis* and *Synechococcus/Anabaena* samples also have a reduced carbon content (42.78 to 48.27 %), compared to *Spirulina* (54.62 %), which may be related to an increased ash content and the high oxygen content of the PHA fraction.

3.2 Conversion of model compounds

3.2.1 Product distribution

The liquefaction of the four model compounds rapeseed oil, corn flour, soy protein and PHB was conducted at four reaction temperatures, ranging from 300 to 360 °C, and the yields of the solid, oil, water residue and gas were recorded (Figure 1a). In accordance with the literature, the product distributions from the different compound classes were found to

compound classes were found to be vastly different (Biller & Ross, 2011; Teri et al., 2014). Whilst rapeseed oil is almost exclusively converted into an oil product, corn flour favours the formation of solids, soy protein the formation of water phase residue and PHB produces very high gas yields, particularly at the higher reaction temperatures.

With the exception of rapeseed oil, the overall mass balance closures obtained from the conversion of the model compounds were poor, particularly for corn flour. Despite this, the results showed high repeatability, which suggests that the deficit must be attributed to systematic causes, rather than experimental error. The most likely explanation is the loss of volatile organic compounds during the evaporation of water from the aqueous phase. Indeed, many of the products previously identified in the water phase from the hydrothermal liquefaction of carbohydrates (glucose) fulfil this requirement, such as acetone (boiling point of 56 °C), formic acid (BP ~ 101 °C), 5-hydroxymetnylfurfural (BP ~ 114 – 116 °C), acetic acid (BP ~ 118 °C), lactic acid (BP ~ 122 °C) and glucoaldehyde (BP ~ 131 °C) (Srokol et al., 2004). As most previous work calculated the water yield by difference rather than direct measurement, this problem has been rarely encountered in literature (Chen et al., 2014).

Analysis by ^{1}H NMR (included in supplementary information) of the rapeseed oil fraction revealed the complete disappeareance of the peaks corresponding to the glycerol backbone (δ = 4.0 – 4.5) and the bis-allylic sites (δ = 2.5 – 3.0), a reduction in the peaks corresponding to the double bonds (δ = 5.0 – 5.5) but almost no change to the ester peaks as reaction temperatures approached 340 °C. This shows that the triglycerides in rapeseed oil fully decomposed into free fatty acids and glycerol, and no further decarboxylation took place.

Increasing the reaction temperature from 300 to 360 °C had different effects on the yields obtained from the various model compounds. Whilst yields obtained from the liquefaction of corn flour and rapeseed oil remained more or less constant, reaction temperature had a large effect on the yields obtained from soy protein and PHB. In the case of the

former, the highest oil yields of 28.6 % were obtained at the highest reaction temperature of 360 °C, which also resulted in the lowest solid (~ 0 %) and water phase residue (35.9 %) yields. Similar to the literature, the increase in oil yields over the investigated temperature range appears to be correlated to a similar reduction in solid yields (Yoo et al., 2015). In contrast, the decreasing water phase residue yields result in a reduced overall mass balance closure, suggesting that water soluble products are broken down into more volatile organic compounds as the reaction temperature is increased.

Table 1: Proximate and ultimate analysis and energy content of model compounds and cyanobacteria used in this study

Compound / Alga	TGA analysis		Biochemical composition				Elemental Distribution (daf)			*Energy density*
	Moisture	*Ash*	*Protein*	*Carbo-hydrate*	*Lipid*	*PHB*	*C*	*H*	*N*	*MJ kg^{-1}*
Spirulina	6.00	9.32	63	20	6	0	54.62	8.78	12.51	20.19
Synechococcus/ Anabaena	7.4	38.1	54.9	16.5	3.5	bdl	42.78	7.74	7.91	9.61
Synechococcus/ Anabaena-N	10.4	28.9	54.2	22.9	6.1	bdl	48.27	9.19	6.17	11.25
Synechocystis	4.5	11.2	53.7	40.5	2.8	7.5	46.12	7.98	3.52	15.37
Soy Protein	6.8	4.5	91	0	3.3	-	53.28	8.32	15.02	21.10
Rapeseed Oil	0	0.53	0	0	100	-	77.45	13.37	0.00	39.37
Corn Flour	11.8	0	0.2	88	0.1	-	44.77	8.02	0.00	15.09
PHB	1.9	0.35	-	-	-	100	*57.09	*7.14	*0.00	$^{+}$22.19

* Elemental distribution of PHB based on molecular formula

$^{+}$ Energy density calculated using Dulong formula

bdl – below detection limit

For PHB, over the investigated temperature range, gas yields steadily increased from 33.0 to 71.6 % whereas water residue yields dropped from 35.7 to 14.3 %. Oil yields were reduced from 7.0 % to 2.6 %, and solid yields were low at all reaction temperatures (2.4 % to 1.6 %). In contrast to soy protein, the overall mass balance closure increased as the temperature was raised from 320 to 340 °C, suggesting a successive break-down of solid PHB, first into heavier water soluble compounds, then into lighter organics and finally into gas products.

HTL of corn flour and soy protein resulted in a significant increase in the carbon and hydrogen content of the biocrude compared to the unconverted model compound (see supporting information). In contrast, the carbon and hydrogen content of the rapeseed oil product appeared slightly reduced, whereas for PHB, carbon and hydrogen were reduced at

300 and 320 °C, but increased at the higher reaction temperatures. For soy protein, the nitrogen content in the biocrude was considerably reduced from an initial value of 13.3 % to a minimum of 6.6 % at 360 °C.

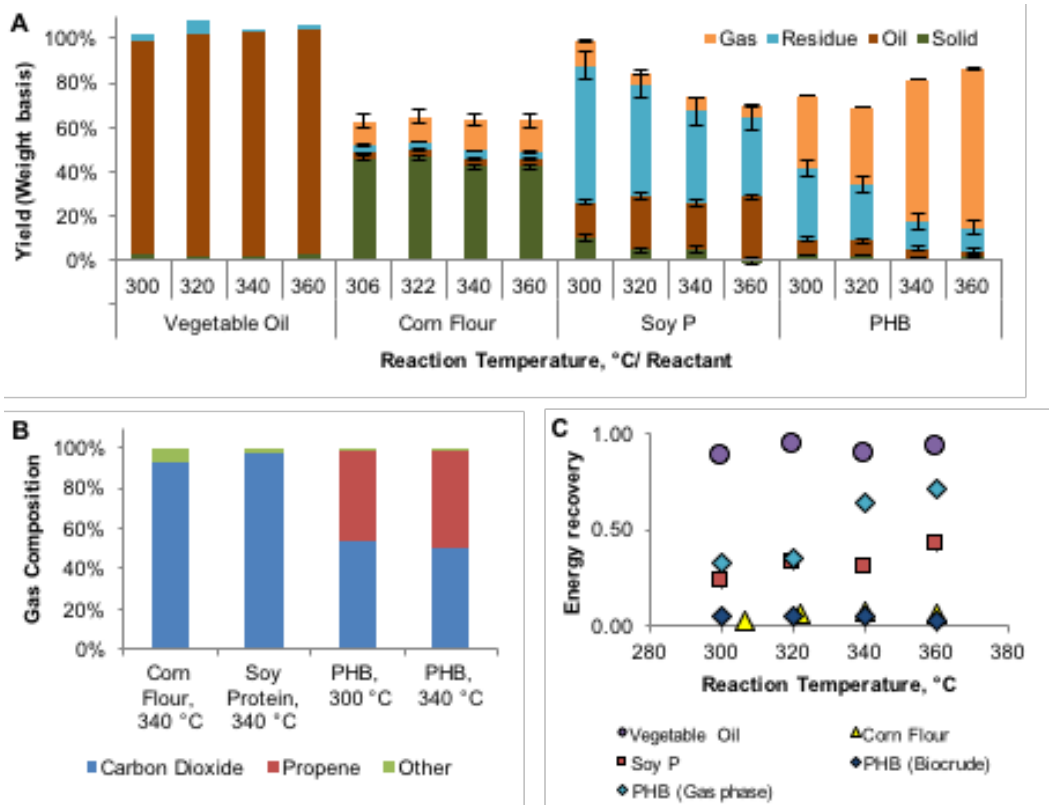

Figure 1: Results from HTL of model compounds representing biochemical compound classes present in cyanobacteria; A) Product distribution; B) Gas compositions, C) Energy recoveries

Consequently the carbon and hydrogen retention for this feedstock, 37.5 % and 34.0 % respectively, were much higher than the nitrogen retention of only 12.5 %, resulting in an increase in the HHV from 20.8 to 35.4 MJ kg^{-1} (all values for 360 °C). Despite this, the residual nitrogen content remains above the acceptable threshold for fuel use, and therefore further treatment of the oil would be required (Chuck et al., 2015). Increasing the reaction temperature from 300 to 360 °C resulted in a large increase in the HHVs obtained for corn flour (23.3 to 29.5 MJ kg^{-1}) and PHB (15.2 to 27.2 MJ kg^{-1}), likely as a result of an increased degree of deoxygenation, and therefore increased carbon and hydrogen concentration. However, the low oil yields obtained from these two models are unlikely to make a major contribution to the overall oil produced from the HTL of actual, PHB-containing cyanobacteria.

3.2.2 Gas phase analysis

Analysis of representative gas samples from the HTL of soy protein and corn flour revealed that, consistent with the literature, carbon dioxide was by far the dominant gas product, exceeding 90% in both cases (Figure 1b), (Jazrawi et al., 2013). Other compounds included ammonia, 2-butene, 2-methyl-1-propylene and 2-methylfuran. In contrast, the gas product formed from the HTL of PHB was considerably different, consisting of approximately equal amounts of carbon dioxide and propylene, particularly at the higher reaction temperature of 340 °C. Based on these results, a potential decomposition mechanism of PHB under hydrothermal conditions to equal amounts of carbon dioxide and propylene is proposed (see supporting information). Propylene is an important precursor for the polymer industry, and therefore the conversion of PHB-containing algae with associated gas separation, could represent a viable value-adding product stream. This, in turn, may help to subsidise the cost of the main oil product and make the overall process more cost effective.

3.2.3 Energy Recovery

An important consideration in evaluating the feasibility of HTL towards the conversion of biomass is the overall energy recovery (ER) into the desired reaction product. This can be calculated using the higher heating values of the product and feedstock (HHV_P and HHV_F) and the product yield (Y_P), using equation (2).

$$ER = \frac{HHV_P \times Y_P}{HHV_F} \quad \textbf{(2)}$$

The HHVs of the oil phases were calculated from the elemental composition using the Dulong formula (Figure 1c). The conversion of rapeseed oil resulted in very high energy recoveries to the oil phase of over 90 %, regardless of reaction temperature. For soy protein, the energy recovery increased with increasing reaction temperature, to a maximum value of 42 % at 360 °C, whereas both corn flour and PHB display only marginal energy recovery to the crude oil phase of less than 8 % for corn flour and less than 5 % for PHB. This suggests that HTL of

these compounds is not viable for the formation of a crude oil product. PHB does however produce a significant yield of propylene. Using the HHV of propylene from the literature (48.96 MJ kg^{-1}) and multiplying this value with the mass fraction of propylene in the gas phase, the energy recovery to the gas phase can be calculated. At temperatures above 340 °C, very high energy recoveries of over 64 % could be obtained. This suggests that HTL could represent an energy-efficient method to convert PHB, present in algal biomass, into propylene.

3.3 Effect of biochemical composition on HTL yields

3.3.1 Synergetic effect of biochemical compounds present in Spirulina

The previous section focused on the conversion of model compounds in an attempt to understand what contribution they could play in the HTL of whole microalgae. This has revealed some interesting differences in the product distributions and energy recoveries obtained from the different algal components, but the liquefaction behaviour of these components in combination is much more complicated. A number of researchers have attempted to correlate bio-oil yields to algae composition and found that overall yields are not simply a weighted average of the yields obtained from model compounds (Chen et al., 2009; Teri et al., 2014). Whilst reasonable correlations were observed between lipid content and bio-crude yield, much weaker correlations are obtained for protein and carbohydrate contents. In general, the recovered biocrude yields were higher than expected (Biller & Ross, 2011; Teri et al., 2014), and it was suggested that the decomposition products from proteins and carbohydrates – amino acids and sugars – could further react via Maillard type reactions to form nitrogen containing cyclic organic compounds such as pyridines and pyrroles. Maillard reactions are complex, and still not fully understood in this complex reaction environment, however nitrogen containing heterocycles are known to be formed through these reactions (Owuso-Apenten, 2004).

To verify these findings, the biochemical composition of the cyanobacteria *Spirulina* was used to calculate theoretical HTL conversion

yields (Y_T), and subtracted these from the actual yields obtained (Figure 2a).

$$\text{Theoretical Yield } (Y_T) = A_{CH} \times Y_{CH} + A_P \times Y_P + A_L \times Y_L \quad \textbf{(3)}$$

Where Y_T, denotes the theoretical yield obtained from the conversion of the algae, A_{CH}, A_P and A_L stand for the concentration of carbohydrates, protein and lipid in the algae, on a daf basis; and Y_{CH}, Y_P and Y_L denote the yields obtained from the HTL of carbohydrates, proteins and lipids (daf basis). Carbohydrate, protein and lipid yields were calculated from the conversion of model compounds, however due to the complexity of these calculations, the corresponding equations are shown in the supplementary information.

The results show a remarkable increase in actual biocrude yields and a similar reduction in solid yields, compared to the theoretical yields based on the conversion of model compounds, consistent with the literature findings. Gas yields are slightly increased at higher reaction temperatures, but the water residue yields don't appear to follow a clear trend, potentially due to competing reactions and the high level of uncertainty in determining these values.

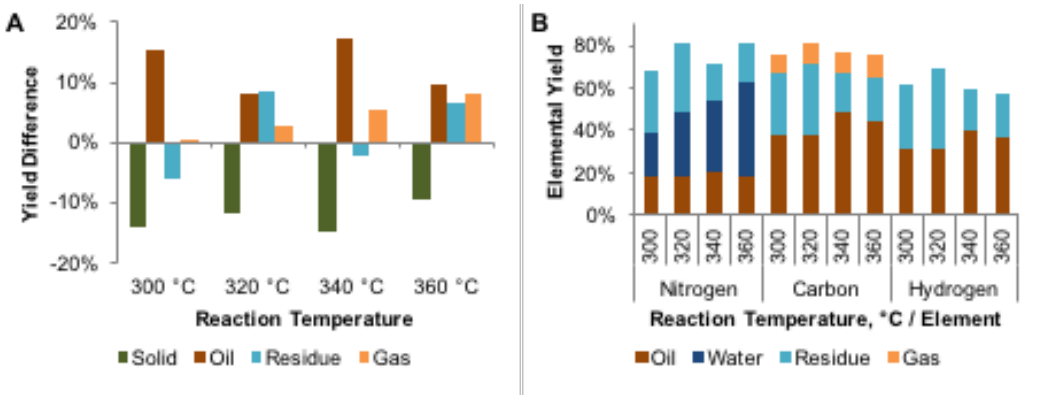

Figure 2: Results from the HTL of *Spirulina*; A) Difference between actual yields and theoretical yields, calculated based on yields from model compounds and composition of *Spirulina*; B) Elemental distribution to the different product phases

As neither the protein nor the lipid models produce notable amounts of solid, the reduction in solid production must be related to lower yields from the carbohydrate fraction present in the algae (20 wt%). This may be a result of catalytic activity from inorganic compounds present in the algal

ash phase, such as K, Mg and C. Potassium, in particular, could help to catalyse the decomposition of carbohydrates into lighter reaction products (Jazrawi et al., 2013). As the carbohydrate model, corn flour is virtually ash free (Table 1), the catalytic effect is not present in the conversion of the model compound on its own.

The increase in oil yields could be related to a simple shift in carbohydrate products from the solid to the biocrude phase, however this is unlikely as oil yields obtained from corn flour were very small, and most non-solid products appeared to partition into the water phase. Instead, the increase in oil yields could result from the reaction of protein and carbohydrate breakdown products, as previously suggested. In this case, the nitrogen distribution to the crude oil phase would be expected to increase in comparison with pure protein.

The elemental distribution was calculated from the elemental analysis for the products obtained from the HTL of *Spirulina* (Figure 2b). Both the carbon and hydrogen retention to the bio-oil are significantly higher than the nitrogen retention, with a visible increase as the temperature is increased from 320 to 340 °C. This demonstrates that HTL is effective in concentrating carbon and hydrogen towards the oil phase, increasing the carbon and hydrogen concentration from 46.3 % and 7.4 %, respectively, in the microalgae to a maximum of 71.6 % and 9.4 %, respectively, (at 340 °C) in the HTL oil product. The nitrogen retention from the HTL of *Spirulina* to the biocrude is approximately twice that of soy protein (21.0 % *vs.* 9.6 % at 340 °C), indicating that increased retention of the protein fraction in the presence of other biochemical products, such as carbohydrates, could indeed play a role in the increase in oil yields. Lastly, energy recoveries to the crude oil phase (not shown) range from 41 % to 49 %, with the highest value obtained at a reaction temperature of 340 °C. This is consistent with the highest oil yield of 36.9 % obtained at this temperature. Consequently this temperature was used for all further HTL reactions.

3.3.2 Liquefaction of Spirulina/PHB mixtures

So far, the results have provided further evidence on the occurrence of Maillard type reactions between amino acids and sugars to help increase oil yields, as indicated by an increased nitrogen content in the oil phase. However, the results do not provide any information on the interaction of PHB with other algal compounds, as *Spirulina* does not contain appreciable levels of these biopolymers.

To investigate this interaction, *Spirulina* was liquefied in the presence of varying levels of PHB (5 to 20 % (w/w)), and the mass balance results were compared to those of the pure substances (Figure 3a). The bright red lines represent the theoretical yields based on weighted averages obtained from the yields from the pure substances.

Although some differences can be observed in the actual and expected gas and water residue yields, the maximum differences of 5.8 % for the gas phase and 6.5 % for the water residue phase are much less than the differences obtained from the conversion of biochemical models and *Spirulina* (up to 16.4 %). More importantly, the deviation in the oil and solid yields is almost negligible, and given the high uncertainty in the gas and water residue yield measurements, based on the overall product distribution, it does not appear as if a significant interaction occurs between PHB and other biochemical compounds during the HTL process.

To further investigate any potential interactions between PHB and the biochemical compounds in *Spirulina*, the carbon dioxide and propylene yields were calculated from the sum of overall gas yields and gas composition (Figure 3b). Again, the theoretical yields, calculated on an additive basis from the pure compounds, are displayed as bright red markers. Most of the theoretical values are within the error of the actual gas yields, with the exception of the CO_2 yield for a 5 % PHB loading and the propylene yield at a 20 % loading. There is however a clear increase in propylene yield as the PHB content increases, with a yield of almost 3 % at a PHB loading of 20 %. Given the large uncertainty in gas yields at 0 and 100 %, upon which the theoretical values are based, it can be

concluded that the trend observed in this chart suggests that no interaction between PHB and the biochemical compounds present in *Spirulina* occurs during HTL.

3.4 Liquefaction of PHB containing microalgae

To verify the results from the PHB/*Spirulina* conversion studies, the *Synechocystis* and *Synechococcus/Anabaena* samples were converted under equivalent HTL conditions. All three cyanobacteria samples produced significantly higher solid yields than those obtained for *Spirulina*, with a maximum solid yield of 22.9 % recovered for the *Synechococcus/Anabaena* sample (Figure 4a). TGA analysis revealed that the solid product from the two *Synechococcus/Anabaena* samples contained an organic (combustible) content of 35.4 % and 35.9 %, whereas the solid produced from *Synechocystis* contained 89.7 % of combustibles. These values were consistent with elevated levels of carbon in the solid fraction (12.3 % for *Synechococcus/Anabaena*, 15.8 % for *Synechococcus/Anabaena*–N and 38.9 % for *Synechocystis*). These results suggest a significant partitioning of organic compounds into the solid phase, similar to the results obtained from the carbohydrate model, corn flour.

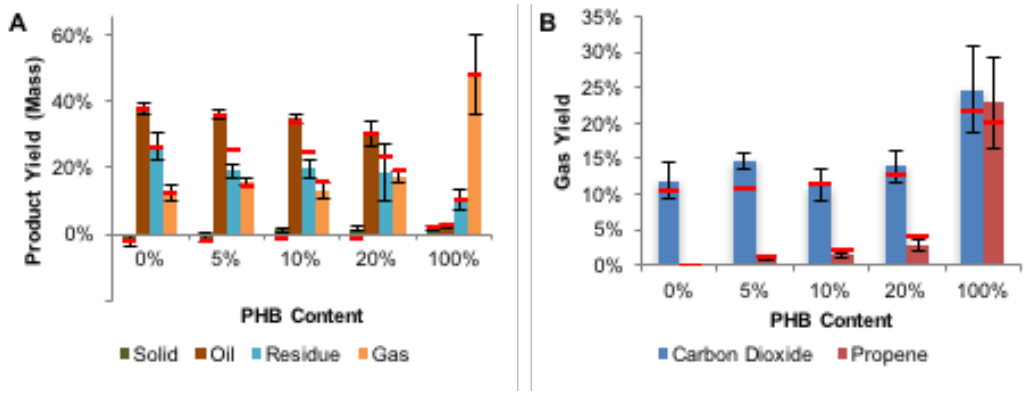

Figure 3: Results from the HTL of *Spirulina* / PHB mixtures; A) Product distribution; B) Absolute yields of major gas compounds. The red markers indicate theoretical yields, based on a weighted average of the yields obtained from the conversion of the pure substances.

The carbohydrate content of *Synechocystis* is approximately twice that of *Spirulina,* 40.5 % compared to 20.0 %. This is presumably due to the high solid yield formed from this algae, combined with its high carbon and

organic content. In contrast, the carbohydrate content of the *Synechococcus/Anabaena* samples were very similar to *Spirulina*, and despite this, the solid yield was increased significantly. Interestingly, the ash content of the mixed *Synechococcus/Anabaena* samples was approximately 3 to 4 times higher than for *Spirulina,* and for the conversion of *Spirulina* it was found that the catalytic properties of the ash might have helped to convert carbohydrates and reduce the solid content. However, it is possible that in this case increasing the ash content above a certain level has no further beneficial impact, but catalyses coking reactions, or binds some of the heavy oils, preventing them from being extracted with chloroform.

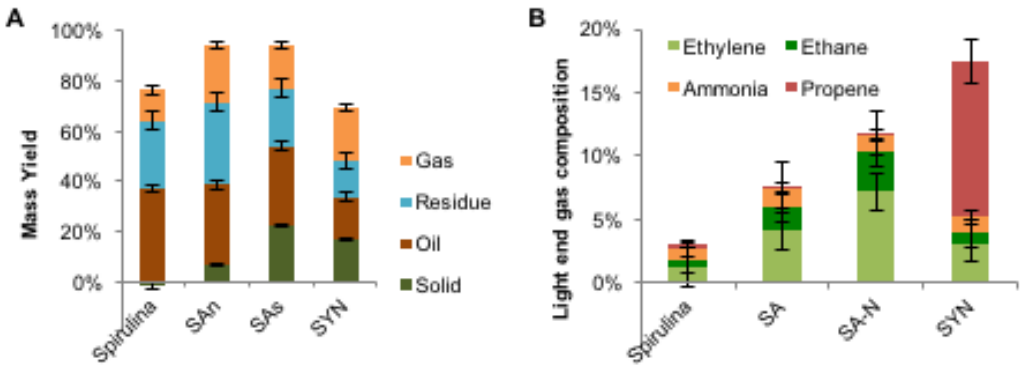

Figure 4: Results from the HTL of PHA-containing cyanobacteria; A) Product distribution; B) Gas composition of the VOC phase, where SA – *Synechococcus/Anabaena*; SA-N – *Synechococcus/Anabaena-N*; SYN – *Synechocystis*

Bio-oil yields from the three cyanobacteria samples were reduced compared to *Spirulina*. However, whilst oil yields from the two *Synechococcus/Anabaena* samples were still in a similar region (31.2 % and 32.0 % compared to 36.9 % from *Spirulina*), oil yields from *Synechocystis* were drastically reduced to only 16.6 %. All oils contained a similar carbon and hydrogen content, ranging from 69.8 % to 71.6 % and 8.6 % to 9.5 %, respectively, whereas the nitrogen content of the cyanobacteria-based oils (4.6 – 6.1 %) was noticeable lower than for *Spirulina* (7.1 %; data included in supplementary information).

The oil with the lowest nitrogen content of 4.6 % was obtained from the HTL of *Synechocystis*, which itself had the lowest N content of all converted cyanobacteria species (3.5 %, see Table 1). For the two

Synechococcus/Anabaena samples, the one grown under nitrogen depleted conditions, produced an oil with a noticeably lower nitrogen content than that grown under normal growth conditions. These results suggest that cyanobacteria grown under nitrogen-starved conditions could potentially produce higher quality HTL oils than protein producers such as *Spirulina*, albeit with reduced product yield.

Water residue yields from the two *Synechococcus/Anabaena* samples appeared similar to those obtained from *Spirulina*, but the yields from *Synechocystis* were almost 50 % lower. In contrast, the carbon content of the water phase residue was by far the highest for *Synechocystis* (68.4 %), compared to 40.3 % for *Spirulina*, and only 12.4 and 15.8 % for the two *Synechococcus/Anabaena* samples. Nitrogen and hydrogen concentrations were lowest in the residue from the *Synechococcus/Anabaena* samples, whereas *Synechocystis* produced the lowest concentration of ammonia, correlating to an ammonia yield of only 0.6 %, compared to 5.7 % for *Spirulina*. It is interesting to note that conversion of the *Synechococcus/Anabaena* samples results in a very high degree of mass balance closure (around 95%), whereas the mass balance closure for *Synechocystis* is low at only 70 %. This suggests the presence of high amounts of light organic compounds, soluble in the water phase, which may help explain the low water phase residue yield obtained from this species.

Gas yields from the alternative cyanobacteria were noticeable higher than for *Spirulina*, which is desirable for the production of volatile organic compounds. Compositional analysis shows that all selected cyanobacteria produce significantly higher concentrations of VOCs than *Spirulina* (Figure 4b). However, whilst *Synechocystis* favours the formation of propylene (12.1 %), the major VOC product from *Synechococcus/Anabaena* is ethylene with a contribution of 7.2 % for the nitrogen depleted sample. These findings are consistent with the PHA analysis, which detected a PHB content of 7.5 % in *Synechocystis*, but no PHB in either of the two *Synechococcus/Anabaena* samples.

The findings suggest that propylene is formed from PHB only. Based on gas yields, the overall propylene yield from *Synechocystis* can be calculated at 2.6 %, very similar to those obtained from the PHB/*Spirulina* mix for a 20 wt% PHB loading. The discrepancy between the measured PHB content (7.5 %), and the higher than expected propylene yield could have multiple causes, including differences in the catalytic effect of the ash present in *Spirulina* and *Synechocystis*, or differences in the polymeric composition and chain length between model PHB and PHB present within the algae. Therefore, PHB containing microalgae represent a viable feedstock for the production of a low nitrogen oil together with a valuable gas by-product.

4 Conclusion

The potential of using HTL for the conversion of cyanobacteria into a crude oil with reduced nitrogen content, and a high value gas by-product was demonstrated. In contrast to cross-reactions between protein and carbohydrate intermediates, which impact on product quality, no synergistic effects were detected when converting PHB in the presence of algal biomass.

Out of the three potential PHA producers, only *Synechocystis* sp. was found to accumulate significant levels of PHB. In agreement with the model compound experiments, the conversion of this species resulted in the formation of elevated amounts of propylene, a valuable precursor for the polymer industry.

5 References

Beacham, T.A., Macia, V.M., Rooks, P., White, D.A., Ali, S.T. 2015. Altered lipid accumulation in Nannochloropsis salina CCAP849/3 following EMS and UV induced mutagenesis. Biotech. Rep. 7, 87-94.

Bellou, S., Aggelis, G. 2012. Biochemical activities in Chlorella sp. and Nannochloropsis salina during lipid and sugar synthesis in a lab-scale open pond simulating reactor. J. Biotechnol. 164, 318-29.

Biller, P., Friedman, C., Ross, A.B. 2013. Hydrothermal microwave processing of microalgae as a pre-treatment and extraction technique for bio-fuels and bio-products. Bioresour. Technol. 136, 188-95.

Biller, P., Ross, A.B. 2011. Potential yields and properties of oil from the hydrothermal liquefaction of microalgae with different biochemical content. Bioresour. Technol. 102, 215-25.

Chen, W., Su, B., Xing, H., Yang, Y., Ren, Q. 2009. Solubilities of cholesterol and desmosterol in binary solvent mixtures of n-hexane+ethanol. Fluid Phase Equilibr. 287, 1-6.

Chen, W.T., Zhang, Y., Zhang, J., Yu, G., Schideman, L.C., Zhang, P., Minarick, M. 2014. Hydrothermal liquefaction of mixed-culture algal biomass from wastewater treatment system into bio-crude oil. Bioresour. Technol. 152, 130-9.

Chuck, C.J., Wagner, J.L., Jenkins, R.W. 2015. Biofuels from Microalgae. in: Chemical Processes for a Sustainable Future, (Eds.) T.M. Letcher, J.L. Scott, D.A. Patterson, Royal Society of Chemistry. Cambridge, pp. 425-442.

Drosg, B., Fritz, I., Gattermayr, F., Silvestrini, L. 2015. Photo-autotrophic Production of Poly(hydroxyalkanoates) in Cyanobacteria. Chem. Biochem. Eng. Q. 29, 145-156.

Faeth, J.L., Valdez, P.J., Savage, P.E. 2013. Fast Hydrothermal Liquefaction of Nannochloropsis sp. To Produce Biocrude. Energ. Fuel. 27, 1391-1398.

Hai, T., Hein, S., Steinbüchel, A., 2001. Multiple evidence for widespread and general occurrence of type-III PHA synthases in cyanobacteria and molecular characterization of the PHA synthases from two thermophilic cyanobacteria: Chlorogloeopsis fritschii PCC 6912 and Synechococcus sp. strain MA19. *Microbiology*, 147, 3047-3060.

Jazrawi, C., Biller, P., Ross, A.B., Montoya, A., Maschmeyer, T., Haynes, B.S. 2013. Pilot plant testing of continuous hydrothermal liquefaction of microalgae. Algal Research, 2, 268-277.

Karr, D.B., Waters, J.K., Emerich, D.W. 1983. ANALYSIS OF POLY-BETA-HYDROXYBUTYRATE IN RHIZOBIUM-JAPONICUM BACTEROIDS BY ION-EXCLUSION HIGH-PRESSURE LIQUID-CHROMATOGRAPHY AND UV DETECTION. Appl. Environ. Microb. 46, 1339-1344.

Li, H., Liu, Z., Zhang, Y., Li, B., Lu, H., Duan, N., Liu, M., Zhu, Z., Si, B. 2014. Conversion efficiency and oil quality of low-lipid high-protein and high-lipid low-protein microalgae via hydrothermal liquefaction. Bioresour. Technol. 154, 322-9.

López Barreiro, D., Prins, W., Ronsse, F., Brilman, W. 2013. Hydrothermal liquefaction (HTL) of microalgae for biofuel production: State of the art review and future prospects. Biomass Bioenerg. 53, 113-127.

Lopez Barreiro, D., Samori, C., Terranella, G., Hornung, U., Kruse, A., Prins, W. 2014. Assessing microalgae biorefinery routes for the production of biofuels via hydrothermal liquefaction. Bioresour. Technol. 174, 256-65.

Markou, G., Nerantzis, E. 2013. Microalgae for high-value compounds and biofuels production: a review with focus on cultivation under stress conditions. Biotechnol. Adv. 31, 1532-42.

Miyake, M., Erata, M., Asada, Y. 1996. A thermophilic cyanobacterium, Synechococcus sp. MA19, capable of accumulating poly-β-hydroxybutyrate. J. Ferment. Bioeng. 82, 512-514.

Nishioka, M., Nakai, K., Miyake, M., Asada, Y., Taya, M. 2001. Production of poly-β-hydroxybutyrate by thermophilic cyanobacterium, Synechococcus sp. MA19, under phosphate-limited conditions. Biotechnol. Lett. 23, 1095-1099.

Owuso-Apenten, R. 2004. Introduction to Food Chemistry. CRC Press.

Panda, B., Jain, P., Sharma, L., Mallick, N. 2006. Optimization of cultural and nutritional conditions for accumulation of poly-beta-hydroxybutyrate in Synechocystis sp. PCC 6803. Bioresour. Technol. 97, 1296-301.

Raikova, S., Smith-Baedorf, H., Bransgrove, R., Barlow, O., Santomauro, F., Wagner, J.L., Allen, M.J., Bryan, C.G., Sapsford, D., Chuck, C.J. 2016. Assessing hydrothermal liquefaction for the production of bio-oil and enhanced metal recovery from microalgae cultivated on acid mine drainage. Fuel Process. Technol. 142, 219-227.

Rao, P., Pattabiraman, T.N. 1989. Reevaluation of the phenol-sulfuric acid reaction for the estimation of hexoses and pentoses. Anal. Biochem. 181, 18-22.

Rippka, R., Deruelles, J., Waterbury, J.B., Herdman, M., Stanier, R.Y. 1979. GENERIC ASSIGNMENTS, STRAIN HISTORIES AND PROPERTIES OF PURE CULTURES OF CYANOBACTERIA. J. Gen. Microbiol. 111, 1-61.

Somleva, M.N., Peoples, O.P., Snell, K.D. 2013. PHA bioplastics, biochemicals, and energy from crops. Plant Biotechnol. J. 11, 233-52.

Srokol, Z., Bouche, A.G., van Estrik, A., Strik, R.C., Maschmeyer, T., Peters, J.A. 2004. Hydrothermal upgrading of biomass to biofuel; studies on some monosaccharide model compounds. Carbohydr. Res. 339, 1717-26.

Stanier, R.Y., Kunisawa, R., Mandel, M., Cohen-Bazire, G. 1971. Purification and properties of unicellular blue-green algae (order Chroococcales). Bacteriological Reviews, 35, 171-205.

Teri, G., Luo, L., Savage, P.E. 2014. Hydrothermal Treatment of Protein, Polysaccharide, and Lipids Alone and in Mixtures. Energ. Fuel. 28, 7501-7509.

Tian, C., Li, B., Liu, Z., Zhang, Y., Lu, H. 2014. Hydrothermal liquefaction for algal biorefinery: A critical review. Renew. Sust. Energ. Rev. 38, 933-950.

Torri, C., Garcia Alba, L., Samorì, C., Fabbri, D., Brilman, D.W.F. 2012. Hydrothermal Treatment (HTT) of Microalgae: Detailed Molecular Characterization of HTT Oil in View of HTT Mechanism Elucidation. Energ. Fuel. 26, 658-671.

Vardon, D.R., Sharma, B.K., Scott, J., Yu, G., Wang, Z., Schideman, L., Zhang, Y., Strathmann, T.J. 2011. Chemical properties of biocrude oil from the hydrothermal liquefaction of Spirulina algae, swine manure, and digested anaerobic sludge. Bioresour. Technol. 102, 8295-303.

Versteegh, G.J.M., Blokker, P. 2004. Resistant macromolecules of extant and fossil microalgae. Phycological Res. 52, 325-339.

Wu, G., Bao, T., Shen, Z., Wu, Q. 2002. Sodium Acetate Stimulates PHB Biosynthesis in Synechocystis sp. PCC 6803. Tsinghua Sci. Technol. 7, 435-438.

Wu, G.F., Wu, Q.Y., Shen, Z.Y. 2001. Accumulation of poly-β-hydroxybutyrate in cyanobacterium Synechocystis sp. PCC6803. Bioresour. Technol. 76, 85-90.

Yang, W., Li, X., Li, Z., Tong, C., Feng, L. 2015. Understanding low-lipid algae hydrothermal liquefaction characteristics and pathways through hydrothermal liquefaction of algal major components: Crude polysaccharides, crude proteins and their binary mixtures. Bioresour. Technol. 196, 99-108.

Yoo, G., Park, M.S., Yang, J.-W., Choi, M. 2015. Lipid content in microalgae determines the quality of biocrude and Energy Return On Investment of hydrothermal liquefaction. App. Energ. 156, 354-361.

3.3 SUPPLEMENTARY INFORMATION

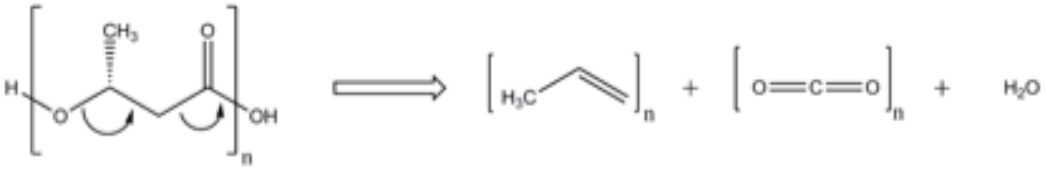

Scheme 3-1: PHB decomposition pathway to propene and carbon dioxide

1 Yields, ultimate analysis and energy density of oil product phase from HTL of model compounds

	300 °C	*320 °C*	*340 °C*	*360 °C*
Corn Flour	**2.4**	**3.3**	**4.0**	**3.6**
Elemental composition				
C	*64.33*	*67.16*	*69.41*	*68.32*
H	*4.96*	*8.54*	*8.83*	*7.49*
N	-	-	-	-
Energy Density, MJ/kg*	23.34	30.56	32.19	29.47
Soy Protein	**16.1**	**24.4**	**21.0**	**28.6**
Elemental composition				
C	*67.38*	*65.70*	*69.31*	*69.91*
H	*9.49*	*9.18*	*9.83*	*9.91*
N	*8.74*	*7.31*	*6.84*	*6.60*
Energy Density, MJ/kg*	33.75	32.09	35.05	35.35
Rapeseed Oil	**96.3**	**100.1**	**100.6**	**101.3**
Elemental composition				
C	*75.63*	*74.83*	*74.72*	*69.64*
H	*12.84*	*13.23*	*11.75*	*12.07*
N	-	-	-	-
Energy Density, MJ/kg*	36.26	37.24	35.03	36.03
PHB	**7.0**	**6.4**	**3.8**	**2.6**
Elemental composition				
C	*47.58*	*53.76*	*61.49*	*59.84*
H	*5.25*	*5.99*	*8.53*	*8.83*
N	-	-	-	-
Energy Density, MJ/kg*	15.17	19.53	27.55	27.18

2 Product analysis from HTL of PHA-rich cyanobacteria

	Spirulina	*SAn*	*SAs*	*SYN*
Solid	**-1.8**	**6.5**	**22.9**	**17.2**
Elemental composition				
C	*5.73*	*12.34*	*15.77*	*38.87*
H	*0.74*	*2.46*	*2.85*	*6.71*
N	*1.05*	*3.35*	*4.70*	*2.97*
TGA analysis				
Ash	nd	61.4	61.2	8.3
Moisture	nd	3.3	2.8	2.0
Organic	nd	35.4	35.9	89.7
Oil	**36.9**	**32.0**	**31.2**	**16.6**
Elemental composition				
C	*71.6*	*69.8*	*69.9*	*70.9*
H	*9.4*	*9.5*	*9.4*	*8.6*
N	*7.1*	*6.1*	*5.3*	*4.6*
Energy Density	31.89	34.47	34.22	33.41
Water Residue	**27.3**	**33.2**	**23.3**	**14.8**
Elemental composition				
C	*40.3*	*12.4*	*15.8*	*68.4*
H	*6.1*	*2.5*	*2.9*	*5.2*
N	*8.0*	*3.4*	*4.7*	*5.3*
Ammonia yield	5.7%	2.4%	1.7%	0.6%
Gas	**12.6**	**23.0**	**17.0**	**21.2**

3 Calculation of theoretical Spirulina yields

Theoretical yields from the conversion of *Spirulina* have been calculated based on its biochemical composition, and HTL yields from the conversion of the models representing the three main biochemical compounds found in the algae.

$$\text{Theoretical Yield } (Y_T) = A_{CH} \times Y_{CH} + A_P \times Y_P + A_L \times Y_L \quad \textbf{(1)}$$

Where Y_T, denotes the theoretical yield obtained from the conversion of the algae, A_{CH}, A_P and A_L stand for the concentration of carbohydrates, protein and lipid in the algae, on a daf basis; and Y_{CH}, Y_P and Y_L denote the yields obtained from the HTL of carbohydrates, proteins and lipids (daf basis).

Although the model compounds displayed high purity in their respective biochemical compound fraction, they still included impurities of other biochemical compounds. To correct for this, the yields obtained from the

conversion of soy protein, corn flour and rapeseed oil were corrected using a set of three simultaneous equations, as outlined below:

$$Y_{SP} = Y_P * SP_P + Y_{CH} * SP_{CH} + Y_L * SP_L \quad \textbf{(2)}$$

$$Y_{RO} = Y_P * RO_P + Y_{CH} * RO_{CH} + Y_L * RO_L \quad \textbf{(3)}$$

$$Y_{CF} = Y_P * CF_P + Y_{CH} * CF_{CH} + Y_L * CF_L \quad \textbf{(4)}$$

Where Y_{SP}, Y_{RO} and Y_{CF} denote the actual yields obtained from the conversion of soy protein, rapeseed oil and corn flour (daf basis), respectively; SP_P, RO_P and CF_P stand for the protein concentrations in the three feedstocks (daf basis), and similar denotations were used for the carbohydrate and lipid content.

Rearrange **(3)**:

$$Y_L = (Y_{RO} - Y_P * RO_P - Y_{CH} * RO_{CH}) / RO_L \quad \textbf{(5)}$$

Insert into **(1)** and **(4)**:

$$Y_{SP} = Y_P * SP_P + Y_{CH} * SP_{CH} + ((Y_{RO} - Y_P * RO_P - Y_{CH} * RO_{CH}) / RO_L) * SP_L \quad \textbf{(6)}$$

$$Y_{CF} = Y_P * CF_P + Y_{CH} * CF_{CH} + ((Y_{RO} - Y_P * RO_P - Y_{CH} * RO_{CH}) / RO_L) * CF_L \quad \textbf{(7)}$$

Rearrange **(6)** and **(7)** for Y_{CH}:

$$Y_{CH} = (Y_{SP} * RO_L - Y_P * SP_P * RO_L - Y_{RO} * SP_L + Y_P * RO_P * SP_L)/(SP_{CH} * RO_L - RO_{CH} * SP_L) \quad \textbf{(8)}$$

$$Y_{CH} = (Y_{CF} * RO_L - Y_P * CF_P * RO_L - Y_{RO} * CF_L + Y_P * RO_P * CF_L) / (CF_{CH} * RO_L - RO_{CH} * CF_L) \quad \textbf{(9)}$$

Combine **(8)** and **(9)**:

$$(Y_{CF} * RO_L - Y_P * CF_P * RO_L - Y_{RO} * CF_L + Y_P * RO_P * CF_L) / (CF_{CH} * RO_L - RO_{CH} * CF_L) =$$

$$(Y_{SP} * RO_L - Y_P * SP_P * RO_L - Y_{RO} * SP_L + Y_P * RO_P * SP_L)/(SP_{CH} * RO_L - RO_{CH} * SP_L) \quad \textbf{(10)}$$

Rearrange for Y_P:

$$\begin{aligned} Y_P = \quad & (Y_{CF} * RO_L * (SP_{CH} * RO_L - RO_{CH} * SP_L) \\ & + Y_{RO} * RO_L * (SP_L * CF_{CH} - CF_L * SP_{CH}) \\ & + Y_{SP} * RO_L * (RO_{CH} * CF_L - CF_{CH} * RO_L)) \\ & / (CF_P * RO_L * (SP_{CH} * RO_L - RO_{CH} * SP_L) \\ & + RO_P * RO_L * (SP_L * CF_{CH} - CF_L * SP_{CH}) \\ & + SP_P * RO_L * (RO_{CH} * CF_L - CF_{CH} * RO_L)) \end{aligned} \quad \textbf{(11)}$$

Now the corrected HTL yields for the protein, carbohydrate and lipid fractions in the algae can be calculated using equations 11, 9 and 5, respectively, and used in equation 1, to determine the theoretical yield for the HTL of the algae.

4 NMR analysis of vegetable oil conversion products

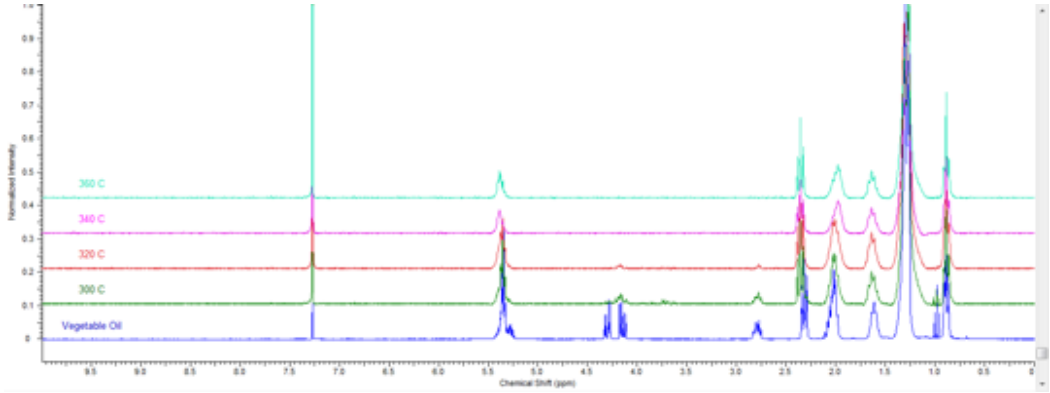

CHAPTER 4

HTL OF LIPID-EXTRACTED ALGAE

The work described in this chapter was conducted during a 3-month internship in the laboratory of Prof. Telma Franco, in the Faculdade de Engenharia Química, at the Unversidade Estadual de Campinas in São Paulo State, Brazil. The internship was funded through the Global Research Scholarship Scheme of the University of Bath.

4.1 INTRODUCTION

The previous chapter demonstrated the possibility of recovering propylene as a valuable by-product from the HTL of PHB-containing cyanobacteria. Propylene yields of up to 2.6 wt% were obtained from *Synechocystis* cf. *salina*, with a PHB content of 7.5 wt%, accounting for 12.1 wt% of the total gas phase. In addition, the conversion of this algae produced a bio-oil with a reduced nitrogen content of 4.6 wt%, compared to 7.1 wt% for the model algae *Spirulina*, although the overall oil yields were significantly reduced from 36.9 wt% for *Spirulina* to only 16.6 wt% for *Synechocystis*. One of the main challenges with using algae for the production of polyhydroxyalkanoates such as PHB is the high metabolic cost associated with the expression of these compounds, requiring carefully controlled, nutrient-limited growth-conditions.[174, 175] Consequently, pending major technological breakthroughs, the biomass production costs remain prohibitively high, preventing large-scale production.

An alternative algae by-product is the lipid fraction itself.[30] Similar to PHB, lipids act as an energy storage compound within the cell, and incur a higher metabolic cost than proteins or carbohydrates.[14] Despite this, a large amount of research has been dedicated to the production of lipid-rich algae, as a potential feedstock for bio-fuels. Compared to the bio-crude oil obtained from algal HTL, algal lipids represent a much higher quality feedstock, which can be readily converted into hydrotreated fuels, fully compatible with the existing transportation infrastructure.

Elevated lipid concentrations of 40 % and higher can be achieved quite easily,[13] but require longer cultivation times, resulting in enhanced production costs. A major limitation to lipid-derived algae fuels is the challenging requirement of producing algae with a lipid content of at least 40 %, at a biomass cost of no more than \$0.25 kg^{-1}.[4] However, by converting the remaining biomass components through HTL, it may be possible to produce a lower value bio-oil to help subsidise the production of higher quality lipids.[186] Furthermore, balancing bio-oil and lipid yields

against cultivation costs could allow the application of faster growing algae with a lower lipid content than required for a solely lipid-based process.

The lipid-extracted algae cake would be expected to consist predominantly of protein and carbohydrate derived material,[186] which in the last chapter, based on the model compounds soy protein and corn flour, were found to produce relatively low maximum oil yields of 28.6 wt% and 4.0 wt%, respectively. A potential method for obtaining enhanced oil yields is the addition of organic solvents to the reaction medium, including ethanol,[63] acetone,[62] or ethylene glycol.[61] Whilst the liquefaction in a pure solvent may be undesirable, due to the high energy costs associated with complete biomass drying, liquefaction in water-ethanol mixtures was found to produce higher yields than reactions in either pure water or ethanol.[63, 64] However, for polar solvents, the subsequent recovery of the bio-oil and reaction solvent may be more challenging, compared to conventional HTL reactions, due to the high miscibility with the aqueous phase.

Liquefaction yields from the conversion of carbohydrates were also found to be positively influenced by the addition of the base catalyst sodium carbonate (Na_2CO_3),[36] whereas the noble metal catalysts Pd/C and Pt/C were found to produce significantly enhanced bio-oil yields with improved flow properties and a reduced nitrogen content.[34, 51] Despite this, due to their high cost, the application of noble metal catalysts for the large-scale HTL of algae is unlikely to represent an economically feasible solution. Consequently, research should focus on identifying alternative low-cost materials that can be added to the liquefaction medium instead.

In this chapter, the HTL of algae cake, recovered from a lipid-extracted algae hydrolysate solution, was investigated. The reactions were conducted both in pure water, and in the presence of varying concentrations of IPA, in an attempt to enhance the overall bio-oil yields. In addition, the effect of adding two iron furnace residues, ladle-furnace-residue (LFR) and electric-arc furnace slag (EAFS), obtained from ArcelorMittal's iron smelter in Piracicaba, SP, Brazil, on the product

distribution obtained from the conversion of the algae cake was evaluated. This work was part of a wider Petrobras-sponsored project, of developing heterotrophic systems for the production of high-quality oils and additional biorefinery products from microalgae. A blend of the microalgal biodiesel together with conventional road-diesel was successfully tested in July 2015.[187]

4.2 BIOMASS WORK-UP

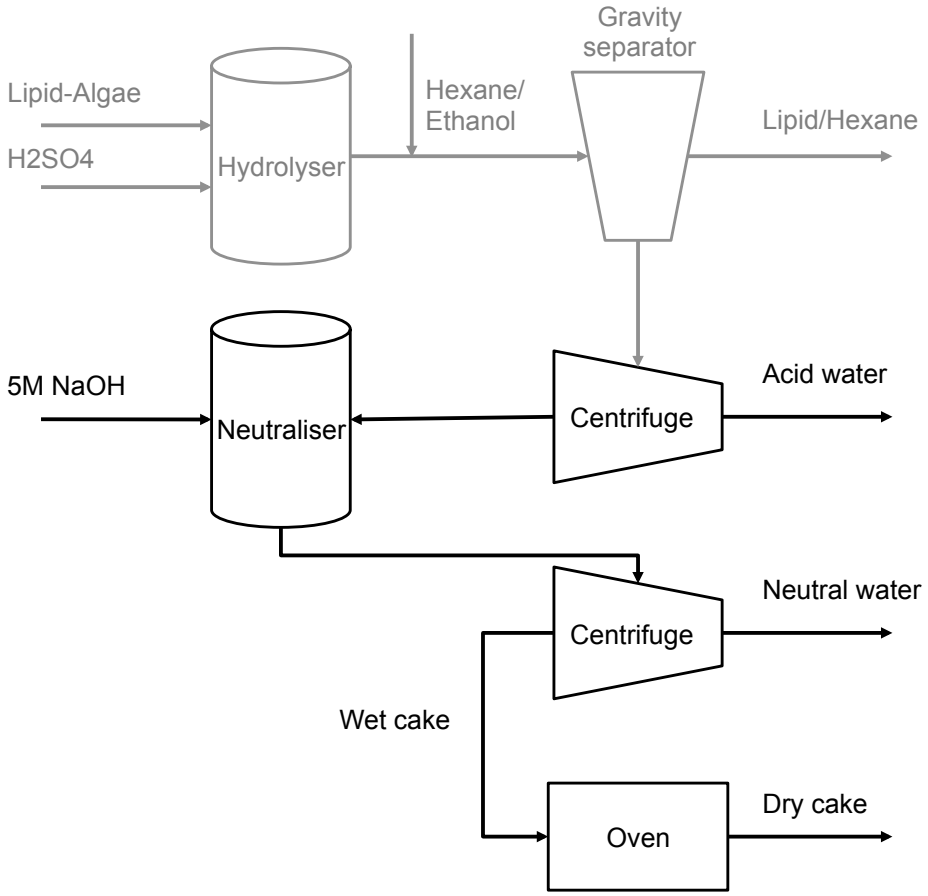

Figure 4-1: Schematic for algae cake work-up

The feedstock for the HTL reaction was prepared from a lipid-extracted hydrolysate of a *Chlorella* sp. strain, produced in the group of Prof. Telma Franco, in the Faculdade de Engenharia Química, at the Unversidade Estadual de Campinas in S.P., Brazil. The algae feed was cultivated under continuous, heterotrophic growth conditions, using glucose as the carbon source to obtain biomass concentration of 30 g L^{-1}. Following harvesting, the biomass was hydrolysed for 1 h at 120 °C in the presence

of 0.1 g H_2SO_4 for each gram of dry biomass. Subsequently, the hydrolysed biomass was extracted five times using a 1:4 mixture of ethanol and hexane (2.5 mL g^{-1} of dry algae), followed by gravity separation of the lipid-containing hexane phase.

Owing to the large amount of sulphuric acid employed for the hydrolysis reaction, the lipid-extracted hydrolysate was highly acidic (pH ~ 0.08). It also had a high water content of 81 % and contained a significant amount of residual hexane. Therefore significant work-up was required before the algae residue could be applied to the HTL reaction (Figure 4-1). First, the hydrolysate was centrifuged to remove any residual hexane and reduce its water content to 78 %. Subsequently it was neutralized using a 5M sodium hydroxide solution, followed by a second centrifugation step to recover a wet biomass cake, containing a residual water content of 72 %. Finally, this cake was dried at 70 °C and finely ground up prior to reactions.

Table 4-1: Composition of dried algae cake produced from lipid extracted algae hydrolysate

Elemental composition	Percentage, wt%
Carbon	34.1
Hydrogen	6.6
Nitrogen	3.5
Sulphur	8.7
TGA analysis	
Residual moisture	2.1
Ash content	52.9

The dry algae cake contained a remarkably high ash content of 52.9 % (Table 4-1), which could be partially attributed to the high amounts of sulphuric acid and sodium hydroxide used in the lipid extraction and algae cake recovery process. Based on the quantity of sodium hydroxide required to neutralize the hydrolysate solution, sodium sulphate (Na_2SO_4) was estimated to account for 33.0 % of the total algae cake weight, or 62.4 % of its ash and 85.6 % of its sulphur content. Even though this salt

is highly water-soluble, it was precipitated into the algae cake during the final oven drying stage. The remaining ash content could be attributed to micronutrients, including calcium chloride, magnesium sulphate and potassium phosphates, as well as oxidation products from the reaction of sulphuric acid with the algae itself, such as ammonium sulphate, and carbonates produced during the cultivation of the algae.

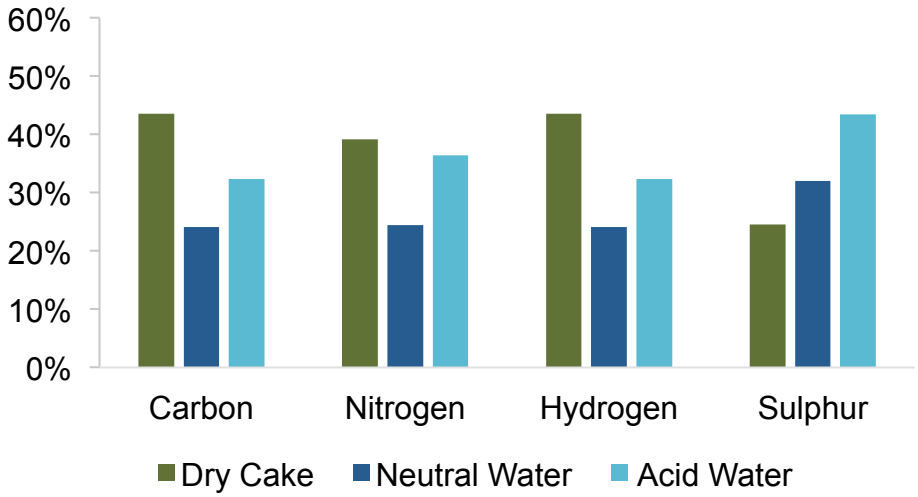

Figure 4-2: Elemental distribution of hydrolysed algae residue during work-up

Whilst the dewatering and neutralization of the hydrolysed algae residue was necessary to produce a suitable HTL feedstock, it also resulted in a significant loss of organic biomass components. Using the results from the total carbon and nitrogen analysis of the water phase, it was possible to calculate the elemental distribution to the dry cake and the two recovered water phases (Figure 4-2). This analysis shows that only 44 % of carbon and 39 % of nitrogen from the lipid-extracted hydrolysate were recovered into the dry cake, whereas the remainder was lost during the water recovery process. 11.6 % of the carbon content in the neutral water and 14.6 % of the carbon content in the acid water could be directly attributed to glucose, one of the main products from the hydrolysis of carbohydrates. However, the lower retention of nitrogen, compared to carbon, to the dry cake suggests that the recovery process resulted in preferential loss of the protein fraction.

The sulphur phase could be predominantly attributed to the sulphuric acid present in the hydrolysate. Even though a large amount of sulphur was

lost during the two centrifugation steps, just under a quarter (24.5 %) of the total sulphur was retained within the dry algae cake.

4.3 HTL IN THE PRESENCE OF IPA

Employing organic solvents such as ethanol, acetone and ethylene glycol was previously found to result in enhanced liquefaction yields, compared to HTL in pure water.[61] At the same time, the reaction in these solvents produced oils with increased nitrogen contents and enhanced solid production.[62]

In this section, the effect of adding IPA to the reaction medium was investigated. IPA was selected due to its ability to act as a hydrogen donor for transfer hydrogenation reactions,[188, 189] potentially helping to improve the quality of the resulting bio-oil. The reactions were conducted at 310 °C and the maximum IPA loading was limited to 50 vol%, for two reasons. Firstly, 50 vol% was seen as the maximum feasible concentration that could be employed industrially, without requiring excessive biomass drying. Secondly, the applied reaction temperature of 310 °C corresponds to the critical temperature of a 40 vol% IPA-water solution, as predicted using the Peng-Robinson equation of state within Aspen Hysys®. Operating at 50 vol% IPA therefore ensured that the maximum possible IPA concentration in the liquid phase was reached, without causing excessive evaporation of IPA, resulting in operation above the design pressure of the reactor.

4.3.1 EFFECT OF PRODUCT RECOVERY METHOD

One of the challenges of conducting HTL is the subsequent separation of the bio-oil and water phase. Even in the absence of solvents, around 20 – 30 % of the total organic product was found to partition into the water phase and could not be recovered using conventional gravity based separation methods.[53] Although these products could be extracted using non-polar solvents such as hexane or cyclohexane, there is currently no consensus on whether the increase in bio-oil yields justifies the additional costs of the solvent extraction procedure.[29]

However, when the HTL reaction is conducted in the presence of alcohols, such as IPA, the solvent would be expected to partition into the water phase and could reduce the fraction of organic products recovered in the bio-oil phase.

To investigate this further, the reaction products from the HTL of the algae cake in pure water and in the presence of 50 vol% IPA were recovered using two different methods. For the first method, the water/IPA phase was decanted and vacuum filtered, and the bio-oil was recovered by washing the reactor walls and retentate with chloroform, followed by vacuum evaporation at 40 °C. The same procedure was applied for the second recovery method, however, in this case, the chloroform phase was first recombined with the aqueous product phase, to extract the reaction solvent (IPA) and any water-soluble organic reaction products, prior to solvent evaporation.

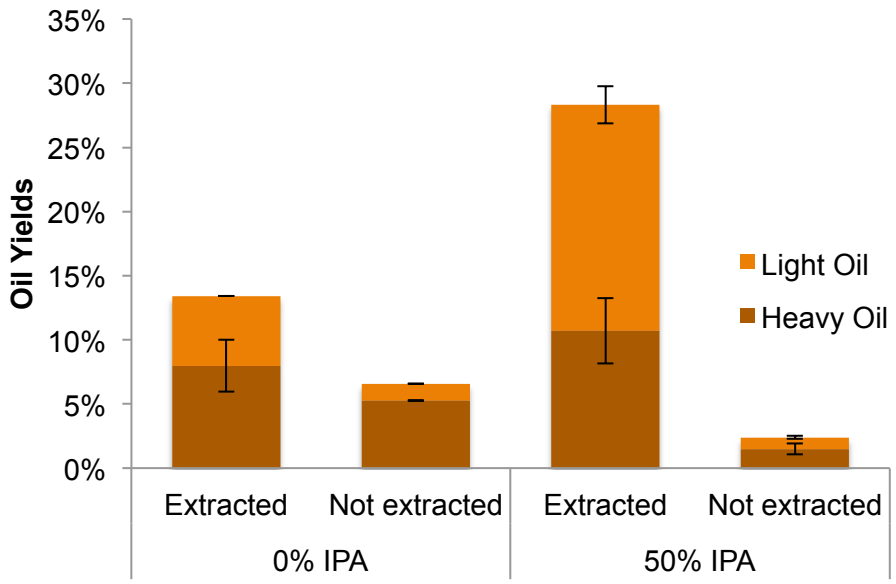

Figure 4-3: Effect of extracting the aqueous phase with chloroform

As expected, the bio-oil yields were significantly enhanced when the aqueous product phase was extracted with chloroform (Figure 4-3). For HTL in pure water, the bio-oil yields more than doubled from 6.6 wt% to 13.4 wt%, predominantly associated with an increase in the light, heptane-soluble oil fraction. An even bigger effect was observed for the reaction conducted in the presence of 50 vol% IPA. Without water

extraction, the total bio-oil yields amounted to only 2.4 wt%, but increased to 28.3 wt% after the aqueous phase was washed with chloroform, a more than 10-fold increase. These results show that HTL of the algae cake in the presence of IPA is only feasible if the water phase is subsequently extracted to recover IPA and organic reaction products.

Even in the absence of IPA, the difference in bio-oil recovery with and without chloroform washing of the water phase was significantly higher than the 20 % or 30 % reported in the literature.[53] This could be related to the complete absence of lipid-derived products from the algae cake used for this study, and a higher proportion of smaller, more polar organics, produced from the carbohydrate and protein fractions.

4.3.2 Effect of IPA concentration on product distribution

In the previous section, it was shown that the addition of IPA to the reaction medium produced significantly enhanced bio-oil yields. To test this effect further, the reaction was conducted over a range of IPA concentrations, and the effect on the overall product recovery was investigated (Figure 4-4a).

Both the light and heavy bio-oil products increased steadily as the IPA concentration was raised from 0 to 50 vol%. However, the increase in the light oil phase (5.4 wt% to 17.6 wt%) was much more pronounced than that of the heavy bio-oil (8.0 wt% to 10.7 wt%). At the same time, the solid yields remained almost constant (4.0 wt% to 4.7 wt%), whereas the water residue yields reduced significantly from 47.7 wt% to 30.8 wt%. Consequently, the overall product recovery remained between 63 wt% to 70 wt% (with the unaccounted fraction likely to be gas product), suggesting that IPA helped to convert or transfer some of the water-soluble products into the bio-oil phase, without being incorporated into the bio-oil itself. This is contrary to previous liquefaction experiments using alcohols, where the product recoveries exceeded the initial amount of biomass added.[61, 62] However, in these cases, the alcohol appeared to react with the lipid fraction to form esters, whereas the algae press cake

used in the present study contained only negligible amounts of residual lipids.

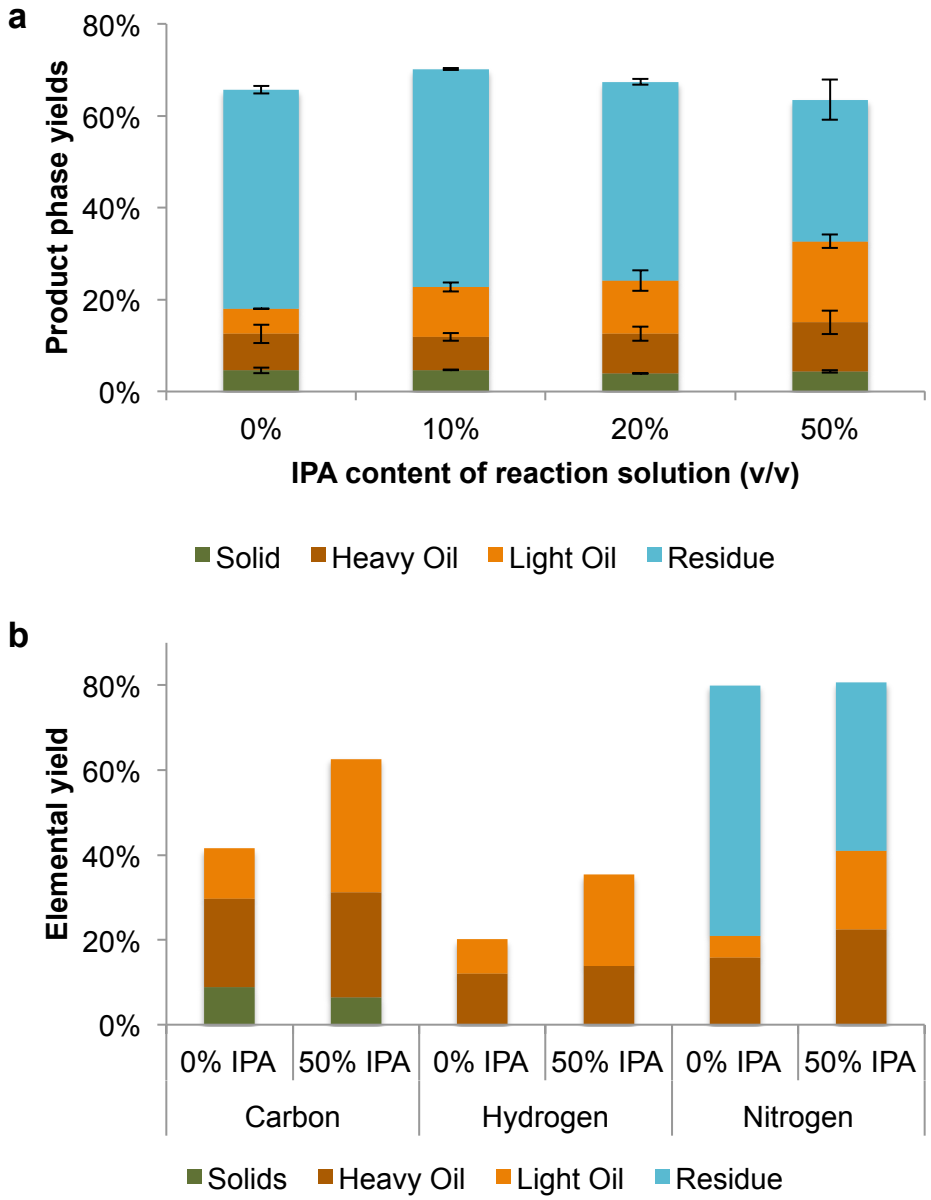

Figure 4-4: Effect of IPA concentration in liquefaction medium for reaction at 310 ºC on (a) overall product distribution, (b) elemental distribution to different product phases

Similar conclusions can be drawn from the elemental balance to the different product phases (Figure 4-4b). Whilst the carbon retention in the solid remained relatively constant, the carbon, hydrogen and nitrogen distribution to the light oil phase increased significantly. The increase in bio-oil nitrogen content matched the reduction of nitrogen that partitioned into the aqueous phase, as calculated from the total nitrogen analysis of

this phase, suggesting a direct transfer of nitrogen containing compounds from the aqueous to the bio-oil phase. (It should be noted that the presence of residual solvent in the water phase made it impossible to obtain meaningful results for the total carbon analysis of the water phase.)

When considering the ash content of the algae cake used for this study (53 wt%), it is remarkable that the solid fraction amounted to only 4 wt% to 5 wt% of the total reaction products. This confirms that a major portion of the ash consisted of highly water-soluble material (mostly sodium sulphate), which was recovered into the aqueous product phase instead. For the reaction in 50 vol% IPA, the combined solid and water phase residue yields amounted to 35 wt%, only just above the estimated sodium sulphate content in the biomass (33 wt%), but significantly less than the total algae cake ash content. Consequently, a significant fraction of the ash appears to have been lost into the gas phase, or volatile water-soluble products, potentially through the thermal decomposition of carbonates into carbon dioxide, or the release of ammonia from ammonium salts.

Given the high ash content of the algal press cake, the bio-oil yields of 28.3 wt% obtained for an IPA loading of 50 vol% correspond to a high recovery of the organic fraction of 60.2 wt%, significantly higher than the yields typically expected from the HTL of proteins (11 % - 18 %) or carbohydrates (6 % - 15 %).[36] However, as discussed already, the press cake contained only 43.6 wt% of the total carbon present in the lipid-extracted hydrolysate, as the remaining carbon was lost during the water removal stages.

In order to try to recover some of this additional carbon, the algae cake was liquefied in the ‘neutral water’ obtained from the second centrifugation step. Even though this resulted in a remarkable increase in product yields from 13.4 wt% to up to 42.8 wt%, the results were not reproducible, due to the formation of hard solid deposits within the reactor (Figure 4-5). These solids were probably formed from the shock precipitation of sodium sulphate present at high levels in the neutral

water, and consequently, the product recovery process should be improved, to reduce the quantity of sulphuric acid required to break up the biomass.

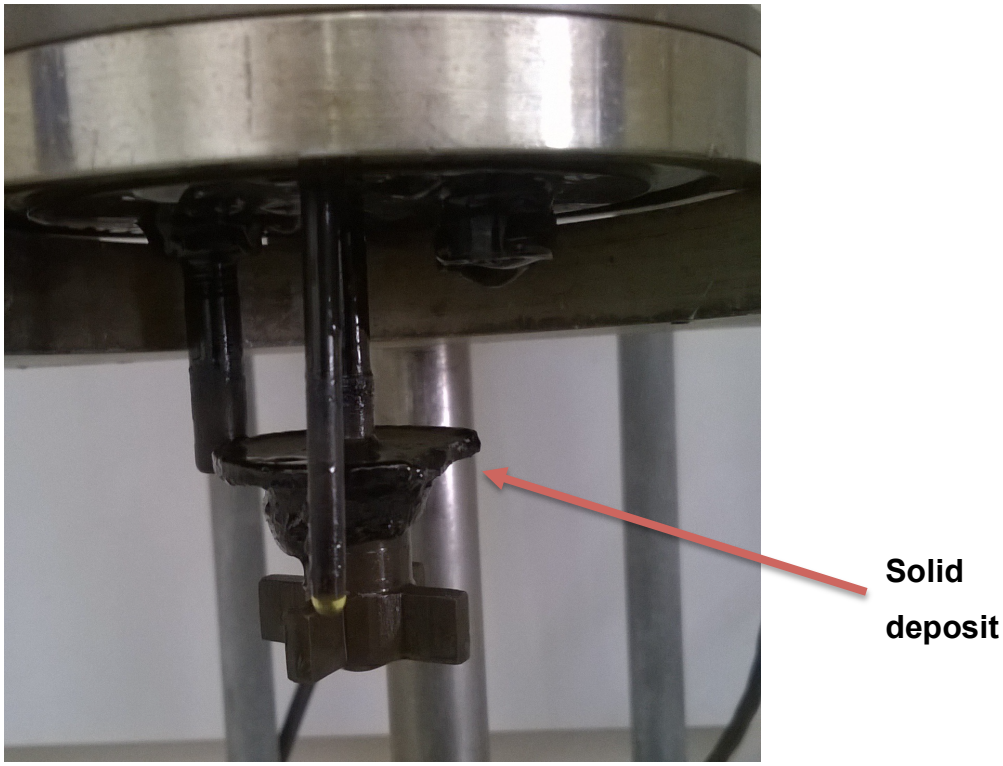

Figure 4-5: Formation of hard solid deposits within reactor for liquefaction in neutral water recovered during algae cake preparation

4.4 HTL IN THE PRESENCE OF FURNACE RESIDUES

In an attempt to increase the product recovery from the HTL of the algae cake and allow the use of lower reaction temperatures, the reaction was studied in the presence of two furnace waste materials, obtained from AcelorMittal's iron smelter in Piracicaba, SP, Brazil.

Consistent with the IPA solvent study above, the reactions were conducted at 310 °C, either in pure water or in the presence of 50 vol% IPA. Additional reactions were also carried out at a much milder temperature of 220 °C. As this temperature is below the critical temperature of pure IPA (235.1 °C), the reaction could be conducted in pure IPA, as well as 50 vol% IPA and pure water.

4.4.1 CATALYST CHARACTERIZATION

Ladle-furnace residue (LFR) refers to the fly ash produced by the combustion of coal, and consists predominantly of calcium and silicon oxides, with smaller amounts of carbon, magnesium and titanium (Figure 4-6a). Base catalysts, particularly sodium carbonate, have been previously shown to be beneficial in the liquefaction of carbohydrates,[36] and consequently the basic group II metal oxides in LFR could be beneficial to the HTL of the dry algae cake.

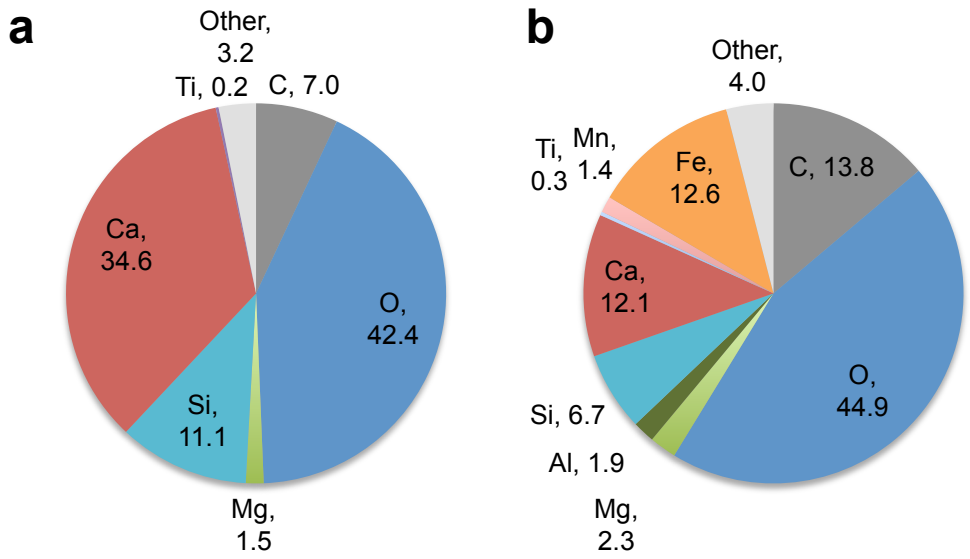

Figure 4-6: Elemental composition from SEM-EDX analysis of materials tested as HTL catalysts; (a) Ladle-furnace residue (LFR), (b) Electric-arc furnace slag (EAFS)

Electric-arc furnace slag (EAFS) refers to aggregates formed on top of molten steel. Like LFR it is made from calcium, silicon and magnesium oxides, but also contained a significant fraction of iron (12.6 wt%) and smaller amounts of aluminium (1.9 wt%), manganese (1.4 wt%) and titanium (0.3 wt%), which could contribute to its catalytic activity (Figure 4-6b).

4.4.2 CATALYST RECOVERY

An important consideration for using catalysts is the ease with which they can be recovered and recycled after the reaction. Consequently, industry

generally prefers heterogeneous over homogenous catalysts, as they do not require significant additional separation steps.

However, as already observed for the algae cake ash content, certain solid compounds can partition into the water phase during the HTL reaction. Not only does this result in a loss of material, but it can also lead to contamination of the water phase, making it more difficult to recycle for further algal growth, or discharge into the environment. It was therefore decided to track the recovery of the major elemental components from the two furnace waste products into the solid phase.

4.4.2.1 Ladle-furnace residue

Apart from oxygen and carbon, which were not tracked as they are also present in the biomass itself, LFR contained significant quantities of calcium (34.6 wt%), silicon (11.1 wt%) and magnesium (1.5 wt%).

During the reaction at 220 °C in pure water, substantial amounts of silicon and magnesium were lost, whereas calcium retention was close to 80 % (Figure 4-7a). Following the introduction of IPA to the reaction medium, the silicon and magnesium recovery increased significantly, with the calcium recovery appearing to drop slightly. The reverse trend was observed at 310 °C. At this temperature the recovery of silicon and magnesium in pure water was significantly enhanced, compared to the reaction at 220 °C, but dropped for the reaction conducted in the presence of IPA.

The data suggests that under HTL conditions, all three elements display high solubility in the water phase. Calcium oxide is known to react with water to form calcium hydroxide, whereas the solubility of magnesium oxides in water increases with increasing temperature. Amorphous silicon dioxide in turn was previously found to display a maximum water solubility of 1660 mg kg^{-1} at a temperature of 340 °C.[190] A potential explanation for the enhanced retention of calcium, compared to silicon and magnesium, is its higher concentration within LFR, resulting in complete saturation of the water phase. Consequently, the recovery of silicon and magnesium increased following the introduction of IPA, as the volume of water

decreased. However, it is clear that this correlation broke down at the higher reaction temperature of 310 °C and suggests that the catalyst underwent chemical changes to modify its solubility in the reaction medium. Calcium could have reacted with the sulphates in the press cake to form gypsum, whereas silicon and magnesium could have been reduced or adapted more stable configurations. The overall water loading and the presence of IPA could have influenced the equilibrium between these reactions, ultimately affecting the final product phase distribution.

In all cases, it should be noted that the data contains a large degree of uncertainty. Apart from the general limitations of using SEM-EDX, this may be related to a non-uniform composition of the solid reaction product as well as the difficulty of fully recovering solid precipitates from the reactor walls.

4.4.2.2 Electric-arc furnace slag

Compared to LFR, EAFS contained less calcium (12.1 wt%) and silicon (6.7 wt%), but a higher amount of magnesium (2.3 wt%). It also contained significant quantities of iron (12.6 wt%), aluminium (1.9 wt%), manganese (1.4 wt%) and titanium (0.3 wt%), and consequently the recovery of all seven elements was tracked following the HTL reaction (Figure 4-7b).

Despite its low concentration, within error, titanium appeared to have been fully recovered into the solid phase at all reaction conditions. The recovery of magnesium and silicon appeared to be increased, compared to LFR, whereas the calcium recovery remained about the same. Iron recovery at 220 °C did not follow a clear trend, reaching around 100 % for an IPA concentration of 50 vol%, but recoveries of only 55 % in pure water and 42 % in pure IPA. The manganese recovery followed a similar trend to iron, remaining around 60 % at all conditions, apart for the 50 vol% IPA loading at 220 °C, whereas the aluminium recovery remained consistently above 80 %. The low recovery of iron and manganese for the reaction in pure IPA is surprising, as only three product phases (solid, oil and gas) were collected from the reactor. A

potential explanation could be the formation of deposits on the reactor walls, which could not be easily recovered after the reaction.

Consistent with the results for LFR, the calculated elemental recoveries showed a high degree of experimental uncertainty. Whilst EAFS appeared to display a higher overall stability than LFR, the reaction still caused a significant portion of magnesium, silicon, iron and manganese to partition into the water phase. Particularly the dissolution of manganese to the water phase could be problematic, due to its known neurotoxicity at elevated groundwater concentrations.[191]

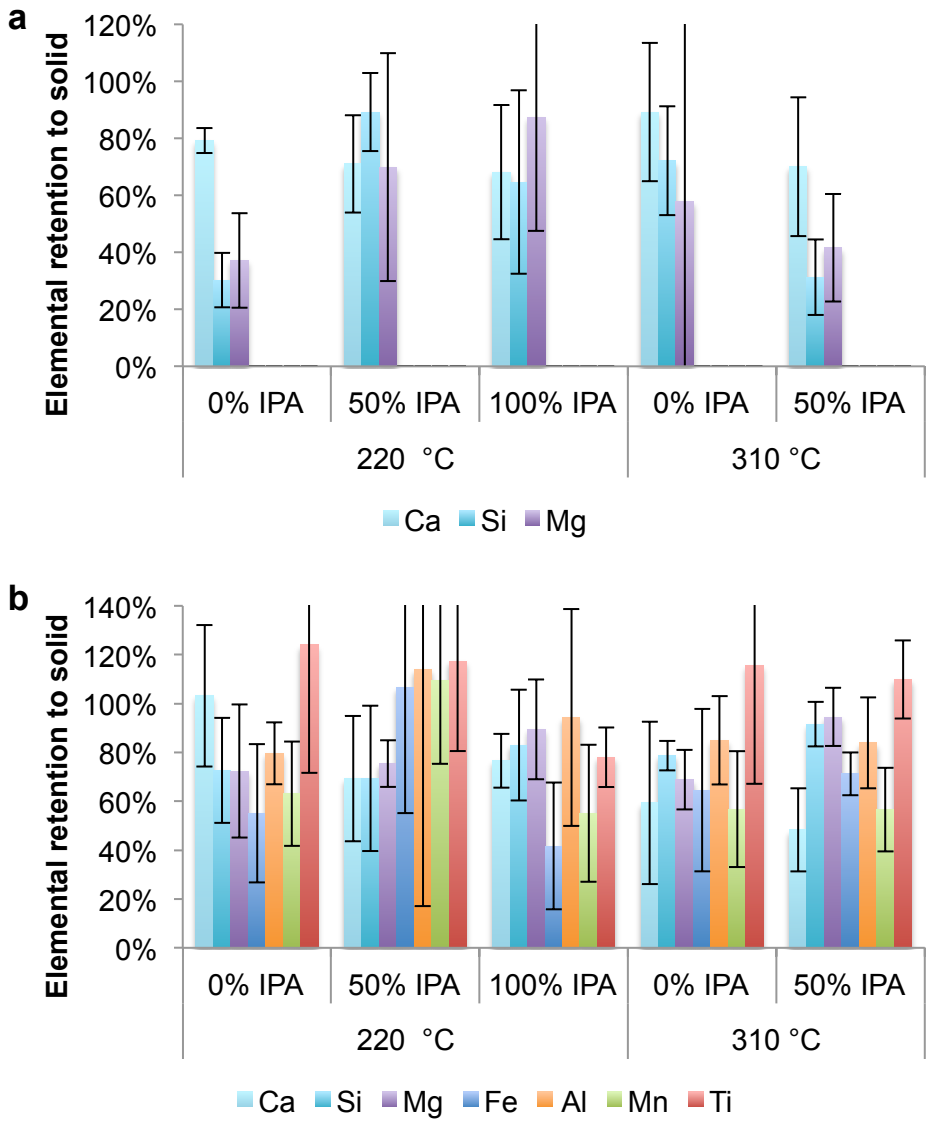

Figure 4-7: Elemental retention of catalyst material in the solid phase, calculated from SEM-EDX analysis, following HTL reactions; (a) Ladle-furnace residue (LFR), (b) Electric-arc furnace slag (EAFS)

4.4.3 PRODUCT DISTRIBUTION

Compared to the water-only reactions, at 220 °C, the addition of 50 vol% IPA to the reaction medium resulted in a significant increase in the bio-oil yields obtained from both the catalytic and the blank reactions (Figure 4-8a). Solid yields remained relatively constant, whereas the water phase residue yields experienced a significant drop, together with a reduction in the overall mass balance closure, indicating enhanced gas formation.

Conducting the reactions in pure IPA resulted in only a small further increase in bio-oil yields, compared to the reactions in 50 vol% IPA. No water phase was present for these reactions, and consequently no water phase residue was recovered. In contrast, the solid yields increased significantly from less than 20 wt% at an IPA loading of 50 vol% to up to 45.7 wt% for the reaction catalysed with LFR. This large increase can be attributed to the high quantity of water-soluble ash present in the algae cake. For reactions conducted in water, these salts dissolved and were subsequently removed together with the aqueous phase (and precipitated as water phase residue), but in the absence of water, the salts remained part of the solid product fraction. Even so, the maximum solid recovery of 45.7 wt% remained below the total ash content of the algae cake (52.9 wt%), suggesting that during the reaction, some of the inorganic press cake components were either dissolved into the IPA phase, or decomposed into gas phase products.

For the reactions at 220 °C, the presence of LFR and EAFS did not appear to have a positive effect on the product distributions obtained from the HTL of the algae cake. In pure water, the overall bio-oil yields were significantly lower for the reactions involving the two catalysts (6.0 wt% for LFR and 5.7 wt% for EAFS), compared to a yield of 8.4 wt% for the non-catalytic reaction. Following the introduction of IPA, the difference became less pronounced, but maximum overall oil yields of 14.5 wt% at an IPA loading of 50 vol% and 18.8 wt% in pure IPA were still obtained for the non-catalytic reactions. However, compared to the blank run,

EAFS appeared to slightly favour the formation of light, hexane-soluble oil.

In contrast, the solid yields obtained in the presence of EAFS were comparable to the non-catalytic reaction at all three IPA loadings, whereas the yields obtained with LFR were significantly enhanced for the reactions conducted in the presence of IPA. Even though the solid yield enhancement appeared to be less significant in pure water, it should be noted that at this condition, a significant amount of catalyst was lost to the water phase, potentially counter-acting the effect of increased solid formation.

At 310 °C the difference between the blank and catalytic runs was much more noticeable than at 220 °C (Figure 4-8b). Both catalysts resulted in a significant reduction in bio-oil yields, and a large increase in solid yields, particularly in the presence of 50 vol% IPA. The water residue yields were approximately equal in pure water, but significantly reduced from 47.7 wt% to 30.8 wt% in 50 vol% IPA for the non-catalytic run and remained unchanged between 41 wt% to 49 wt% for the catalytic reactions. This suggests that the presence of IPA helped to transfer organics from the water-phase into the bio-oil, whereas the catalysts increased the formation of solids, potentially through enhanced coke or char formation on the catalyst surface.

Previous work has shown that the presence of inorganic salts, including potassium carbonate and calcium acetate, can enhance secondary char formation during the pyrolysis of lignocellulosic biomass.[192, 193] The presence of these metals appeared to reduce the pyrolysis temperature of the biomass, as well as influencing the relative rates of polymerization and cracking reactions of intermediate decomposition products to favour either char or gas formation.[194] Whilst pyrolysis reactions are mostly limited to the solid and gas phase, secondary HTL reactions proceed within the aqueous phase. Consequently, higher salt concentrations may be required to have a similar effect, resulting in higher char yields in the presence of calcium-rich LFR, compared to the more stable EAFS.

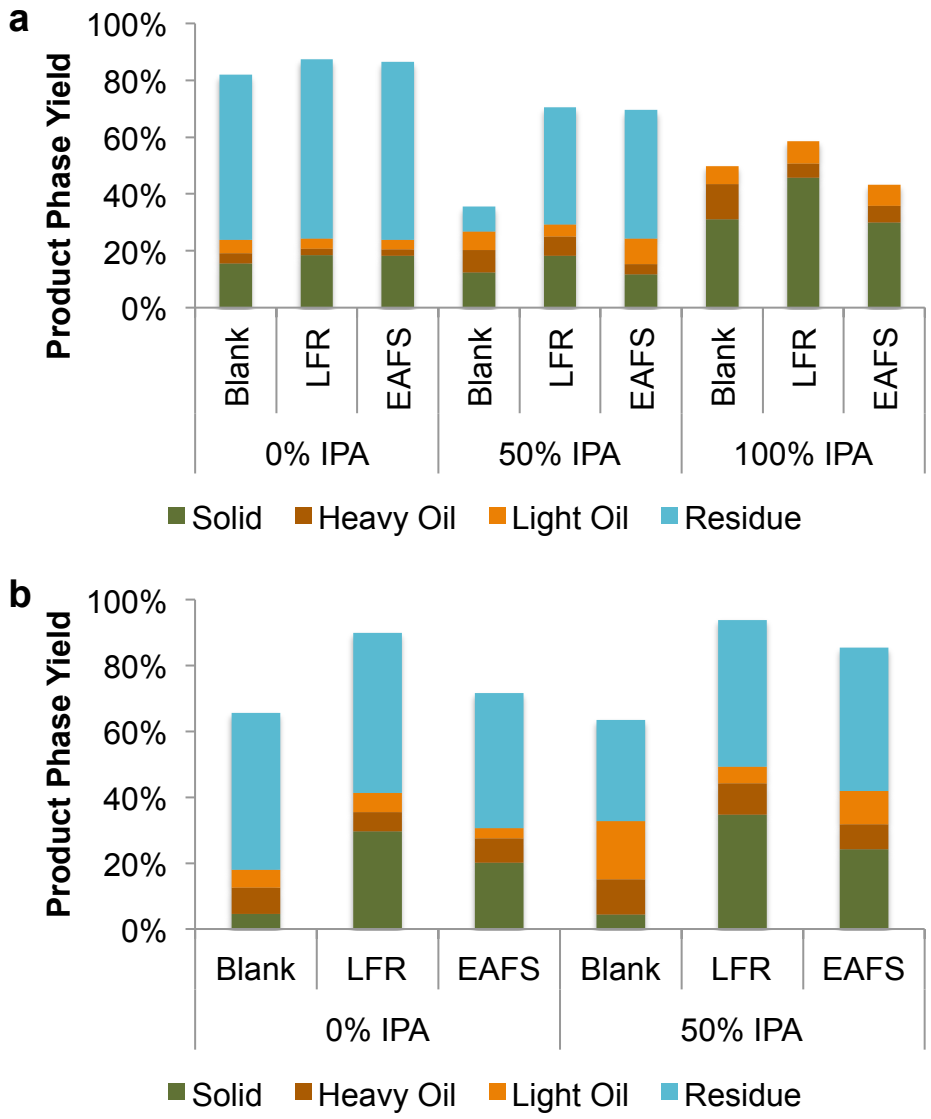

Figure 4-8: Effect of using the furnace waste materials ladle-furnace residue (LFR) and electric-arc furnace slag (EAFS) during the liquefaction of algae cake in the presence of varying concentrations of IPA; (a) reaction at 220 °C, (b) reaction at 310 °C

Comparing the results obtained for the non-catalytic reactions shows that the overall bio-oil yields obtained at 220 °C in the presence of 50 vol% IPA (14.5 wt%) and pure IPA (18.8 wt%) were higher than the bio-oil yields obtained at 310 °C and in pure water (13.4 wt%). The same trends were observed for the bio-oil yields obtained from the catalytic reactions, however it should be noted that the reactions at 310 °C, in 50 vol% IPA, always yielded the highest oil yields of all conditions studied. Solid yields, in turn, were lower for both non-catalytic reactions at 310 °C, than for any

of the reactions at 220 °C, but the opposite trend was observed for the reactions involving LFR and EAFS.

4.4.4 ELEMENTAL RECOVERY

To study the effect of reaction temperature, IPA content and the presence of the catalysts in more detail, the distribution of carbon, hydrogen and nitrogen to the oil and solid phases was calculated for the reactions in pure IPA at 220 °C and the two reaction conditions at 310 °C, in pure water and with a 50 vol% IPA loading (Figure 4-9).

Consistent with the higher oil yields obtained at 220 °C in pure IPA, compared to the reaction at 310 °C in pure water, the carbon and hydrogen recoveries to the oil phase for the non-catalytic reactions were slightly increased from 32.8 % to 34.9 % and 20.2 % to 29.5 %, respectively. At the same time, the nitrogen recovery was significantly elevated from 21.0 % to 35.6 %, resulting in an overall increase in the nitrogen content of the bio-oil from 4.7 wt% to 6.6 wt%. Similarly, the contribution of the unaccounted elemental fraction (predominantly oxygen) to the overall oil yield increased from 13.5 wt% to 18.8 wt%.

The addition of 50 vol% IPA to the reaction medium at 310 °C resulted in a large increase in the total carbon and hydrogen recovery to the bio-oil, and was comparable to the simultaneous increase in nitrogen recovery, resulting in similar overall nitrogen contents in the oil of 4.7 wt% for the reaction in pure water and 4.8 % in the presence of IPA. Despite this, the increased retention of carbon, hydrogen and nitrogen could not account for the entire increase in oil yields, resulting in an increase in the unaccounted elemental fraction from 13.5 wt% to 19.0 wt%. The H/C mass ratio only increased marginally from 0.118 to 0.121, suggesting limited transfer of hydrogen from IPA to the bio-oil. This is not surprising, as this reaction generally requires a good hydrogenation catalyst, such as RANEY® Nickel.[188] Carbon recoveries to the solid phase were significantly higher at the lower reaction temperature (43.3 %) than at 310 °C (8.8 % in pure water and 6.4 % in 50 vol% IPA), consistent with

the differences in solid yields and the absence of a water phase residue for the reaction in pure IPA.

Slightly different trends were obtained for the reactions over the two catalysts. Whilst the highest carbon and nitrogen recoveries were still obtained at 310 °C and in the presence of IPA, the hydrogen recovery was reduced compared to the reaction at 220 °C, and the nitrogen content in the bio-oil was higher for the reaction in pure water. The carbon recovery to the solid phase at 310 °C was also decreased in the presence of 50 vol% IPA, contrary to the simultaneous increase in solid yields. This suggests that the increase in solid yield can be mostly attributed to reduced dissolution of inorganic material from the algae cake and the catalysts, whilst IPA helped the recovery of organic carbon.

These findings show that the addition of IPA to the liquefaction medium can result in a significant enhancement of liquefaction yields, potentially allowing the reaction to proceed at much milder conditions compared to the pure water-phase reaction. However, the bio-oil quality obtained at 220 °C was also reduced, as indicated by an increased oxygen and nitrogen content. This was probably the result of incorporating lighter, water-soluble organics into the bio-oil, which contained high concentrations of oxygen and nitrogen. Furthermore, the reaction in pure IPA is unlikely to be feasible for industrial scale production, as it requires highly energy-intensive drying steps to obtain the fully dried biomass. In contrast, liquefaction in the presence of 50 vol% IPA at 310 °C offered a good compromise between enhanced oil yields and reduced biomass drying. Whilst it caused a reduction in the carbon and nitrogen content in the bio-oil, due to the increased incorporation of oxygen, it only had a limited impact on the nitrogen content from the non-catalytic reaction, and even reduced the nitrogen content for reaction with the two furnace residue materials.

Neither of the two catalysts employed for this study resulted in an increase in bio-oil yields. LFR in particular caused an increase in solid yields and decreased the bio-oil yields without having any obvious beneficial impact on bio-oil composition. It was previously hoped that the

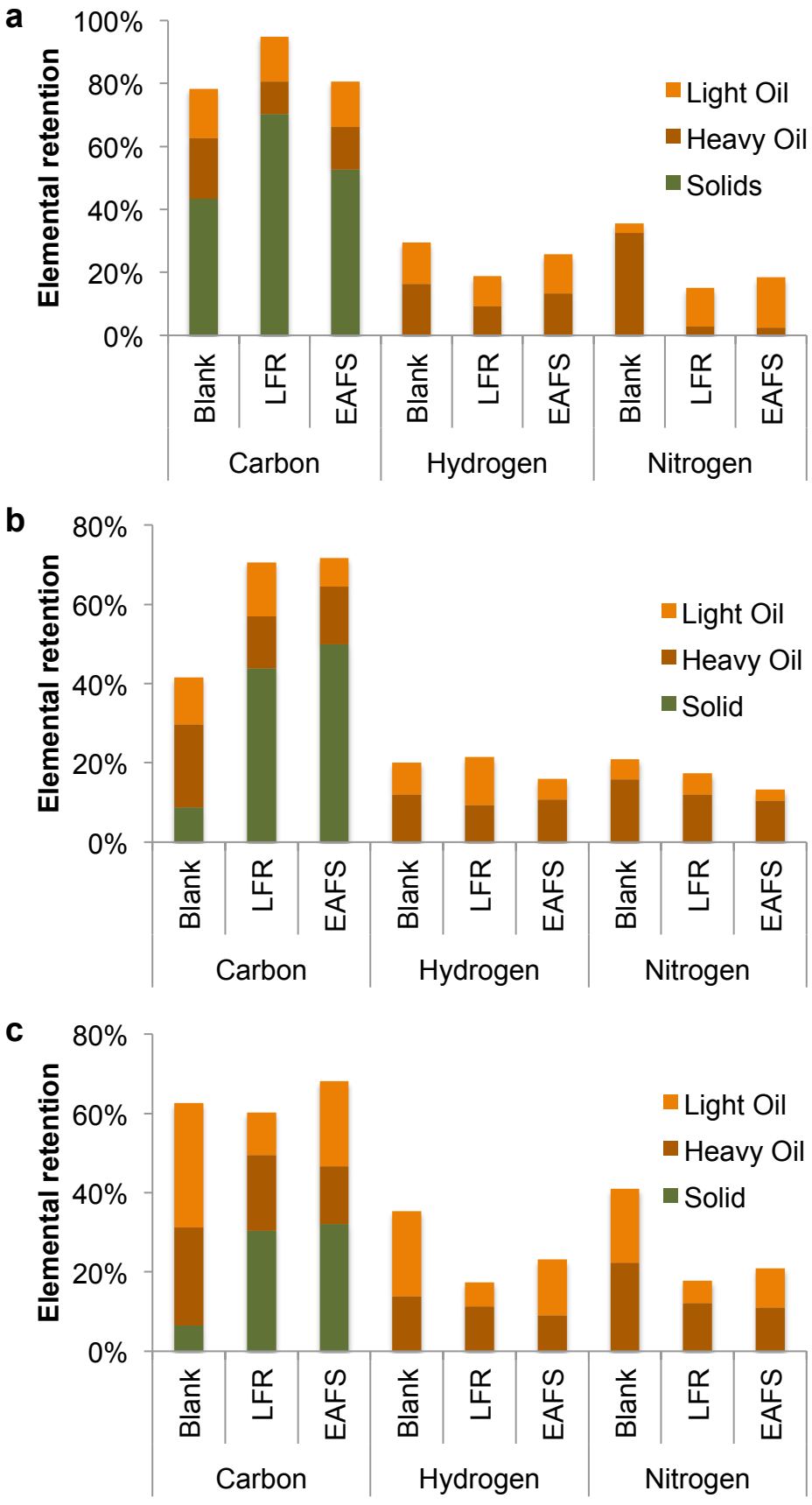

Figure 4-9: Effect of catalyst on elemental distribution to the bio-oil phase; (a) 220° C, 100 vol% IPA, (b) 310° C, 0 vol% IPA, (c) 310° C, 50 vol% IPA

basic nature of the catalysts would help the conversion of carbohydrates into bio-oil products. However, it is possible that the high ash content of the microalgae cake itself (53 wt%) provided sufficient quantities of base catalyst, and therefore the presence of LFR had no further beneficial impact. EAFS also reduced bio-oil yields and increased solid content, but had a beneficial impact on the carbon and hydrogen contents of the bio-oils obtained by the reaction, related to a reduced oxygen concentration. This suggests that the iron catalysed the deoxygenation reaction, however as iron only accounted for a small fraction of the overall catalyst material (12.6 wt%), the beneficial impact was out-weighed by the reduction in bio-oil yields.

4.4.5 CONCLUSIONS

In this chapter, the conversion of algal cake, recovered from a lipid-extracted hydrolysate, in the presence of IPA and two furnace waste materials, was investigated.

Prior to the reaction, the hydrolysate required a significant amount of pre-treatment, to neutralize the acid used for the hydrolysis reaction, and reduce the concentration of sodium sulphate. This process resulted in a loss of 56 % of the residual carbon and 61 % of the nitrogen, whilst producing an algae cake with a remarkably high ash content of over 50 wt%, owing to the high concentration of residual sodium sulphate. Although the liquefaction study attempted to recycle the carbon lost within the neutral wash water, this reaction was found to form hard, solid deposits, which hindered the recovery of the reaction products, and rendered this approach unsuitable for industrial application. Based on these findings, the harsh treatment conditions employed for the lipid-extraction process appear incompatible with the efficient recovery of residual biomass for the HTL reaction, and should be adapted accordingly. For example, by applying higher hydrolysis temperatures, it might be possible to employ lower concentrations of acid to form a lipid-rich solid-residue, which could be separated from the hydrolysate solution and solvent extracted. The remaining solid phase could then be

recombined with the hydrolysate solution for further HTL at a higher temperature. Alternatively, techniques such as steam explosion could be explored, although they may not prove energetically favourable.

The addition of IPA loadings of up to 50 vol% to the reaction medium resulted in a significant increase in overall bio-oil yields, owing to the transfer of light organic products from the aqueous to the oil phase. However, this approach was only feasible when extracting the water phase with a non-polar solvent, due to the high miscibility of IPA with this phase. Even in the absence of IPA, oil yields more than doubled after extracting the water phase with chloroform, owing to the large number of protein and carbohydrate derived reaction products.

Reactions conducted in pure IPA allowed the application of much lower reaction temperatures of 220 °C to obtain comparable bio-oil yields and carbon and hydrogen recoveries to reactions conducted in pure water and at 310 °C, but produced oils with significantly increased nitrogen contents and enhanced solid product formation. In contrast, the addition of 50 vol% IPA to the reaction medium at 310 °C, increased the overall bio-oil yields from 13.4 wt% to 28.3 wt%, corresponding to an increase in carbon recovery from 32.8 % to 56.2 %. At the same time, the nitrogen content of the oil remained approximately constant at around 4.7 % to 4.8 %, although the carbon and hydrogen contents decreased, due to increased incorporation of oxygen. The hydrogen to carbon ratio remained approximately constant, indicating that IPA did not act as a hydrogen donor in this reaction.

Adding the two furnace waste residues LFR and EAFS to the reaction medium had no beneficial impacts on bio-oil yields. Instead, the presence of these catalysts, particularly LFR, resulted in significantly increased solid yields, correlated to increased carbon retention, potentially due to the formation of char and coke over the catalyst surface. Calcium salts, in particular, were previously found to enhance char formation during the pyrolysis of lignocellulosic biomass. At the same time, the liquefaction reaction resulted in significant leaching of calcium, silicon, magnesium,

iron and manganese to the water phase. The loss of manganese, in particular, could be a major problem due to its known neurotoxic effect. Nevertheless, the presence of EAFS had a positive effect on the carbon, hydrogen and nitrogen contents of the bio-oils produced in 50 vol% IPA, suggesting that it could have a low activity towards deoxygenation and denitrogenation reactions, most likely catalysed by its iron content of 12.6 wt%. Future work could therefore explore the use of more stable, iron-based catalysts, to obtain more favourable bio-oil compositions.

CHAPTER 5

CONTINUOUS HTL OF ALGAE USED FOR WASTEWATER REMEDIATION

Part of this work was orally presented at the RRB-12 Renewable Resources and Biorefineries Conference in Ghent (30th May to 1st June 2016), and in the form of a poster at the ChemEngDay UK 2016 in Bath (31st March/1st April 2016).

5.1 INTRODUCTION

The previous two chapters investigated bio-oil production from the HTL of microalgae combined with the recovery of higher value by-products. In Chapter 3 it was shown that the HTL of PHB-containing algae resulted in the formation of gaseous propylene, in addition to the bio-oil phase, whereas Chapter 4 converted algae residue following the extraction of higher value lipids. These by-products have the potential to subsidise the overall fuel production costs from the HTL of microalgae, however, these benefits may be outweighed by the increased algae cultivation costs required to express these by-products in the first place.

In addition, all reactions described in the previous two chapters were conducted in batch reactors. Whilst these batch systems are a good way to evaluate and compare different feedstocks and reaction conditions, they are not directly applicable to large-scale industrial processing, which heavily relies on continuous flow processes with much higher volumetric productivities. Furthermore, batch systems are unable to provide the same level of control as continuous systems and struggle to combine high heating rates, which have been shown to be beneficial for higher bio-oil yields,[47] with extended reaction times, required to achieve full biomass conversion.

In this chapter a different approach was used and the conversion of algae produced during wastewater treatment was investigated under continuous reaction conditions. The algae was obtained from a collaboration with the Algae Research Group (Department of Biology and Biochemistry, University of Bath) and Wessex Water, a local water company, who are trying to use it as a cheap and natural alternative to domestic wastewater treatment. As the specific purpose of the algae is to take up P and N salts from the wastewater, no or little additional nutrients are required, resulting in a significant reduction in cultivation costs. Furthermore, if the algae production costs are effectively covered by the value of the wastewater treatment itself, the algae represents an almost free source of biomass for the HTL process.[166]

The reactions themselves were conducted using a specially designed continuous reaction system, which allowed the variation of system flow and temperature to determine the effect of these parameters on the product distribution and composition from the HTL of the algae. Significant operational challenges were encountered during the commissioning of this system, requiring extensive modifications to allow the steady processing of algae. As these challenges could have a significant bearing on the future design of industrial systems, both the initial design and the modifications resulting in the final design are discussed in this chapter and compared to the systems previously used in the literature. Liquefaction reactions were conducted under a range of different operating conditions and the results were compared to baseline data obtained from a batch system.

5.2 CONTINUOUS HTL SYSTEM DESIGN

5.2.1 DESIGN BASIS

The objective of this work was to study the continuous liquefaction of wastewater algae using a range of flowrates and reaction temperatures. This required the design of a continuous reaction system that could fulfil a number of fundamental requirements: (1) deliver the algae/water slurry at the required reaction pressure, (2) heat this slurry to, and maintain it at, the desired reaction temperature until the reaction is complete, (3) recover and separate the resulting four-phase product mixture (solid, water, oil and gas), (4) provide good control of temperatures, flow and pressures throughout the system, (5) ensure safe operation within the design envelope of all system components. An additional objective was to minimize the overall system costs, to develop a cheaper alternative to the systems currently used in the literature and provide an inexpensive laboratory method for the screening of different algae species and operating conditions.

The desired system flow rate was set in the range of 5 mL min^{-1} to 10 mL min^{-1} with a maximum operating temperature of at least 350 °C, to allow operation within the most widely studied range of HTL temperatures

(300 °C to 350 °C). This required a minimum operating pressure of 165 bar, the vapour pressure of water at this temperature.

5.2.2 INITIAL DESIGN

In the initial design (Figure 5-1), pre-mixed algae feed was supplied from a 1 L feed reservoir (V1) and pushed through the system using high-pressure nitrogen from a gas cylinder. A second, smaller back-up reservoir (V2), with an internal volume of 150 mL, was installed in parallel via a valve manifold, allowing continuous flow to continue when topping up V1. A drain-line on the outlet of V1 allowed the main feed reservoir to be fully emptied to enable flow to be switched from water to algae, or vice versa, during system start-up and shutdown.

The system pressure was controlled from the front, using the high-pressure regulator on the nitrogen cylinder (BOC, single-stage, 0-241 bar outlet range) and fine-tuned using a pressure reducing valve (Tescom, model number 44-1115-24-314) with an outlet range of 1.7 to 276 bar and a Cv of 0.02, installed upstream of the feed reservoirs.

The HTL reaction itself was carried out inside a vertical plug flow reactor, made from ¼ “ tubing (ID = 4.57 mm) and heated inside a carbolite tube furnace (model VST 12/600), with a heating zone length of 600 mm. Algae was fed from the bottom and three thermocouples, connected to datalogging software, were installed at one third and two thirds along the length of the reactor and at its outlet, allowing monitoring of the reactor temperature profile.

The reacted product mixture was cooled inside a double-pipe heat exchanger, with an inner tube diameter of ⅜ “ (ID = 6.3 mm), with counter-current cooling-water flow on the outside. An additional thermocouple on the cooler outlet (T4) was used to monitor the cooling performance.

Cooled reaction products were then passed through a solid collection pot, with the feed line entering through a tee from the top, inserted approximately ⅔^{rds} of the way into the vessel (Figure 5-2). The collection

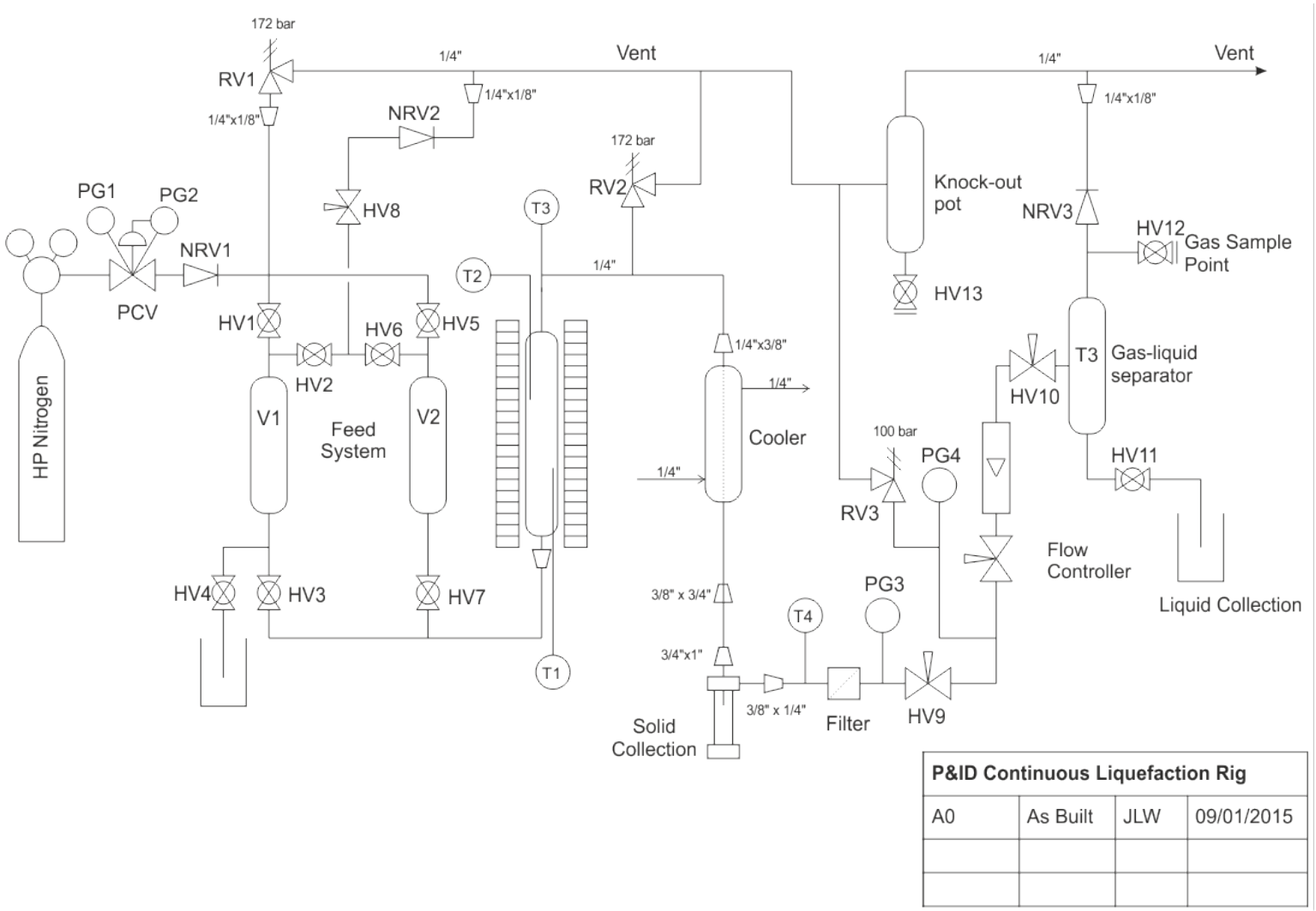

Figure 5-1: P&ID of initial design for the continuous HTL system

pot outlet was also located at the top, requiring the products to reverse their direction of flow, pass back up the annulus of the pot while allowing the solids to settle at the bottom. A fine particle filter with a mesh size of 15 µm (SS-4F-K4-15) was installed at the outlet of the pot to prevent the carry-over of any solid particles.

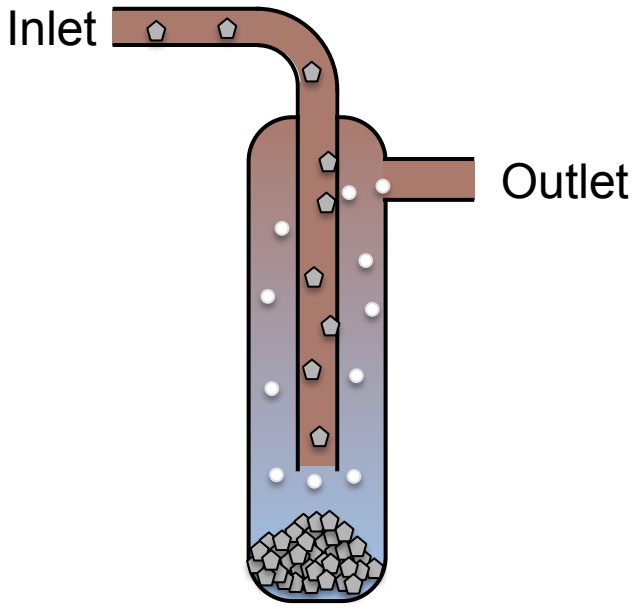

Figure 5-3: Schematic of solid collection pot design. Feed enters through an inner tube from the top, and solids are allowed to settle as the products flow back out through the annulus of the vessel

The remaining flow was controlled using a variable area liquid flowmeter, consisting of a needle valve and flow gauge, calibrated for a water flow range of 5 to 50 mL min^{-1} (Swagelok, VAF-M1-A1L-1-0). As the maximum design pressure of the flowmeter was limited to 130 bar (20 °C), a micro metering precision valve, HV9 (Rice Lake Weighing System, 57168), was installed upstream of the flowmeter to reduce the pressure accordingly. The system backpressure was therefore held against valve HV9, whereas the system flow was controlled using the variable area flowmeter. The outlet from the flowmeter was close to atmospheric pressure and routed into a gas/liquid separator, allowing gas to be vented from the top, and the water and oil phases to be collected via a drain valve from the bottom.

5.2.2.1 Safety considerations

HTL of microalgae requires high temperatures and pressures and therefore it is paramount that all system components are fully rated to the maximum possible reaction conditions. Consequently, a full list of the design ratings and maximum expected operating conditions of the system components was compiled (Table 5-1).

The weakest system component was the variable area flowmeter, with a maximum inlet pressure of 130 bar at 20 °C. This required the installation of pressure reducing valve HV9 upstream of the flowmeter to reduce its inlet pressure to below 100 bar. Pressure gauge PG4 was used to set and monitor the inlet pressure to the flowmeter, and a relief valve with a set-pressure of 100 bar was installed to protect against overpressure from failure or accidental opening of valve HV9.

All other system components were rated to a pressure of at least 172 bar, limited by the design pressure of the ⅛ “ ball valves. Therefore, the design pressure of the system was limited to this value and the maximum operating pressure was set to 163 bar, after applying a 5 % safety margin. Based on the VLE data for water, this pressure allowed a maximum reaction temperature of 349 °C, slightly below the maximum desired operating temperature of 350 °C. However, if needed, it would have been possible to replace these valves with higher-pressure alternatives to allow operation at temperature above 350 °C.

The design temperatures of a number of system components were also significantly below 350 °C. However, these components were either located upstream of the reactor, or downstream of the product cooler, with an operation temperature close to ambient, and were therefore not expected to be exposed to reaction temperatures.

Two potential scenarios were identified that could result in overpressure inside the system. In the first scenario, regulator failure at the inlet could have exposed the system to a pressure of up to 230 bar, the maximum delivery pressure inside the nitrogen cylinders. The second scenario

Table 5-1: Design ratings of components used in continuous HTL rig

Description	Design Rating	Max. Operating Conditions	Supplier
Gas Cylinder Regulator	241 bar	230 bar / 35 °C	BOC
Inlet pressure regulator (PCV)	276 bar	230 bar / 35 °C	Tescom Corporation UK
Feed Reservoir (T1)	207 bar	172 bar / 35 °C	FTI Ltd.
Needle Valve, V5	232 bar / 232 °C	172 bar / 35 °C	Swagelok
¼" Reactor (x = 0.035 in.)	175 bar / 374 °C	172 bar / 340 °C	Swagelok
1" Solid Collection Pot	175 bar / 374 °C	172 bar / 60 °C	Swagelok
Filter	248 bar / 371 °C	172 bar / 60 °C	Swagelok
Pressure reducing valve, V9	690 bar	172 bar / 60 °C	Condec (MPV-10k)
Variable area flowmeter	130 bar / 20 °C	100 bar / 60 °C	Swagelok
Pressure Relief Valves	338 bar / 121 °C	172 bar / 100 °C	Swagelok
⅛" Ball Valves	172 bar / 148 °C	172 bar / 60 °C	Swagelok
⅛" Check Valves	206 bar / 37 °C 150 bar / 190 °C	172 bar / 60 °C	Swagelok
⅛" fittings	360 bar / 374°C	172 bar / 340 °C	Swagelok
¼" fittings	368 bar / 374°C	172 bar / 340 °C	Swagelok
⅜" fittings	295 bar / 374°C	172 bar / 340 °C	Swagelok
¾" fittings	261 bar / 374°C	172 bar / 340 °C	Swagelok
1" fittings	245 bar / 374°C	172 bar / 60 °C	Swagelok
⅛" Tubing (x = 0.028 in.)	480 bar / 374 °C	172 bar / 340 °C	Swagelok
¼" tubing (x = 0.65 in.)	575 bar / 374 °C	172 bar / 340 °C	Swagelok
⅜" tubing (x = 0.035 in.)	186 bar / 374 °C	172 bar / 340 °C	Swagelok

could have arisen from a system blockage, either inside the reactor itself or within the product collection system, resulting in the expansion or vaporisation of trapped liquid with no real upper pressure limit. To protect against these two scenarios, pressure relief valves with set-pressures of 172 bar (as calibrated using HP nitrogen) were installed both at the system inlet and directly downstream of the reactor. The outlets from both relief valves were routed to the top of the fume hood, via a knock-out pot to collect any entrained liquid.

Finally, insufficient feed volume inside the feed cylinder could have resulted in the loss of liquid flow through the system, causing a significant increase in the temperature inside the reactor. During system operation, the furnace temperature had to be set to a value significantly above the desired reaction temperature, to ensure a sufficient temperature gradient to overcome heat transfer limitations. A reduction in liquid flow would therefore reduce the available heat sink, causing the reactor temperature to rise. This in turn would have been expected to result in partial vaporisation of the water, causing the pressure to rise. Even though the relief valves should have opened once the design pressure of 172 bar was reached, venting the entire reactor inventory and maintaining the reactor temperature at the corresponding temperature of 353 °C, the collected liquid volume was monitored continually to prevent the loss of flow in the first place.

5.2.3 OPERATING PROBLEMS AND DESIGN CHANGES

During the commissioning of the system, a number of significant operational issues became apparent, resulting in poor flow and temperature control as well as the formation of blockages forcing the shutdown of the system. These issues were addressed through a series of design iterations until smooth and controlled system operation could be achieved.

5.2.3.1 Flow Control Issues

The original design employed a variable area liquid flowmeter to control the flow of fluid through the system. An additional pressure reducing valve (HV9) was installed upstream of this flowmeter, reducing the flowmeter inlet pressure below its design pressure of 130 bar.

When commissioning the system, large fluctuations in liquid flow were observed, even when flowing the system with water only. A potential explanation for these fluctuations was the high pressure drop across the flow meter, requiring operation close to its design limit. Alternatively, the pressure reduction across the pressure reducing valve HV9 and the flowmeter itself could have resulted in the release of dissolved nitrogen and the formation of gas bubbles, leading to cavitation and temporary obstruction of the restrictions within the valve.

To address this issue, the pressure drop across valve HV9 was increased, reducing the inlet pressure to the liquid flowmeter to 20 bar. This helped to improve the flow control sufficiently to allow the introduction of algae to the system. However, after flowing around 300 mL of a 5 wt% algae slurry, the outlet pressure and liquid flow rate started to drop, requiring shut-down of the system. When dismantling the system, the filter element and the two control valves were found to be covered in a black, sticky, chloroform-soluble substance (Figure 5-4). The accumulation of this bio-oil within the system restrictions suggested that its viscosity at the collection temperature was too high to allow it to pass through the flow control system.

In order to address this, and raise the oil collection temperature, the system was modified by relocating the solid collection pot and particle filter upstream of the product cooler, and substituting the cooling water flow (~ 15 °C) with pre-heated water at 60 °C.

Even with these changes in place, the system outlet temperature remained close to ambient, probably as a result of heat losses from the pipes and the cooling effect from the expansion of dissolved nitrogen across the control valves. Consequently, it was decided that the installed

liquid flowmeter was unable to provide sufficient flow control through the system, and that a more fundamental redesign of the flow control system was required.

Figure 5-4: Accumulation of black, sticky substance within particle filter during HTL of algae using initial design

5.2.3.2 Redesign of product collection and flow control system

As the flow control issues were strongly related to the high viscosity of the bio-oil at near ambient conditions, it was decided to collect the reaction products at elevated temperatures, using two liquid collection pots with an internal volume of 150 mL each, similar to the design used by Elliott *et al*.[66] (Figure 5-5). Valve manifolds at the inlet and the outlet of the pots allowed batch-wise collection of the liquid reaction product into either one of the pots, whilst venting and draining the products from the other. Prior to use, the pots were filled with high-pressure nitrogen using a by-pass line from the system inlet, and the liquid flow into the pots was controlled by regulating the flow of nitrogen (and reaction gases) out of the system, using a low-pressure manual rotameter (KDG 1100). The system backpressure was maintained using the Tescom regulator, relocated from the system inlet, which was set to control the rotameter inlet pressure to

10 bar. To account for gas expansion, the volumetric gas flow through the rotameter was set to a value approximately 160 times that of the desired liquid flow, and the system flow was calibrated manually each time liquid was drained from the collection pots using a stop-watch and measuring cylinder.

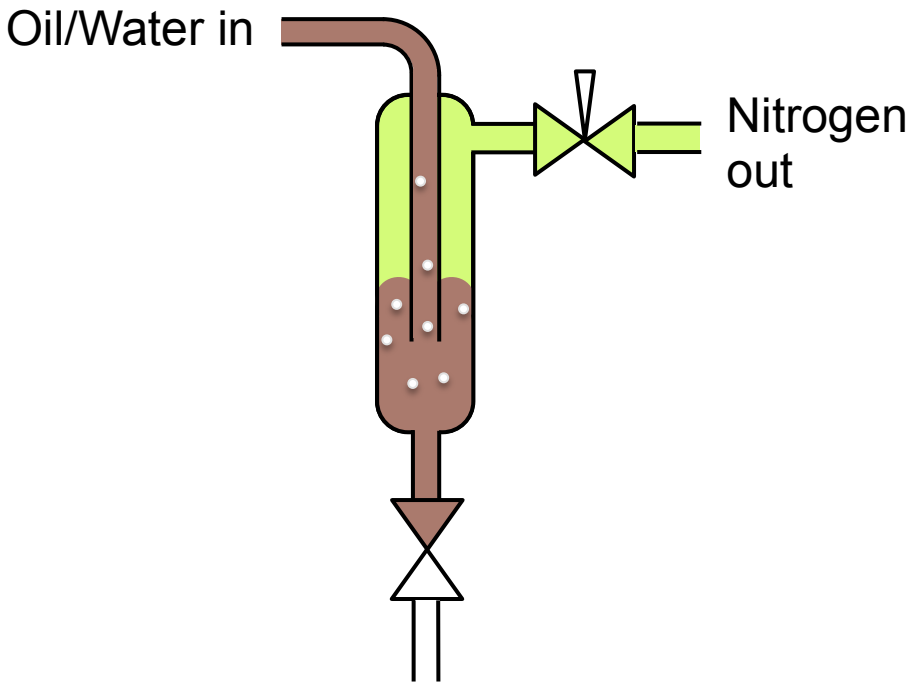

Figure 5-5: Liquid collection pot design. Prior to use, each pot was charged with high-pressure nitrogen, and the gas outlet flow was controlled to allow the ingress of liquid reaction products into the collection pot.

Depending on the desired system flow rate, the pots had to be switched over every 15 (7 mL min^{-1}) to 30 minutes (3 mL min^{-1}), to prevent overflow of the liquid into the gas lines. It should also be noted that the collection volume of the pots restricted the maximum flowrate to 7 mL min^{-1}, rather than the initially specified 10 mL min^{-1}, as faster switchover of the collection pots proved to be impractical. However, this problem could be addressed by increasing the volume of the liquid pots.

Implementation of this modification resulted in a significant improvement in flow control, but every time the collection pots were repressurised with nitrogen from the inlet, large spikes were observed in the reactor temperature profile (Figure 5-6a). These spikes were attributed to the small reductions in inlet pressure caused by the repressurisation process, which in turn led to a temporary reduction or even cessation of liquid flow

through the system, thereby increasing the reactor hold-up time. To prevent this, a separate gas cylinder was installed to re-pressurise the collection pots, with a set-pressure as close as possible to the operating pressure of the system. This adjustment led to a significant reduction of the undesired temperature spikes, and allowed steady reaction temperatures to be maintained over an extended period of time (Figure 5-6b).

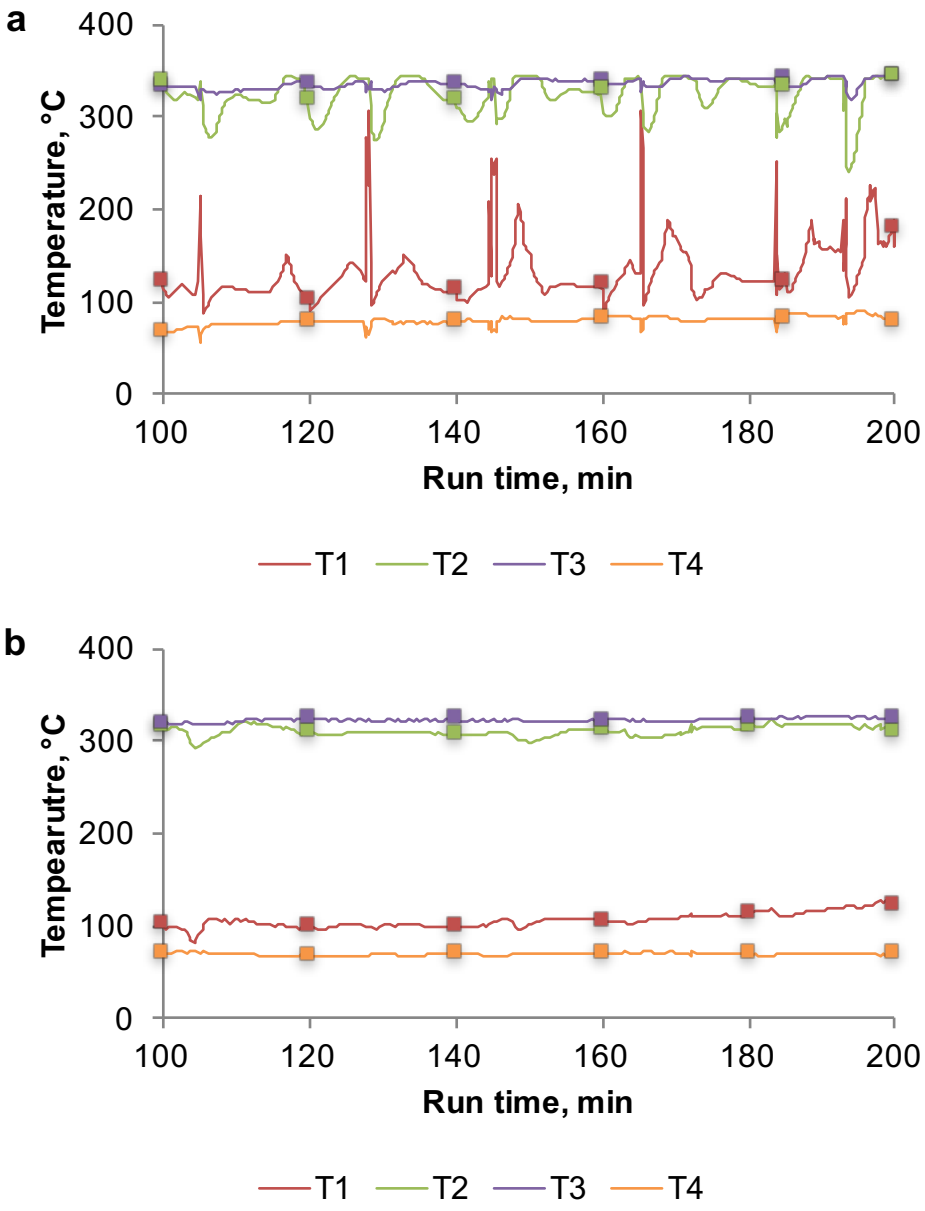

Figure 5-6: Reactor temperature profiles during repressurisation of liquid collection pots using (a) nitrogen from the inlet, (b) separate nitrogen cylinder

5.2.3.3 Reactor blockage issues

Using the re-configured product collection and flow control system, it was possible to return the system to liquefaction conditions and re-introduce a 5 wt% algae slurry feed (5 mL min^{-1}). However, almost as soon as the algae were introduced, the outlet pressure started to decrease and the experiment was aborted after 55 minutes, when the system pressure had fallen to below 100 bar. After dismantling the rig, a hard solid blockage, with an estimated length of 10 to 15 cm, was found approximately ⅔ ^{rds} of the way up the reactor.

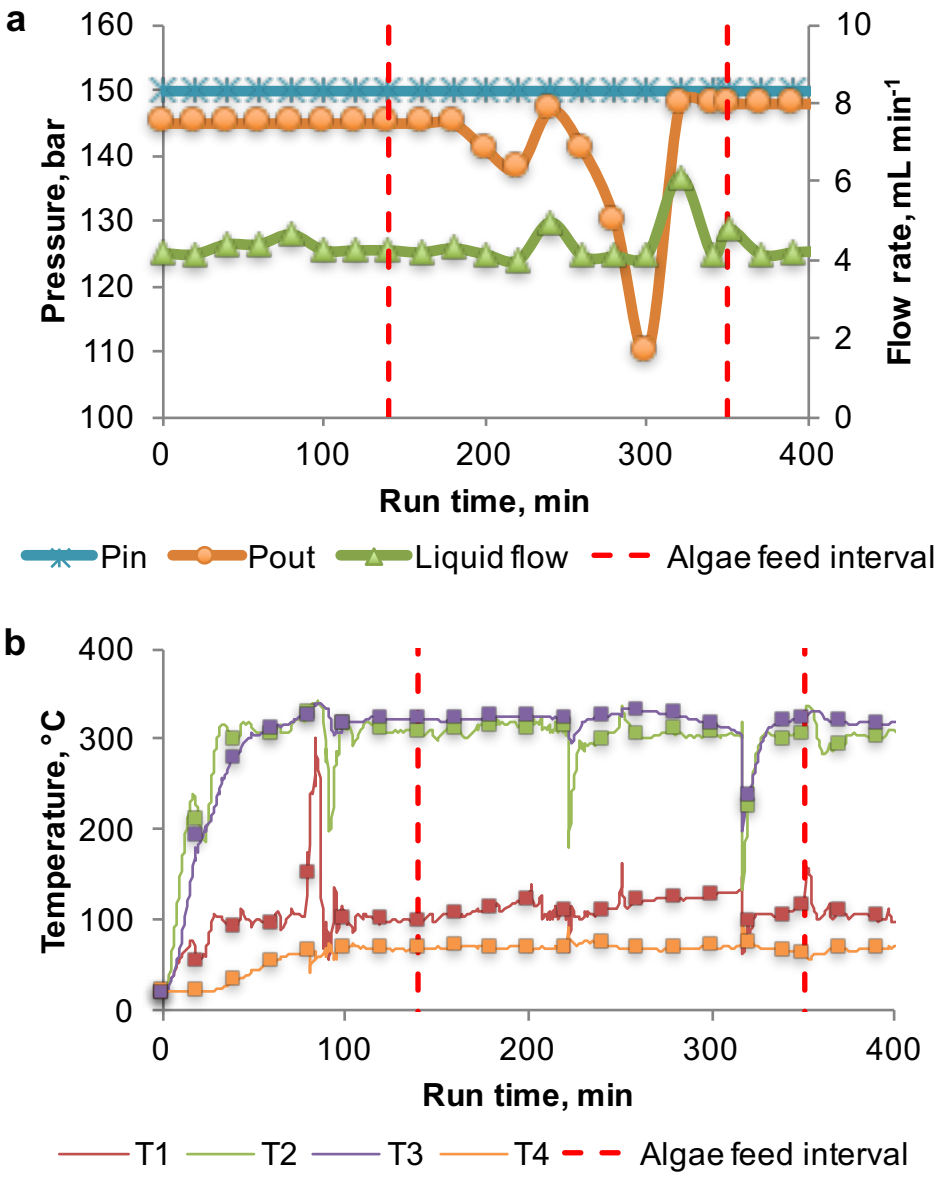

Figure 5-7: Reactor blockages leading to: (a) fluctuations in outlet pressure and liquid flow, (b) negative temperature spikes

To reduce the risk of further blockages, the reactor diameter was increased from ¼ " to ⅜ " tubing (ID = 6.22 mm) and this resulted in a marked improvement in operation (Figure 5-7). Nevertheless, the outlet pressure still reduced over time, before suddenly recovering to its initial value. This pressure jump was associated with a sudden increase in liquid flow through the system, resulting in large negative temperature spikes, increasing in magnitude after each event (Figure 5-7b). These fluctuations were attributed to the formation of blockages within the reactor, which were suddenly pushed through the system when the pressure drop reached a critical value. Even though it was possible to process the entire inventory of the algae feed reservoir, the fluctuations in operating conditions were too large to meet the project objectives of studying their impact on the HTL reaction.

5.2.3.4 Reconfiguration of reactor design to minimise risks of blockages

One of the most credible explanations for the formation of the reactor blockages was the incomplete suspension of solid products within the other product phases, leading to their accumulation within the reactor tube. The benefit of increasing the reactor diameter further could therefore be outweighed by the reduction of flow velocity, increasing the extent of solid accumulation even further.

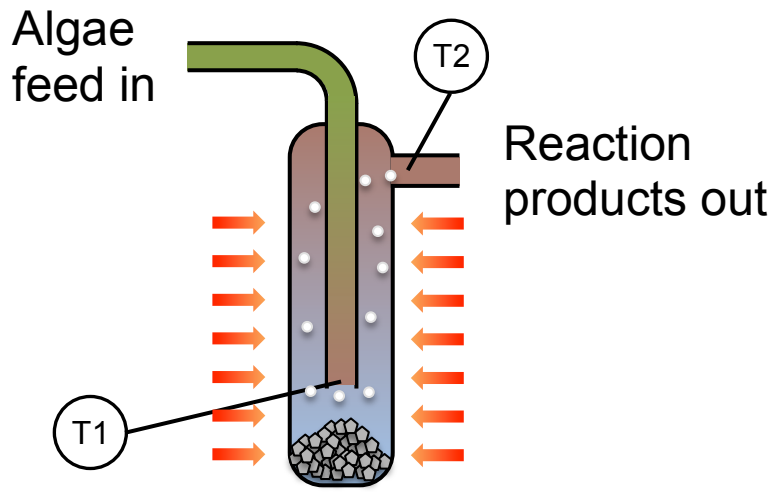

Figure 5-8: Configuration of the modified HTL reactor

It was therefore decided that more fundamental reactor modifications were required to eliminate the risk of reactor blockages. Consequently,

the upflow plug reactor was replaced with a double-tube design, using a configuration similar to that of the solid collection pot (Figure 5-8). In this design, the cold algae feed entered through an inner tube from the top, in which it was quickly heated to the reaction temperature. As the feed flowed out from the inner tube and up the annulus of the reactor, the reaction was allowed to proceed to completion, and the oil, water and gas product exited from a tee-piece at the top. Reaction temperatures were monitored using two thermocouples located at the bottom of the inner tube (T1) and at the reactor outlet (T2), and the separate solid collection pot and particulate filter were removed.

Figure 5-9 Solid recovered from the bottom of the modified HTL reactor, containing cylindrical sections of compressed solid

Initially, respective inner and outer tube diameters of ⅜” (ID = 6.22 mm) and 1 ” (ID = 21.18 mm) were selected, which allowed the processing of 1 L of a 5 wt% microalgae slurry. Smaller pressure fluctuations of up to 30 bar were still observed, resulting in spikes in the temperature profiles, and approximately 1” long cylindrical sections of compressed solid were found at the bottom of the reactor following reaction (Figure 5-9). As these cylinders had the same diameter as the inner reactor tube, they

appeared to have formed within the inner tube, resulting in a partial blockage and pressure build-up, until the pressure drop became sufficient to push the plugs into the bottom of the reactor.

To mitigate against these pressure fluctuations, the reactor dimensions were increased further to an inner tube diameter of ½ ” (ID = 9.4 mm) and an outer tube diameter of 1 ” (ID = 20.12 mm), and this finally enabled virtually smooth flow and minimal temperature fluctuations throughout the entire reaction period (Figure 5-10).

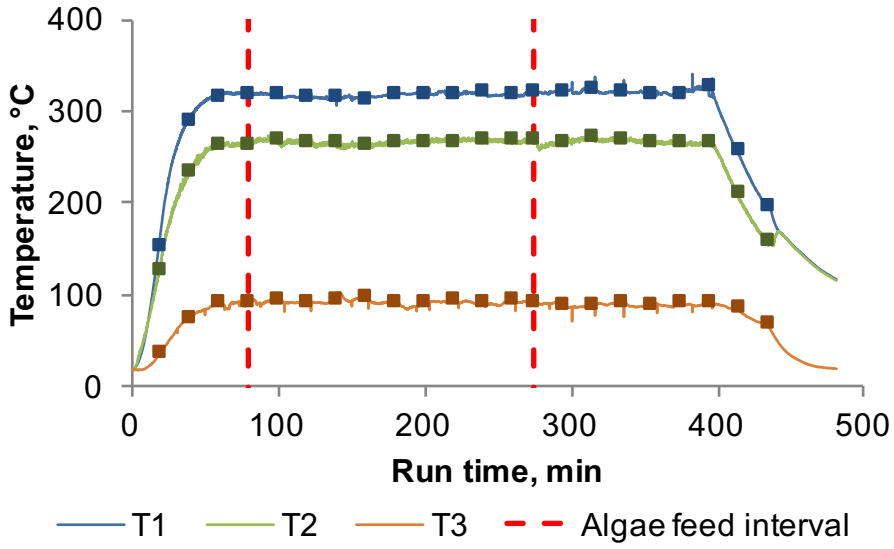

Figure 5-10: Reaction temperature profile of final reactor configuration

5.2.4 FINAL DESIGN

Following the changes discussed above, the final system design (Figure 5-11) retained the feed delivery system, consisting of two parallel feed reservoirs, pressurised from a high-pressure nitrogen cylinder and connected via a valve manifold. A second gas cylinder was connected to this manifold to allow independent repressurisation of the liquid collection pots without affecting the system inlet pressure.

The vertical plug flow reactor was replaced with a double-tube design, allowing the collection of solids at the bottom of the reactor and preventing their accumulation within the flow line. This eliminated the need of a separate solid collection pot and the product filter was removed for operational reasons. Liquid reaction products were collected at

elevated temperatures within two parallel, nitrogen-filled collection pots and rather than controlling the liquid flow directly, the system flow was maintained by regulating the flow of nitrogen and reaction gases from the liquid collection system. Ambient cooling within the product lines, connecting the top of the reactor with the liquid collection pots, was sufficient, as monitored using thermocouple T3, eliminating the need of a separate product cooler.

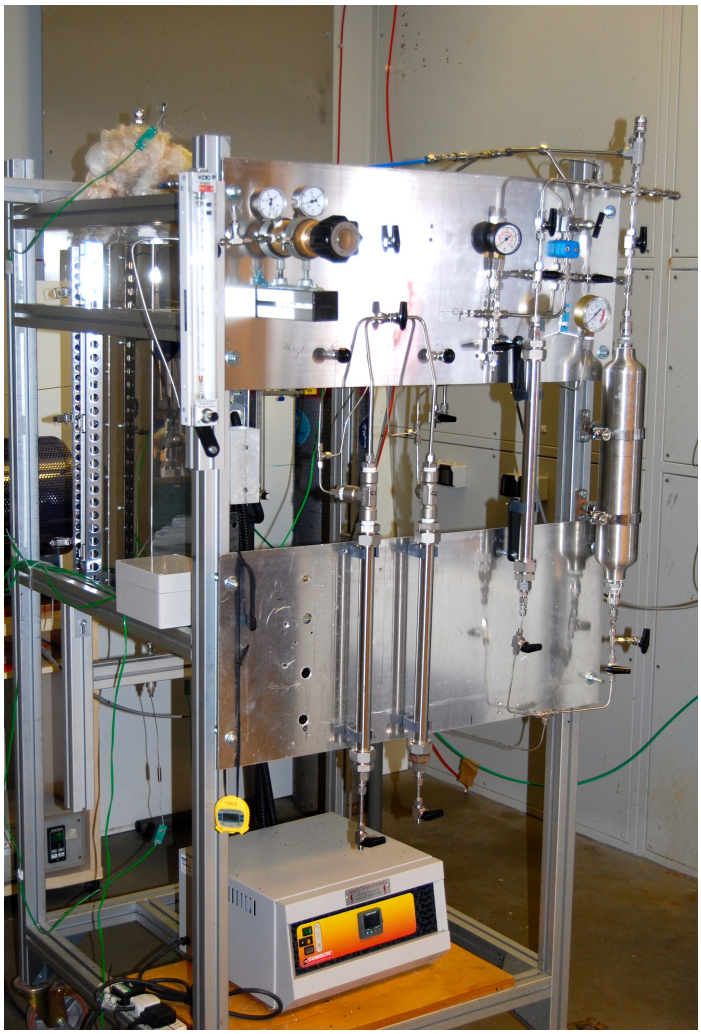

Figure 5-11: Final design of the continuous HTL system

Whilst the modified system contained a slightly increased liquid inventory, the pressure interface between the reaction system and liquid flow control meter was eliminated, reducing the risk of system overpressure. Relief valves at the system inlet and reactor outlet were retained to protect against the risks of regulator failure and the heating of trapped liquid

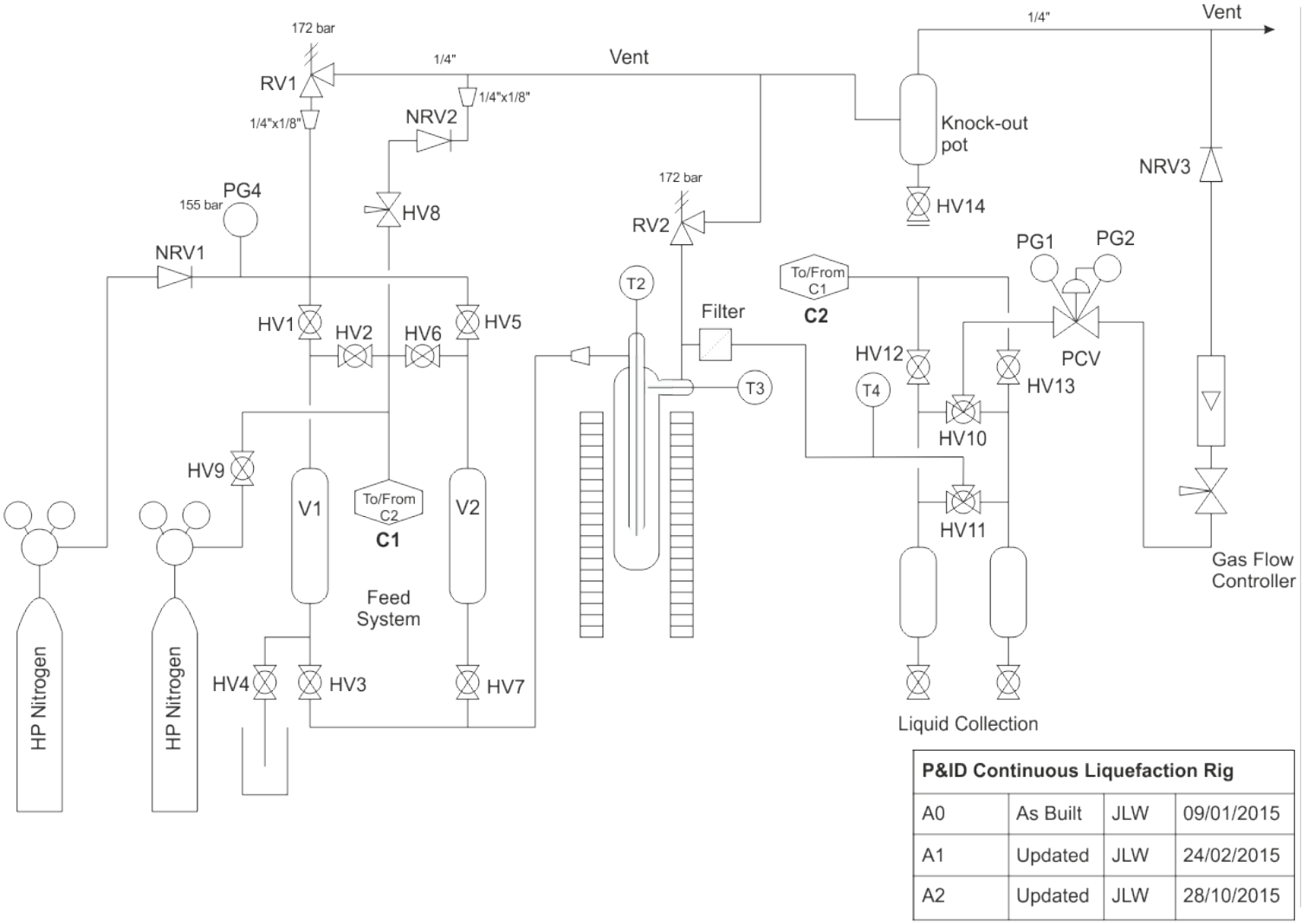

P&ID Continuous Liquefaction Rig			
A0	As Built	JLW	09/01/2015
A1	Updated	JLW	24/02/2015
A2	Updated	JLW	28/10/2015

Figure 5-12: P&ID of the final design of the continuous HTL system

within the reactor. The P&ID of the final system has been included for reference (Figure 5-12).

5.2.4.1 Flow delivery

All the liquefaction systems described in the literature have used high-pressure mechanical pumps to push the algae through the systems. These pumps include triplex piston pumps,[44, 54] an HPLC pump,[68] a hydraulic diaphragm metering pump,[69] a double screw press,[65] and a modified dual syringe pump system.[66]

The dual syringe pump system used by Elliott *et al*. appeared to be one of the most effective, allowing the injection and flow metering of a microalgae slurry with a loading of up to 35 wt%,[66] however, it proved to be prohibitively expensive for application in this project. In contrast, the flow range of the triplex piston pump system used by Jazrawi *et al*.[44] and Cole *et al*.[54] (15-90 L h^{-1}) greatly exceeded the desired flow range of 5 to 10 mL s^{-1} (0.3 to 0.6 L h^{-1}). Finally, Patel and Hellgardt experienced operational problems when feeding the biomass through their HPLC pump, which limited the maximum biomass concentration to 1.5 wt%.[68]

Many of the operational challenges of the laboratory-scale systems can be attributed to the inverse scaling problems described by Jazrawi *et al*.,[44] where smaller flowrates require smaller pumps and control valves with reduced clearances which are more prone to be blocked by algal biomass particles. This is presumably why Garcia-Moscoso *et al*., used water from a high precision pump to activate a vertical piston arrangement to push algae through the system.[75] Whilst their design eliminates the risk of blockages within the cavities of the high precision pumps, it still relies on moving parts, requiring high-pressure seals and limits the injection volume to the capacity of the piston.

By using high-pressure nitrogen to push the algae through the system, the present design eliminates the need of using mechanical pumps completely. It provides a high degree of flexibility both in terms of flowrate and feed pressure and the double feed cylinder arrangement allows

continuous feeding of algae. This approach offers a lower cost alternative to the systems previously used in the literature, and can be used to investigate the continuous HTL of algae under laboratory conditions.

Obviously, there are also a number of disadvantages. First and foremost, nitrogen feeding does not provide the precise metering functionality of some of the mechanical pumps. Consequently, the system flowrate needs to be controlled separately, as will be discussed in a later section. Secondly, nitrogen is a compressible fluid, and therefore variations in the pressure drop through the system could have a larger effect on the algae flowrate, than in a liquid based feed system. Finally, partial dissolution of nitrogen in the reaction medium could result in the dilution of reaction gases, which might impact the ability to recover gaseous by-products.

5.2.4.2 Reactor Configuration

Consistent with the present design, most continuous HTL systems described in the literature, and used for the liquefaction of microalgae, have employed plug flow reactors, including long stainless steel heating coils heated inside fluidized sandbaths,[44, 54, 69] a stainless steel tube heated inside a horizontal tube furnace,[75] a quartz lined-reactor, heated inside a clamp heater,[68] and a microfluidic chip design, made from glass and silicon, containing square channels with a cross-section of 200 by 200 µm and total length of 1320 mm, mounted inside a temperature controlled stainless steel heating block.[31] The only major exception is a system used by Barreiro *et al.* who employed a simple CSTR with a reaction temperature of 350 °C and a residence time of 15 minutes.[65] Elliott *et al*., in turn, used a CSTR to pre-heat the algae feed from 133 °C to the final reaction temperature, before allowing the reaction to complete in a plug-flow reactor.[66] This system was chosen to prevent plugging problems, previously experienced with lignocellulosic feedstocks, using a plug-flow system only.

None of the cited papers reported significant plugging problems within the reactor itself, but it should be noted that in many cases the algae loadings were significantly lower than in the present work,[31, 68, 75] or the authors

employed a co-solvent to prevent plugging issues in the first place.[54, 68] Furthermore, the ash content of the wastewater algae used in this project was particularly high (~ 30 %), which may have further contributed to the severity of the reactor blockage issues experienced using the initial vertical plug flow reactor design. It is interesting to note however, that the internal reactor diameters of some of the literature designs were significantly smaller than the diameters used in this project, most notably the 200 µm channels used by Cheng *et al.*,[31] and this suggests that blocking issues are not necessarily caused by size limitations within the reactor.

This is consistent with the reasoning of replacing the simple vertical up-flow reactor with a double-tube design, which argued that the benefit of increasing the reactor diameter may be outweighed by a reduction in flow velocity, resulting in increased solid accumulation within the reactor. However, after adapting the double-tube reactor, it was found that an increase of the inner tube diameter from ¼ " to ½ " still helped to prevent the formation of solid plugs, which temporarily restricted flow and led to temperature and pressure fluctuations in the system.

Following these changes, the final reactor design consistently allowed the processing of 1 L of a 5 wt% algae slurry without any noticeable blockage issues and this suggests that the collection of reactor solids may indeed be beneficial. The final design also provides much faster and more consistent biomass heating within the inner reactor tube, whilst preventing the presence of hot spots, which might catalyze the formation of radicals, which in turn could initiate polymerization reactions. Even though the CSTR designs employed by Barreiro *et al.*[65] and Elliott *et al.*[66] were capable of providing even higher heating rates, the former group found that oil yields were reduced compared to batch reactors, and this was associated with the cross-reaction of the final oil product with intermediates formed at early reaction stages. These cross-reactions do not occur in a plug flow reactor, and consequently the final design offers a good combination of fast heating rates within a plug flow arrangement.

An additional advantage is the partial heat recovery from the hot reaction product in the reactor itself, without causing the plugging problems reported by Elliott *et al*. when pre-heating the reaction feed above 133 °C.[66]

It is obvious however, that the solid collection capacity of the reactor is not unlimited, and this would be a particular challenge for larger scale industrial operation. Any industrial design would therefore have to incorporate a solid removal system, possibly similar to those installed in oil-water separators used in the oil and gas industry.

5.2.4.3 Product collection

In the final system design, liquid reaction products were collected in two parallel, nitrogen filled collection pots, and the flow of algae through the system was controlled indirectly, by regulating the outflow of nitrogen from the system. This system is similar to the arrangement used by Elliott *et al*.,[66] who managed to process a feed with an algae content of up to 35 wt%. They also employed a separate solid collection system, prior to liquid collection, consisting of a combination settler/filtration unit, where solids fell to the bottom of a vessel and the liquids passed overhead through a filter.

In all other studies, the liquid reaction products appear to have been passed through a back-pressure regulator directly,[31] although most publications provided little detail. One exception are Jazrawi *et al*., who reported significant pressure fluctuations in their system as the result of transient blockages of their back-pressure control valve.[44] Increasing the control valve orifice reduced the extent of the blockages at low algae concentrations, but the maximum concentration that could be processed was still limited to 10 wt%.

These problems are similar to those encountered with the initial system design used in the present study, which used a pressure reducing valve and a liquid flowmeter at the system outlet to control the flow of fluid through the system. The high viscosity of the bio-oil at room temperature

resulted in the clogging of the control valves, causing significant operational problems and requiring the eventual redesign of this system.

Controlling the system backpressure on the outflow of gas instead, helped to significantly reduce the risk of system blockages, as it avoided having to pass the viscous bio-oil through the restrictions within the control valve. Whilst the current arrangement, requiring batch-wise removal of liquid problems followed by collection pot repressurisation, would not be practical on a larger scale, the system could be adapted to control the outflow of liquid using a level controller. In this case, the system pressure and flowrate would still be controlled independently from the liquid outflow from the system, minimizing the risk of temporary processing upsets.

5.2.4.4 Flow Control

All systems described in the literature controlled the system flow from the inlet, using the metering function of the various mechanical pumps used to deliver the system flow. This is a big advantage over the present system, where the system flowrate is controlled by regulating the flow of nitrogen from the outlet. In this set-up the system flowrate is controlled indirectly and does not take into account the gases formed during the reaction. Because of this, the liquid flow was determined after each collection interval, using a stopwatch and measuring cylinder.

Whilst this approach is not ideal, a simple modification to install a mass flow controller on the nitrogen inlet of the algae feed reservoirs, and replacing the pressure control valve at the collection pot outlet with a backpressure regulator, would result in a significant improvement of the flow control in the system. At the same time, this modified system would retain the benefit of significantly reduced costs, compared to the alternative systems used in the literature.

5.3 BIOMASS CONVERSION

This section describes the results from the conversion of algae used in the remediation of wastewater in the laboratory scale, continuous HTL reaction system, described in the previous section.

Prior to converting the algae in this system, a set of baseline experiments were conducted under batch conditions to investigate the effect of reaction temperature and heating rate on the resulting product distribution. Subsequently, the continuous system was characterized over a range of flowrates and temperatures, before analysing their effect on the liquefaction reaction itself.

5.3.1 ALGAE CHARACTERIZATION

The algae used for this project came from a collaboration with the Algae Research Group (Department of Biology and Biochemistry, University of Bath) and Wessex Water, a local water company, where the algae is being used to provide tertiary removal of N and P from domestic wastewater.

The algal community was a mixture of locally sourced *Scenedesmus* and *Chlorella* strains selected specifically for its efficiency in phosphate uptake, as well as its ability to settle out quickly to facilitate its recovery following wastewater treatment.

All experiments in this study were conducted using the same batch of algae, which was separated by gravity and further concentrated to a biomass content of 21.7 % using centrifugation. This algae paste was thoroughly mixed and frozen in 50 g batches. For each experiment, the required quantity of algae was defrosted and mixed with distilled water to achieve an approximate concentration of 5 wt%.

5.3.1.1 TGA analysis

The dried wastewater algae was analysed by TGA (in air) to 900 °C to determine its ash and moisture content (Figure 5-13a). Heat flow analysis revealed two endothermic peaks, ranging from 30 to 200 °C (Zone I) and

720 and 850 °C (Zone III), and a large exothermic zone from 200 to 630 °C, which can be further divided into a lower temperature region with a maximum at 350 °C (Zone IIa), and a higher temperature region with a maximum at 545 °C (Zone IIb).

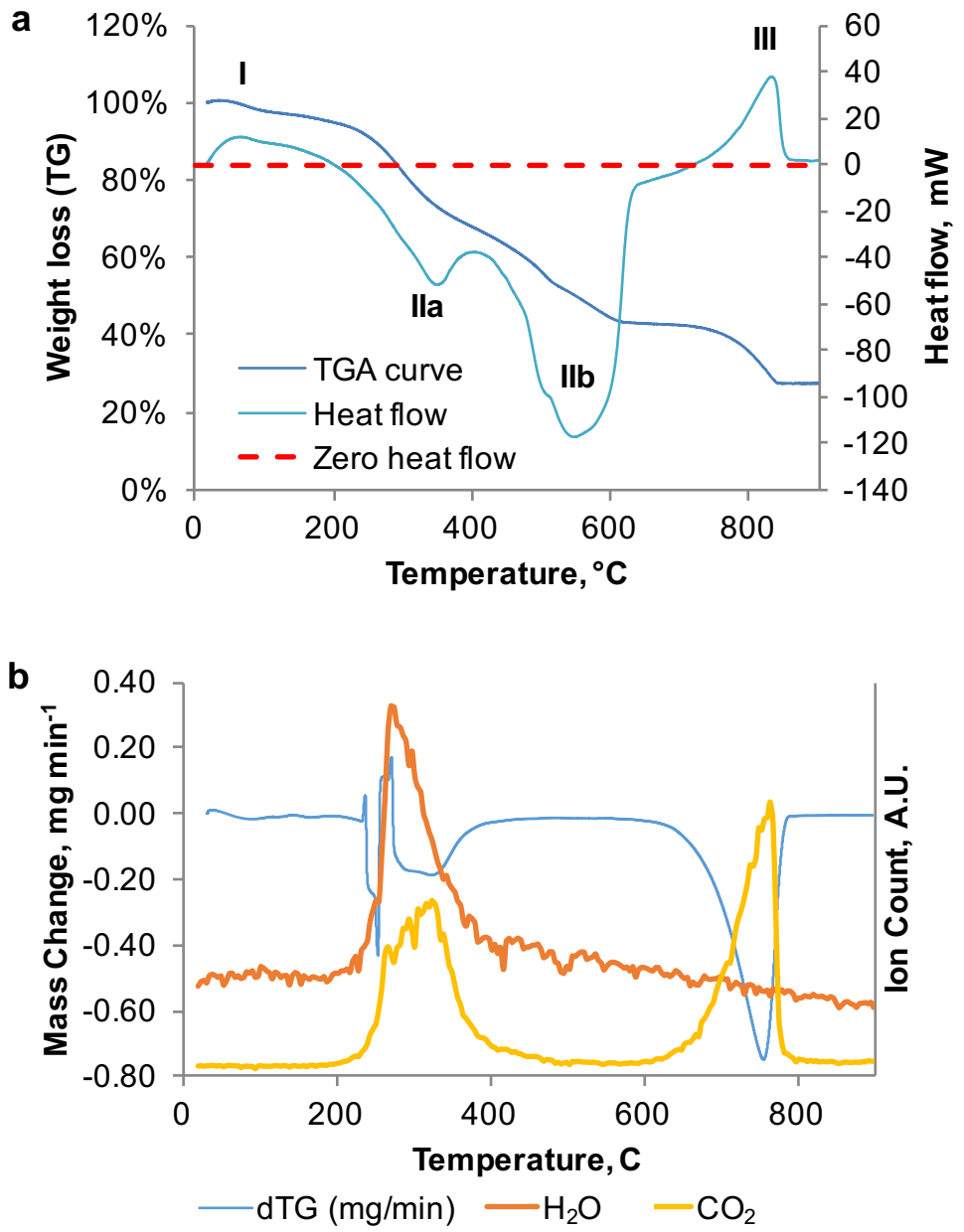

Figure 5-13: Thermogravimetric analysis of wastewater algae, a) TGA curve and heat flow, b) TGA-MS analysis

The first endothermic region with maximum heatflow at 67 °C can be attributed to the loss of residual water from the biomass. This accounts for just over 5 % of the initial biomass weight. In contrast, the exothermic peaks can be associated with the combustion of the biomass, and the two

distinct regions point towards a step-wise combustion process. The source of the second endothermic peak, with a maximum heat flow at 831 °C, is not immediately obvious. This feature was not observed during the analysis of alternative microalgae samples, including *Spirulina* and the PHB containing algae presented in Chapter 3, or the lipid-extracted algal residue discussed in Chapter 4. It cannot be attributed to an exothermic combustion process, but instead, could be the result of thermal decomposition of inorganic salts present in the biomass.

To investigate this in more detail, the analysis was repeated using a TG-MS analyser, which determines the composition of the produced off-gas (Figure 5-13b). From this analysis, the only two gas products that could be detected in significant quantities were water and carbon dioxide. Helium, nitrogen and oxygen were already present in the carrier, purge and blanket gases, and therefore their corresponding peaks were ignored.

At temperatures below 170 °C, water was the only gaseous product, and this confirms that the initial endothermic peak could be attributed to the release of residual moisture. As the temperature was increased further, two distinct regions of weight loss were detected, ranging from around 183 to 360 °C and from 467 to 566 °C. Interestingly, the relative release of water and carbon dioxide over the two regions was very different. Whilst the lower temperatures favoured the release of water, the major product of the higher temperature combustion was carbon dioxide.

A potential explanation for this two-step combustion process could be the sequential combustion of the different biochemical components present in the algae. However, when considering the maximum differences in the C to H elemental ratios of the model compounds used in Chapter 3 (1.07 for soy protein and 0.93 for corn flour), they are too small to explain the large variation in water and carbon dioxide release between the lower and higher temperature region.

Instead, the lower temperature peak could be the result of cross-reactions between different biomass components, including dehydration,

polymerisation, dehydrogenation and cyclization reactions, which release hydrogen and water. Full combustion of the carbon-enriched biomass is only achieved at much higher temperatures, resulting in the release of carbon dioxide.

Finally, over the high-temperature endotherm (630 to 760 °C), the only detected gas product was carbon dioxide, which could be formed by the thermal decomposition of carbonates present in the algae. This would suggest that the wastewater algae is able to sequestrate atmospheric carbon in both organic and inorganic form, which could have important implications on the carbon capture potential of this algal mixture, provided that the carbonates do not decompose during the HTL process.

Using these results, it is finally possible to calculate the ash content of the algae. As this is generally defined as the inorganic biomass fraction, it should include the suspected carbonate fraction, released at high temperatures. Consequently, the ash content was calculated from the sample weight at 650 °C, and amounted to 29.9 %. This compares to a residue weight of only 20.8 % at 900 °C.

5.3.1.2 Algae composition

Table 5.2: Characterization of algae used for wastewater remediation

Biochemical composition	
Lipid	7.85 wt%
Proteins	77.54 wt%
Carbohydrates	13.12 wt%
Elemental Composition	
C	40.1 wt%
H	5.8 wt%
N	6.1 wt%

The biochemical composition of the algae was determined by Tracey Beacham at PML (Table 5.2). Based on this analysis, the algae consisted predominantly of proteins and contained only low amounts of lipids and carbohydrates. However, the total amount of these three biochemical

components adds up to 98.5 wt%, significantly above the total expected organic biomass content of 70.1wt%.

In contrast, the elemental analysis of the algae revealed a nitrogen content of only 6.1 wt% and by applying the standard Jones' factor of 6.25,[195] the protein content can be estimated at 38.1 wt%. A potential explanation for the discrepancy of the protein content, determined by the biuret method, is an interface in the assay as a result of very strong green pigmentation, resulting in the overestimation of protein content.

The actual protein content is therefore likely to lie somewhere between these two estimates, but limited to a maximum value of 49.1 wt%, based on the algae ash content of 29.9 %.

5.3.2 BATCH REACTIONS

The batch reactions were conducted in the same reactors used for the conversion of model compounds and PHB containing algae described in Chapter 3. Reactors were filled with a fixed amount of premixed algae slurry and heated inside a vertical tube furnace. As soon as the desired reaction temperature was reached, the reactors were removed from the furnace and left to cool (Figure 5-14).

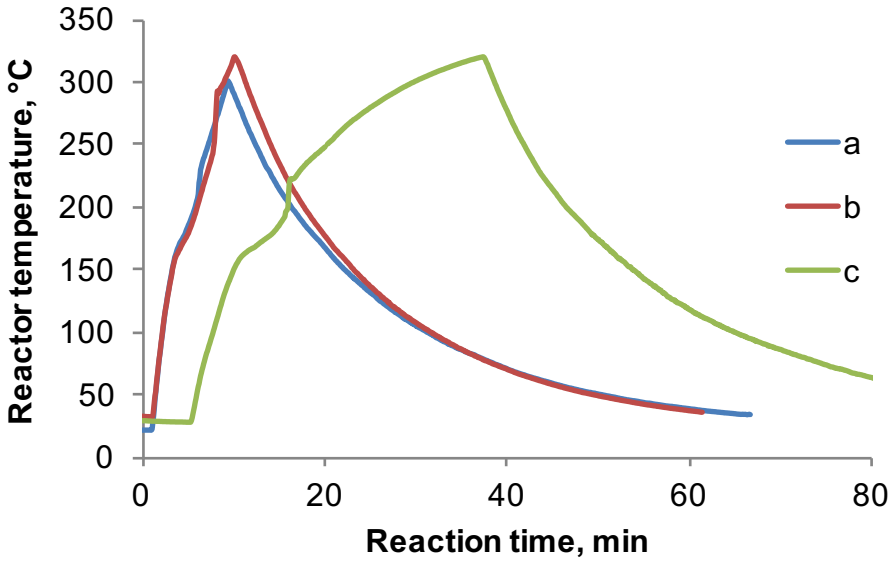

Figure 5-14: Batch reactor temperature profiles obtained with different furnace and reaction temperatures; (a) Reaction temperature (RT): 300 °C, furnace temperature (FT): 700 °C; (b) RT: 320 °C, FT: 700 °C; (c) RT: 320 °C, FT: 500 °C

Consequently, the actual reaction time at the final reaction temperature is zero and the majority of reactions are expected to occur during the heating stage itself. The advantage of this transient system is that it allows much faster heating rates, which have been shown to be beneficial for the formation of bio-oil. However, it does not provide the extended reaction times of the more commonly used isothermal systems, such as that used for the conversion of lipid-extracted algae residue in Chapter 4.

Batch reactions were conducted at 3 different temperatures and at four different heating rates. Each reaction was done in triplicate to allow calculation of the standard error.

5.3.2.1 Effect of reaction temperature

The conversion of wastewater algae was studied at 303 °C, 322 °C and 339 °C, and the effects on the product distribution (Figure 5-15a) and CHN recovery to the bio-oil phase (Figure 5-15b) were investigated. The furnace temperature was kept constant at 700 °C, resulting in respective heating times of 8.1, 9.1 and 10.0 minutes, corresponding to averaged heating rates ranging from 33.8 °C min^{-1} at 339 °C to 37.6 °C min^{-1} at 303 °C.

Increasing the reaction temperature from 303 °C to 339 °C resulted in a clear reduction in solid yields from 43.6 wt% to 38.2 wt%. These findings are consistent with the results from the conversion of model compounds, reported in Chapter 3 and can be associated with an increase in algae conversion, resulting in reduced retention of the organic biomass components into the solid phase.

As the reaction temperatures were increased from 303 °C to 321 °C, the water phase residue yields also experienced a remarkable decrease from 29.9 wt% to 20.7 wt%, however, increasing the temperature further to 339 °C resulted in a small increase to 24.0 wt%. The initial reduction in residue yields at 321 °C can be partially attributed to the simultaneous increase in bio-oil yields (12.1 wt% to 17.1 wt%) and a reduction in the overall mass balance closure by 6.3 wt%, suggesting the increased formation of volatiles.

The subsequent residue yield increase of 3.3 wt% at the highest temperature closely matches the simultaneous reduction in solid yields (41.5 wt% to 38.2 wt%), even though a slight decrease in oil yields (17.1 wt% to 15.9 wt%) was also experienced over this range.

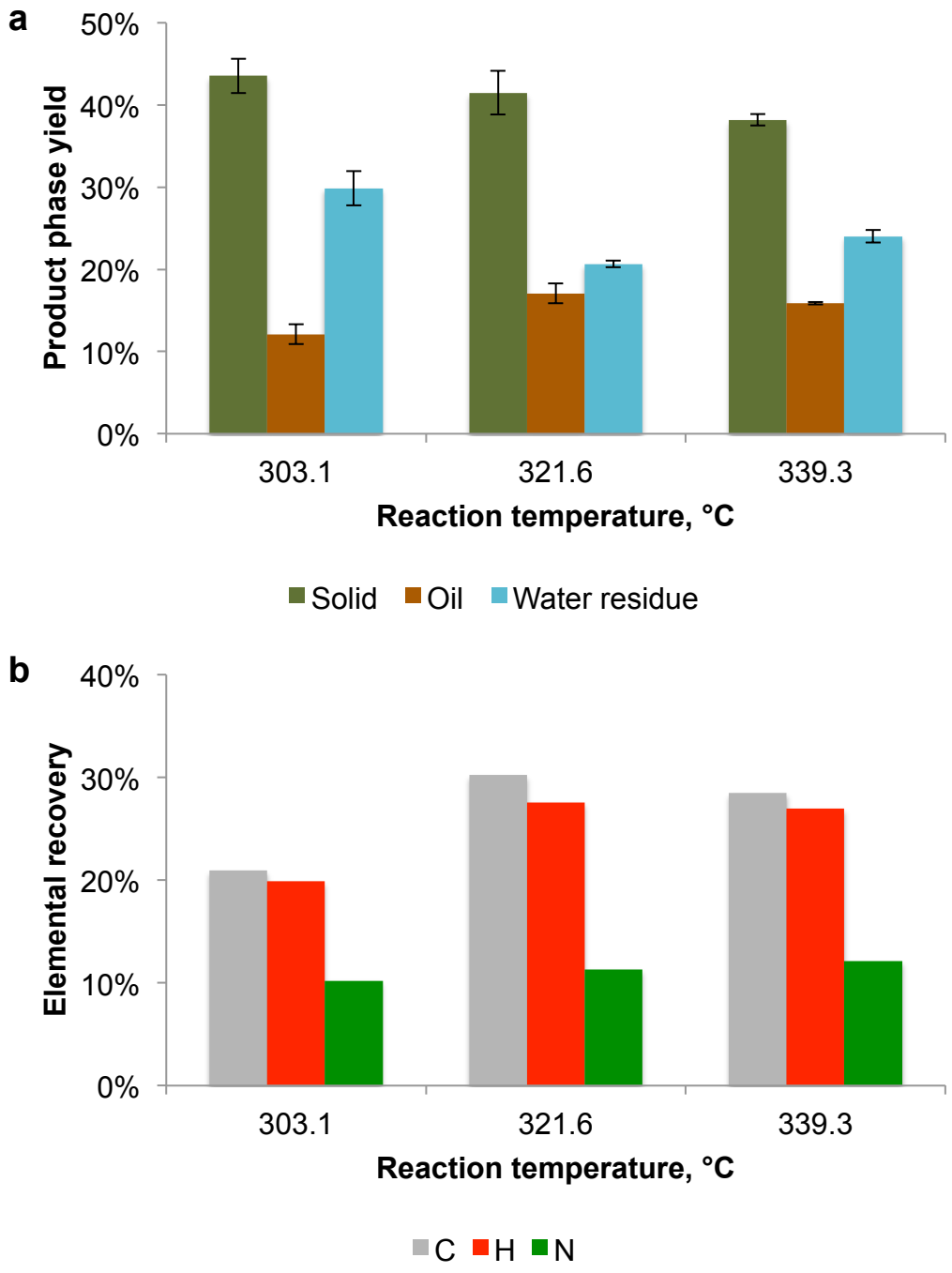

Figure 5-15: Effect of reaction temperature on the conversion of wastewater algae; (a) effect on product distribution, (b) effect on CHN distribution to bio-oil

The highest carbon (30.2 %) and hydrogen (27.6 %) recoveries to the bio-oil were achieved at the medium reaction temperature, and at 4.0 wt% this oil also possessed the lowest overall nitrogen content. In

contrast, the carbon and hydrogen recoveries at 303 °C were much lower which correspond to the low overall oil yields obtained at this temperature.

Interestingly, the difference in nitrogen recoveries was much smaller, and this could suggest that the majority of nitrogen-containing compounds were already incorporated into the bio-oil at very low reaction temperatures, whereas more carbon and hydrogen-rich molecules were added later. Alternatively, some of the nitrogen added into the oil at lower temperatures could be removed via denitrogenation reactions occurring at the more severe reaction conditions, counteracting the incorporation of additional nitrogen containing compounds.

Increasing the reaction temperature further, led to increased nitrogen and decreased hydrogen and carbon distribution to the oil, which does suggest that nitrogen containing compounds continued to be added at all reaction temperatures. Even though the unaccounted elemental fraction in the bio-oil (predominantly oxygen) reduced from 15.5 wt% to 13.5 wt% over the same temperature range, the undesired increase in nitrogen content, along with the reduction in bio-oil yield, suggests that increasing the reaction temperatures significantly above 320 °C had no beneficial impact.

5.3.2.2 Effect of heating rate

To study the effect of heating rate on the HTL of the wastewater algae, the reaction temperatures were kept constant at 320 °C. Heating rates ranging from 10.1 °C.min^{-1} to 52.6 °C.min^{-1} were obtained by changing the furnace temperature from 500 °C to 800 °C, as calculated by dividing the final reaction temperatures by the respective heating times (6.1 min to 31.8 min). Therefore, the heating rates represent an average rather than an absolute value, particularly for the lower furnace temperatures, where the heating rates were found to drop off significantly as the reaction temperature was approached.

At the two lowest heating rates, the solid yields remained approximately constant at around 40 %, but raising the heating rates to 35.2 and

52.6 °C min^{-1} resulted in a small increase in the solid yields to 41.5 wt% and 42.8 wt%, respectively (Figure 5-16a). Oil yields, in turn, increased almost linearly from 14.9 wt% to 17.1 wt% as heating rates were increased from 10.1 to 35.2 °C min^{-1}, but dropped off to 13.5 wt% at the highest heating rate of 52.6 °C min^{-1}. Residue yields at last, showed the opposite trend to oil yields, decreasing from 24.7 wt% at the lowest heating rate to 20.7 wt% at 35.2 °C min^{-1}, before recovering to 27.7 wt% at the highest heating rate.

The trend in solid yields can be explained by the reduction in reaction severity at the higher heating rate, resulting in insufficient reaction time to achieve full volatilisation of the biomass. This effect became less important at heating rates below 21.8 °C min^{-1}, as almost full solid conversion was achieved.

Oil and residue yields, in turn, appeared to be closely related. As heating rates increased from 10.1 to 35.2 °C.min^{-1}, the product distribution shifted from water phase residue towards bio-oil, but at the highest heating rate, the oil yields were at their lowest, with maximum water phase residue yields. The trend of increasing oil yields with increasing heating rates has already been reported by Faeth *et al*.,[47] and Garcia Alba *et al*.[27] but these publications did not include the corresponding water phase residue yields. Furthermore, neither of these two publications measured the reaction temperatures directly, and consequently the relative effect of heating rate and final reaction temperature on bio-oil yields cannot be clearly separated. However, Faeth *et al*. did employ a range of reaction times for each heating rate, and found that the optimized oil yields at lower heating rates were still significantly below the oil yields obtained at higher heating rates.

In a later publication by the same authors,[49] bio-oil yields were found to be higher when reducing the total reactor loading from 60 vol% to 10 vol%, whilst maintaining the same algae composition, reaction time and heating rate. Whilst these differences were explained in terms of changes to the apparent biomass concentration, as some of the water evaporates to generate the reaction pressure, an alternative (and more

likely) explanation is that the reaction became kinetically and heat-transfer limited as the reaction volume was increased. This could also explain the sharp drop in bio-oil yields at the maximum heating rate, observed in this work, as the reaction time is potentially too short to achieve full conversion of the water phase residue into bio-oil.

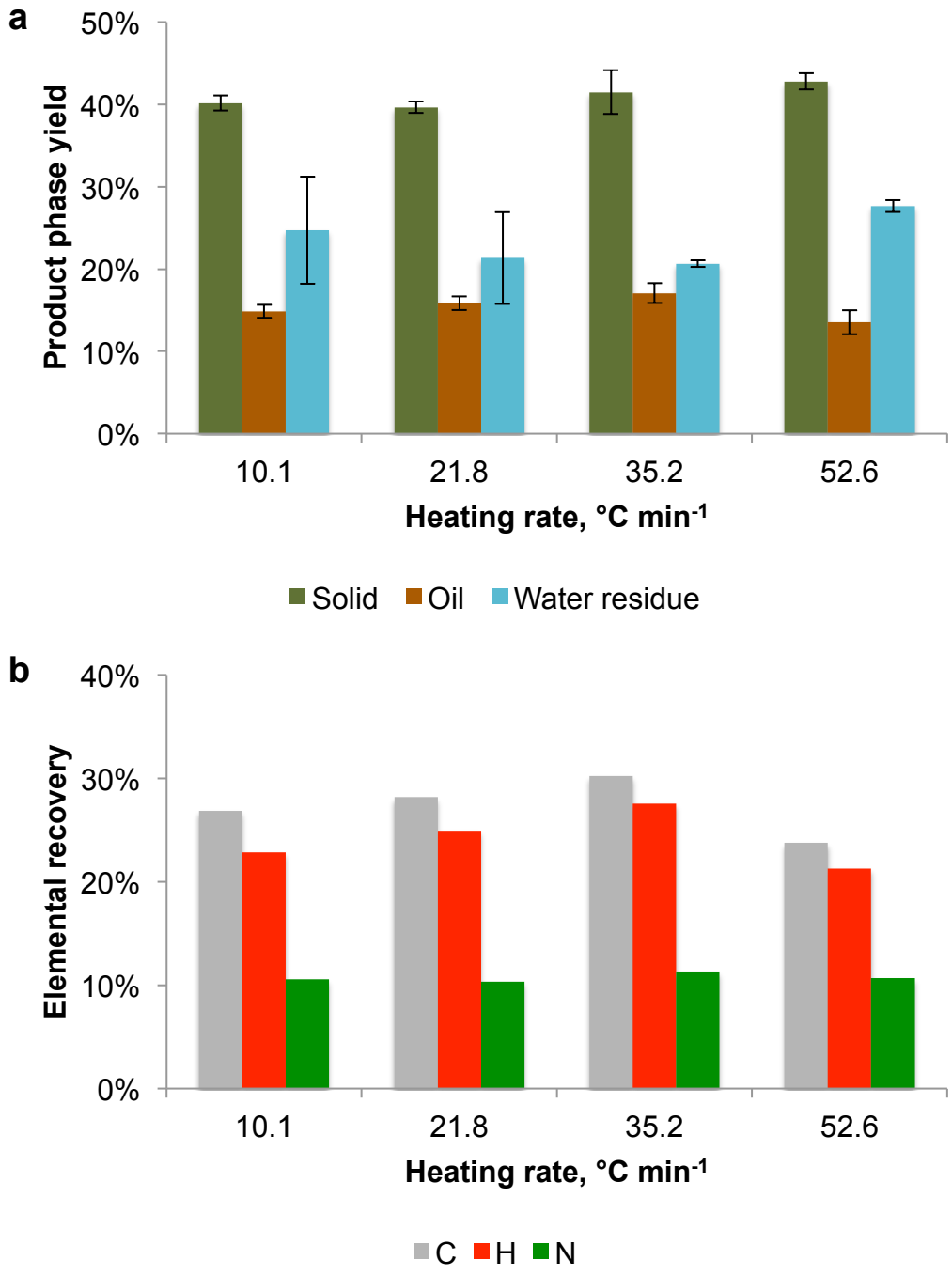

Figure 5-16: Effect of heating rate on the conversion of wastewater algae; (a) effect on product distribution, (b) effect on CHN distribution to bio-oil

As expected from the oil yields, the highest carbon and hydrogen retentions were obtained at the heating rate of 35.2 °C min^{-1}. The reduction in carbon, hydrogen and nitrogen retentions at lower heating rates can be attributed mostly to the reduction in oil yields, whilst the oil composition remained relatively constant. In contrast, the oil obtained at the highest heating rate had a significantly higher nitrogen content of 4.8 wt% than the oil obtained at a heating rate of 35.2 °C min^{-1} (4.0 wt%). Similarly to the results obtained at different reaction temperatures, this suggests that nitrogen containing compounds preferentially partition to the bio-oil at lower reaction severities, and subsequently become denitrogenated as the reaction temperature, or residence time, is increased.

5.3.2.3 Reaction mechanism

The trends in water phase residue and bio-oil yields suggest that the two product phases are closely related. Low reaction temperatures and very high heating rates appear to favour the formation of molecules that partition into the water residue, which are further converted into bio-oil as the reaction severity is increased. At the same time, some of the nitrogen incorporated at low temperatures and heating rates was removed via denitrogenation, reducing the nitrogen content of the oil and resulting in the formation of more volatile reaction products, which were not recovered in this project.

The results suggest a stepwise reaction mechanism; first the algae is broken up into water soluble compounds, which then further react to form the bio-oil and more volatile reaction products. This is consistent with the previously suggested Maillard type reaction pathways, where carbohydrates and proteins in the biomass were first decomposed into sugars and amino acids, which then further reacted via dehydration reactions to form heavier, water-insoluble compounds.[22, 38]

However, the algae decomposition reaction into intermediates and their subsequent reactions to form oil, water phase and gaseous products, can follow many different pathways and the ultimate product distribution

depends on the relative reaction kinetics between these pathways. Low heating rates would therefore favour reactions with lower activation energies, consuming a significant proportion of the reaction intermediates before the temperature rises to a level where higher energy reactions can occur. Based on the trends observed for bio-oil yields and heating rate, the reactions resulting in the formation of bio-oil appear to have higher activation energies than the reactions resulting in the formation of alternative product phases.

However, at the highest heating rates, the reaction time is insufficient to allow full conversion of the biomass or the reaction intermediates, resulting in a sharp drop off in bio-oil yield. Unfortunately, the transient batch reactors used in this study do not allow the combination of high heating rates with extended reaction times, potentially limiting the maximum bio-oil yield that can be obtained. Consequently, continuous systems, which combine higher heating rates with extended reaction times, may provide more favourable product distributions.

5.3.3 CONTINUOUS REACTIONS

The continuous reaction system was operated at four different temperatures (302 to 344 °C) and three different flowrates (3 mL min^{-1}, 5 mL min^{-1} and 7 mL min^{-1}). However, due to the limited amount of algae available, and the extended reaction time for each experiment, it was not possible to obtain repeats for each reaction conditions. Instead the standard deviation was calculated based on repeats for a single reaction setting with a temperature of 320 °C and a system flowrate of 7 mL min^{-1}.

In comparison to the batch system, where the reaction temperature is relatively uniform throughout the whole reactor, the temperature profile across the continuous system is more complicated. Furthermore, whilst only a single oil phase was recovered during batch reactions, several oil phases were recovered from the continuous system, and their relative distribution was found to depend strongly on the reaction conditions. Consequently, the system was first characterized before analysing the liquefaction data.

5.3.3.1 Temperature profiles

Three thermocouples, located at the bottom of the inner reaction tube (T1), at the reactor outlet (T2), and at the inlet to the liquid collection pots (T3) were used to monitor the temperature distribution across the continuous HTL system (Figure 5-10). The highest temperatures were recorded by T1, and consequently this temperature was used to control the system temperature. In order to achieve the desired reaction temperature, the furnace had to be set to a much higher value, ranging from 435 °C for the lowest flowrate of 3 mL min^{-1} (RT of 320 °C) to 500 °C for the highest system flowrate of 7 mL min^{-1} (RT of 340 °C).

Based on the location of thermocouple T1 at the outlet of the inner reaction tube, it was assumed that most of the heating occurred as the algae mix flowed down this tube. Consequently, the inner tube volume (33.5 mL) and the range of reaction temperatures (300 °C to 344 °C) and system flowrates (3 mL min^{-1} to 7 mL min^{-1}) could be used to estimate the range of heating rates as 28.8 °C min^{-1} to 67.6 °C min^{-1}.

Similarly, the residence times of the hot reagents/products in the outer tube volume (122.5 mL) was calculated to have varied between 17.7 and 41.8 minutes, even though temperature drops ranging from 45 to 58 °C were recorded between the bottom and outlet of the reactor. These temperature drops were attributed to heat exchange between the hot reaction products flowing up the reactor annulus and the cold algae feed flowing down the inner tube, as well as some external heat losses. The highest temperature drops were observed for the highest system flowrate, probably as a result of reduced reactor residence times, reducing the degree of convection and temperature equilibration across the reactor.

Significant further cooling occurred as the reaction products flowed from the reactor outlet towards the inlet of the product collection pots, and once again the temperature drop was strongly related to the system flowrates. However, in this case, the highest temperature drop of 217 °C was obtained at the lowest flowrate (3 mL min^{-1}) compared to a temperature drop of only 147 °C for the highest flowrate (7 mL min^{-1}).

This is the result of the increased product residence times within the reactor outlet piping as the flowrate is reduced, resulting in increased heat loss to the atmosphere.

5.3.3.2 Product distribution

For all reactions, the solids recovered from the reactor accounted for at least 95 % of all recovered solids, with little correlation to the selected reaction conditions (temperature and flow). This suggests that gravity settling was highly effective in the recovery of this fraction.

The oil product in turn was collected as three different fractions: (1) oil collected from the outlet during system operation; (2) oil recovered from the system piping and liquid collection pot walls; (3) oil recovered from the reactor itself. The relative distribution of the first two fractions was found to be highly dependent on T3, the temperature at the collection pot inlet (Figure 5-17a).

Increasing this temperature resulted in an almost linear increase in the oil fraction collected from the outlet from 29.8 % at 56 °C to 55.9 % at 126 °C. Conversely, the oil recovered from the reactor outlet piping decreased by a similar amount, from 46.1 % to 19.9 %, over the same temperature range. This suggests that oil recovery from the system outlet was strongly dependent on the pipework temperature and may be related to the increased oil viscosity and reduced miscibility with water as the collection temperature is decreased. This is also consistent with the problems encountered with the initial design, where the low collection temperatures resulted in the accumulation of oil within restrictions in the flow path, resulting in almost full blockage of the system.

It should, however, be noted that all experiments were conducted with approximately the same amount of algae (1 L of a 5 wt% slurry). Therefore, it is unclear, whether oil accumulation within the system pipework was linear over the entire reaction period, or whether oil accumulation reached a saturation point, after which all additional oil exited from the system. This could be important as continuing oil accumulation would eventually result in a reduction in pipe diameter

leading to flow restrictions, whereas in the latter case, the system would eventually reach steady state.

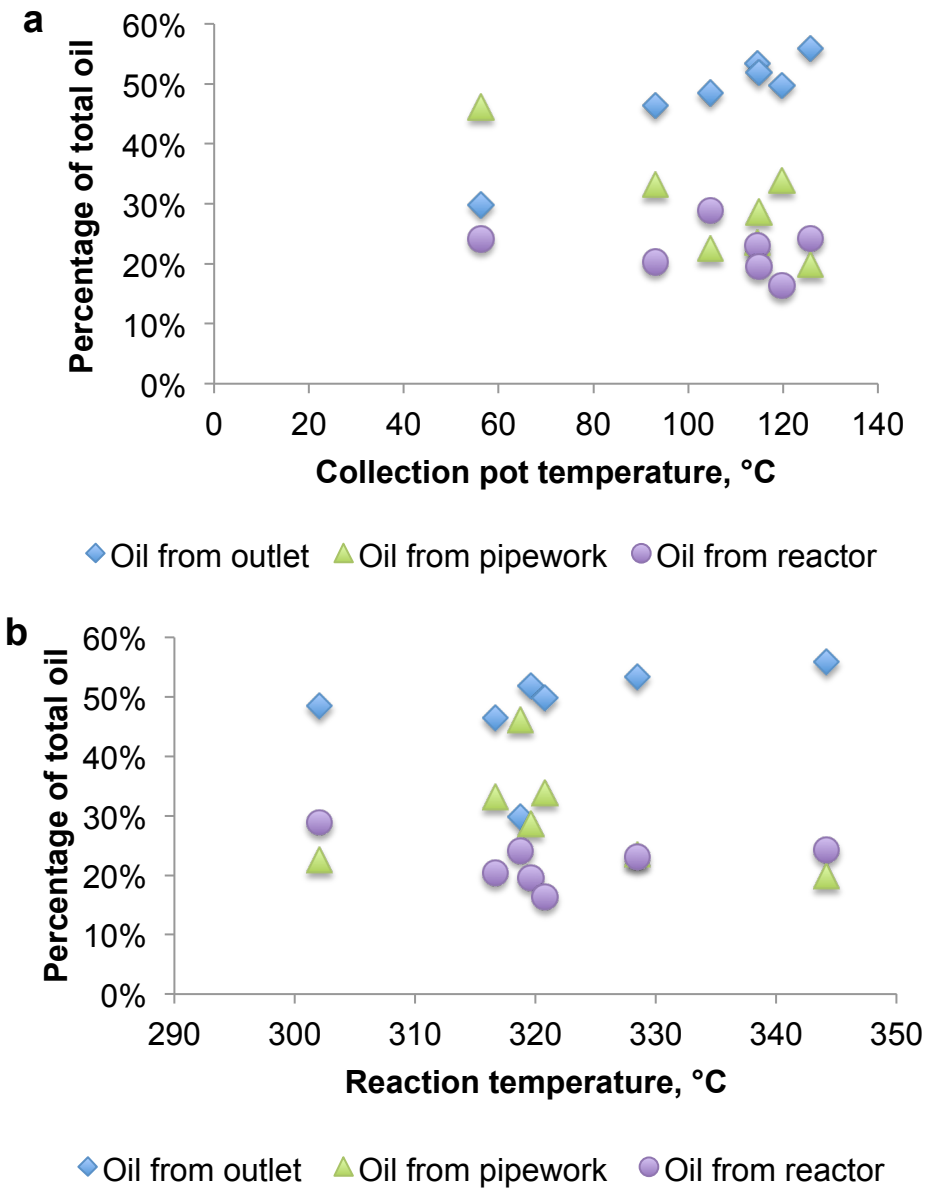

Figure 5-17: Effect of (a) the product collection temperature (T3) and (b) reaction temperature (T1), on oil recovery from the HTL system

In contrast to the oil recovered from the pipework and outlet, the oil collected from the reactor showed no correlation to the collection pot temperature. Instead, this fraction was found to decrease slightly with increasing reaction temperatures (Figure 5-17b). Similar to the relationship between pipe temperature and oil collection from the outlet, the retention of oil within the reactor could be viscosity related, i.e. higher reaction temperatures reduce the viscosity of the oil, reducing its

retention within the reactor. However, given the large difference between the minimum reactor outlet temperature (248 °C) and the maximum collection pot inlet temperature (126 °C), viscosity effects appear less likely. Instead, the differences in oil recovery from the reactor could be the result of chemical differences of the oil formed in the first place. Higher reaction temperatures would be expected to result in a higher degree of cracking, forming a higher fraction of lighter products with lower viscosity. The oil remaining in the reactor is therefore expected to consist mostly of heavy and highly viscous products, whereas most of the lighter components are removed during the reaction itself and subsequent water purging.

As the partitioning between oil stuck in the pipework and oil recovered from the outlet appeared to depend mostly on the collection temperature, rather than chemical differences in the oils, these two fractions were combined into a single, light-oil phase. The reactor oil in turn was kept as a separate fraction for two reasons. Firstly, its chemical nature appeared significantly different to the other two oil phases, and secondly, this oil could not be easily recovered from the system during continuous flow, but required full dismantling of the system and extensive solvent washing of the solid product phase, which may be impractical in an industrial set-up.

5.3.3.3 Effect of reaction temperature

The effect of reaction temperatures on the product distribution was studied at a constant system feed flow rate of 7 mL min^{-1} (Figure 5-18a). Solid yields generally decreased with increasing reaction temperatures, although there was a high degree of experimental uncertainty, possibly related to the difficulty of recovering all of the reaction solids from the bottom of the reactor. Water phase residue yields in turn displayed a much clearer trend, decreasing steadily from 19.8 wt% at 302 °C to 13.4 wt% at 344 °C. Finally, the trends in oil yields were more complex. The maximum heavy oil yields (5.8 wt%) were obtained at the lowest reaction temperature, but whilst this fraction was lowest at 320 °C, it started to increase again as the temperature was raised further.

Conversely, the lowest light oil yields were obtained at the lowest reaction temperature of 302 °C (14.3 wt%), and remained reasonably constant at 15 to 16 wt% at all other temperatures.

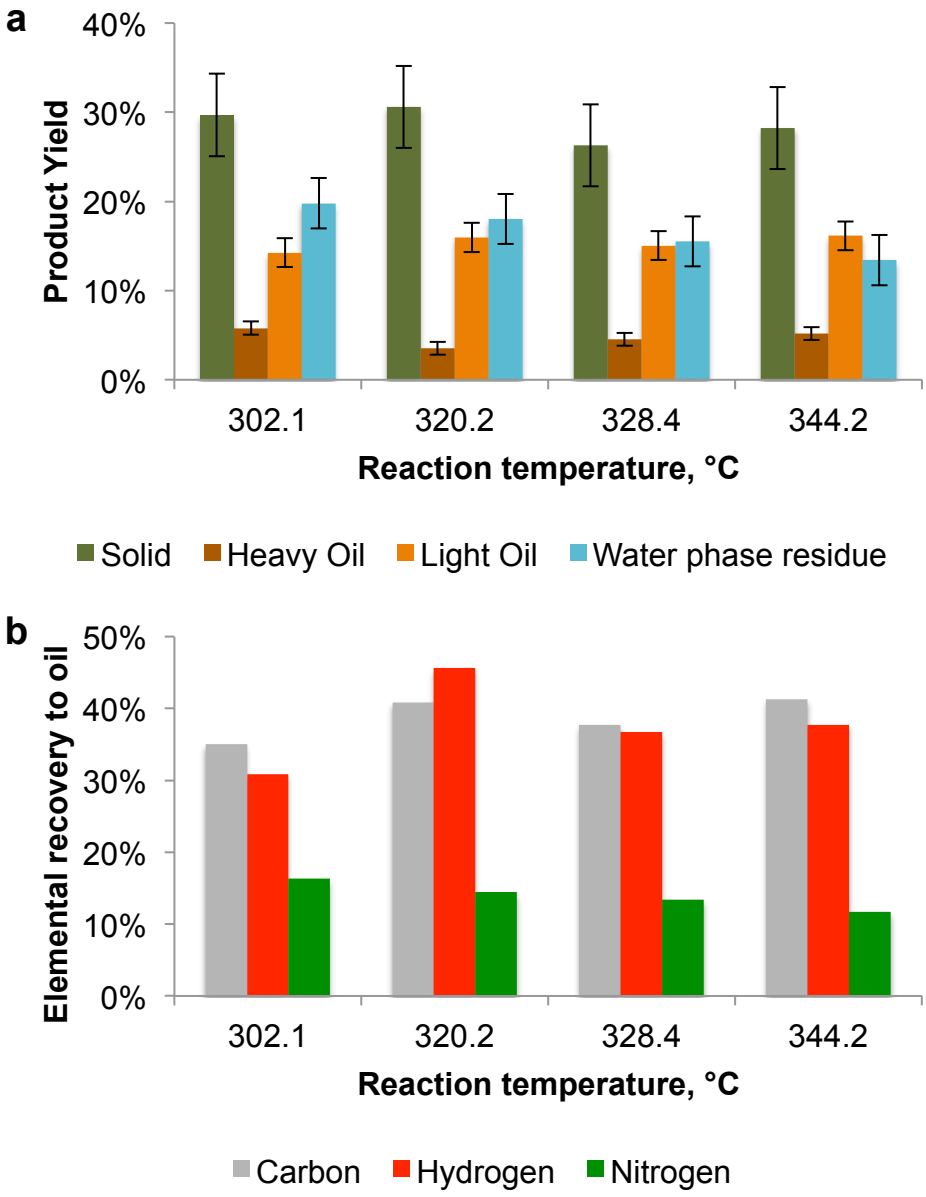

Figure 5-18: Effect of reaction temperature on the continuous liquefaction of wastewater algae; (a) overall product distribution, (b) CHN retention in bio-oil

The correlation between solid and water phase residue yields with reaction temperature is consistent with the findings from the batch study, and can be attributed to increased biomass conversion at higher reaction temperatures. In contrast, the residue and total oil yields show little correlation, and the reduction in water phase residue yields (19.8 wt% to 13.4 wt%) can be mostly attributed to a decrease in the overall mass

balance closure from 69.5 wt% to 63.0 wt%, suggesting the formation of more volatile reaction products.

The initial reduction in heavy oil yield from 5.8 wt% to 3.5 wt%, as reaction temperatures were increased from 302 °C to 320 °C, closely matched the increase in light oil yields from 14.3 wt% to 16.0 wt% over the same temperature range. This could be the result of increased cracking reactions of heavy oil components to form lighter compounds, which were carried over into the light oil phase. Conversely, the subsequent increase in heavy oil yields at higher reaction temperatures could be caused by the polymerisation of more stable reaction intermediates, or further conversion of the solid or aqueous phase product. In all cases, the net formation of light oil appeared to be complete at temperatures above 320 °C, although it is possible that additional oil formation was balanced by gasification, denitrogenation and deoxygenation reactions, which would improve the oil quality at higher reaction temperatures. It is also interesting to note, that in contrast to the batch system, oil yields did not reduce at higher reaction temperatures. This is particularly surprising as the continuous reaction system provides longer reaction times, which would be expected to favour a higher amount of cracking reactions. Consequently, it appears that these effects are outweighed by an increase in oil formation, either as a result of faster heating rates, or the extension of reaction times.

To investigate this in more detail, the carbon, hydrogen and nitrogen balance to the oil phase was calculated from the elemental analysis of the two bio-oil fractions (Figure 5-18b). Increasing the reaction temperature from 302 °C to 320 °C resulted in a significant increase in carbon retention from 35.0 % to 40.8 %, but at higher temperatures the carbon retention remained approximately constant. Nitrogen retention, in turn, reduced steadily from 16.3 % at 302 °C to 11.7 % at 344 °C, which is opposite to the trend observed during the batch experiments. This could suggest that the extended residence time in the continuous flow reactor allowed more denitrogenation reactions to take place. Finally, the hydrogen retention was highest at 320 °C and dropped sharply as the

reaction temperature was increased further. This can be explained by the participation of hydrogen in the denitrogenation pathway to form ammonia and is consistent with the steady increase in the yield of ammonia in the water phase from 1.7 wt% to 3.0 wt%, corresponding to a nitrogen recovery of 23.2 % and 41.1 %, respectively, as the reaction temperature was raised from 302 °C to 344 °C.

5.3.3.4 Effect of system flowrate

The effect of the system flowrate on the product distribution was studied at three different values, 3 mL min^{-1}, 5 mL min^{-1} and 7 mL min^{-1}, and at a constant reaction temperature of 320 °C (Figure 5-19a). Only a few publications investigated the effect of flowrate on the continuous liquefaction of algae in the past, with both Biller *et al.*[69] and Jazrawi *et al.*[44] obtaining higher oil yields at higher system flowrates.

Increasing the flowrate resulted in a clear increase in solid yields from 27.7 wt% at 3.0 mL min^{-1} to 35.2 wt% at 6.9 mL min^{-1}. Residue yields increased from 13.8 wt% to 20.5 wt% for a flowrate increase from 3.0 to 5.0 mL min^{-1}, but remained constant as the flowrate was increased further. In contrast, both the heavy and light oil yields were lowest at the medium flowrate of 5.0 mL min^{-1} (3.6 % and 13.9 %, respectively). Whilst the maximum light oil yield was obtained at 6.9 mL min^{-1} (17.6 %), the heavy oil yield was highest at the lowest flowrate of 3.0 mL min^{-1} (4.9 %).

The trend in solid yields is similar to the one observed for the batch system, where higher heating rates produced more solid, probably as a result of reduced reaction times. However, all the solid yields from the continuous system (maximum of 35.2 wt%) were much lower than those from the batch reactor (minimum of 39.7 wt%). This is unsurprising, as even at the fastest flow rate, the reaction time in the continuous system (17.8 min) exceeded the reaction times obtained with the batch system. Furthermore, the solid products remained in the reactor for the entire period of system operation, resulting in solid reaction times of several hours.

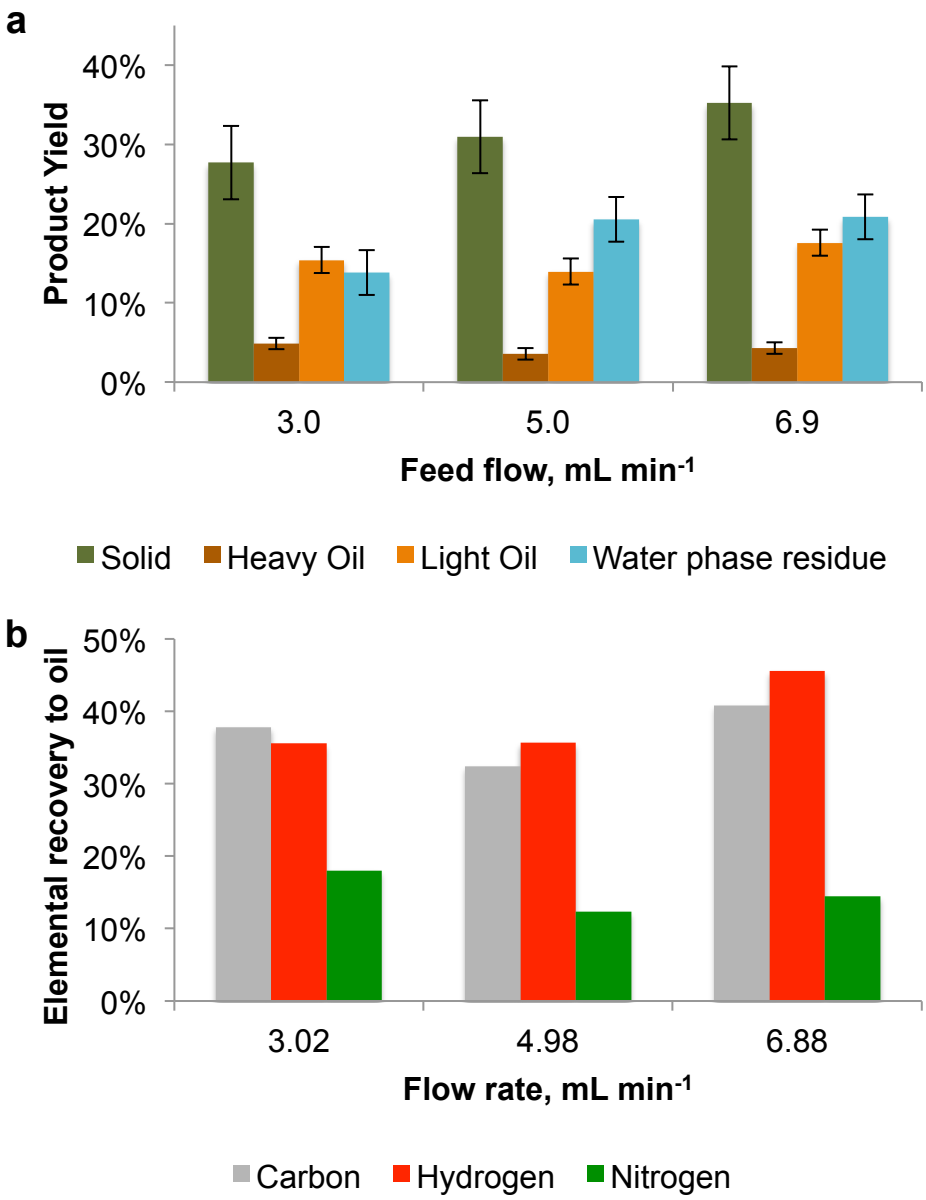

Figure 5-19: Effect of feed flowrate on the continous liquefaction of wastewater algae; (a) overall product distribution, (b) CHN retention in bio-oil

Indeed, on this basis, the strong correlation between system flow and solid yields is surprising, and suggests that it is not related to the total solid residence time. Instead, higher heating rates could disrupt the decomposition pathway of the biomass, resulting in the formation of more stable solid products. Alternatively, the solid yields could be equilibrium controlled by the product concentration in the aqueous phase. At high flowrates the residue concentration in the water phase was higher, inhibiting the full conversion of the solid. Finally, whilst the reaction temperature was determined at the outlet of the inner tube, the temperature at the bottom of the reactor could be significantly higher,

particularly at lower flowrates with lower turbulence. Consequently, the increased solid conversion could be related to the presence of hot spots within the reactor, catalysing polymerisation reactions.

Like the solid yields, the water phase residue yields obtained from the continuous reactor (13.8 wt% to 20.9 w%) were significantly lower than those from the batch reactor (20.7 wt% to 27.7 wt%). Furthermore, increasing the system flowrate, and therefore the heating rate, caused the residue yields to increase, whereas for the batch system, the residue yields tended to decrease with increasing heating rate. These opposing trends suggest that whilst high heating rates may have favoured the initial conversion of residue into oil product, the remaining water soluble compounds were more stable, requiring extended reaction times to break down further.

A similar explanation can be used to explain the complex trend in oil yields. The highest overall oil yields were obtained at the fastest system flowrate, and could be associated with the conversion of the less stable water-soluble intermediates produced at high heating rates. However, the reaction times were insufficient to allow full conversion of the remaining, more stable, aqueous phase products. Reducing the system flowrate to 5 mL min^{-1}, reduced the heating rates and resulted in the formation of more stable intermediates, which were less readily converted into bio-oil. However, reaction times were still insufficient to allow full conversion of these more stable intermediates into bio-oil. Finally, at the lowest system flowrate, full conversion of the more stable reaction intermediates was achieved, resulting in an increase in the oil yield.

Based on this explanation, the oil formed from the more stable reaction intermediates would be expected to have a different composition to the oil formed at high heating rates, and to verify this, the elemental retention of C, H and N to the oil phase was calculated (Figure 5-19b). Indeed, the oil formed at a flowrate of 3.0 mL min^{-1} contained a lower hydrogen and a higher nitrogen content than the oil phases formed at the higher system flowrates. Even though the carbon recovery of 37.8 % was higher than at the medium flowrate, it was still lower than the carbon recovery at

6.9 mL min^{-1} (40.8 %). Combined with a much higher hydrogen, and lower nitrogen recovery, the best results, both in terms of oil yields and quality, were obtained at the highest system flowrate. Even the yields of light oil on their own (17.6 %), exceeded the total oil yields from the batch reactor, which demonstrates the advantage of continuous over batch processing. Therefore, research on continuous flow reactors, does not only provide results which are much more applicable to large-scale industrial processing, but also has the potential to yield improved bio-oil yields and product compositions.

5.4 CONCLUSIONS

This chapter described the design of an inexpensive, laboratory scale continuous liquefaction system for the HTL of microalgae obtained from a wastewater remediation process. The design employed high pressure nitrogen as the driving force to push algae through the system, and thereby eliminated the need of the more expensive mechanical pumps typically used in the literature.

Significant operational problems faced during system commissioning required an extensive reconfiguration of the system, but provided important lessons for the future design of these systems. Most notably, maintaining a minimum product collection temperature of around 60 °C was found to be necessary to prevent bio-oil solidification and the formation of blockages within system restrictions. This was achieved by recovering the liquid products from two nitrogen-filled liquid collection pots, and controlling the system flow indirectly, via the outflow of nitrogen from the system. Further modifications to control the outflow of liquid via level controllers in the collection pots, whilst regulating the system back-pressure via the outflow of reaction gases from this system, could make the design more industrial relevant.

The initial design of the HTL reactor, consisting of a simple upflow plug reactor, was also found to be inadequate for achieving smooth flow through the system. This was attributed to the accumulation of solids within the reactor tube, possibly as a result of insufficient liquid flow

velocities. The modified design included solid collection within the reactor itself, which eliminated the formation of blockages, whilst maximising solid conversion.

Results from the liquefaction of wastewater algae in the batch system confirmed previous work in the literature, which suggested that increased heating rates could help to improve bio-oil yields. This was attributed to the competition of reactions resulting in oil formation from aqueous phase products with alternative reactions, producing solids, more stable intermediates or gas products. However, at very high heating rates, bio-oil yields dropped-off sharply and this was attributed to the short reaction times, which may not enable full biomass conversion.

These limitations were not present within the continuous reaction system, which combined fast heating rates with extended reaction times. Consequently, this system produced higher bio-oil and lower solid and water phase residue yields than the batch system. The effect of system flowrate on bio-oil yield appeared to be more complex, and this was explained by a balance between the impact of heating rates and reaction times on the HTL reaction. However, the highest bio-oil yields were obtained for the highest system flowrate, consistent with previous literature findings made in the literature.

Overall, the project objectives were met to design a low-cost laboratory system, that was able to process an algae slurry containing a biomass loading of 5 wt%. The system yielded a significantly different product distribution to a batch system, which reaffirmed the importance of conducting research under continuous flow conditions, which are more representative of large-scale industrial processes. Furthermore, product yields were significantly enhanced, due to the combination of high heating rates with prolonged reaction times, which is difficult to achieve within batch systems.

CHAPTER 6

CATALYTIC UPGRADING OF HTL BIO-OIL

6.1 INTRODUCTION

The previous chapter described the design of a cheap, laboratory scale, continuous hydrothermal liquefaction system, which was tested for the conversion of microalgae obtained from wastewater treatment. This system combined high heating rates, required to minimise side reactions leading to the formation of undesired solid or gas products, with extended reaction times, ensuring full conversion of the algae biomass. As a result, the system managed to produce much higher oil yields than a batch reactor, operated at equivalent reaction temperatures and algae loadings.

Even so, the bio-oil is still a long-way off being a good fuel, and requires significant upgrading to reduce its viscosity, smell, colour and heteroatom content. Particularly the high nitrogen content, ranging from 3.4 wt% to 6.0 wt%, is a challenge, as it lies significantly above the acceptable thresholds of the catalysts used in conventional crude oil refineries (around 0.25 wt%).[70] Despite this, surprisingly little research has been done on the upgrading of the bio-crudes produced by the liquefaction of microalgae,[196] and has been mostly confined to noble metal and sulphided transition metal catalysts.[66, 69, 76, 81, 83, 84, 87-90] However, noble metal catalysts are expensive, whereas transition metal sulphides are more active for the removal of sulphur rather than nitrogen. Furthermore, in order to maintain their activity, the transition metal sulphides require sulphur-containing compounds, not normally present within the algae bio-oils.[81]

An alternative group of catalysts are transition metal phosphides, particularly, Ni_2P, which have been found to display high activities for the denitrogenation of model compounds and have attracted increasing attention for the hydrodenitrogenation of petroleum feedstocks.[128-130, 132] Unlike sulphides, they adopt spherical particles rather than layered structures and may therefore allow greater access to active corner and edge sites on the crystallite surfaces,[129, 130] whilst the presence of P protects the catalysts from deactivation. Despite this, to the knowledge of

the author, these catalysts have not yet been applied to the upgrading of bio-oil produced by the HTL of algae.

Most transition metal phosphides have been either supported on silica[135, 137] or used in the bulk phase,[144, 197, 198] but increasingly alternative supports such as alumina,[150] MCM-41[127, 146] and zeolites[129, 145] have been tested. Aluminium containing supports possess additional acid sites which may help to protonate the nitrogen group, facilitating the cleavage of the aliphatic C-N bonds via E_2 elimination reactions.[123, 124] The acid sites may also help catalyse cracking reactions to break up large polyaromatic compounds into lighter oil fractions,[145] thereby reducing the oil viscosity.

However, the synthesis of phosphide catalysts on aluminium containing supports is much more difficult, due to the strong interaction between aluminium and phosphates to form $AlPO_4$ during calcination.[108] Because of this, large excesses of P[146, 147] and much higher reduction temperatures are required[136, 199] to form the desired Ni_2P phosphide phase, resulting in poorer metal dispersion and adverse effects to the support structure.[199]

In this chapter, a range of Y zeolite supported nickel phosphide catalysts were synthesized and tested for the upgrading of the algal bio-crude produced from the continuous liquefaction of the wastewater derived algae.

During the synthesis stage, the effect of using different phosphorus precursors and impregnation methods was investigated to obtain materials that retained the zeolite structure and contained well-dispersed nanoparticles with the desired Ni_2P metal phase. Furthermore, different zeolite counterions and Si/Al ratios were used to moderate the metal/support interactions and change the acidity of the resulting catalyst. Finally, the effects of using more open zeolite structures, obtained via base-leaching of the supports, were investigated.

Prior to using the catalysts for the upgrading of the bio-oil, they were tested for the denitrogenation of quinoline, a widely studied

denitrogenation model compound. Based on these results, the most promising catalysts were selected and applied to the upgrading of the light bio-oil phase, obtained from the continuous HTL of the wastewater algae.

6.2 CATALYST SYNTHESIS

The main objective of the catalyst synthesis was to obtain well-dispersed nanoparticles containing the active Ni_2P phase. Secondary objectives were to retain the structure of the zeolite supports and obtain a range of materials with different support properties, which may affect the denitrogenation pathway.

All catalysts synthesised in this work were supported on Y zeolites, containing the FAU framework structure. This zeolite was chosen as it is already widely used as a catalyst support within the refining industry and is therefore available in commercial quantities.

The properties of the support were modulated by changing the zeolite counterion, affecting the acid site strength, varying the Si/Al ratio, determining the total number of acid sites, and exposing the zeolite to base-treatment, in order to introduce additional porosity and change its surface properties.[200]

In addition, the synthesis procedure applied two different sources of P (ammonium phosphate and ammonium hypophosphite), different Ni/P ratios and tested three different methods of impregnation.

Post impregnation, all catalysts were dried at 120 °C, calcined at 400 °C and reduced under flowing hydrogen at 550 °C. Post reduction, the catalysts were passivated in 1 % O_2/N_2.

6.2.1 SUPPORT PREPARATION

All supports were prepared from three commercial zeolites: NH_4^+ Y and Na^+ Y zeolites, both containing a Si/Al ratio of 2.56, and low aluminium H^+ Y (H^+Y_{low}) zeolite, with a Si/Al ratio of 15. K^+ Y and Ni^{2+} Y were prepared by ion exchange of the Na^+ Y precursor with solutions of KNO_3

and $Ni(NO_3)_2.6H_2O$ solutions, respectively, whereas H^+ Y was obtained from the calcination of NH_4^+ Y at 550 °C for 5 hours. The base-treated zeolites were obtained from a collaboration with the Department of Chemistry.[200] These zeolites were prepared via base leaching with solutions of NaOH and tetrapropyl ammonium bromide of the NH_4^+ Y and the low-aluminium H^+ Y_{low} zeolite precursors.

6.2.1.1 Characterization of ion-exchanged/calcined zeolites

Calcination of the commercial NH_4^+ Y zeolite resulted in a weight loss of 27.6 %, significantly above the nominal ammonia loading of 10 wt%. This additional weight loss can be attributed to the removal of absorbed water, which was previously determined to be around 17 wt% for the same type of zeolite.[201] Based on the nominal Al_2O_3 content of 22 wt%, the NH_4^+/Al ratio of the commercial support can be calculated as 1.29. The support also contained a residual Na_2O content of 2.5 wt%, corresponding to a Na^+/Al ratio of 0.19. Therefore, a significant excess of NH_4^+ appeared to be present within the zeolite, which could be adsorbed on its surfaces, or deposited within the zeolite pores.

Table 6.1: Properties of zeolites obtained by ion exchange and calcination of commercial precursors

Label	Molar ratios vs Al				BET Surface area, $m^2\ g^{-1}$	Cubic unit cell parameter, Å
	Na^+	K^+	Ni^{2+}	NH_4^+		
Na^+ Y	0.97*	-	-	-	888.2	24.24
NH_4^+ Y	0.19*	-	-	1.29*	764.5	24.61
H^+ Y	0.19*	-	-	-	843.9	24.47
K^+ Y	0.36	0.61	-	-	780.8	24.55
Ni^{2+} Y	0.38	-	0.30	-	802.6	24.60

** Based on supplier information*

According to supplier's information, the commercial Na^+ Y zeolite contained 13 % Na_2O and 22 % Al_2O_3, corresponding to a Na^+/Al ratio of 0.97. Following ion exchange, the zeolites were recovered by centrifugation and washed with D.I. water, and the water phase was analysed using a sodium ion electrode, calibrated against sodium nitrate solutions. Based on this analysis, it was possible to calculate the counter-

ion to aluminium ratios of the exchanged materials (Table 6.1). In both cases, the single pass ion exchange replaced approximately 60 % of the sodium with K^+ or Ni^{2+}.

This compares to slightly higher exchange ratios, of 77 % for K^+Y and 64 % for Ni^{2+}, obtained from SEM-EDX analysis. Elemental mapping by TEM of the Ni-exchange zeolite indicated a uniform distribution of Ni across the entire zeolite crystal (Figure 6.1).

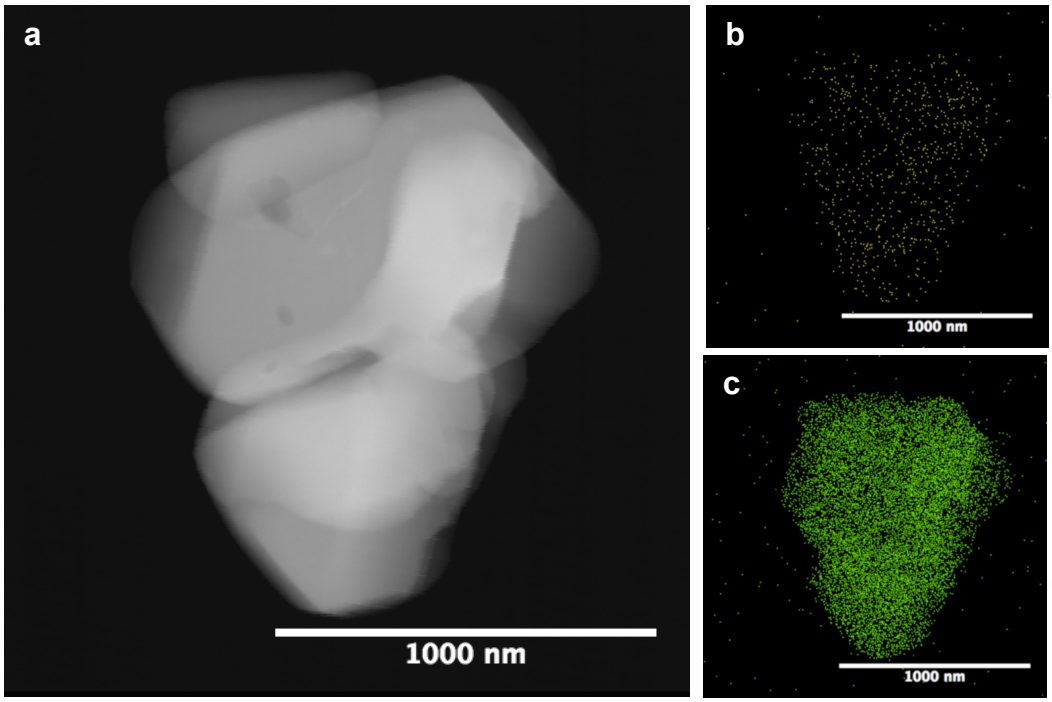

Figure 6.1: Elemental mapping by TEM of Ni^{2+} Y zeolite. (a) Electron image, (b) P distribution, (c) Ni distribution

Analysis by X-ray powder diffraction confirmed that the Y zeolite structure was maintained for all of the calcined and ion-exchanged supports (Figure 6.2). The diffraction patterns were used to calculate the zeolite unit cell parameters, which were found to range from 24.24 Å for Na^+ Y to 24.61 Å for NH_4^+ Y (Table 6.1). Calcination of NH_4^+ Y to form H^+ Y resulted in a decreased unit cell size whereas ion exchange of Na^+ Y with K^+ and Ni^{2+} increased the unit cell size. Therefore, for both treatment types, the unit cell sizes followed the expected trend of increasing for larger counter-ions. In contrast, the H^+ Y zeolite had a larger unit cell size than the Na^+ Y zeolite, despite containing a smaller counter-ion. This could be related to small differences in the two commercial precursors,

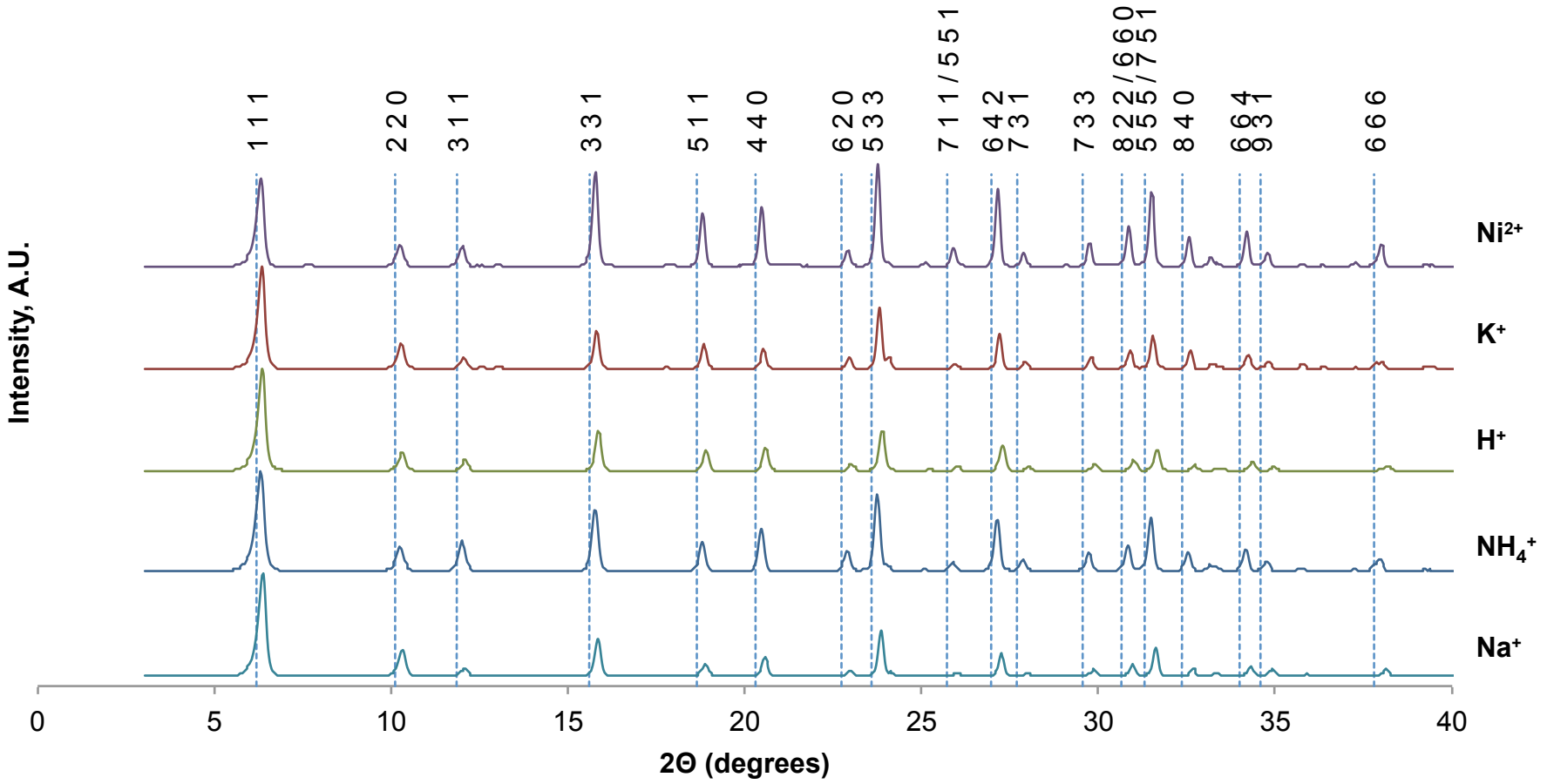

Figure 6.2: X-ray diffraction patterns of zeolites produced by calcination and ion exchange of commercial precursors

such as variations in the Si/Al ratios, as well as changes in the zeolite structure as a result of consecutive ion exchange and thermal treatment to produce NH_4^+ Y and H^+ Y, respectively.

The BET surface areas obtained from nitrogen adsorption experiments ranged from 764.5 m^2 g^{-1} for NH_4^+ Y zeolite to 888.2 m^2 g^{-1} for Na^+ Y zeolite. Ion exchange with K^+ and Ni^{2+} caused a slight decrease in surface area, possibly as a result of introducing a larger cation. In contrast, calcination of the NH_4^+ Y zeolite increased the surface area, due to the smaller size of the remaining H^+ ion and the loss of excess ammonium from the zeolite surface.

6.2.1.2 Characterization of base-treated zeolites

Two series of base-treated zeolites were prepared using the commercial NH_4^+ Y and H^+Y_{low} precursors. Each treatment was conducted with constant concentrations of NaOH (0.38 g g^{-1}) and either low concentrations of TPABr (0.2 g g^{-1}) or high concentrations (0.92 g g^{-1}), denoted as mild (MT) and harsh chemical treatment (HT), respectively. (The untreated zeolites were labelled NT for no treatment.) One of the objectives of base-leaching was the introduction of additional porosity and previous analysis identified the formation of pores within the 2-17 nm range for the chemically treated H^+Y_{low} zeolite supports.[200]

X-ray powder diffraction confirmed that the zeolite structure was maintained for both sets of zeolites and under both treatment conditions (Figure 6.3). The unit cell diameters for the H^+Y_{low} zeolites were significantly smaller than those of the NH_4^+ Y zeolite series (Table 6.3). This could be the result of the reduced number of counterions, as well as the reduced counter-ion size.

SEM-EDX analysis was applied to determine both the Si/Al ratio and the Na^+/Al ratio (Table 6.3). Whilst the Si/Al ratio for the NH_4^+ precursor remained relatively constant at around 2.5, the ratio for the H^+Y_{low} precursor reduced significantly from 17.87 without treatment to 11.53 after harsh base treatment. This analysis is consistent with previous findings showing that silicates were preferentially removed over

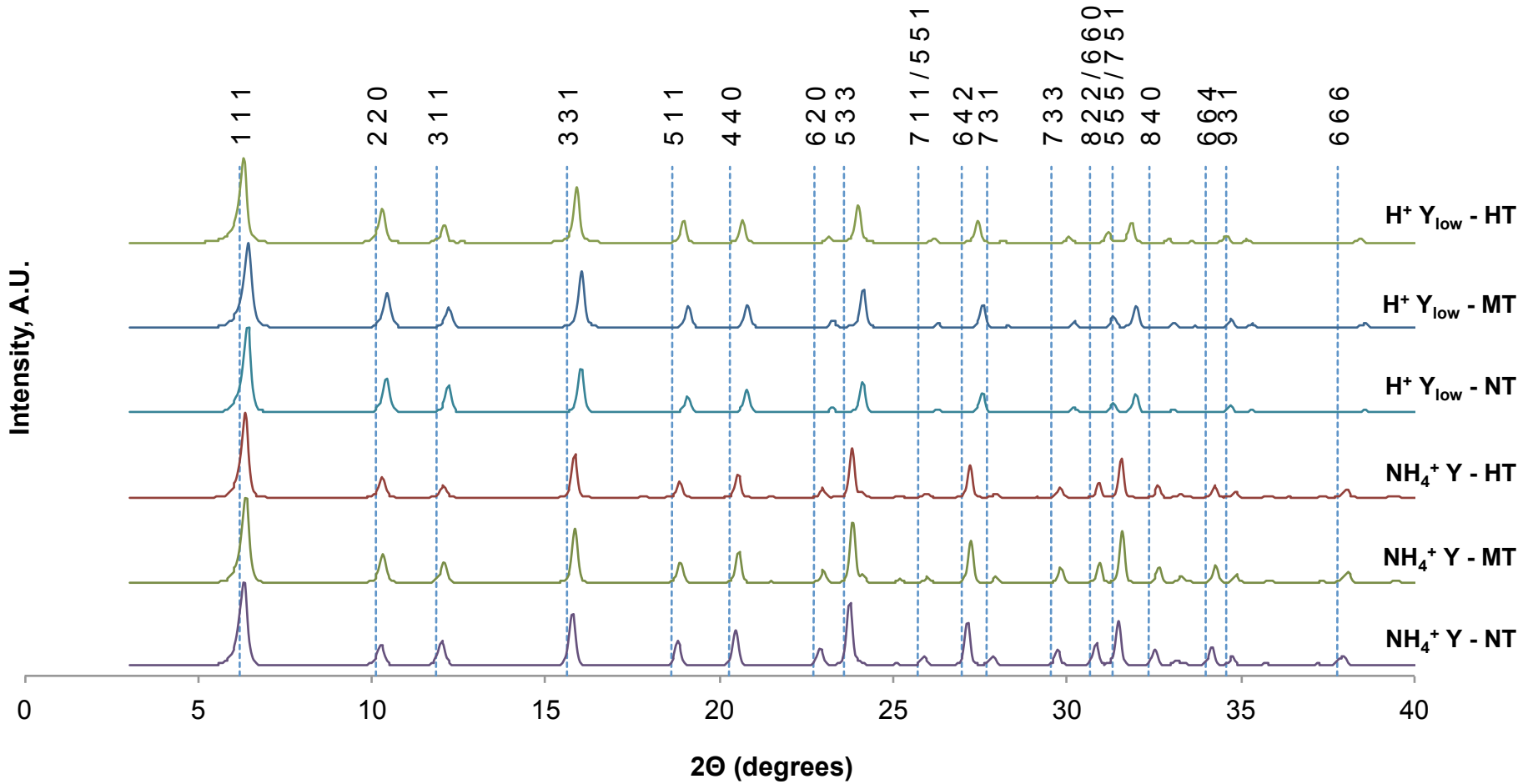

Figure 6.3: X-ray powder diffraction patters of NH_4^+ Y and low-aluminium H^+ Y_{low} zeolites, either with no treatment (NT), mild chemical treatment (MT) with 0.2 g g^{-1} TPABr, or harsh chemical treatment (HT) with 0.92 g g^{-1} TPABr.

aluminates.[202] However, at higher aluminium contents the overall stability of the catalyst appeared to be increased, resulting in a reduced loss of silica.

Both of the precursors contained only small quantities of sodium, probably left over from the initial zeolite synthesis. Following base-treatment, the Na^+/Al ratio for both zeolites increases above unity, suggesting significant ion exchange of the zeolite with the Na^+ ions of the sodium hydroxide solution. This in turn could have a significant impact on the properties of the resulting catalysts.

Table 6.2: Properties of chemically modified zeolites

Name	Si/Al ratio (from SEM-EDX)	Na^+/Al ratio (from SEM-EDX)	BET Surface area, $m^2\ g^{-1}$	Cubic unit cell parameter, Å
NH_4^+ Y-NT	2.51	0.19	764.5	24.61
NH_4^+ Y-MT	2.61	1.07	897.8	24.52
NH_4^+ Y-HT	2.49	1.07	855.6	24.53
H^+ Y_{low}-NT	17.87	0.02	919.1	24.23
H^+ Y_{low}-MT	12.16	0.73	683.8	24.33
H^+ Y_{low}-HT	11.53	1.23	716.2	24.22

Finally, base treatment of the NH_4^+ Y zeolite resulted in an increase in the BET surface area, whereas the area reduced for the H^+ Y_{low} zeolite series. A potential explanation for the increase in area for NH_4^+ Y derived zeolites could be the removal of excess NH_4^+ absorbed on the zeolite surface, as well as exchange of ammonia with the smaller sodium ions. In contrast, for the H^+ Y zeolites, a loss of zeolite structure, as a result of silica dissolution, and the introduction of the larger Na^+ counterions could have caused the reduction in surface area.

6.2.2 Effect of phosphorus precursor

The most commonly used method of synthesizing metal phosphide catalysts in the literature is the reduction of phosphates together with a metal salt in the presence of hydrogen.[105, 127, 150] However, lower-oxidation state phosphorus precursors, such as phosphites and

hypophosphites are increasingly used to lower reduction temperatures, prevent sintering and form more dispersed catalysts.[137, 144]

This section investigates the benefit of using ammonium hypophosphite rather than ammonium phosphate for the synthesis of H^+Y zeolite supported Ni_2P catalysts. Both sets of catalysts were prepared by successive incipient wetness impregnations with aqueous solutions of nickel nitrate and the phosphorus precursor, followed by drying at 120 °C, calcination at 400 °C and reduction at 550 °C or 650 °C. For all catalysts, the target Ni loading was kept constant at 5 wt%, whereas two different Ni/P ratios were applied for each P precursor.

The XRD patterns for the catalysts prepared with ammonium hypophosphite and a Ni/P ratio of 0.53 do not exhibit the characteristic Ni_2P peaks at either the lower (550 °C) or the higher (650 °C) reduction temperature (Figure 6.4). Instead, strong signals for metallic nickel at 2Θ values of 44.5 [1 1 1], 51.8 [2 0 0] and 76.4 [2 2 0] are apparent. Ni_2P peaks at 2Θ = 40.7 [2 -1 1], 44.6 [2 0 1], 47.4 [3 -1 0], 54.2 [3 0 0] and 74.8 (3 -1 2) are only present for the catalyst prepared with the lower Ni/P ratio of 0.35, but this material also exhibits peaks for the $Ni_{12}P_5$ phase at 2Θ = 38.4 [1 1 2], 41.8 [4 0 0], 47.0 [4 -2 0] and 49.0 [3 1 2].

In contrast, the materials prepared with ammonium phosphate displayed Ni_2P peaks for both the higher (0.65) and lower (0.26) Ni/P ratios and both reduction temperatures (Figure 6.5). Whilst the material with the lower Ni/P ratio appeared to contain the pure Ni_2P phase, materials prepared with the higher Ni/P ratio also displayed $Ni_{12}P_5$ peaks, and interestingly these peaks appeared to be enhanced at the higher reduction temperature.

These findings show that regardless of the phosphorus source, and consistent with the literature,[146, 149] a large excess of P was required to form the desired Ni_2P phase. However, it is clear that a significant difference exists between the nickel phases produced from the two phosphorus precursors. Whilst the phosphate precursor yielded Ni_2P even at high Ni/P ratios of 0.65, synthesis with the hypophosphite salt

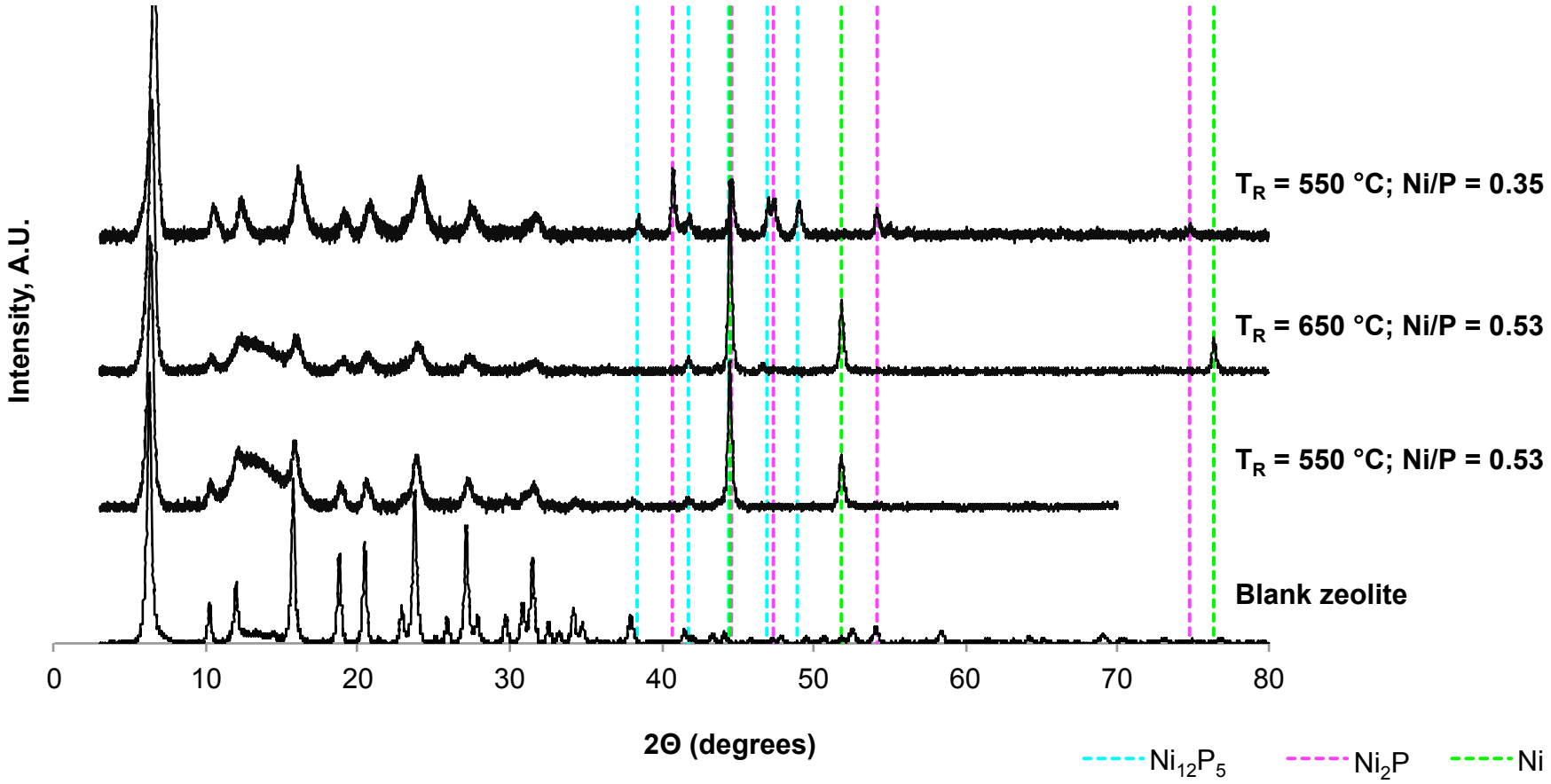

Figure 6.4: X-Ray diffraction patterns for catalysts prepared with ammonium hypophosphite

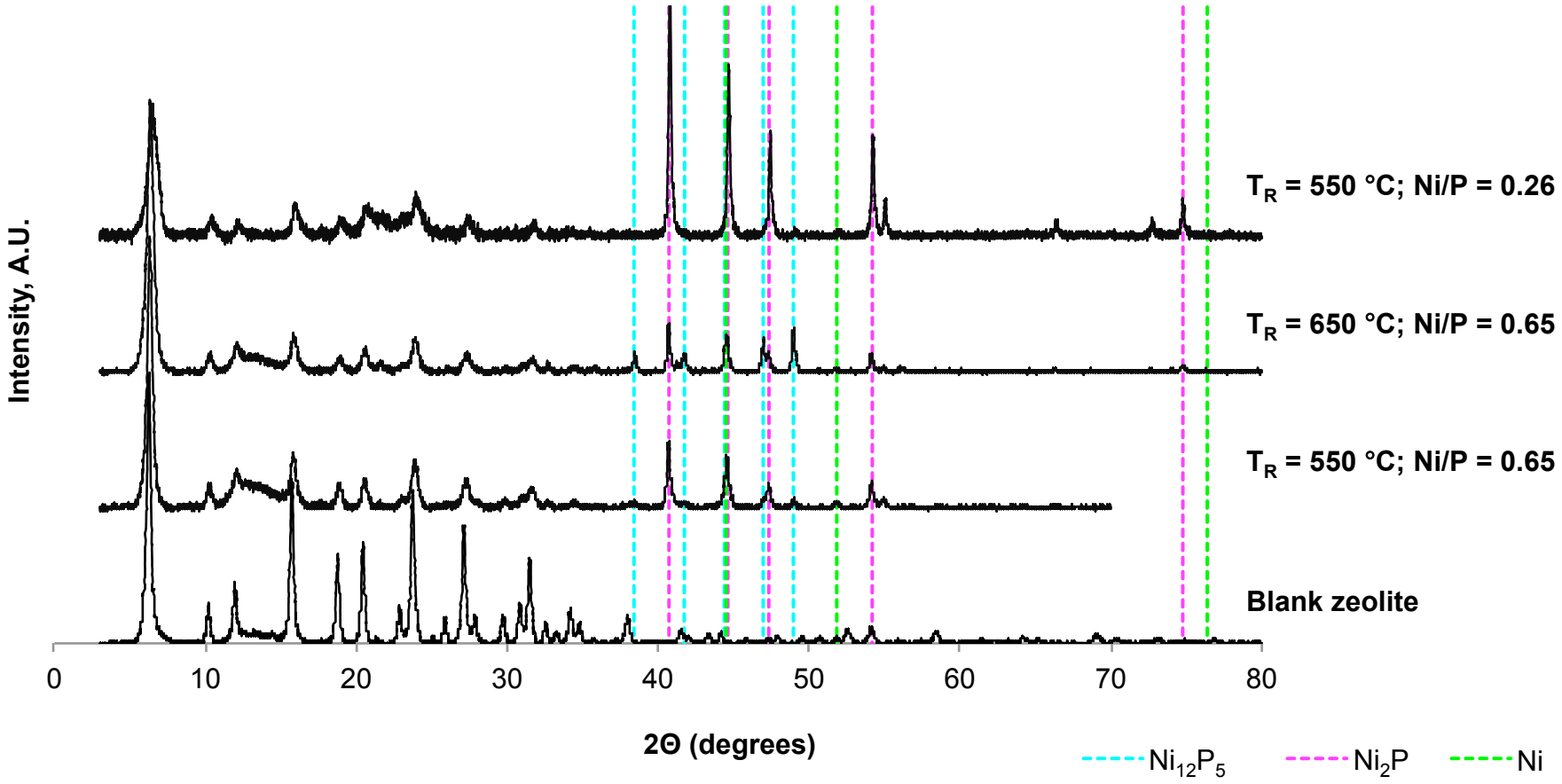

Figure 6.5: X-Ray diffraction patterns for catalysts prepared with ammonium phosphate

required a much larger excess of phosphorus (Ni/P ratio of 0.35) to form this phase.

A potential explanation for this discrepancy is the loss of phosphine gas (PH_3) during the disproportionation reaction of hypophosphite. D'Aquino *et al.* found that for unsupported NaH_2PO_4 this reaction took place in argon at temperatures ranging from 262 °C to 306 °C,[203] significantly below the calcination temperature of 400 °C employed in the present study. Consequently, it is possible that a substantial amount of phosphorus was lost prior to the reduction of nickel, leaving only the phosphate fraction, accounting for just over 50 % of the initially loaded P, to be available for the reaction with nickel.

A similar explanation was given by Song *et al*., who obtained a pure Ni_2P phase at reduction temperatures of 250 °C, but observed $Ni_{12}P_5$ at the higher reduction temperature of 300 °C.[144] However, unlike in the present work, their catalysts were supported on SiO_2, allowing the use of lower reduction temperatures. In contrast, d'Aquino *et al.* found that the reduction temperature required to form Ni_2P on alumina or silica-alumina supports was around 200 °C higher than for a SiO_2 support, at 500 °C.[203] The loss of P at increased reduction temperatures could also explain the enhancement of $Ni_{12}P_5$ peaks at 650 °C for the catalysts prepared with ammonium phosphate.

Given that in the present work pure Ni_2P could be formed by reduction of the phosphate precursor at 550 °C, there appeared to be little benefit of using the hypophosphite salt instead and all subsequent catalyst studies were conducted with the phosphate precursor only.

6.2.3 Effect of impregnation method

Supported Ni_2P catalysts have typically been prepared via one of two methods: Incipient wetness (pore volume) impregnation, where the desired amount of catalyst precursor is dissolved in the exact amount of solvent required to fill the pores of the support,[150, 198] and solution based impregnation, where the support is suspended in a solution of the metal salt, stirred for an extended period of time, before the solvent is allowed

to evaporate.[146, 204] As nickel phosphate is insoluble in neutral water, impregnation solutions have either been acidified, typically with nitric acid,[105, 205] or impregnation was conducted in two successive steps, first with the metal salt, followed by drying and a second impregnation step with the phosphorus precursor.[144, 145]

In this section the effect of applying three different impregnation methods for the synthesis of H^+Y supported Ni_2P catalysts was investigated.

Method 1 used a two-step incipient wetness impregnation process, first with a solution of nickel nitrate, followed by a solution of ammonium phosphate, method 2 employed single step incipient wetness impregnation with nickel phosphate dissolved in 2.5 M nitric acid, and method 3 used solution-based impregnation with 10 mL of a nickel phosphate solution in 0.5 M nitric acid per 1 g of support. For all three methods, the target nickel loadings and Ni/P molar ratios were kept constant at 5 wt% and 0.33, respectively. Following impregnation all catalysts were dried at 120 °C, calcined at 400 °C and reduced in hydrogen at 550 °C.

6.2.3.1 SEM-EDX analysis

SEM-EDX analysis was used to determine the Ni loading and Ni/P ratio for the catalysts prepared by the different impregnation methods (Table 6.3). For all three methods, the Ni/P ratios obtained from the EDX analysis were significantly higher than those used during the catalyst preparation (0.33). This confirms the loss of phosphorus during the calcination and reduction procedure, as previously reported in the literature.[129, 146]

Table 6.3: Metal loadings and Ni/P ratios of H^+Y supported catalysts prepared with three different impregnation methods

Impregnation method	Loading Parameters		SEM-EDX analysis	
	Ni Loading	Ni/P ratio	Ni loading	Ni/P ratio
Method 1	4.84 wt%	0.33	5.82 wt%	0.58
Method 2	4.26 wt%	0.33	4.33 wt%	0.48
Method 3	4.05 wt%	0.33	2.69 wt%	0.41

The best match between the Ni loading determined by the EDX analysis and the actual loading was obtained for the catalyst prepared using method 2 (4.33 wt% vs 4.26 wt%). A higher degree of discrepancy was observed for impregnation method 1 (5.82 wt% vs 4.84 wt%) and particularly method 3 (2.69 wt% vs 4.05 wt%). As EDX analysis only provides a snapshot of a very small sample, this could indicate that method 2 produces a more uniform metal distribution than the other two methods. The solution-based impregnation required the evaporation of water after the mixing step, and it is possible that settling of the support caused more nickel to precipitate at the top of the sample, resulting in a non-uniform nickel distribution. Similarly, for the two-step impregnation, partial resolubilisation of the impregnated nickel salts during phosphorus addition could have introduced non-uniformity in the nickel loading across the sample. Indeed, it was not possible to obtain a uniform colour following the second impregnation step, due to leaching of the green nickel salts. In contrast, the single-step impregnation delivers a uniform nickel concentration to the entire sample surface, resulting in the best metal distribution.

6.2.3.2 X-ray diffraction

The powder diffraction patterns for the three materials show that the two-step incipient wetness impregnation (method 1) was the only method that resulted in the formation of clear Ni_2P peaks (Figure 6.6). In contrast, both the spectra for the single-step incipient wetness impregnation (method 2) and the solution-based impregnation (method 3) exhibited strong metallic nickel peaks. Interestingly, the catalyst prepared with method 1 also possessed the highest Ni/P ratio, indicating the highest degree of P loss during the calcination and reduction procedure. A possible explanation is that the initial impregnation with the Ni precursor shielded the aluminium sites, reducing the interaction between P and the support, allowing it to react with Ni instead.

Considering the full width at half maximum (FWHM) of the [1 1 1] peak (2θ = 6.19) (shown in Table 6.4), indicates that the catalysts prepared

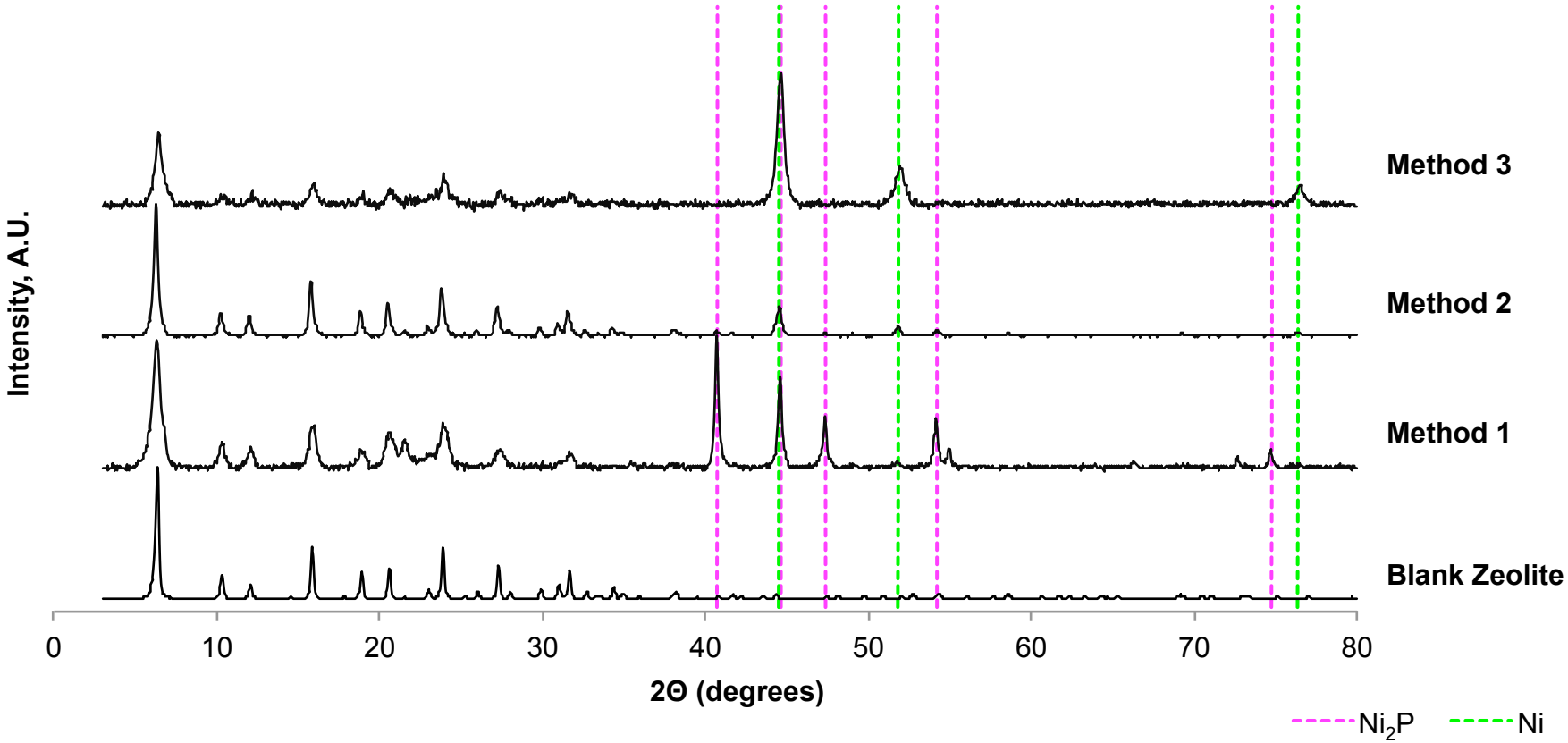

Figure 6.6: X-ray diffraction patterns of nickel phosphide catalysts supported on H^+ Y zeolite prepared with different impregnation methods. Method 1: Two-step incipient wetness impregnation with solutions of nickel nitrate followed by ammonium phosphate; Method 2: Single step incipient wetness impregnation with nickel phosphate solution acidified with nitric acid (2.5 M); Method 3: Solution impregnation with nickel phosphate solution acidified with nitric acid (0.5 M)

with impregnation methods 1 and 3 suffer a much higher loss in crystallinity than the material prepared with impregnation method 2. This material also possesses a much higher BET surface area (314.1 $m^2 g^{-1}$) than the materials prepared by methods 1 and 3 (91.9 and 123.8 $m^2 g^{-1}$, respectively), but still significantly below the area of the virgin zeolite (843.9 $m^2 g^{-1}$).

Table 6.4: Properties of H^+ Y supported Ni_2P catalysts prepared with three different impregnation methods

Name	BET Surface area, $m^2 g^{-1}$	Ni-P particle size, nm	FWHM of [1 1 1] zeolite peak, degrees	Unit cell parameter, Å
Blank support	843.9	*na*	0.197	24.47
Method 1	91.9	33.19 ±1.16	0.492	24.42
Method 2	314.1	26.70 ±1.51	0.246	24.53
Method 3	123.8	17.24 ±3.09	0.443	24.37

Compared to the catalysts prepared by methods 1 and 3, the metal peak intensities of the method 2 catalyst were much smaller, suggesting smaller metal particles, or improved dispersion. To investigate this in more detail, the sizes of the nanoparticles were estimated using Scherrer's equation with the FWHMs of the strongest metal peaks, corresponding to the dominant Ni phase ([2 -1 1], [2 0 1] and [3 -1 0] for Ni_2P and [1 1 1], [2 0 0] and [2 2 0] for Ni). This analysis showed that the smallest particles were obtained from the solution-based impregnation, whereas the largest particles were obtained from the 2-step incipient wetness impregnation. The low intensity of the Ni peaks for the material prepared by method 2 could therefore be related to incomplete reduction, rather than improved dispersion, a masking by the stronger signal from the zeolite, or the formation of a highly dispersed phase that cannot be detected by powder diffraction.

6.2.3.3 TEM analysis

Further analysis of the material prepared using method 2 by TEM (Figure 6.7) showed the clear presence of nanoparticles at the zeolite surface, with an average diameter of 61 nm. Elemental mapping confirmed that Ni

was mostly confined to the particles, whereas P was much more evenly distributed over the entire zeolite, with only slightly increased concentrations on the nanoparticles themselves. Together with the XRD analysis results, it appears that the catalyst reduction temperature was insufficient to yield a fully reduced Ni phase and was mostly confined to smaller nanoparticles.

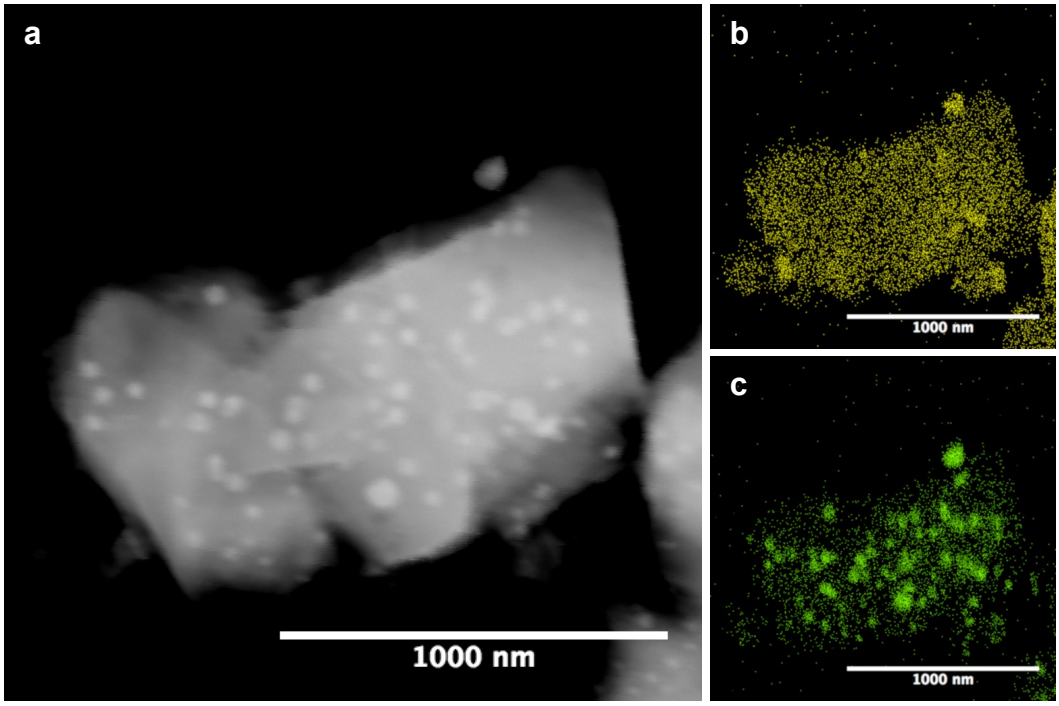

Figure 6.7: Elemental mapping by TEM of H^+Y supported Ni-P catalyst prepared by impregnation method 2. (a) Electron image, (b) P distribution, (c) Ni distribution

This suggests that this material is more difficult to reduce than the other two materials, potentially due to improved dispersion or the use of strong nitric acid (2.5 M) during the preparation procedure.

Nevertheless, compared to the other two preparation methods, this material displayed high metal dispersion and good retention of the zeolite structures. Method 1, in turn, resulted in the formation of the desired Ni_2P with adequate dispersion, whereas method 3 yielded a poorly dispersed material with the undesired Ni metal phase. Consequently, further studies were focused on impregnation methods 1 and 2 only.

6.2.4 EFFECT OF ZEOLITE COUNTER ION

Previous research suggested that the nature of the zeolite counterion can have a large impact on the preparation and activity of supported phosphide catalysts. Rh phosphide catalysts, for example, displayed much lower reduction temperatures when supported on Na^+ MFI, rather than H^+ MFI, allowing the formation of smaller nanparticles, potentially with higher catalytic activity.[136] The cracking activity of H^+ USY supported Ni_2P catalysts, in turn, was significantly reduced following ion exchange with potassium, due to a lower number of Bronsted acid sites.[129]

To investigate this further, nickel phosphide catalysts were supported on the Y zeolites containing NH_4^+, Na^+, K^+ and H^+ counterions, previously described in section 6.2.1.1, using both the single and two-step incipient wetness impregnation methods. The target metal loading and Ni/P ratio was kept constant for all catalysts at 5 wt% and 0.33, respectively, and all materials were dried, calcined at 400 °C and reduced at 550 °C, following impregnation.

6.2.4.1 Catalyst characterization

The XRD patterns for the catalysts prepared by two-step impregnation displayed clear Ni_2P peaks for all four supports (Figure 6.8). However, unlike the H^+ Y supported catalysts, the catalysts supported on the K^+ and Na^+ exchanged zeolite also exhibited peaks for the $Ni_{12}P_5$ phase, whereas the NH_4^+ Y supported catalyst displayed a weak metallic Ni phase. For the single-step impregnation, the catalysts supported on K^+ Y and Na^+ Y still displayed a mixed $Ni_2P/Ni_{12}P_5$ phase, whereas the H^+Y zeolite contained only metallic Ni (Figure 6.9). The NH_4^+ Y supported catalyst appeared to display a pure Ni_2P phase, however the signal intensity was much lower than for the other three supports.

Once again, the catalysts prepared with method 2 displayed a much better retention in crystallinity (lower FWHM of [1 1 1] zeolite peak) than the catalysts prepared with method 1 (Table 6.5). Particularly the NH_4^+ Y zeolite experienced a remarkable loss of crystallinity, potentially due to the release of ammonia during the calcination, which could have been

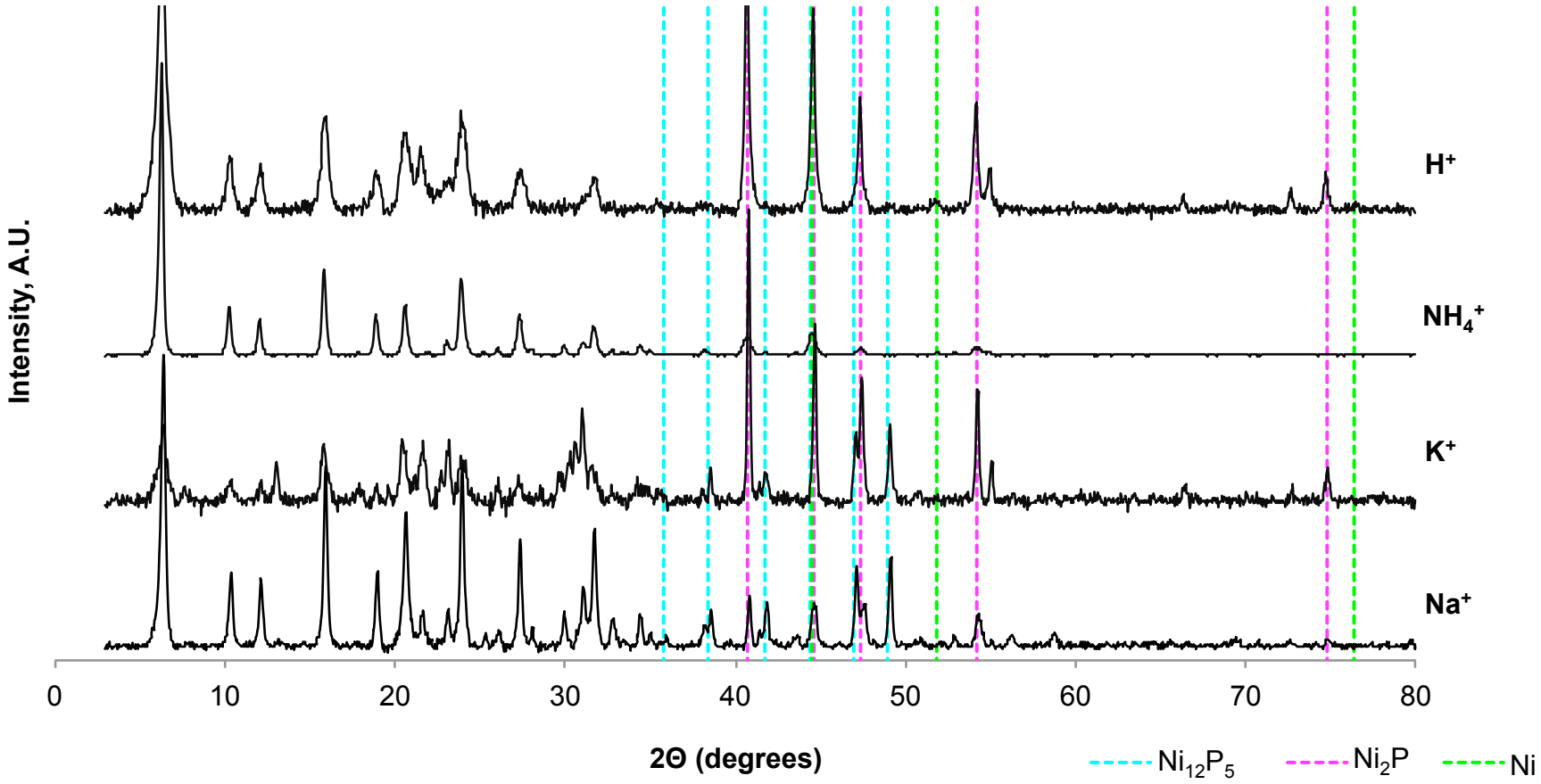

Figure 6.8: Effect of zeolite counterion on X-ray powder diffraction patterns of catalysts prepared using method 1

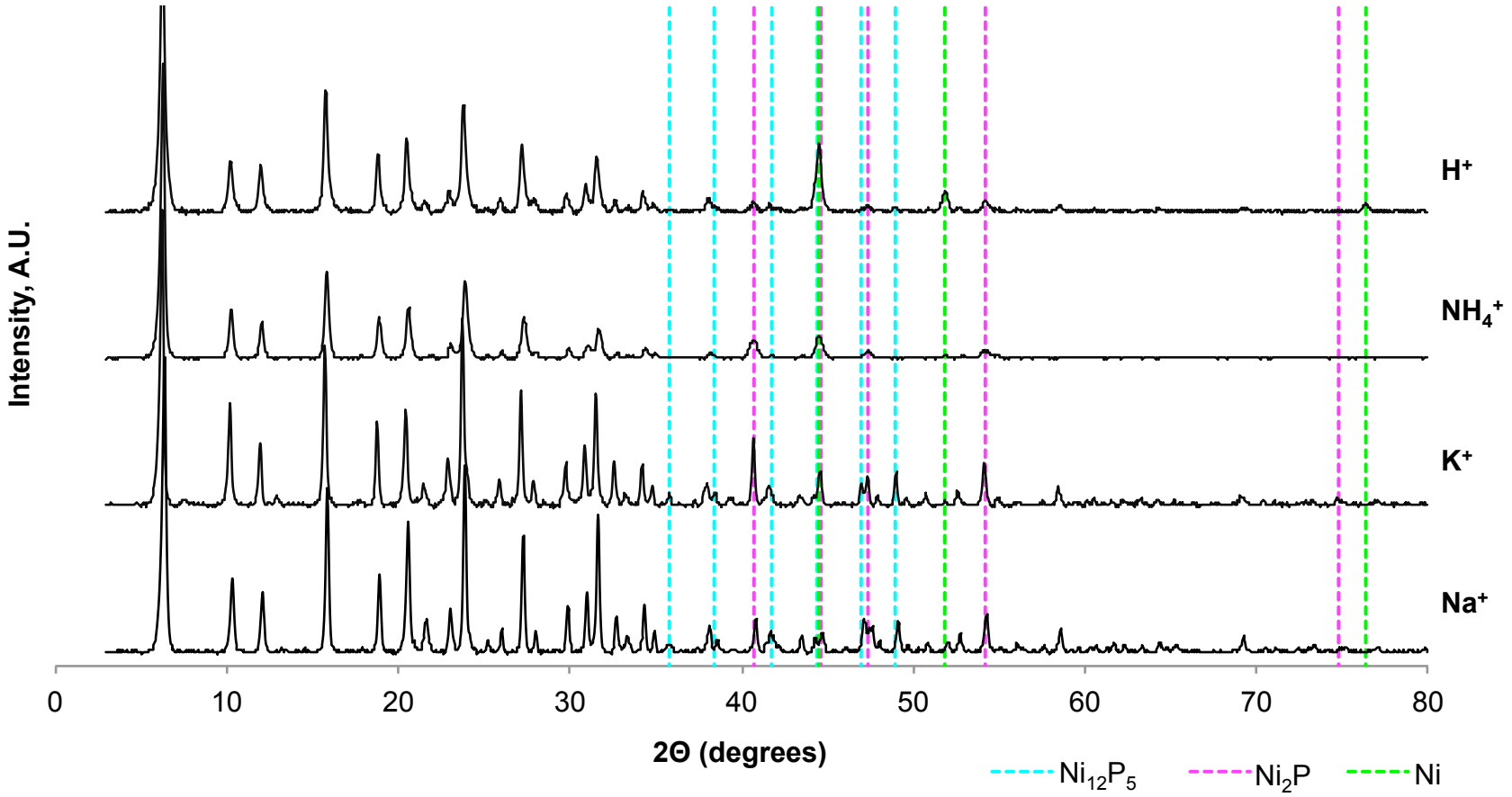

Figure 6.9: Effect of zeolite counterion on X-ray powder diffraction patterns of catalysts prepared using method 2

impeded by the blockage of pores with the catalyst precursors. Similar observations were made for the BET surface areas, which, with the exception of Na^+ Y, were generally an order of magnitude higher for the single step impregnation.

Table 6.5: Properties of Ni_2P catalysts supported on Y zeolites with different counterions

Support	BET Surface area, $m^2\ g^{-1}$	FWHM of [1 1 1] zeolite peak, degrees	Ni-P particle size, nm	Ni phase
NH_4^+ Y, method 1	7.9	0.836	26.53 ±1.37	Ni_2P/Ni
NH_4^+ Y, method 2	225.7	0.246	18.08 ±1.40	Ni_2P
H^+ Y, method 1	91.9	0.492	33.19 ±1.16	Ni_2P
H^+ Y, method 2	314.1	0.246	26.70 ±1.51	Ni
Na^+ Y, method 1	214.0	0.246	41.27* ±4.56 38.72$^+$ ±2.07	Ni_2P/$Ni_{12}P_5$
Na^+ Y, method 2	321.9	0.197	35.81* ±4.45 36.73$^+$ ±3.76	Ni_2P/$Ni_{12}P_5$
K^+ Y, method 1	21.6	0.443	43.34$^+$ ±2.15	Ni_2P/$Ni_{12}P_5$
K^+ Y, method 2	264.8	0.197	44.10$^+$ ±7.17	Ni_2P/$Ni_{12}P_5$

** $Ni_{12}P_5$, +Ni_2P*

The presence of the $Ni_{12}P_5$ phases over the K^+ Y and Na^+ Y supports for both methods of impregnation suggests that unlike the H^+ Y supported catalyst the formation of Ni_2P was P-limited. Indeed, the results from SEM-EDX analysis displayed higher Ni/P ratios for the K^+ Y and Na^+ Y supported catalysts (0.55 and 0.58, respectively), compared to H^+ Y (0.48), indicating a higher degree of P loss. This is consistent with previous findings which suggested that the presence of sodium reduced the interaction between phosphates and the support.[136] The small amount of metallic Ni observed on the NH_4^+ Y supported catalyst prepared with method 1 could be related to the loss of zeolite structure, preventing the reaction of Ni with P. In contrast, the catalyst prepared with method 2 over the same support displayed a pure, if weak, Ni_2P phase. This

suggests that on this support, P was more readily available than on the H^+ Y support, allowing it to react with any reduced Ni.

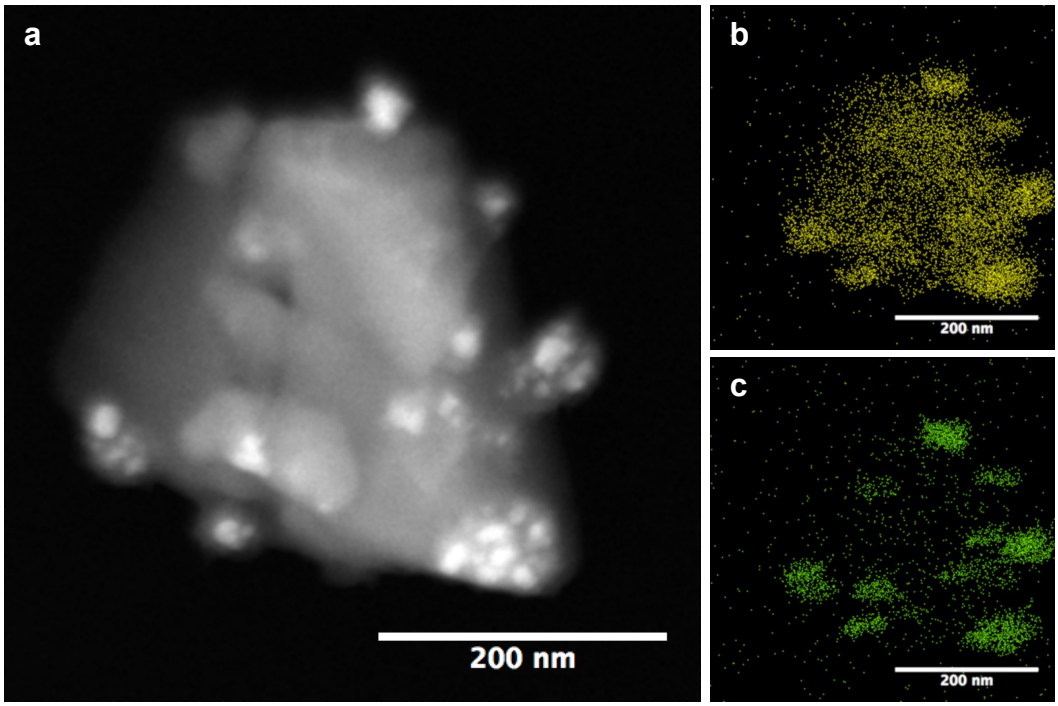

Figure 6.10: Elemental mapping by TEM of NH_4^+Y supported Ni-P catalyst prepared by impregnation method 2. (a) Electron image, (b) P distribution, (c) Ni distribution

The estimated nanoparticle sizes were generally smaller for the catalysts prepared by method 2, with the smallest particles obtained over NH_4^+ Y. In contrast, the Na^+ Y and K^+ Y supported catalysts both contained significantly larger particle sizes and were less affected by the impregnation method. This difference in size could be related to a reduced interaction of the catalyst precursors with these two supports, resulting in increased sintering and particle agglomeration during the reduction process. Furthermore, the calcination and reduction of the NH_4^+ Y supported catalysts is expected to release ammonia, which could have interacted with the catalyst precursors.

TEM images of this catalyst show a very disperse nanoparticle phase with an average diameter of 25.1 nm. Consistent with the analysis of the H^+ Y supported catalyst, elemental mapping confirmed that most of the nickel is confined to the particles, whereas P is present over the entire zeolite surface (Figure 6.10). However, a clear increase in P

concentration can be observed in the vicinity of the nanoparticles, confirming the presence of a Ni-P phase.

6.2.5 EFFECT OF BASE-TREATMENT

Catalysts supported on the base-treated zeolites were prepared using the single-step impregnation (method 2) only, applying the same metal loading (5 wt%), Ni/P ratio (0.33) and reduction conditions (calcination at 400 °C, reduction at 550 °C) as before.

X-ray diffraction patterns for the catalysts supported on the NH_4^+ Y zeolites show that a pure Ni_2P was formed on the unmodified zeolite, whereas chemical treatment resulted in the expression of a mixed $Ni_2P/Ni_{12}P_5$ phase (Figure 6.11). The emergence of this phase could be related to the ion exchange with Na^+ during the base treatment, reducing the interaction between the P precursor and the support.

Table 6-6: Properties of Ni_2P catalysts supported on chemically modified zeolites

Support	SEM-EDX analysis		BET Surface area, $m^2\ g^{-1}$	FWHM of [1 1 1] zeolite peak, degrees	Ni-P particle size, nm
	Ni loading	Ni/P ratio			
NH_4^+ Y, NT	2.59*	0.23*	225.7	0.246	17.01 ±2.22
NH_4^+ Y, MT	4.00	0.48	328.4	0.197	39.12 ±5.29
NH_4^+ Y, HT	3.76	0.50	330.2	0.246	35.74 ±3.68
H^+ Y_{low}, NT	4.99	0.76	597.3	0.197	30.11 ±6.32
H^+ Y_{low}, MT	3.22	0.60	534.8	0.246	26.21 ±2.45
H^+ Y_{low}, HT	3.30	0.63	426.2	0.197	28.77 ±3.84

**from TEM*

In contrast, the catalysts supported on the low-aluminium zeolites displayed almost pure Ni_2P, regardless of chemical treatment (Figure 6.12). (Note that the $Ni_{12}P_5$ peak at $2\Theta = 38.4$, associated with the [1 1 2] crystal plane overlaps with the Y zeolite peak corresponding to the [6 6 6] crystal plane). Despite this, the Ni/P ratio, as determined by SEM-EDX analysis, of this series of catalysts (0.60 to 0.76) is significantly higher

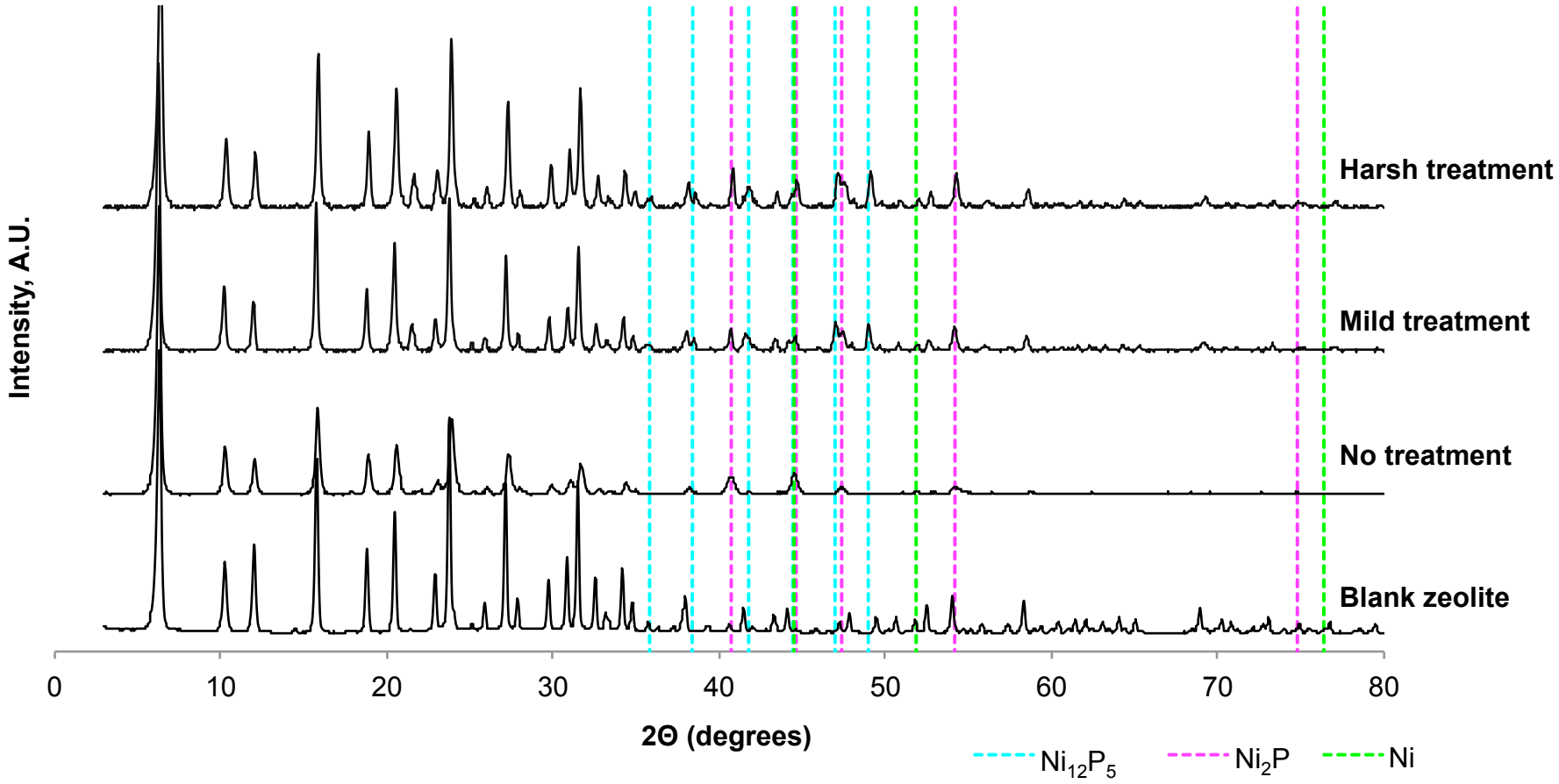

Figure 6.11: X-ray powder diffraction for Ni_2P catalysts supported on base-treated NH_4^+ Y zeolites

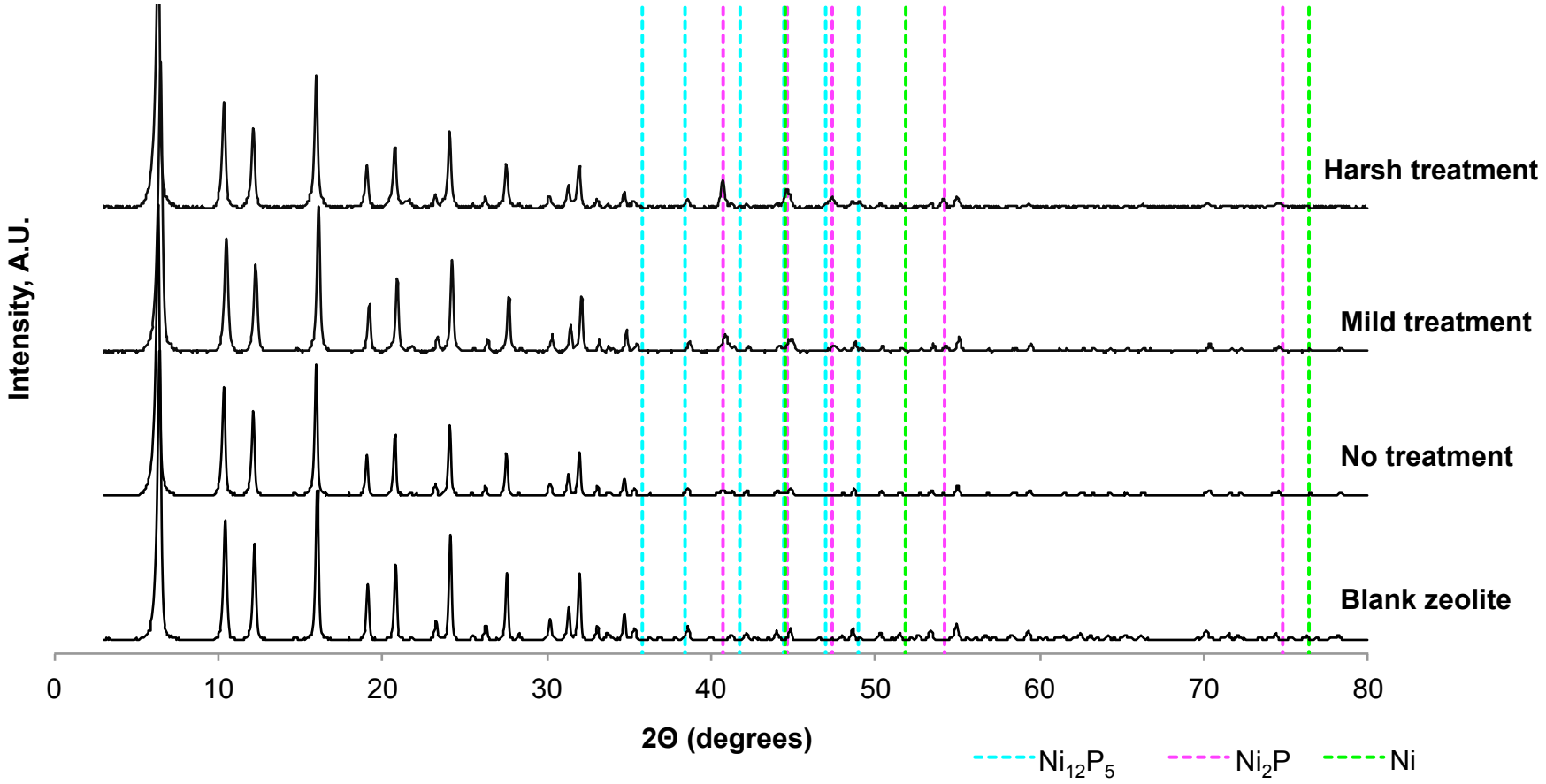

Figure 6.12: X-ray powder diffraction for Ni_2P catalysts supported on base-treated H^+ Y_{low} zeolites

than that of the NH_4^+ Y catalysts (0.48 to 0.50) (Table 6-6). The reduced retention of P on the $H^+ Y_{low}$ supported catalysts can be related to their reduced aluminium content. Consequently, the P retention increases for the base-treated supports, as the Si/Al ratio falls from 17.87 to 11.53 (Table 6.2).

Base treatment appeared to have only limited effect on the zeolite crystallinity, as indicated by relatively constant FWHM values for the [1 1 1] zeolite peak (Table 6-6). However, the surface area for the NH_4^+ Y zeolites was substantially increased following base-treatment, whereas it reduced for the $H^+ Y_{low}$ supported zeolites. The increased area for the NH_4^+ Y can be explained by the exchange of NH_4^+ with the smaller Na^+ ions, as well as the removal of excess ammonia from the support surface. In contrast, the reduction in areas for the $H^+ Y_{low}$ supported catalysts could be the result of silica leaching, introducing defects within the zeolite structure. Even so, the surface areas for this catalyst series remained significantly above those of the NH_4^+ Y supported catalysts, probably as a result of the reduced interactions between the catalyst precursors and the support.

6.2.5.1 TEM analysis

The catalysts supported on the unmodified supports, and those exposed to harsh base treatment, were further analysed by TEM.

For the NH_4^+ Y supported catalysts, the untreated zeolite formed much smaller Ni-P particles (average diameter of 25.1 nm) than the base-treated support (61.9 nm), consistent with the trend of estimated particle sizes from the XRD data (Table 6-6). In contrast, the average particle size decreased from 37.8 nm to 29.5 nm following base treatment of the $H^+ Y_{low}$ supports. Despite this fall, base-treatment appeared to have a lesser effect on particle size for this support than for the NH_4^+ Y support.

Elemental mapping of the base-modified NH_4^+ Y catalyst showed clearly defined nickel-containing particles, with increased P concentration (Figure 6.13). However, the P background concentration remained high, as expected due to the high aluminium content of the support.

In contrast, the P-background loading for the $H^+ Y_{low}$ supported catalyst was much lower and appeared to reduce following base-treatment, despite the

reduction in Si/Al ratio (Figure 6.14 and Figure 6.15). A clear accumulation of P can be observed on top of the Ni particles, consistent with the presence of the mixed $Ni_2P/Ni_{12}P_5$ phase, as detected by XRD.

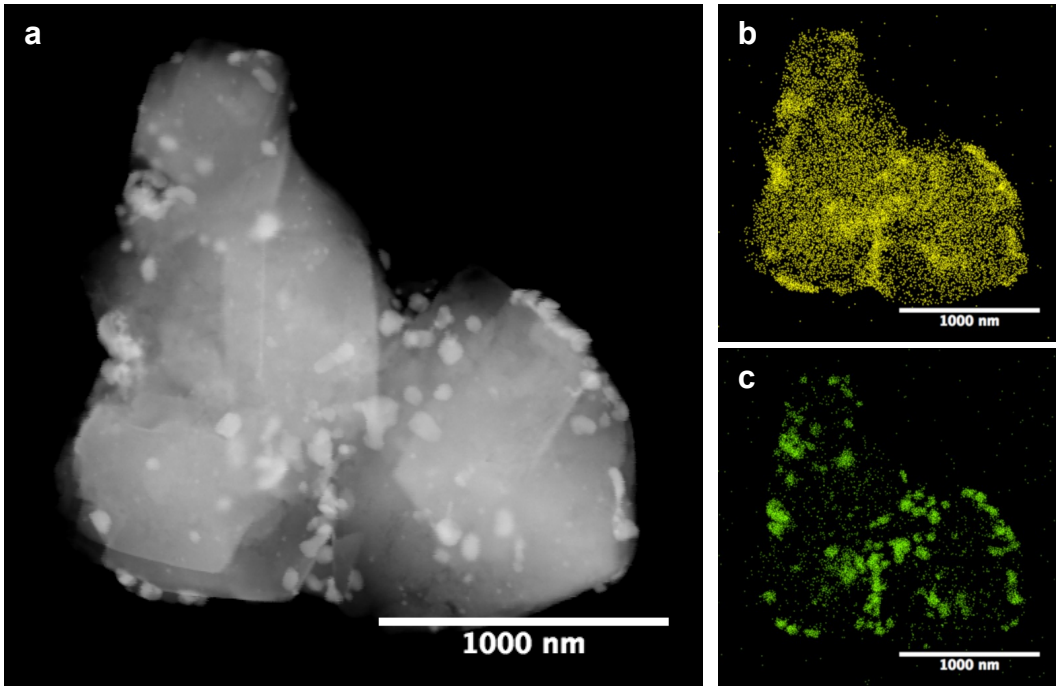

Figure 6.13: Elemental mapping by TEM for Ni-P catalyst supported on base-treated (HT) NH_4^+Y zeolite. (a) Electron image, (b) P distribution, (c) Ni distribution

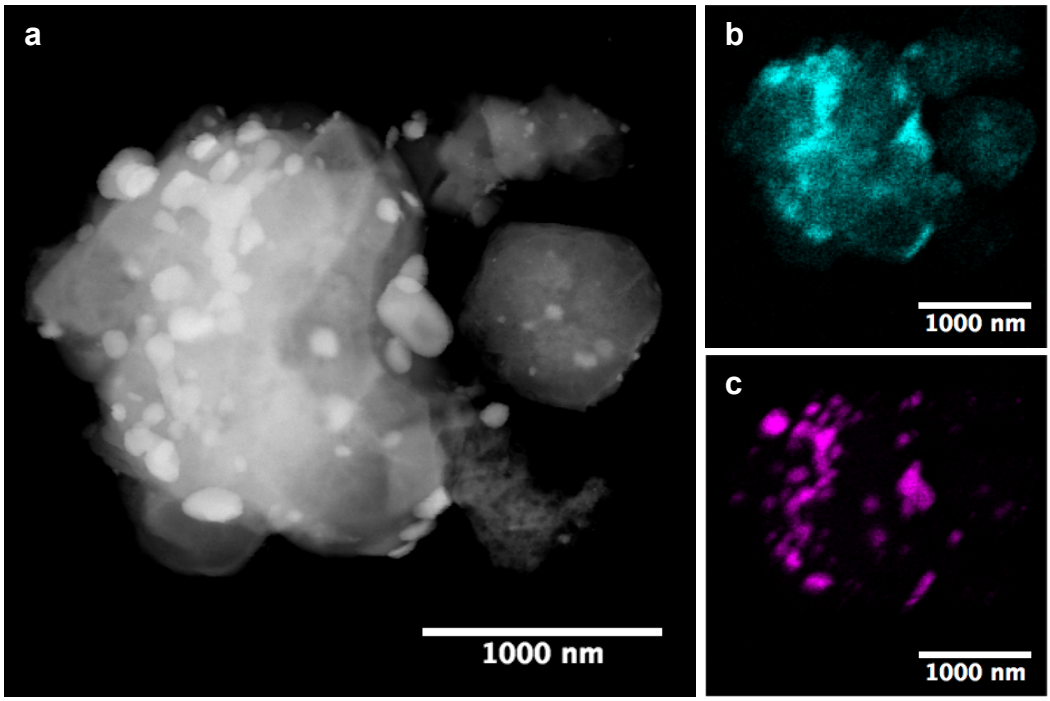

Figure 6.14: Elemental mapping by TEM for Ni-P catalyst supported on untreated H^+ Y_{low} zeolite. (a) Electron image, (b) P distribution, (c) Ni distribution

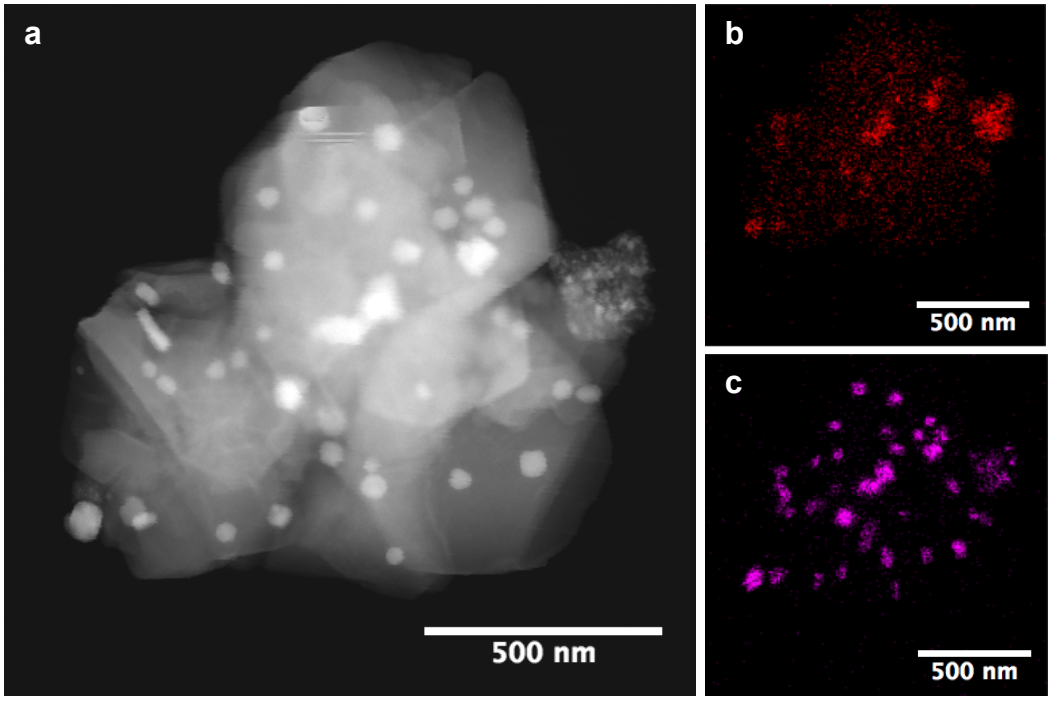

Figure 6.15: Elemental mapping by TEM for Ni-P catalyst supported on base-treated (HT) H^+ Y_{low} zeolite. (a) Electron image, (b) P distribution, (c) Ni distribution

6.2.6 TPR ANALYSIS

The catalyst precursors for the H^+ Y, H^+ Y_{low}, and the unmodified and based treated NH_4^+ Y-NT and NH_4^+ Y-HT supported catalysts were further analysed by Dr Laura Torrente Murciano (Department of Chemical Engineering and Biotechnology, University of Cambridge, UK) using temperature programmed reduction (Figure 6.16).

The TPR curve for the H^+ Y supported catalyst shows a clear maximum at a temperature of 652 °C, significantly above the reduction temperature employed in this study. This is consistent with the analysis in section 6.2.3, concluding that the catalyst phase was only partially reduced. However, smaller peaks at 211 °C and 367 °C could account for the formation of the metallic Ni phase previously observed on the XRD. The TPR curve also contains a high temperature peak at 957 °C, probably related to the reduction of aluminium bound phosphorus.[149]

TPR analysis of the unmodified NH_4^+ Y supported precursor showed a much sharper reduction peak than for the H^+ Y catalyst and at a higher temperature of 675 °C, which could be related to increased interaction with the support,

potentially through the formation of smaller particles.[150] Again the spectrum contains a low temperature peak at 217 °C and a slight step around 457 °C, which could account for the presence of the Ni_2P phase in the XRD spectrum. The high temperature reduction peak is lowered to 865 °C, indicating a weaker interaction between P and the support, compared to the H^+ Y zeolite.

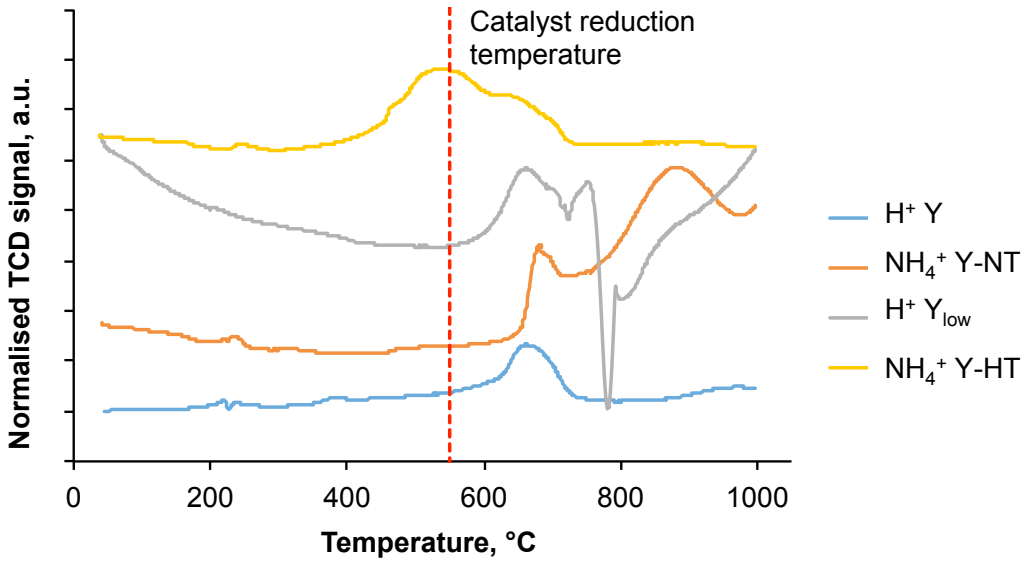

Figure 6.16: TPR curves for selected zeolite supported Ni-P catalysts

Following base-treatment, the reduction temperature of the NH_4^+ Y-HT precursor is significantly reduced, with a maximum at around 515 °C. This is consistent with the emergence of a stronger $Ni_2P/Ni_{12}P_5$ signal on the corresponding XRD and could be related to the ion-exchange with sodium, which was previously found to reduce the reduction temperature over MFI supported Rh phosphide catalysts.[136] Unlike the curves for the untreated support, the spectra does not contain a high temperature reduction peak, which could indicate a much lower interaction between the P precursor and the support.

Finally, the TPR curve for the low-Al H^+ Y_{low} supported catalyst displays a maximum at 648 °C, very close to the peak temperature obtained for the other H^+ Y zeolite support. This suggests that the reduction temperature is directly affected by the nature of the counterion, regardless of the acid site density (Si/Al ratio). However, the spectrum displays a strong negative peak at

780 °C, which could be related to a sudden release of gases, affecting the TPR measurement.

6.3 MODEL COMPOUND CONVERSION

In order to establish their denitrogenation activity, the Ni_2P catalysts were tested for the conversion of the model compound quinoline in dodecane solvent. This allowed the evaluation of the three reaction mechanisms associated with denitrogenation reactions, which would be difficult to achieve with the complex bio-oil: (1) hydrogenation of the nitrogen ring, to convert the aromatic carbon-nitrogen bonds into single, aliphatic bonds; (2) sequential hydrogenolysis of the C-N bonds to release nitrogen as ammonia and (3) saturation of the aromatic rings adjacent to the nitrogen heterocycle.[96]

The quinoline denitrogenation pathway is given in Figure 6.17.

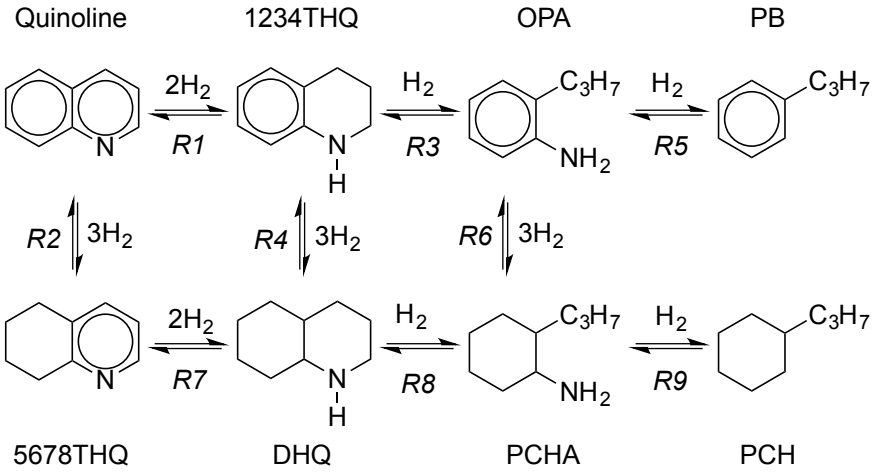

Figure 6.17: Denitrogenation pathway for quinoline

Denitrogenation of quinoline can follow a number of reaction pathways to either yield the fully hydrogenated reaction product propylcyclohexane (PCH) or the aromatic product propylbenzene (PB). In both cases, the nitrogen-containing ring must first be hydrogenated to form the partial hydrogenation compound 1234-tetrahydroquinoline (1234THQ) or the fully hydrogenated compound decahydroquinoline (DHQ), via the intermediate 5678-tetrahydroquinoline (5678THQ). Hydrogenolysis of 1234THQ forms orthopropylaniline (OPA), which can either undergo direct hydrogenolysis to

yield propylbenzene or be hydrogenated into propylcyclohexylamine (PCHA), which is rapidly converted further into propylcyclohexane (PCH). PCHA is also formed by the hydrogenolysis of DHQ to yield PCH as the final reaction product.

6.3.1 BASELINE REACTIONS

A number of baseline reactions were conducted without catalyst (blank), with Pd/C and with two supported transition metal catalysts, optimized for HDS (NiCoMo/Al) and HDO ($NiMo/CeO_2$) reactions (Figure 6.18).

6.3.1.1 Catalyst information

Pd/C was selected due to its high hydrogenation activity, which is a key requirement for a successful denitrogenation catalysts.[96] The two transition metals were chosen to represent conventional sulphided refining catalysts and were obtained from a collaboration with the PetroVietnam Research and Development Center for Petroleum Processing, part of the Vietnam Petroleum Institute, and sulphided with DMSO prior to use. The $NiMo/CeO_2$ catalyst was previously tested for the HDO of guaiacol for 3 h at 250 °C, after initial reduction at 350 °C in 10 bar hydrogen.[206]

Table 6-7: Properties of baseline catalysts, as obtained via personal communication[207]

Catalyst	Composition	BET surface area, $m^2\ g^{-1}$	Peak reduction temperature, °C
Pd/C	5 wt% Pd	*nd*	*na*
$NiCoMo/Al_2O_3$	1.6 wt% Ni 1.6 wt% Co 15 wt% Mo	143	430
$NiMo/CeO_2$	6.0 wt% NiO 30 wt% MO_3 64 wt% CeO_2	27	550

It possessed a much lower BET surface area, and had a higher peak reduction temperature than the $NiCoMo/Al_2O_3$ (Table 6-7). This was attributed to stronger interactions between Mo species and the CeO_2 support, compared to the same catalyst supported on Al_2O_3.[206] However, in comparison to a $NiMo/Al_2O_3$ catalyst, the ceria supported catalyst displayed a slightly improved guaicaol conversion of 23 % and favoured the formation of cylcohexanol

(27.1 %) over phenol (0.8 %), indicating stronger hydrogenation activity for the aromatic ring.

6.3.1.2 Conversion results

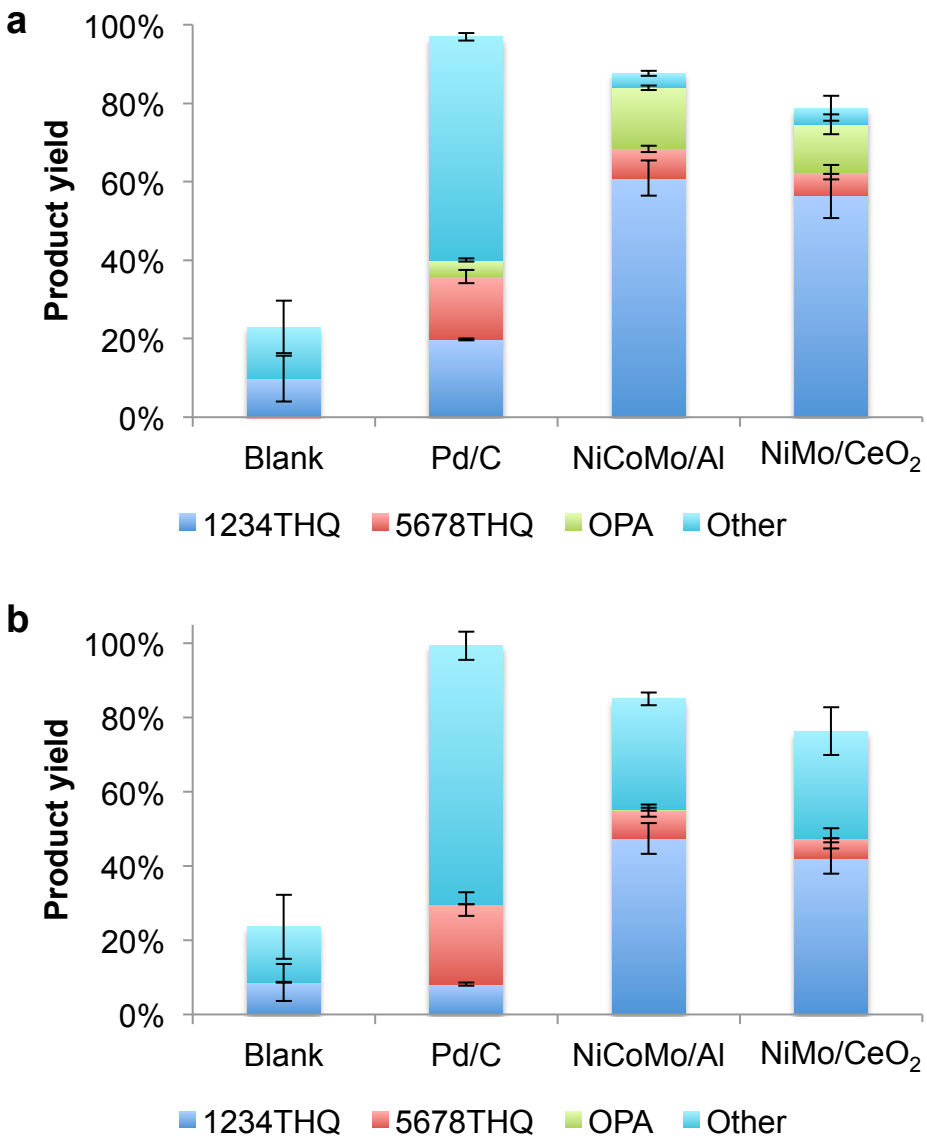

Figure 6.18: Quinoline conversion over baseline catalysts: (a) results from ^{1}H NMR analysis, (b) results from GC-MS analysis

The results from the ^{1}H NMR analysis show that in comparison to the blank runs (conversion of 21 %) the addition of any of the three catalysts resulted in a significant increase in quinoline conversion to 79 % for $NiMoCeO_2$, 88 % for $NiCoMo/Al_2O_3$ and 97 % for Pd/C (Figure 6.18a). However, the product distribution obtained over Pd/C was significantly different to the distributions produced by the two transition metal catalysts. Whilst the latter favoured the

formation of the partial hydrogenation product 1234THQ (61 % and 56 %) together with smaller quantities of OPA (16 % and 12 %), 5678THQ (7 % and 6 %) and other products (both 4 %), Pd/C yielded comparable amounts of 1234THQ (20 %) and 5678THQ (16 %), but favoured the formation of the unidentified 'other' product fraction (57 %).

Similar overall conversions were obtained from the GC-MS analysis, however in this case the 1234THQ yields were reduced and no OPA product was detected for either of the three catalysts (Figure 6.18b). This, in turn, resulted in an increase in the fraction of unidentified reaction products.

The complete absence of OPA peaks from the GC-MS spectra suggests that contrary to the results from the ^{1}H NMR analysis this product was not formed during the conversion of quinoline over the model catalysts. A potential explanation is the overlap of the ^{1}H NMR integral assigned to the OPA-C peak used for quantification (δ = 6.71– 6.65 ppm) with the peaks of a reaction by-product, which does not form part of the direct quinoline denitrogenation pathway. Potential culprits could be cracking and isomerisation products such as indoline, isoquinoline, *o*-toluidine, *o*-phenylpropylamine, aniline, toluene and *o*-ethylaniline which were previously detected during the HDN of quinoline.[208] Indeed, a number of these compounds possess ^{1}H NMR peaks that fall into this region, including indoline ((δ = 6.69 ppm) or *o*-toluidine (δ = 6.676 ppm).[209]

In contrast, the differences in the 1234THQ yields obtained from the ^{1}H NMR and GC-MS analysis can be assigned to calibration errors, either as a result of assuming equivalent GC responses for 1234THQ and quinoline, or the distortion across the ^{1}H NMR spectrum, already identified during the NMR peak assignment (refer to Section 8.4.8.1).

1.1.1.1 Denitrogenation performance

The results from the ^{1}H NMR analysis suggest that the transition metal catalysts had a high activity for the hydrogenation of the nitrogen ring, but yielded only low amounts of the alternative hydrogenation products 5678THQ and DHQ or the denitrogenation products PB and PCH. As the product initially assigned to OPA does not form part of the direct quinoline denitrogenation

mechanism, the C-N bond cleavage activities of these catalysts under the selected reaction conditions appeared to be low.

Pd/C, in turn, yielded similar amounts of the partial hydrogenation products 1234THQ and 5678THQ and therefore appeared to hydrogenate both aromatic rings at equal rates. It also formed a large amount of 'other' reaction products, which could include the fully hydrogenated intermediate DHQ as well as the fully denitrogenated products PB and PCH. At the same time, additional peaks at δ = 8.18 ppm and 7.01 ppm were already identified for the Pd/C products during the assignment of the ^{1}H NMR integrals for 1234THQ and 5678THQ (refer Section 8.4.8.1)). These peaks could not be attributed to any of the direct quinoline denitrogenation intermediates, and may therefore correspond to side products such as indoline or *o*-toluidine which possess peaks that fall within a similar area.

To investigate this further, the Pd/C conversion product was analysed by ^{13}C NMR and the resulting peaks were compared to the peaks expected for the direct quinoline denitrogenation products (Table 6-8). As expected from the ^{1}H NMR and GC-MS analysis, almost all the peaks associated with 1234THQ and 5678THQ could be detected. In contrast, only three out of eight peaks were present for OPA, and compared to the 1234THQ and 5678THQ peaks they were much lower in magnitude. As virtually no OPA product was detected by either the ^{1}H NMR or GC-MS analysis, it is likely that the three detected peaks belong to an alternative side product. Based on the ^{13}C NMR spectrum, there was no evidence for the formation of either of the two DHQ stereoisomers or the denitrogenation product PB, however it did contain most of the peaks associated with PCH. The ^{13}C NMR spectrum also contained additional peaks at δ = 154.42, 146.66, 136.45, 134.95, 131.47, 37.00, 32.85, 32.28 and 28.55 ppm, which could not be assigned to any of the direct quinoline denitrogenation products.

Even though the ^{13}C NMR analysis is not quantitative, it suggests that Pd/C is more active for the denitrogenation of quinoline than either of the two transition metal catalysts. A potential explanation is its higher activity towards the hydrogenation for the second aromatic ring, eliminating the need for the

Table 6-8: ^{13}C NMR analysis for conversion product of quinoline over Pd/C. Theoretical peaks are listed on the left, whereas the actual peaks are assigned to each product and missing peaks are denoted by an X.

Chemical Shift, ppm	1234THQ	5678THQ	OPA	tDHQ	cDHQ	PCH	PB
157.28		157.28					
146.73		146.76					
144.80	144.65						
144.14			x				
142.67							x
136.60		136.56					
132.12		132.10					
129.48			129.48				
129.40	129.38						
128.51							x
128.26							x
126.83			x				
126.65	126.61						
126.64			126.56				
125.67							x
121.26	121.26						
120.80		120.72					
118.62			x				
116.77	116.87						
115.49			x				
114.12	114.06						
53.28				x			
50.49					x		
47.31				x			
45.52					x		
43.85				x			
42.52				x			
41.93	41.92						
40.04						x	
38.18							x
37.56						37.51	
36.54					x		
34.74					x		
34.43				x			
33.64				x			
33.58						33.39	
33.33			33.31				
32.52		32.38					
30.57				x			
30.11					x		
28.86					x		
28.73		28.69					
27.00	x						
26.89						26.91	
26.85					x		
26.61						26.63	
26.53				x			
26.31				26.33			
25.05					x		
24.62							x
23.09		23.17					
22.90					23.01		
22.71		2.79					
22.17	22.16						
21.86							
20.04						x	
14.46						14.36	
14.13			x				
13.83							x

direct deamination of OPA, which is known to be inhibited by the presence of Co and Ni promoters.[100] The absence of the fully

hydrogenated intermediate DHQ suggests that the second hydrogenation step is slower than the C-N bond cleavage reactions to form PCHA and PCH, in line with previous literature findings.[118]

6.3.2 EFFECT OF IMPREGNATION METHOD

The H^+ Y zeolite supported catalysts, prepared by the three different impregnation methods described in section 0 were tested together with the blank zeolite for the conversion of quinoline (Figure 6.19).

Based on ^{1}H NMR analysis very similar conversions were achieved over the catalysts prepared via methods 1 (92 %) and 2 (89 %), whereas the catalyst produced via method 3 converted only 62 % of quinoline and the blank zeolite only 42 % (Figure 6.19a). The main reaction product over all three Ni catalysts was 1234THQ (41 to 58 %), together with lower amounts of the 'other' product phase (18 to 20 %). Catalysts prepared by methods 1 and 2 also produced 5678THQ, with method 1 yielding approximately twice the amount of this product (16 %) than method 2 (7 %). In contrast, the blank zeolite yielded mostly unidentified products, grouped together as 'other' (27 %) and 1234THQ (11 %).

The same trends were obtained from the GC-MS analysis but, consistent with the results from the conversion over the baseline catalysts (section 6.3.1), the 1234THQ product fraction was reduced in favour of unidentified reaction products and no OPA product was detected (Figure 6.19b). Overall quinoline conversions were slightly reduced for catalysts produced via methods 1 and 2, unaltered for method 3, and increased by 9 % for the blank zeolite.

It is apparent that for both analysis methods the experimental variation for the material prepared via method 3 was much higher than for the other two catalysts. This may be related to the poor dispersion of nickel, identified during SEM-EDX analysis, resulting in differences in catalytic compositions from one experiment to the next. Conversely, this suggests that the high experimental repeatability over the other two catalysts, particularly the catalyst prepared via method 2, could be related to a much more uniform bulk material composition. (Note that the results for

the blank support are based on a single experiment, and consequently do not include error bars.)

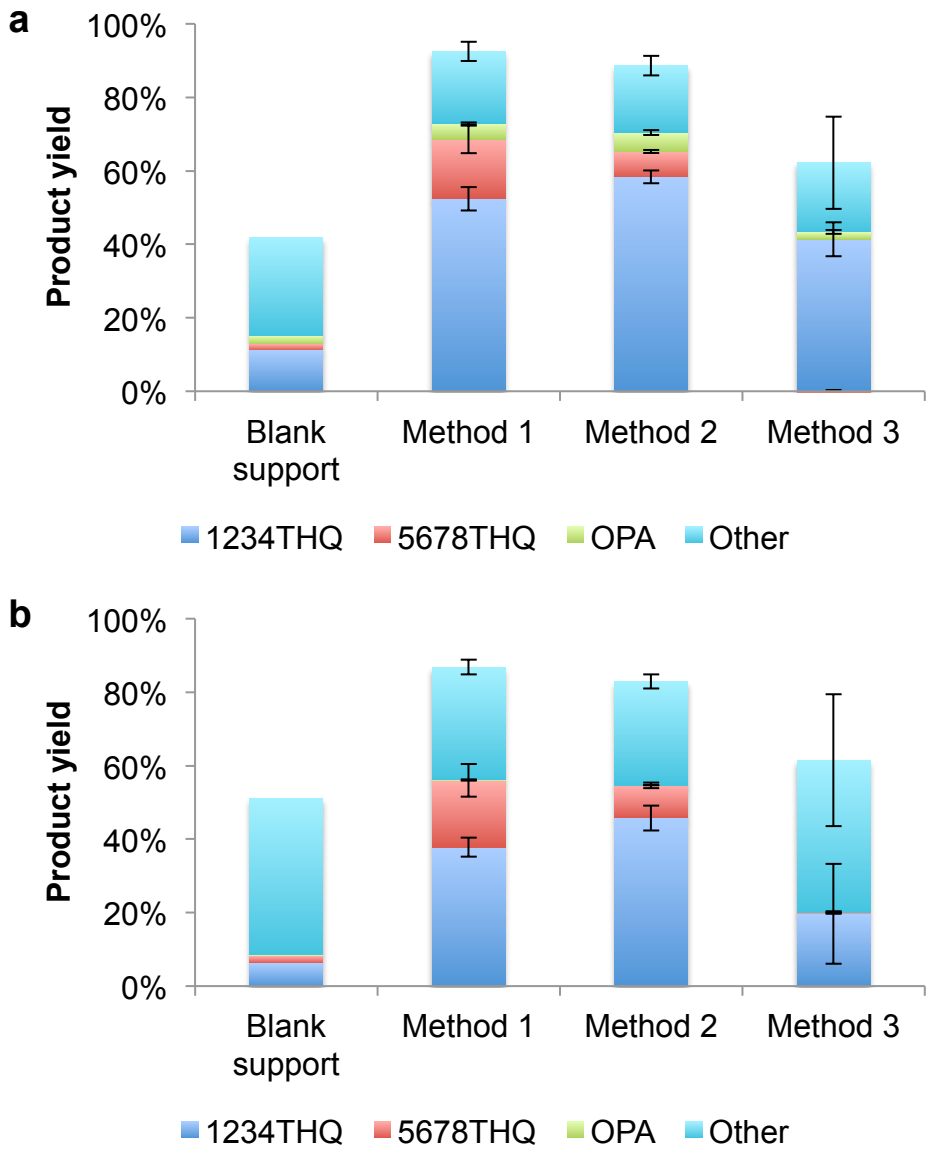

Figure 6.19: Conversion of quinoline over nickel phosphide catalysts, supported on H^+ Y zeolite, prepared by two-step incipient wetness impregnation (method 1), single-step incipient wetness impregnation (method 2) and solution based impregnation (method 3). (a) analysis by ^{1}H NMR, (b) analysis by GC-MS.

The quinoline conversions over the materials produced via methods 1 and 2 (92 % and 89 %, respectively) were higher than those obtained over the two baseline transition metal catalysts (79 and 88 %). Their selectivity towards 1234THQ was comparable, but the Ni_2P catalysts favoured the formation of 'other' reaction products instead of OPA. In addition, the catalyst prepared by method 1 produced higher amounts of 5678THQ (16 %) than either of the two transition metal catalysts (6 %

and 7 %). In contrast, the performance of the method 3 catalyst was significantly lower, reaffirming the conclusions from the catalyst characterization that impregnation method 3 was inferior to the other two impregnation methods.

In the previous section, the fraction assigned as OPA by the ^{1}H NMR analysis was already attributed to undesired by-products, which are not involved in the general quinoline denitrogenation pathway. Therefore, the reduced formation of this compound over the Ni_2P catalysts compared to the transition metal catalysts is desirable as it could indicate that the unidentified 'other' fraction contained more denitrogenated reaction products. A higher activity for the hydrogenation of the second aromatic ring, as observed for the method 1 catalyst, is also advantageous, as it is necessary for the formation of DHQ, which appeared to be rate limiting in the denitrogenation of quinoline over Pd/C.

A potential explanation for the increased formation of 5678THQ over this catalyst could be the presence of a pure Ni_2P phase, whereas the method 2 material contained only partially reduced metallic Ni. Even if phosphorus isn't directly involved in the reaction, it may help to reduce the binding forces between Ni and nitrogen, preventing poisoning of the active sites.[70]

6.3.3 Effect of zeolite counterion

Following these results, the effect of the zeolite counterion (H^+, K^+, NH_4^+ and Na^+) on the quinoline conversion performance using the blank zeolites, and the catalysts prepared by impregnation methods 1 and 2, was evaluated.

6.3.3.1 Conversion over blank supports

With the exception of Ni^{2+} Y, the reactions over the blank zeolite supports resulted in low quinoline conversions, ranging from 24 % over Na^+ Y zeolite to 42 % for H^+ Y zeolite (Figure 6.20a), but higher than the conversion achieved during the blank run without catalyst (21 %). The four zeolites NH_4^+ Y, H^+ Y, Na^+ Y and K^+ Y all produced similar amounts

of 1234THQ (10 to 14 %), comparable to the amount formed without catalyst (10 %). This suggests that the formation of 1234THQ was not catalysed by the zeolites, but may instead have been catalysed by the reactor wall (stainless steel). The increase in the 'other' product fraction was most likely associated with the formation of cracking products, catalysed over the zeolite acid sites. As these reactions were solely conducted for comparative purposes, the results are based on a single reaction, and consequently no error bars are displayed.

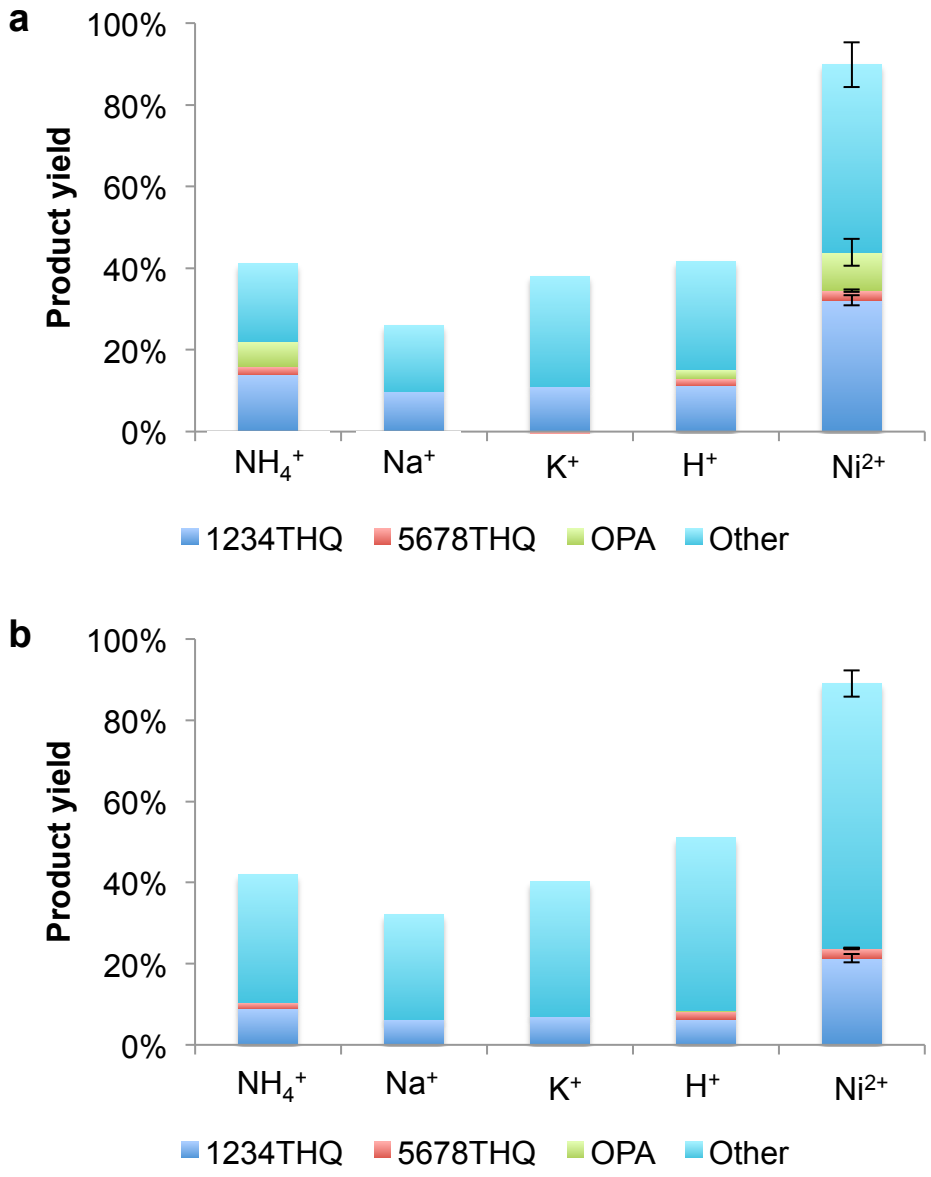

Figure 6.20: Conversion of quinoline over blank Y zeolite supports, containing different counterions. (a) analysis by ^{1}H NMR, (b) analysis by GC-MS.

Compared to the other zeolites, the yields obtained over Ni^{2+} Y were remarkably different, with an overall conversion of 90 %, 1234THQ yields of 32 %, and 46 % of unidentified 'other' products. The 9 % OPA yield also indicates the formation of undesired side products. To obtain more information on the denitrogenation activity of this zeolite, the product phase was analysed by ^{13}C NMR (Table 6-9), however no peaks corresponding to OPA, DHQ, PB or PCH could be detected. This suggests that the unidentified product phase consisted predominantly of cracking and isomerisation products.

6.3.3.2 Conversion over catalysts prepared with method 1

Out of the materials prepared by the two-step impregnation, the catalysts supported on H^+ Y and NH_4^+ Y appeared more active, achieving quinoline conversions of 91 % and 92 %, respectively, compared to conversions of 81 % and 78 % for the Na^+ and K^+ Y alternatives (Figure 6.21a). These two catalysts also produced significantly higher yields of 5678THQ (9 % and 16 %, respectively), compared to the Na^+ Y and K^+ Y catalysts (1 % and 2 %). It is also noticeable that K^+ Y showed a very high selectivity towards 1234THQ, with very little formation of other reaction products. In contrast, Na^+ Y showed the lowest overall selectivity towards the partially hydrogenated quinoline products (1234THQ and 5678THQ) and produced the highest amount of unidentified 'other' products.

The differences in product distribution could be related to the differences in the nickel phase present on the catalysts. XRD analysis identified a pure Ni_2P phase for the H^+ Y supported catalyst, a mixed $Ni_2P/Ni_{12}P_5$ phase for the Na^+ Y and K^+ Y catalysts and a mixed Ni_2P/Ni^0 phase for the NH_4^+ Y catalyst. This suggests that the Ni_2P phase displayed a higher hydrogenation activity for the 2nd aromatic ring than either metallic Ni or $Ni_{12}P_5$ and is consistent with previous findings that the Ni_2P phase is more active than the metal rich $N_{12}P_5$ phase.[140]

Alternatively, the differences in 5678THQ selectivity could also be related to differences in particle size. The Na^+ Y and K^+ Y supported catalysts contain much larger particles (41.3 nm and 43.3 nm, respectively) than

the NH_4^+ Y and H^+ Y supported catalysts (26.5 nm and 33.2 nm). Previous studies identified that Ni_2P contains two different types of catalytic sites: tetrahedral sites, which are more predominant in the bulk phase, and square pyramidal sites which are more predominant in smaller nanoparticles, and are more active towards hydrogenation reactions.[210]

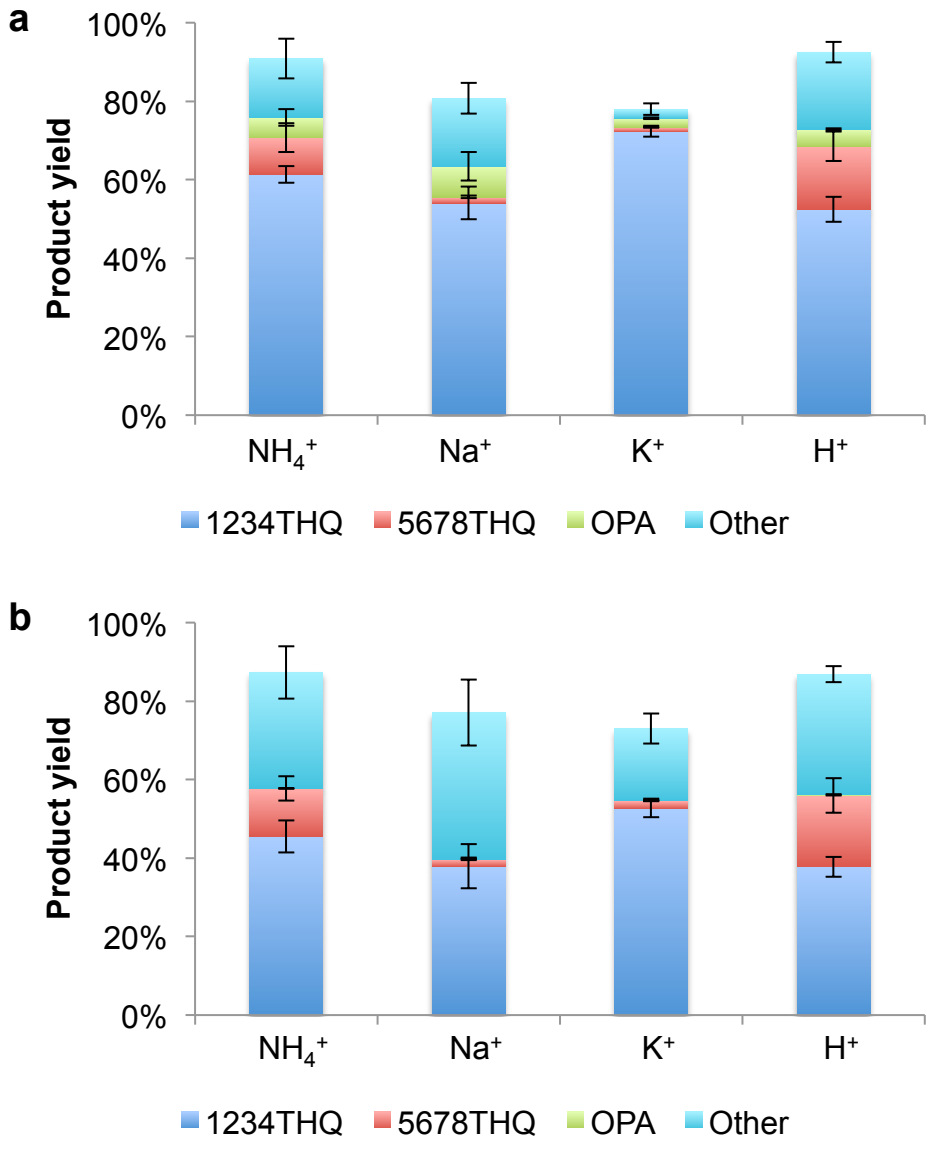

Figure 6.21: Effect of Y zeolite counterion on the conversion of quinoline over Ni phosphide catalysts prepared via two-step incipient wetness impregnation. (a) analysis by ^{1}H NMR, (b) analysis by GC-MS.

The high selectivity of the K^+ Y supported catalyst towards 1234THQ compared to the other catalysts and the unimpregnated support, suggests that the catalyst preparation method reduced the isomerisation

Table 6-9: ^{13}C NMR analysis for conversion product of quinoline over Ni^{2+} Y zeolite. Theoretical peaks are listed on the left, whereas the actual peaks are assigned to each product and missing peaks are denoted by an X.

Theoretical peaks	1234THQ	5678THQ	OPA	tDHQ	cDHQ	PCH	PB
157.28		x					
146.73		x					
144.80	144.66						
144.14			x				
136.60		x					
132.12		x					
129.48			129.40				
129.40	129.40						
126.83			x				
126.65	126.62						
126.64			126.62				
121.26	121.28						
120.80		120.93					
118.62			x				
116.77	116.88						
115.49			x				
114.12	114.08						
53.28				x			
50.49					x		
47.31				x			
45.52					x		
43.85				x			
42.52				x			
41.93	41.92						
40.04						x	
37.56						x	
36.54					x		
34.74					x		
34.43				x			
33.64				x			
33.58						x	
33.33			x				
32.52		x					
30.57				x			
30.11					x		
28.86					x		
28.73		28.69					
27.00	26.91						
26.89						26.91	
26.85					x		
26.61						x	
26.53				x			
26.31				x			
25.05					x		
23.09		x					
22.90					x		
22.71		x					
22.17	22.16						
21.86							
20.04						x	
14.46						14.36	
14.13			x				

and cracking activity of this material. A previous study showed that a K^+ USY supported Ni_2P catalyst displayed significantly lower cracking activity than an H^+ Y equivalent, and contained a much lower number of Brønsted acid sites.[129]

6.3.3.3 Conversion over catalysts prepared with method 2

The reactions over the catalysts prepared via single-step incipient wetness impregnation (method 2) generally followed similar trends to those over the catalysts prepared by method 1: The NH_4^+ Y and H^+ Y supported catalysts achieved higher overall conversions and were the only materials to yield significant quantities of 5678THQ, whereas the highest selectivity towards 1234THQ was achieved over the K^+ Y catalyst.

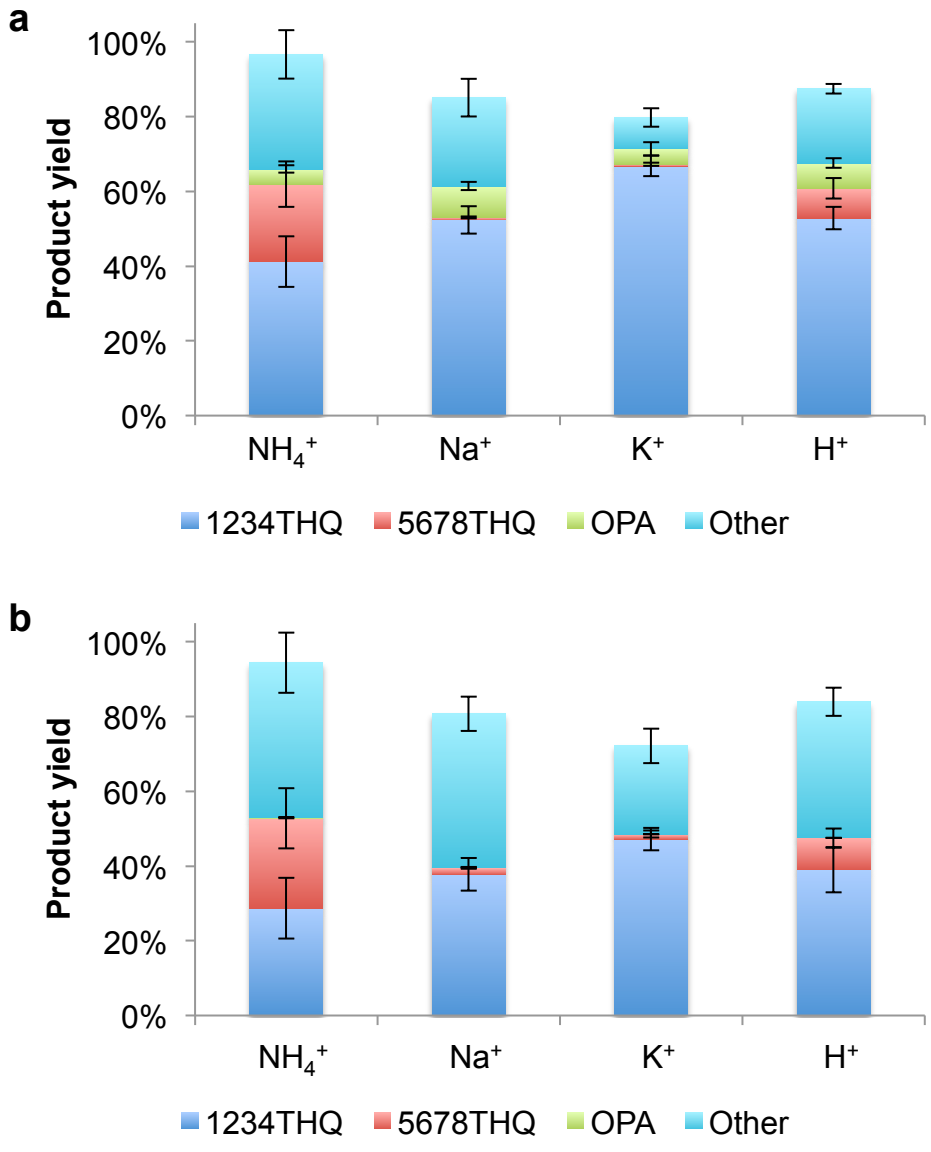

Figure 6.22: Effect of Y zeolite counterion on the conversion of quinoline over Ni phosphide catalysts prepared via single-step incipient wetness impregnation. (a) analysis by ^{1}H NMR, (b) analysis by GC-MS.

However, whilst for the H^+ Y catalyst the 5678THQ yield was reduced from 16 % to 8 % compared to the catalyst prepared by dual-step impregnation, it was increased from 9 % to 21 % for the NH_4^+ Y supported catalyst. The latter catalyst was also the only of the four materials, prepared by single-step impregnation, that displayed a pure Ni_2P phase, whereas the H^+ Y supported catalyst contained mostly metallic nickel and the Na^+ Y and K^+ Y catalysts displayed a mixed $Ni_2P/Ni_{12}P_5$ phase.

The increase in 5678THQ yields for the NH_4^+ Y catalyst prepared by method 2 rather than two-step impregnation could once again be related to a smaller particle size (17.01 nm vs 27.1 nm), increasing the relative contribution of the square pyramidal sites, responsible for hydrogenation reactions.

6.3.4 EFFECT OF ZEOLITE STRUCTURE

As described in section 6.2.5, catalysts supported on the base-treated zeolites ($H^+ Y_{low}$ and NH_4^+ Y) were prepared by the single-step impregnation method only. These catalysts were then tested for the conversion of quinoline along with the blank zeolite supports.

6.3.4.1 Conversion over blank supports

For both sets of zeolites, the materials produced by mild and harsh base leaching showed much lower quinoline conversions than the unmodified supports (Figure 6.23). Consistent with the previous section, the 1234THQ yields of all the supports were comparable to the non-catalytic blank, whilst the remaining products mostly fell within the unidentified 'other' product fraction. Interestingly, the overall quinoline conversions over the modified supports were comparable to the blank reaction run, which suggests that the materials were no longer catalytically active. Even so, the results from the material analysis (section 6.2.5) suggested that the zeolite structure had been retained and the BET surface area was increased for NH_4^+ Y and only reduced slightly for the H^+ Y zeolites.

A potential explanation is the ion exchange of NH_4^+/H^+ with Na^+, as the zeolite containing the Na^+ counterion was the least active out of all the blank zeolites tested so far. In addition, the base treatment could have neutralized the acid sites in the zeolite for example through the absorption of TPABr.

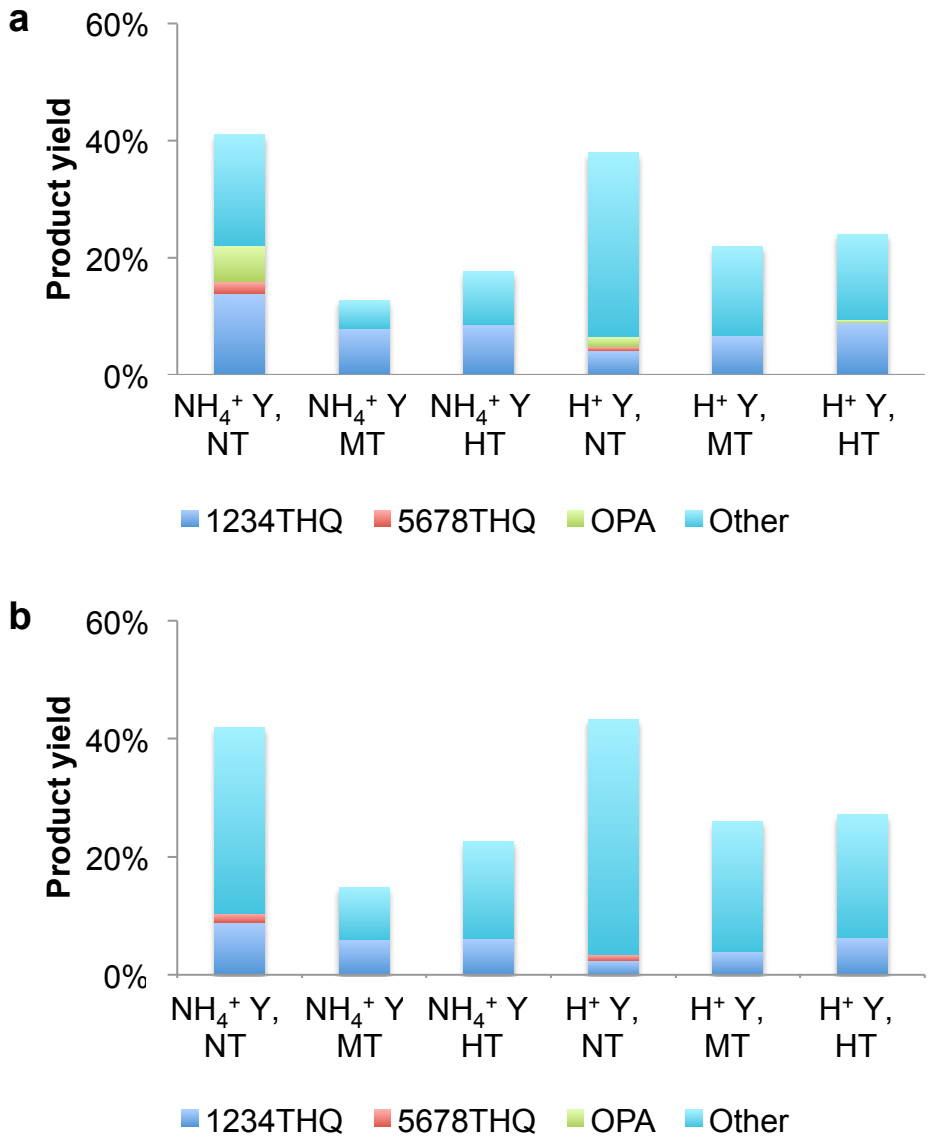

Figure 6.23: Conversion of quinoline over NH_4^+ Y and low aluminium H^+ Y_{low} zeolites, either with no treatment (NT), mild chemical treatment (MT) with 0.2g g^{-1} TPABr, or harsh chemical treatment (HT) with 0.92 g g^{-1} TPABr: (a) analysis by ^{1}H NMR, (b) analysis by GC-MS

6.3.4.2 Conversion over catalysts prepared with method 2

Similar to the unloaded zeolite supports, quinoline conversion over the Ni catalysts was reduced for most of the chemically modified supports

(Figure 6.24). It is noticeable that the reduction was higher for the NH_4^+ Y series than for the H^+ Y_{low} supported catalysts. The former also experienced a larger change in product distribution, away from 5678THQ, towards 1234THQ and OPA. In contrast, the 5678THQ yield for the low-Al supports remained approximately constant at around 12 %, lower than the yield over the unmodified NH_4^+ Y catalyst, but higher than its modified versions.

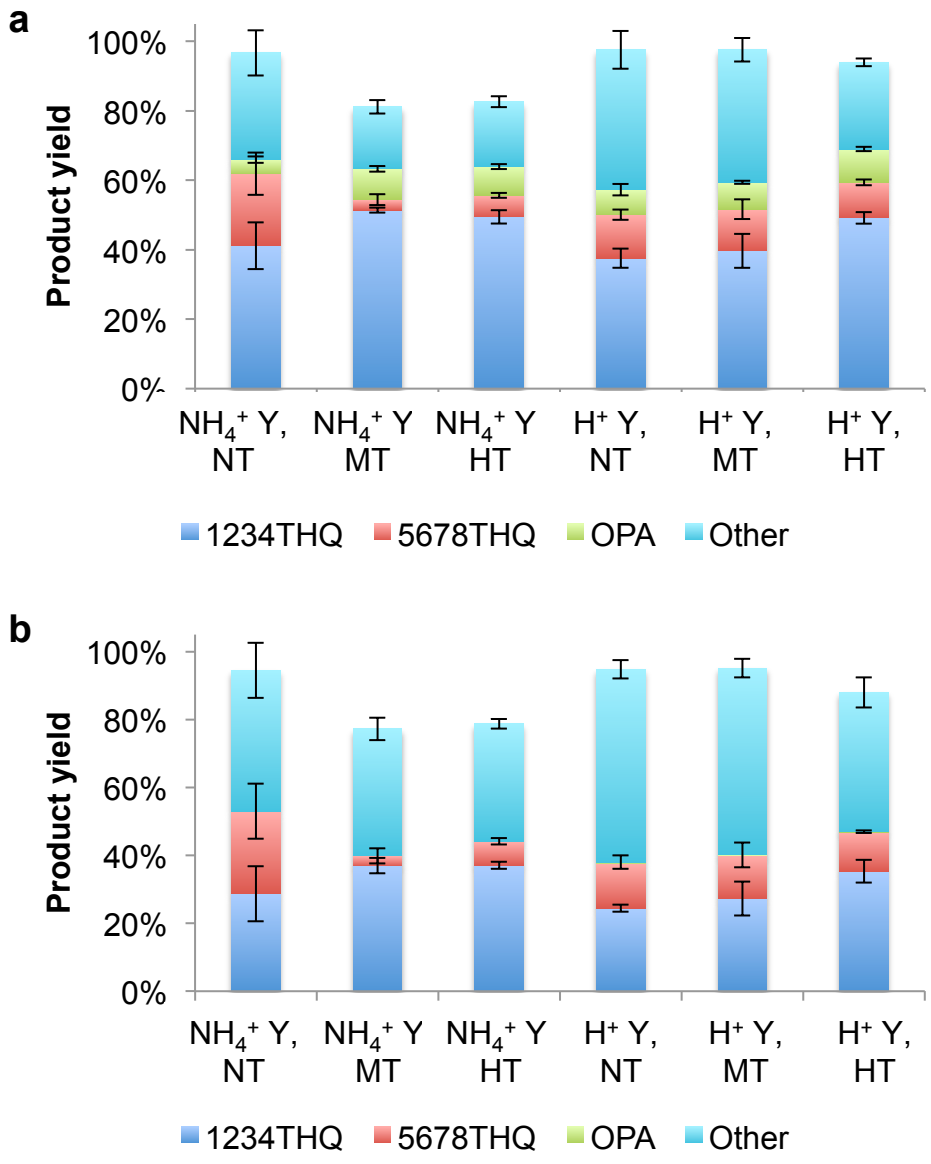

Figure 6.24: Conversion of quinoline over nickel phosphide catalyst supported on NH_4^+ Y and low aluminium H^+ Y_{low} zeolites, either with no treatment (NT), mild chemical treatment (MT) with 0.2g g^{-1} TPABr, or harsh chemical treatment (HT) with 0.92 g g^{-1} TPABr: (a) analysis by ^{1}H NMR, (b) analysis by GC-MS

The shift from 5678THQ towards 1234THQ for the modified NH_4^+ Y supported catalysts could once again be associated with the emergence of the $Ni_{12}P_5$ phase, which was not present on the unmodified support, and a significant increase in particle size from 17.0 nm to 39.1 nm, reducing the number of square pyramidal edge sites. In contrast, the reduction in overall conversion was mostly associated with a reduction in the 'other' product fraction, as already observed for the blank supports. This in turn suggests that the formation of this product fraction was catalysed by the zeolite surface, rather than the Ni sites, and could include isomerisation and cracking products, not directly involved in the quinoline denitrogenation pathway.

For the H^+ Y_{low} supports, the 5678THQ selectivity remained the same, as the pure Ni_2P phase was expressed over all three supports, and the particle size was more consistent ranging from 26.2 nm and 30.1 nm. Only a minor reduction of the 'other' product phase was observed following zeolite modification, which could suggest that the changes to the zeolite surface, resulting in a reduction in 'other' products for the blank zeolites, were reversed during catalyst preparation.

6.4 BIO-OIL UPGRADING

The oil upgrading studies converted the light-oil phase produced during the continuous HTL experiments of the wastewater-derived microalgae, described in Chapter 5. This oil phase accounted for up to 17.6 wt% of the total algae biomass. For the upgrading experiments, the light-oil products from all continuous reaction runs were combined to obtain a consistent feedstock. This mixed oil had an average nitrogen content of 4.57 wt% (± 0.69 wt%) and oxygen content of 12.84 wt% (± 1.32 wt%), as determined by CHN analysis of three separate samples.

The upgrading studies were conducted in the same reactors as the model compound reactions; however, to allow a more precise determination of the nitrogen content in the reaction product using elemental analysis, the oil was converted without additional reaction solvent. Because of this, the reaction volume was significantly reduced from 1 mL for the model

reactions to between 100 mg and 150 mg of bio-oil, potentially reducing the contact between catalyst and bio-oil.

6.4.1 CATALYST SELECTION

The quinoline conversion studies indicated that a number of the synthesised zeolite supported Ni_2P catalysts displayed comparable, if not higher, hydrogenation activities than the baseline, sulphided transition metal catalysts. With exception of Ni^{2+} Y, the zeolites alone displayed only slightly higher quinoline conversion activities than the non-catalytic reaction, and these reactions were mostly associated with cracking and isomerisation reactions, not directly contributing to the denitrogenation pathway.

The reactions over the catalysts supported on zeolites containing different counterions suggested that the NH_4^+ Y and H^+ Y catalysts produced a more favourable product distribution than the Na^+ Y and K^+ Y alternatives, with the highest hydrogenation activity observed over the NH_4^+ Y catalyst prepared with single-stage incipient wetness impregnation.

Reactions with the base-modified catalysts suggested that base pretreament had no beneficial effect on the conversion of quinoline, but may have resulted in reduced side product formation through cracking and isomerisation reactions. At the same time, the catalysts supported on the low-Al zeolite, $H^+ Y_{low}$, displayed a lower 5678THQ selectivity than the catalyst supported on the unmodified NH_4^+ Y zeolites, but showed higher stability in conversion following base treatment.

Based on these results, it was decided to select five of these catalysts for the bio-oil upgrading, in addition to the three baseline catalysts Pd/C, NiCoMo/Al and $NiMo/CeO_2$, and non-catalytic blank runs.

The catalysts supported on the unmodified NH_4^+ Y, H^+ Y and $H^+ Y_{low}$ zeolites were selected as they displayed the highest hydrogenation activities (highest 5678THQ selectivity) of all the studied materials. In addition, the catalyst supported on the modified NH_4^+ Y-HT zeolite was selected as it displayed a significantly reduced cracking/isomerisation

activity compared to the untreated zeolite. Finally, the blank Ni^{2+} Y zeolite was selected for its high cracking activity, which may not contribute directly to the quinoline denitrogenation pathway, but may still be useful for the upgrading of the heavy bio-oil produced in the liquefaction reaction. All chosen catalysts were prepared using impregnation method 2, to allow a direct comparison between the different zeolites, even though for the H^+ Y supported catalysts, the material prepared using method 1 appeared to display a higher hydrogenation activity, related to improved reduction of the Ni phase to Ni_2P.

6.4.2 UPGRADING REACTIONS

For all four baseline reactions (without catalyst and with Pd/C, NiCoMo/Al and $NiMo/CeO_2$), the carbon and hydrogen recovery to the bio-oil was significantly higher than the recovery of nitrogen, indicating a substantial reduction in nitrogen content (Figure 6.25a). The highest carbon recoveries were obtained over the two sulphided catalysts NiCoMo/Al (69 %) and $NiMo/CeO_2$ (70 %), corresponding to the highest upgraded bio-oil yields overall, of 62.1 wt% and 64.3 wt%, respectively (Table 6-10). In contrast, Pd/C displayed the lowest carbon recovery and bio-oil yield of 60 % and 55.6 wt%, respectively, however this catalyst also had the lowest nitrogen recovery, of only 27 %, corresponding to a reduction in nitrogen content by 52.3 %. This value is significantly higher than the nitrogen reductions achieved during the blank run (36.4 %) and with the two sulphided catalysts NiCoMo/Al (36.7 %) and $NiMo/CeO_2$ (31.2 %). Even though the nitrogen removal for the latter catalyst appears reduced compared to the blank, all three values are within experimental error, as indicated by the range of their standard deviations (1.7 – 3.9 %).

The upgrading reactions also resulted in similar reductions in oxygen content (calculated by difference), from 12.8 wt% in the raw bio-oil to 8.3 % for the blank, 7.3 % for Pd/C and 6.1 % and 5.8 % for the two sulphides. Consequently, the sulphided catalysts displayed higher deoxygenation activities than Pd/C, potentially due to the presence of

acid sites, which might help to catalyse cracking reactions to release CO or CO_2.

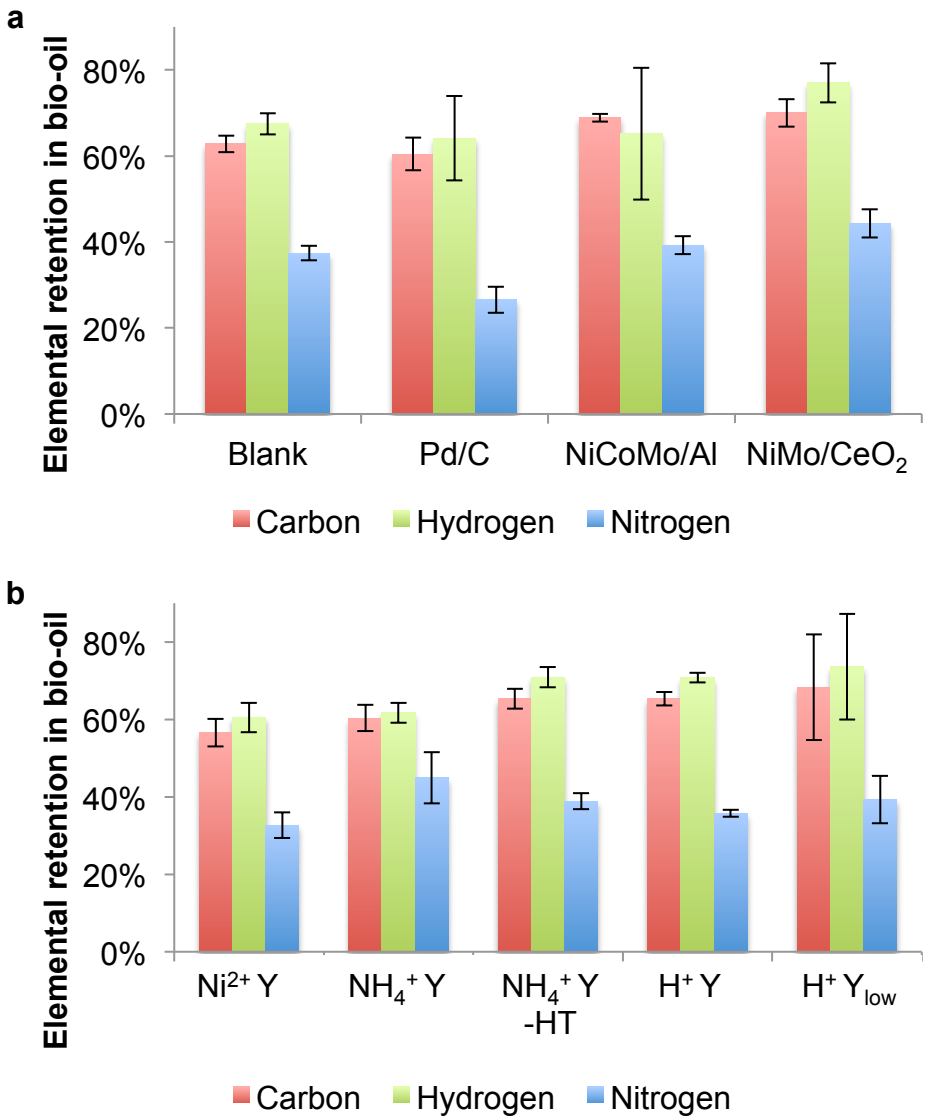

Figure 6.25: Elemental recovery of C, H and N into upgraded bio-oil. (a) baseline reactions, (b) reactions over zeolite supported Ni_2P catalysts

The zeolite-supported Ni-P catalysts also resulted in significantly lower retentions of nitrogen in the upgraded oil than of carbon or hydrogen (Figure 6.25b). The lowest nitrogen retention of 33 % was obtained over the unimpregnated Ni^{2+} Y zeolite, however this catalyst was also relatively inefficient in retaining carbon (57 %) and hydrogen (60 %), resulting in a low upgraded bio-oil yield of only 53.1 %, with a nitrogen reduction of 38.6 %. In contrast, the H^+ Y supported catalyst also retained a low fraction of nitrogen (36 %), but produced much higher bio-oil yields of 60.8 wt%, resulting in a nitrogen reduction of 41.2 %. Even so, the

difference compared to the blank run is below the combined standard deviation of the two sets of experiments.

Table 6-10: Bio-oil conversion activity of baseline catalysts and selected zeolite supported nickel phosphides

Catalyst	Oil Yield, wt%	Oil composition, wt%				N reduction, %
		C	*H*	*N*	*O*	
Raw Bio-oil	n/a	72.81	9.84	4.57	12.84	n/a
Blank	58.9 ±1.4	77.6	11.2	2.9	8.3	36.4 ±3.9
Pd/C	55.6 ±3.8	79.2	11.3	2.2	7.3	52.3 ±3.3
NiCoMo / Al	62.1 ±0.9	80.7	10.3	2.9	6.1	36.7 ±3.4
NiMo / CeO_2	64.3 ±3.2	79.4	11.7	3.1	5.8	31.2 ±1.7
Ni^{2+} Y	53.1 ±2.7	77.5	11.1	2.8	8.6	38.6 ±4.3
Ni-P / NH_4^+ Y-NT	59.6 ±3.5	73.7	10.2	3.4	12.6	24.8 ±8.4
Ni-P / NH_4^+ Y-HT	60.6 ±2.9	78.4	11.3	2.9	7.2	35.9 ±0.5
Ni-P / H^+ Y	60.8 ±1.6	78.2	11.4	2.7	7.8	41.2 ±2.3
Ni-P / H^+ Y_{low}	63.5 ±12.0	78.2	11.4	2.9	7.6	37.6 ±3.6

Within error, the nitrogen reductions and upgraded oil yields over the other three zeolite supported catalysts (Ni-P/NH_4^+ Y-NT, Ni-P/NH_4^+ Y-HT and Ni-P/H^+ Y_{low}) were also comparable to the blank run, suggesting limited denitrogenation activity for the bio-oil. However, most of the supported Ni-P catalysts displayed a slightly enhanced oxygen removal capability compared to the blank run, but less than the two sulphided transition metal baseline catalysts.

These findings suggest that at the chosen reaction conditions, and compared to the blank reactions, both the sulphided baseline catalysts and the zeolite supported Ni-P catalysts displayed only limited denitrogenation activities for the bio-oil. A potential exception is the Ni-P/H^+ Y catalyst, which resulted in a nitrogen reduction of 41.2 %, compared to 36.4 % in the blank, however the difference was insufficient to account for experimental error. This is contrary to the much higher hydrogenation activities of all these catalysts, observed during the model

compound conversion study, and suggests that the bio-oil upgrading mechanism is more complex than for quinoline.

To investigate this further, the O/C and N/C molar ratios of the upgraded oils were plotted against the H/C ratio, in a Van Krevelen-like diagram (Figure 6.26). This plot shows that the oxygen content of the bio-oil appeared to be inversely related to the hydrogen content, whereas the correlation between nitrogen and hydrogen content is much weaker. This confirms the suggestion that the nitrogen removal capability of the catalysts is not directly related to their hydrogenation ability. The results for the NiCoMo/Al catalysts have been highlighted, as they do not appear to be representative due to the high experimental uncertainty of the hydrogen retention achieved over this catalyst (see Figure 6.25a).

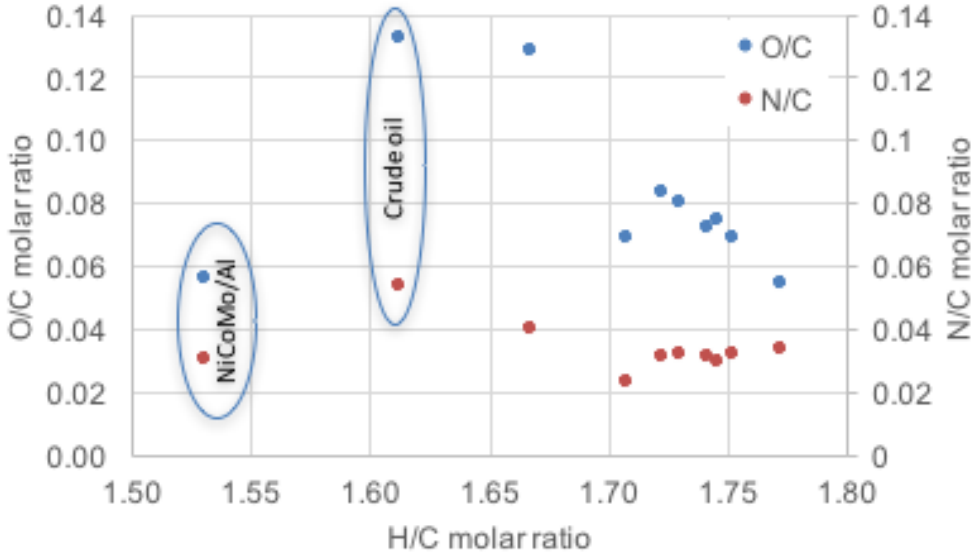

Figure 6.26: Van Krevelen like diagram for the upgrade bio-oil

The results from this study are consistent with previous findings made in the literature, where the presence of catalysts did not appear to have a significant effect on nitrogen removal.[83, 90] Barreiro *et al.* found that the presence of Pt/Al_2O_3 and HZSM-5 catalysts had limited beneficial impact on the upgrading of bio-oils produced by the HTL of *Scenedesmus almeriensis* and *Nannochloropsis gaditana* and they suggested that the reactions could be mass transfer-limited within their batch system.[81] Consequently, they suggested that more work should be done within

continuous upgrading systems, which provide better contact between catalysts, bio-oil and hydrogen.

Another potential limitation of the current work is the use of only partially reduced catalysts, as indicated by the XRD, TEM and TPR analysis conducted in section 6.2. Furthermore, all catalysts were passivated under a flow of 1% O_2/N_2 to form an oxide monolayer at the catalyst surface and prevent pyrophoric combustion during exposure to the atmosphere. With the batch reactors used for the current study, it was not possible to re-reduce the catalysts prior to introducing the reagents, and therefore, the catalysts could have remained in a less active state.

6.5 CONCLUSIONS

In this chapter, a range of Y zeolite supported nickel phosphide catalysts were synthesized for the upgrading of bio-oil obtained during the continuous HTL of wastewater algae.

6.5.1 CATALYST SYNTHESIS

The catalyst synthesis investigated the effect of the zeolite properties (selection of counterion, effect of base pretreatment, Si/Al ratio) and the synthesis procedure (impregnation method, Ni/P ratio, choice of P precursor) on the formation of the active Ni_2P phase.

Consistent with previous literature findings, a large excess of P was required to form the active phase. This could be partially attributed to the loss of P during the calcination and reduction process, particularly when using an ammonium hypophosphite precursor, and partially to the interaction of P with the support, proportional to the Al content of the zeolite.

Incipient wetness impregnation methods were found to yield catalysts with better metal dispersion than a solution based method, and single stage impregnation with an acidified nickel phosphide solution was less destructive to the zeolite support than two-step impregnation, resulting in higher BET surface areas. However, unlike the material produced by two-

stage impregnation, the single-stage catalyst was not fully reduced at 550 °C, resulting in the formation of metallic Ni, rather than Ni_2P. These results were confirmed using TPR analysis, indicating that temperatures of up to 720 °C were required to achieve full catalyst reduction.

The selection of the zeolite counterion had an important effect on the formation of the active phase. Na^+ Y and K^+ Y supported catalysts formed a mixed $Ni_2P/Ni_{12}P_5$ phase for both single and two-stage impregnation, whereas H^+ Y formed a pure Ni_2P phase with two-stage impregnation but only partially reduced metallic Ni after single stage impregnation. The NH_4^+ Y supported catalyst was the only of the four materials supported on the aluminium rich zeolites that formed the pure Ni_2P phase for single-stage impregnation, however TPR data once again suggested that the reduction was not complete at this temperature.

In contrast, the catalysts supported on the low aluminium H^+ Y_{low} support formed the desired Ni_2P for both methods of impregnation, probably due to reduced interaction of P with the support. Base-treatment had a lesser impact on the behaviour of this support than on NH_4^+ Y, which resulted in a shift towards the $Ni_{12}P_5$ phase, consistent with the ion exchange of NH_4^+ with Na^+, and TPR data displayed a broader reduction peak with a much lower onset temperature.

6.5.2 QUINOLINE CONVERSION

During the conversion of quinoline over the synthesised nickel phosphide catalysts it was found that catalysts containing the pure Ni_2P phase displayed a much higher hydrogenation activity than catalysts containing metallic Ni or the mixed $Ni_{12}P_5$ phase. Furthermore, the size of the nanoparticles appeared to be an important factor, with smaller nanoparticles displaying higher hydrogenation activities, possible due to the presence of a higher number of square pyramidal sites.

Consequently, the NH_4^+ Y and H^+ Y supported catalysts displayed a higher hydrogenation activity for quinoline than the Na^+ Y and K^+ Y alternatives. Base treatment of the NH_4^+ Y supported catalysts appeared

to have no beneficial impact on the hydrogenation activity of this catalyst, but appeared to reduce its cracking activity. In contrast, base treatment had limited impact on the low-Al H^+ Y_{low} supported catalysts. Most catalysts displayed comparable, if not higher hydrogenation activities than the two sulphided transition metal catalysts, but lower activities than Pd/C. The Pd/C catalyst was also the only catalyst that was shown to produce propylcyclohexane, one of the direct denitrogenation products from quinoline.

6.5.3 BIO-OIL UPGRADING

The upgrading of the light bio-oil phase, produced by the continuous HTL of wastewater-derived algae, was conducted over a selected number of catalysts and characterized using the nitrogen removal capability of each material. Whilst the presence of Pd/C resulted in a significant increase in bio-oil denitrogenation, compared to a blank run, neither of the two sulphided transition metal catalysts resulted in a statistically significant increase in nitrogen removal. However, these two catalysts performed slightly better in terms of oxygen removal than Pd/C and the blank reaction.

Similar findings were made for the four tested zeolite-supported Ni-P catalysts. The highest nitrogen removal of 41.2 % was obtained over Ni-P/H^+ Y; however, the difference compared to the blank run was insufficient to account for experimental error, as estimated by the standard deviations of the two reactions. Whilst the upgraded bio-oil oxygen content appeared to be inversely proportional to its hydrogen content, the correlation between nitrogen and hydrogen content was much weaker. This suggests that a high hydrogenation activity on its own is insufficient to yield active catalysts for the denitrogenation of bio-oils, and consequently, the results from the model compound studies may not be fully representative of the ultimate catalyst performance.

Overall, the results are comparable to previous findings in the literature, and could be related to limitations of the batch set-up used in this study, providing a poor interface between the catalyst, reagents and hydrogen.

Furthermore, the reduction temperatures employed during the catalyst preparation were insufficient to produce a fully reduced material, and the passivation procedure, required to protect the catalysts from pyrophoric combustion, could have further deactivated the catalysts. Consequently, further work is required to optimize the catalyst reduction procedure and transfer the upgrading work to a continuous reaction system.

CHAPTER 7

CONCLUSIONS AND FUTURE WORK

7.1 SUMMARY AND CONCLUSIONS

Microalgae are a promising feedstock for the production of 3rd generation biofuels: they can display much higher solar-to-biomass efficiencies than plants, they do not require agricultural land, and therefore do not directly compete with food production, and they can provide secondary functions such as wastewater treatment, carbon sequestration or the production of valuable by-products. However, the cultivation of lipid-rich algae is expensive, and consequently, the current algal fuel production costs, based on lipid-extraction technology, significantly exceed the short- to medium-term cost predictions for transportation fuels.

A potential alternative solution is to convert the algae via hydrothermal liquefaction, a thermochemical method, which converts the entire algae, not just lipids, and can therefore utilise much faster growing algae. This technology also allows the processing of wet biomass, with a water content of up to 95 %, significantly reducing the energy requirements associated with algae harvesting and drying. Finally, HTL allows a significant fraction of nitrogen and phosphorus to partition to the water phase, potentially facilitating their recovery for further algae growth, or as a natural, bio-derived fertilizer.

Despite this, a number of challenges remain to be overcome, before this technology can be applied to large-scale fuel production. Compared to lipid-derived fuels, the bio-oils produced via the HTL reaction are much more complex, display poor flow properties and contain high concentrations of heteroatoms, particularly nitrogen, which prevent their processing within conventional petrochemical refineries. Consequently, the bio-oils require significant upgrading before they can be fractionated into fuels. Furthermore, most research to date has been conducted using batch reactors, and consequently, the results cannot be directly applied to large-scale industrial processes, which are heavily based around continuous flow processes. Finally, fuels are a low-value product and are therefore unlikely to pay for the entire process on their own. Therefore,

additional value streams must be identified and developed which could help to subsidise the overall fuel production process.

The current project sought to investigate potential solutions for all three challenges, through a number of interlinked studies. Initially, the effect of the biochemical composition of the algae on the resulting bio-oil yields and quality was investigated using the model compounds rapeseed oil (lipid), soy protein (protein), corn flour (carbohydrates) and the cyanobacteria *Spirulina*. This work confirmed previous literature findings that, in isolation, the bio-oil yields obtained from lipids are significantly higher than those obtained from proteins or carbohydrates. However, during the conversion of *Spirulina*, the bio-oil yields were much higher than expected, due to the cross-reaction of protein- and carbohydrate-derived intermediates through so-called Maillard reactions. As these reactions also resulted in a significant increase in the nitrogen content of the bio-oils, the biochemical composition of the algae should be carefully balanced to obtain the best compromise between bio-oil yields and quality.

Subsequently, the possibility of using HTL to recover additional value from PHB-accumulating cyanobacteria was explored. On its own, PHB was almost fully converted into equal amounts of carbon dioxide and propylene, a valuable precursor for the polymer industry. Unlike for proteins and carbohydrates, the conversion of PHB was not affected by the presence of other algae components and a total propylene yield of 2.6 wt% was obtained from a specially grown algae, *Synechocystis* cf. *salina*, which had a PHB content of 7.5 wt%. Despite these promising results, the production of significant quantities of PHB-containing algae does not appear to be feasible in the short-term, due to the requirement of carefully controlled, nutrient-limited growth conditions, resulting in prohibitively expensive cultivation conditions.

An alternative algal by-product is the lipid fraction itself, which represents a higher-value feedstock for the production of fuels and chemicals than the lower quality HTL bio-oils. Although cost projections for lipid-based processes on their own have not been found to be competitive with

conventional transportation fuel technologies, the production of a lower-value HTL bio-oil from the lipid extracted residue could help to subsidise the overall process, and may allow the use of faster growing algae with a lipid content below the 40 wt% target.

To study the possibility of combining the two processes, a lipid-extracted hydrolysate solution of a *Chlorella* sp. strain was used as a feedstock for the HTL reaction. As the algae residue was expected to consist mostly of proteins and carbohydrates, which yield only limited bio-oil yields on their own, the study investigated the effect of adding IPA to the reaction solution and applied two low-value furnace waste materials, LFR and EAFS, as potential liquefaction catalysts.

The lipid extraction process used very high concentrations of sulphuric acid to help break up the biomass. Because of this, the algae hydrolysate required significant work-up to produce a neutral algae cake that could be converted through the liquefaction reaction. In this process, over 56 % of the carbon present in the hydrolysate was lost to the water phase, and could not be returned to the HTL process, due to the formation of hard, solid deposits, from the precipitation of sodium sulphate at the reaction conditions. These findings indicate that the lipid-extraction process has an important bearing on the usability of the resulting algae residue, and consequently alternative lipid-extraction processes should be explored.

Liquefaction yields from the conversion of the dry algal cake itself could be strongly increased by the addition of IPA to the reaction medium, although this process proved only feasible if the resulting aqueous phase was subsequently solvent-extracted to recover IPA and water-soluble bio-oil components. At 220 ºC, reactions in 50 vol% IPA and pure IPA yield yielded higher bio-oil yields than reactions conducted at 310 ºC and in pure water, however, the resulting bio-oils contained significantly higher amounts of nitrogen and the reaction enhanced solid formation. In contrast, the addition of 50 vol% IPA to the reactions conducted at 310 ºC caused the bio-oil yields to more than double from 13.4 wt% to 28.3 wt%, with minimal impact on the nitrogen content of the bio-oil.

The furnace waste residue LFR consisted predominantly of calcium, silicon and magnesium oxides, whereas EAFS also contained significant amounts of iron, aluminium, manganese and titanium. Neither of these two materials appeared to have any beneficial impact on the overall bio-oil yields, but instead resulted in increased solid yields, potentially due to the formation of char and coke over the catalyst surface. Furthermore, the reaction caused significant leaching of the catalyst components into the aqueous phase, which would be expected to cause downstream processing issues within a commercial fuel production plant. Nevertheless, the presence of EAFS appeared to have a slight positive effect on the carbon, hydrogen and nitrogen contents of the bio-oils produced in 50 vol% IPA, suggesting that it could have a low activity towards deoxygenation and denitrogenation reactions, most likely catalysed by its iron content of 12.6 wt%.

An alternative strategy of developing additional value streams is to combine the algae cultivation stage with a secondary objective, such as carbon sequestration or wastewater treatment. Using algae for wastewater treatment is a particularly promising option, as it has the potential to eliminate the requirement of external nutrients for algae growth, significantly reducing the financial and environmental costs of this processing stage, as well as improving the quality of wastewater discharged back to the environment. Consequently, the project investigated the conversion of algae used for the tertiary removal of N and P from domestic wastewater. But rather than converting this algae under batch conditions only, it was decided to design and commission a continuous flow process, which would be more representative of the conditions expected in a large-scale, commercial fuel production process.

Only few studies have been published so far on the continuous HTL of algae. All of these used mechanical pumps to push the algae slurry through the system and often encountered significant operational problems when attempting to deliver representative concentrations of algae. The most successful systems were also the most expensive, and due to their scale and complexity may not be applicable to laboratory-

scale operation. Consequently, the objective of this work was to design an inexpensive laboratory-scale alternative, that would allow the screening of different algal species under varying operating conditions. To do this, the system employed high-pressure nitrogen to push the algae through the system, thereby eliminating the limitations of mechanical pumps of delivering very low flows of a viscous biomass slurry at high pressures. The initial commissioning of the system identified a number of operational challenges, including the formation of blockages within the reactor itself and the high viscosity of the bio-oil close to ambient conditions. Consequently, the reactor was re-designed to allow in-situ collection of the solid product, eliminating the accumulation of this product phase within the flow path, and the system outlet was reconfigured to allow product collection at elevated temperatures above 60 ºC and close to reaction pressure. Using this system, it was possible to successfully process 1 L of a 5 wt% algae slurry at flowrates ranging from 3 mL min^{-1} to 7 mL min^{-1} and at reaction temperatures of up to 340 ºC.

When converting the wastewater-derived algae in a batch reactor it was found that bio-oil yields were significantly enhanced when increasing the heating rates from 10.1 °C min^{-1} - 35.2 °C min^{-1}. This effect was related to competitive side reactions occurring during the heating period which consume part of the water-soluble intermediates before they can produce the desired bio-oil phase at higher reaction temperatures. However, when increasing the heating rates further, the oil yields from the batch system were found to decrease sharply, potentially as the overall reaction time was insufficient to achieve full biomass conversion. These problems were not observed with the continuous reaction rig, which combined very fast heating rates with extended reaction times, and consequently produced significantly higher bio-oil yields than the batch system. These findings highlight the importance of conducting HTL reactions under continuous reaction conditions, which are more representative of large-scale industrial processes.

Despite this, the nitrogen content of the resulting bio-oil remained significantly above the acceptable threshold for refining operations,

requiring significant further upgrading. Only limited research has been published on the upgrading of the bio-oils obtained from the HTL of algae, and has mostly focused on the use of expensive noble metal catalysts, or sulphided transition metal catalysts, which require the presence of sulphur-containing compounds, and may therefore not be the most suitable catalysts for the upgrading of the low-S algal bio-oils. A promising alternative class of catalysts are transition metal phosphides, which have been shown to display high activities for the denitrogenation of petroleum model compounds.

In this project, a number of Y-zeolite supported Ni-P catalysts were synthesised and tested for the denitrogenation of the model compound quinoline, as well as the upgrading of the bio-oil obtained from the continuous HTL of the waste-water derived algae. This work confirmed previous literature findings that the catalyst synthesis requires a large excess of P to yield the active Ni_2P phase. Replacing the most commonly used P precursor ammonium phosphate with the lower-oxidation state alternative, ammonium hypophosphite, did not have a beneficial impact on the formation of the active phase, potentially due to excessive loss of P, before the Ni became reduced. Incipient wetness impregnations were found to produce more dispersed catalysts than a solution-based alternative, and single-stage impregnation was less destructive to the zeolite phase than a two-step impregnation process. However, the two-step process produced a purer Ni_2P phase than the single step process, potentially through the shielding of Al sites in the zeolite with Ni, preventing their reaction with the P precursor.

The nature of the zeolite counter-ion was also found to influence the formation of the Ni_2P phase, potentially through modifying the reduction temperature as indicated by TPR data. The K^+ and Na^+ supported catalysts appeared to reduce more easily, however the nickel phosphide formation appeared to be P-limited, resulting in the production of a mixed $Ni_2P/Ni_{12}P_5$ phase. In contrast, H^+ Y and NH_4^+ Y supported zeolites produced pure Ni_2P phases following two-step impregnation, but produced only partially reduced materials for the single-step impregnation

process. Catalysts supported on H^+ Y zeolite with a reduced aluminium content appeared to be reduced more easily, probably due to reduced interaction of P with the support. Base-treatment of the zeolite, at last, appeared to increase the reducibility of the NH_4^+ Y supported catalyst, probably due to ion exchange with Na^+.

During the conversion of quinoline, the catalysts containing a pure Ni_2P phase and smaller nanoparticles appeared to display the highest hydrogenation activities, indicated by higher yields of the hydrogenation product 5678THQ, and this was presumably related to the presence of a higher number of square pyramidal edge sites. Most phosphide catalysts displayed comparable, if not higher, quinoline conversion activities than two sulphided transition metal baseline catalysts, however the only catalyst that was shown to produce the denitrogenation product propylcyclohexane was the baseline catalyst Pd/C.

Based on the results from this model compound conversion, a number of catalysts were selected for the upgrading of the bio-oil produced by the continuous HTL of the wastewater-derived algae. However, with the exception of Pd/C, none of the tested catalysts displayed statistically significant enhancements in denitrogenation activities compared to a blank reaction run. This suggests that the bio-oil upgrading is more complex than the conversion of quinoline, and cannot be directly linked to the hydrogenation activity of the catalysts. Furthermore, the catalyst reduction temperature used in this study was not optimized, resulting in only partially reduced materials. In addition, all upgrading reactions were conducted in batch reactors which may have provided a poor interface between the catalyst, reagents and hydrogen.

7.2 FUTURE WORK

The current project explored a number of avenues for developing additional value streams that could help to subsidise the biofuel production from the HTL of microalgae.

HTL of PHB-containing cyanobacteria was found to produce elevated amounts of propylene, a potential precursor for the polymer industry. However, the high metabolic cost for expressing PHB within the algae requires prohibitively expensive cultivation conditions, and consequently, barring major technological breakthroughs, it is the authors opinion that no further studies should be conducted on the HTL of PHB containing algae.

In contrast, algal lipid production is much more established, and HTL could provide the solution to sufficiently reducing production costs to make this process economically viable. However, it is clear, that this area requires a more in-depth analysis. The lipid extraction process and HTL of the algae residue must be much better integrated to prevent the introduction of excessive quantities of contaminants, such as sodium sulphate. A potential option is to apply thermochemical methods for the lipid extraction process, even if this results in a slight reduction of the overall lipid recovery. Alternatively, research could be focused on reducing the strength of the algal cell wall, and thereby allowing the use of milder extraction conditions. Based on this data, the economic feasibility of the whole process needs to be assessed, and the algal lipid concentration optimized to maximise the product yields of lipids and bio-oil and minimise the processing costs, predominantly associated with algal cultivation.

Combining algae production with wastewater treatment is particularly promising as it combines two of the most pressing challenges of this century: sustainable energy production and the maintenance of clean water sources. Whilst the overall bio-oil yields obtained from the wastewater-derived algae were relatively low, owing to its high ash content, closer integration between the wastewater treatment process

and the algae conversion could help to produce an algae feedstock with a more favourable biochemical composition. However, as the algae was specifically chosen for its ability to quickly settle in a gravity separator, thereby reducing post-treatment costs, and therefore requires a high ash content, it is likely that HTL will only serve as a secondary process to utilising the biomass produced from the wastewater treatment. Nevertheless, the studies should be conducted on a larger scale and over a longer period of time, to assess the effect of seasonal and local variations on the algae composition and its conversion during HTL reactions. The project which provided the algae for this study is already moving towards pilot scale production, which is expected to be fully operational by the end of 2016. Once again, this data should feed into lifecycle and techno-economic analyses, to identify the feasibility of using algal wastewater treatment in the first place, and compare biomass conversion by HTL, with alternative processes such as anaerobic digestion or gasification reactions.

Finally, value-adding processes are not restricted to the options explored in this project. Alternatives include the combination of algae cultivation for carbon sequestration, the recovery of alternative by-products such as polysaccharides and proteins, and further utilisation of the other three product phases.

One of the main objectives of this work was to develop an inexpensive laboratory-scale system to study the continuous HTL of algae slurries. Employing high-pressure nitrogen to deliver the algae produced a flexible system which was able to fulfil this requirement. Nevertheless, the operation of the system required a lot of manual intervention, increasing the risk of operator error and limiting the precision of temperature and flow control. These limitations could be addressed relatively easily, through the installation of a mass flow controller on the nitrogen inlet and controlling the furnace temperature directly off the reactor temperature.

Whilst the results from the continuous system showed a significant enhancement in bio-oil production compared to an equivalent batch system, all experiments employed the same biomass concentration, feed

volume and algal species. Further studies should therefore investigate a wider range of operating conditions, including the use of higher biomass loadings, and maintain the liquefaction reaction for a longer period of time. Overall, more liquefaction studies need to be conducted under continuous flow conditions, to allow a better evaluation of the industrial applicability of this technology and identify and address potential operating challenges.

All bio-oils produced in this project contained a significant amount of nitrogen, which restrict their conversion within conventional petrochemical refineries. To address this, a number of zeolite-supported nickel phosphide catalysts were synthesised and applied to the upgrading of this oil. Even though the catalysts displayed enhanced hydrogenation activity during the conversion of the model compound quinoline, they proved poorly active for the denitrogenation of the bio-oil. Consequently, further work is required to further improve the synthesis of the catalysts, particularly the reduction procedure, as well as improving the reactor design used for the actual upgrading reaction. Continuous flow systems would be expected to provide much better contact between the catalysts, bio-oil and hydrogen, as well as allowing pre-activation of the catalyst under the flow of hydrogen.

CHAPTER 8

EXPERIMENTAL

This chapter provides additional experimental detail for the results discussed in Chapters 3 to 6. The chapter has been divided into four sections, which correspond to each research chapter.

8.1 HTL OF PHB CONTAINING MICROALGAE

As Chapter 3 has been submitted by publication, the experiment detail is fully included within its methodology sub-section.

8.2 LIQUEFACTION OF LIPID-EXTRACTED ALGAE CAKE IN THE PRESENCE OF IPA AND FURNACE RESIDUES

This section provides the experimental detail for the work described in Chapter 4. All experiments were carried out in the laboratory of Prof. Telma Franco, in the Faculdade de Engenharia Química, at the Universidade Estadual de Campinas in S.P., Brazil.

8.2.1 MATERIALS

Ladle-furnace-residue (LFR) and electric-arc furnace slag (EAFS), were obtained from ArcelorMittal's iron smelter in Piracicaba, SP, Brazil.

Lab-grade solvents (IPA, chloroform and heptane) and chemicals (sodium hydroxide) were provided by the University of Campinas.

8.2.2 ALGAE CAKE PREPARATION

8.2.2.1 Algae cultivation and lipid extraction

The algae cultivation (*Chlorella* sp. strain obtained from the Canadian Pycological Culture Centre) and lipid extraction work was carried out by Renato Sano Coelho, in the group of Prof. Telma Franco, using the procedure outlined below.[211]

Algae cultivation

Axenic stock cultures were maintained on synthetic modified BBM medium with the following composition: 50 mg L^{-1} Na_2EDTA, 3.1 mg L^{-1} KOH, 25 mg L^{-1} $CaCl_2.2H_2O$, 75 mg L^{-1} $MgSO_4.7H_2O$, 75 mg L^{-1} K_2HPO_4, 175 mg L^{-1} KH_2PO_4, 25 mg L^{-1} NaCl, 0.71 mg L^{-1} MoO_3, 4.98 mg L^{-1} $Fe_2SO_4.7H_2O$, 1 µL L^{-1} H_2SO_4, 11.42 mg L^{-1} H_3BO_3, 8.82 mg L^{-1} $ZnSO_4.7H_2O$, 1.44 mg L^{-1} $MnCl_2.4H_2O$, 1.57 mg L^{-1} $CuSO_4.5H_2O$, 0.49 mg L^{-1} $Co(NO_3)_2.6H_2O$. Glucose was added as a carbon source at

concentrations of 10 g L^{-1}. $NaNO_3$ was added as a nitrogen source to achieve C/N ratios of 20 and the pH was adjusted at 6.8.

Algae production was started in a fed batch mode until a biomass concentration of 30 g L^{-1} (by dry cell weight) was obtained. At this point, fresh sterile growth medium was introduced at four different dilution rates, ranging from 0.005 h^{-1} to 0.02 h^{-1}, whilst the algae broth was harvested at the same flow rate to maintain a constant reactor volume. The growth medium had the same composition as the synthetic modified BBM medium used for the axenic stock cultures, but was six times more concentrated.

Lipid extraction

Prior to lipid extraction, the algae slurry was hydrolysed in a PHOENIX AV100 Plus autoclave at 120 °C for 1 h, and in the presence of 0.1 g H_2SO_2 for each gram of dry cell weight (dcw) and was subsequently cooled back down to room temperature.

The lipids were extracted using a 1:4 mixture of ethanol and hexane at a ratio of 2.5 mL g^{-1} (dcw). The solvent/algae mixture was stirred for 1 min and allowed to rest until spontaneous phase separation occurred, followed by recovery of the top phase containing hexane and lipids. This procedure was repeated four more times (using hexane only) and the recovered hexane-lipid phase was separated by evaporation under vacuum.

8.2.2.2 Hydrolysate work-up

Following lipid-extraction, the algae hydrolysate was centrifuged to remove any residual hexane and reduce the water volume by 43 %. Subsequently, the remaining biomass was neutralized using a 5 M sodium hydroxide solution, followed by a second centrifugation step to achieve a wet paste with a water content of 72 wt%. Finally, the cake was oven-dried at 70 °C, and finely ground up prior to reactions.

8.2.2.3 Algae analysis

CHNS analysis of the algae cake was carried out by the Laboratório de Recursos Analíticos e de Calibração (LRAC) on a vario MACRO cube analyser, Elementar (Hanau, Germany), with a combustion tube temperature of 1150 °C and a reduction tube temperature of 850 °C.

TGA analysis of the press cake was carried out by LRAC on a TGA/DSC1 analyser by METTLER (Zürich, Switzerland), using a ramp rate of 10 °C min^{-1} to a maximum temperature of 700 °C.

The total organic carbon (TOC) and total nitrogen (TN) contents in the 'acid water' and 'neutral' water were analysed using a Shimadzu TOC/TN analyzer, at dilutions of 2 vol%.

The glucose content in the 'acid water' and 'neutral water' phase was determined using a commercial enzymatic glucose-oxidase assay kit by Bioliquid® using a 10-fold dilution.

8.2.2.4 Mass balancing

Following work-up of the algae hydrolysate solution 977.4 g of dry algae cake were recovered. Elemental analysis of the cake revealed carbon, hydrogen, nitrogen and sulphur contents of 34.1 wt%, 6.6 wt%, 3.5 wt% and 8.7 wt% respectively. Whilst the carbon, hydrogen and nitrogen content was split between water-soluble compounds precipitated during algae cake drying, and water-insoluble compounds, it was assumed that the sulphur content was mostly associated with water soluble sulphates. Algae cake drying removed 2521.9 g of water, and consequently the aqueous sulphur concentration was estimated to be 33.8 g L^{-1}.

The volume of water recovered from the neutralized hydrolysate amounted to 3.3 L and contained carbon and nitrogen concentrations of 56.05 g L^{-1} and 6.43 g L^{-1}, respectively, corresponding to 185.0 g of carbon and 21.2 g of nitrogen. Assuming a constant C/H mass ratio of 0.43 (from the dry algae cake), the amount of organic hydrogen in the neutral water phase was estimated at 35.7 g. The weight of sulphur in turn was calculated as 111.5 g, using the sulphur concentration

calculated above. Finally, the water contained a significant amount of sodium. The neutralization of the hydrolysate employed a total of 2.1 L of 5M NaOH, corresponding to a sodium weight of 241.5 g. Based on a total amount of water in the neutralized hydrolysate of 5.821 L, the sodium concentration was estimated at 41.5 g L^{-1}, and consequently, the neutral water phase contained 136.9 g of sodium, whereas the dry cake contained 104.6 g. The total weight of neutral water could therefore be calculated from the sum of water, carbon, hydrogen, sulphur and sodium at 3790.2 g.

During centrifugation of the acid hydrolysate, the recovered volume of 'acid water' amounted to 2.860 L, containing total carbon and nitrogen concentrations of 86.50 g L^{-1} and 11.05 g L^{-1}, respectively. Consequently, the total amount of carbon and nitrogen were calculated at 247.4 g and 31.6 g, respectively, whereas the amount of hydrogen was estimated at 47.7 g, once again employing the C/N ratio obtained from the dry algal cake. The amount of sulphur, in turn, was calculated as 151.1 g using the sulphur concentration in the neutral water, corrected for the dilution obtained following the addition of sodium hydroxide. The total weight of acid water was therefore estimated at 3337.8 g.

The total amounts of carbon, hydrogen and nitrogen recovered into the algae cake, 'acid water' and 'neutral water' amounted to 1000.3 g, compared to a sulphur weight of 347.7 g, corresponding to a sulphuric acid weight of 1063.4 g. The sulphuric acid to CHN ratio is thus significantly higher than the hydrolysis concentration of 0.1 g g^{-1} (dcw), however the calculation does not account for the biomass oxygen content or ash content, the lipid removed during the solvent extraction, and assumes that all the sulphur in the algae cake was derived from sulphuric acid. However, the quantity of NaOH used for the neutralization procedure accounted for only 85.6 % of the sulphur (in the form of Na_2SO_4).

8.2.3 HYDROTHERMAL REACTIONS

8.2.3.1 Reactor set-up

Hydrothermal conversion reactions of the dry algal cake were conducted in a 100 mL Parr reactor. Each reaction converted 5 g of biomass, in the presence of a total of 50 mL of reaction solvents, consisting of varying concentrations of D.I. water and/or IPA. Catalytic reactions employed an additional 5 g of finely ground material, either FLR or EAFS.

Prior to reaction, the reactor was carefully sealed and charged with 10 bar nitrogen to reduce the vaporisation of the reaction solvent. Reactions were stirred at 180 rpm, and allowed to proceed for 1 h, once the desired reaction temperature (220 °C or 310 °C) had been reached. Reactor pressures ranged from 22 bar for reactions at 220 °C in pure water to 132 bar at 310 °C and an IPA loading of 50 vol%. Following reaction, the heating mantle was removed and the reactor was allowed to cool down to room temperature (< 40 °C). Heating times ranged from 56 to 71 minutes, whereas reactor cooling required between 90 and 120 minutes, giving a total contact time between reagents and catalysts of up to 4 hours.

8.2.3.2 Product recovery

Following reaction, the gases were vented, the reactor was opened and the reaction products were vacuum filtered through pre-weighed filter paper. This allowed the recovery of the aqueous product phase, and a small aliquot of this phase was oven-dried overnight at 70 °C, to determine the yield of the water phase residue. Subsequently, the reactor and filter paper residue were washed with chloroform, until the solvent remained clear.

In order to extract IPA and water-soluble organics from the water phase, the aqueous and solvent phases were recombined and thoroughly mixed prior to gravity separation. To determine the impact of this additional processing step, baseline reactions were conducted at 310 °C with IPA

loadings of 0 and 50 % (v/v), without recombination of the aqueous and solvent phases.

Following recovery of the oil phase, the solvent was removed at 60 °C and under vacuum (120 mbar), before further separating the bio-oil product into a heptane soluble (light-oil) and chloroform soluble (heavy-oil) fraction. The filter paper was dried at 70 °C overnight, before determining the solid product weight. For reactions involving catalysts, the catalyst weight was subtracted before calculating the solid yield.

8.2.3.3 Product analysis

CHNS analysis of the liquefaction oils produced from the HTL of the algae cake was carried out by LRAC on a vario MACRO cube analyser, Elementar (Hanau, Germany), with a combustion tube temperature of 1150 °C and a reduction tube temperature of 850 °C.

The composition of the solid reaction products was also determined by LRAC using SEM-EDX analysis. Prior to analysis, the samples were gold coated using a MITECH Sputter Coater, Model K450 (Kent, United Kingdom). The samples were then analysed using an LEO Electron Microscope (Cambridge, UK), model number Leo 440i using a 6070 EDX detector. The accelerating potential was 20kV with a beam current of 600 pA. Elemental composition was determined from an average of 10 different area scans.

8.3 CONTINUOUS HTL OF WASTEWATER ALGAE

The design of the continuous liquefaction reactor has already been described in detail in Chapter 5. This section provides further detail on the biomass preparation, the system operation itself, and the product recovery, separation and analysis. In addition it provides the experimental detail for the batch reactions.

8.3.1 BIOMASS PREPARATION

The algae used for this project was obtained from a collaboration with the Algae Research Group (Department of Biology and Biochemistry,

University of Bath) and Wessex Water, a local water company. It consisted of a community of locally sourced *Scenedesmus* and *Chlorella* strains, selected for their high phosphate uptake efficiency during domestic wastewater treatment.

After harvesting, the algae were allowed to settle for a number of days, and the excess water was decanted. The aqueous biomass was subsequently centrifuged to obtain an algae slurry with a biomass concentration of 21.7 wt%. This slurry was separated into 50 g batches and stored in a freezer.

For each experiment, the required amount of algae was defrosted and diluted with D.I. water to obtain the experimental biomass concentration of 5 wt%. The exact algae loading was determined by obtaining aliquots of the well-mixed algae slurry and drying them in an oven overnight.

8.3.1.1 Algae analysis

TGA analysis of the dried algae was conducted in air on a Setaram TG-92 microbalance, using a ramp rate of 10 °C min^{-1} to 500 °C, followed by a ramp of 20 °C min^{-1} to 900 °C. This analysis was repeated with the same ramp rate on a TG-DSC-EGA analyser, to determine the gas phase composition.

Biochemical analysis of the biomass was conducted by Tracey Beacham at PML. The carbohydrate assay was carried out according to Taylor,[212] incorporating an upfront two-step hydrolysis protocol adapted from Kostas *et al*.[213]. The protein content was determined using the biuret method, described in Chapter 3. The lipid content was determined post conversion to fatty acid methyl esters (FAMEs) using GC-MS analysis, also described in Chapter 3.

8.3.2 SYSTEM OPERATION

8.3.2.1 Start-up and shut-down

Prior to each reaction run, the system was leak tested and topped up with distilled water until steady flow was established. The flow was then adjusted to the desired flow-rate of 3 mL min^{-1}, 5 mL min^{-1} or 7 mL min^{-1}

by regulating the gas flow through the rotameter at the collection pot outlet and calibrated by measuring the volume of water accumulating within the liquid collection pots over a set time period, using a stop-watch and measuring cylinder. Depending on the flowrate, the collection pots were switched over every 15, 20 or 30 minutes. Each time the collection pots were switched over, the system inlet and outlet pressure, the reactor temperatures and the collection volume were recorded. The total collection volume was monitored to ensure that sufficient liquid feed was left in the feed reservoirs at all times and prevent the system from running dry. When the estimated volume in the main feed reservoir (V1) reduced below 100 mL, flow was switched to the back-up reservoir (V2) and V1 was isolated, depressurised and topped up.

Once steady flow was established, the furnace was turned on and datalogging of the system temperatures was commenced. The furnace temperature was increased gradually until the desired reaction temperature (300, 320 or 340 °C) was reached, as measured by T1, the thermocouple located at the bottom of the inner reactor tube.

At this point, the reaction was started, by isolating V1 (whilst maintaining flow through V2), draining any left-over water, re-filling the feed reservoir with pre-mixed algae slurry, and switching flow back through V1. Any oil and water product collected from the liquid collection pots was retained and separated as described in section 8.3.2.2.

The reaction was allowed to continue until most of the algae feed had been used up (as calculated from the collected liquid product volume), before switching the system back to distilled water flow. Water flow (and product recovery) at the reaction temperature was maintained for at least 2 hours after the end of the reaction, to allow the purging of any material trapped within the system. Once the water at the system outlet started to become clear, the furnace was turned off and flow was maintained until the furnace temperature had dropped below 300 °C. At this point, the system was isolated and allowed to cool fully overnight.

8.3.2.2 Product recovery

Oil and water products recovered from the liquid collection pots were collected and separated using vacuum-filtration through pre-weighed filter paper. After each collection interval, a 20 mL aliquot of reaction water was re-filtered by gravity and retained for further analysis. Any remaining water was re-filtered under vacuum and combined into two separate samples: water collected during algae flow and water collected post reaction, during water purging. The oil product was recovered by washing all filter papers with chloroform and combined into a single fraction. Solid carry-over to the outlet was determined by re-weighing the dried filter papers following oil removal.

At the end of each reaction run, the system was fully dismantled to allow the recovery of solids and oil products from the reactor itself and the system pipework. The reactor contents were filtered and thoroughly washed with water and chloroform to obtain the solid products and a heavy oil fraction, labelled 'reactor oil'. Chloroform washing of the reactor outlet piping and collection pots allowed the recovery of 'pipe oil', which was eventually combined with the oil product from the system outlet to form the 'light oil' fraction.

8.3.3 BATCH REACTIONS

Batch liquefaction reactions and sample work-up were conducted using the same set-up as described in Chapter 3. Different heating rates ranging from 10.1 °C min^{-1} to 52.6 °C min^{-1} were obtained by changing the furnace temperature from 500 °C to 800 °C.

All reactions were conducted in triplicate, and the experimental variation was displayed in terms of the standard deviation.

8.3.4 PRODUCT ANALYSIS

Elemental (CHN) analysis of the crude bio-oil samples was obtained externally at London Metropolitan University on a Carlo Erba Flash 2000 Elemental Analyser. For the batch reactions, only the most representative

of the three repeats (yield closest to average) was analysed for each reaction condition.

The concentration of ammonium ions in the water phase was determined using a Randox Urea analysis test kit. Prior to analysis, the samples were diluted with D.I. water to a concentration of 20 vol%. Subsequently 10 µL of sample was reacted for 5 min with 1000 µL of a urease reactant, followed by the addition of 200 µL of sodium hypochlorite solution to induce the colour change. Finally, the sample absorbance was measured at 600 nm and calibrated using a reagent blank and standard solution.

8.4 CATALYTIC UPGRADING OF HTL BIO-OIL

8.4.1 MATERIALS

Nickel (II) nitrate hexahydrate (99.999 % trace metals basis), potassium nitrate (99.999 % trace metals basis), Na^+ Y and NH_4^+ Y zeolites (Molecular sieves, powder, catalysts support, Si/Al ratio: 2.56), Ammonium phosphate dibasic (puriss, p.a., ≥99.0 %) and ammonium hypophosphite (≥ 97.0 %) used for the catalyst synthesis were all purchased from Sigma-Aldrich.

H^+ Y zeolite (SiO_2/Al_2O_3 mol ratio: 30:1, powder form) was obtained from Alfa Aesar.

Quinoline (reagent grade, 98 %), dodecane (reagent grade, ≥ 99 %), and silica gel (grade 62, 60-200 mesh, 150 Å), used for the model compound reactions, and decahydroquinoline (97 % mixture of *cis* and *trans*), propylbenzene (98 %) and 2-propylaniline (97 %), used for instrument calibration were all obtained from Sigma-Aldrich.

8.4.2 SUPPORT PREPARATION

8.4.2.1 Calcination

H^+ Y zeolite was obtained by calcination of the commercial NH_4^+ Y zeolite in a muffle furnace, in open alumina boats Calcination was conducted in 15 g batches, in static air, using a ramp rate of 2 °C min^{-1} to 120 °C, hold

time of 10 h, followed by ramping at 10 °C min^{-1} to 550 °C and a hold time of 5 h. The calcination procedure resulted in a weight loss of 27.6 %.

8.4.2.2 Zeolite Ion exchange

Ni^{2+} Y and K^{+} Y zeolites were prepared by ion exchange of the commercial Na^{+} Y zeolite with solutions of nickel nitrate, $Ni(NO_3)_2.6H_2O$, and potassium nitrate, KNO_3, respectively.

Ion exchange was carried out in 1 g batches, inside 50 mL centrifuge tubes, using a 2:1 excess of the counter-ion to be exchanged.

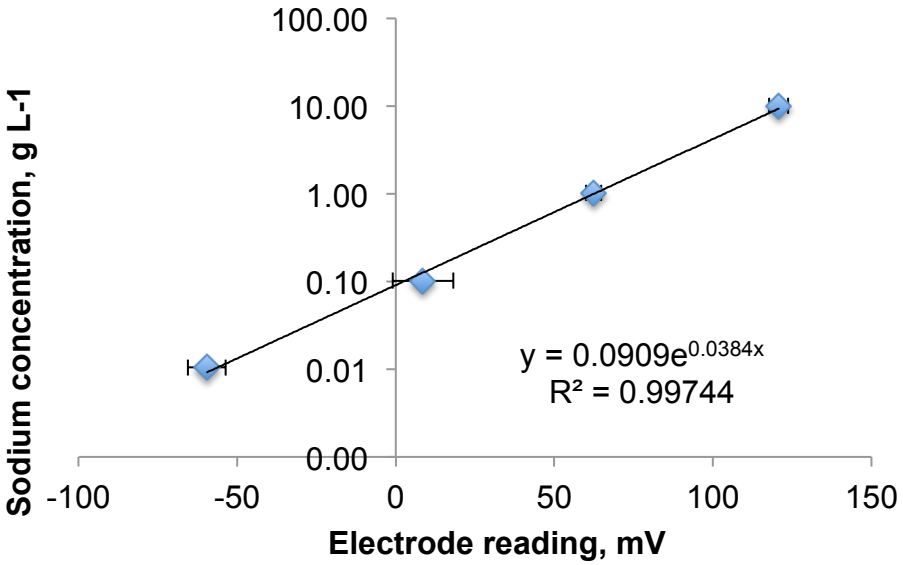

Figure 8.1: Calibration curve for sodium ion selective electrode with $NaNO_3$ solutions

The Na^{+} Y zeolite had a nominal Na_2O loading of 13 wt%, corresponding to a molar sodium loading of 0.00419 mol g^{-1}. Consequently, for ion exchange with Ni^{2+}, 2.440 g of $Ni(NO_3)_2.6H_2O$ were added to the dried zeolite, followed by the addition of 50 mL of deionized water. (Similarly, 0.848 g of KNO_3 were added for ion exchange with K^{+}.)

The solution was stirred at 600 rpm at room temperature for a minimum of 6 hours, followed by centrifugation at 3000 rpm for 10 min. Subsequently, the aqueous phase was decanted off, the zeolite was re-suspended in 50 mL D.I. water and the centrifugation step was repeated to recover the ion-exchanged zeolite.

The ion exchange solutions recovered after the first centrifugation step were analysed using a sodium ion selective electrode calibrated with four $NaNO_3$ solutions, with concentrations of 10 g L^{-1}, 1 g L^{-1}, 0.1 g L^{-1} and 0.01 g L^{-1}, to determine the amount of sodium exchanged from the zeolite (Figure 8.1).

8.4.2.3 Base-treatment

Base-treatment of the commercial NH_4^+ Y and H^+ Y_{low} zeolites was conducted by Emyr Jones, in the Department of Chemistry.[200] For each treatment, a base solution containing 1.25 g of NaOH in 50 mL of D.I. water was combined with a solution containing either 0.64 g (for mild treatment, MT) or 3.22 g (for harsh treatment, HT) of TPABr in 50 mL D.I. water. After mixing for 30 minutes, 3.3 g of zeolite was added to the solution and the suspension was stirred for a further 30 minutes at a temperature of 65 °C. The product was filtered and dried for 24 h at 65 °C in a preheated oven.

8.4.3 CATALYST IMPREGNATION

The catalyst precursors were prepared by impregnating the zeolites with pre-mixed solutions of nickel nitrate hexahydrate, $Ni(NO_3)_2.6H_2O$, ammonium phosphate, $(NH_4)_2HPO_4$, and ammonium hypophosphite, $NH_4H_2PO_2$.

8.4.3.1 2-stage incipient wetness impregnation (method 1)

Prior to catalyst impregnation, the pore volume of the zeolites was determined by drop-wise addition of D.I. water to a 2 g sample of NH_4^+ Y zeolite until the sample became fully wetted, as indicated by a sudden phase change from solid to a viscous slurry. Prior to the measurement, the sample was dried at 120 °C overnight, in a pre-weighed sample vial. The dry and wet sample weights were determined and the water uptake was calculated as 1.05 g g^{-1}. A similar value of 1.07 g g^{-1} was obtained for Na^+ Y zeolite, and for simplicity a universal value of 1 g g^{-1} was adopted for all zeolite impregnations.

To achieve a 5 wt% Ni loading, the required solution concentration was calculated as follows:

MW of $Ni(NO_3)_2.6H_2O$: 290.79 g mol^{-1}

MW of Ni: 58.6934 g mol^{-1}

Required Ni concentration = 0.05 g g^{-1} (Ni/zeolite) / 1 g g^{-1} (water/zeolite)
= 0.05 g g^{-1} (Ni/water)

⇨ Conc. of $Ni(NO_3)_2.6H_2O$ = C-Ni x MW- $Ni(NO_3)_2.6H_2O$ / MW-Ni
= 0.05 x 290.79 / 58.6934
= 0.2477 g g^{-1} ($Ni(NO_3)_2.6H_2O$/water)

Similar calculations were conducted to obtain the required concentrations of ammonium phosphate or ammonium hypophosphite, to achieve the desired P/Ni molar ratio.

Prior to metal impregnation, each zeolite sample was dried at 120 °C overnight in a pre-weighed sample vial and the dry zeolite weight was calculated by difference. The impregnation solution was applied drop-wise until the sample was fully wetted, at which point the sample was immediately re-weighed to allow calculation of the actual amount of metal (or phosphorus) added. Subsequently, the procedure was repeated with the metal-loaded zeolite to add the phosphate solution and allow calculation of the applied Ni/P ratio.

8.4.3.2 Single-stage incipient wetness impregnation (method 2)

The same procedure was applied as for the two-step impregnation, but rather than applying the nickel nitrate and ammonium phosphate solutions separately, the two salts were dissolved together in a 2.5 M nitric acid solution, with a nominal P/Ni molar ratio of 3.

8.4.3.3 Solution-based impregnation (method 3)

Solution based impregnation was conducted by mixing 2 g of dry zeolite with 20 mL of a nickel phosphate solution. The solution contained $Ni(NO_3)_2.6H_2O$ and $(NH_4)_2HPO_4$ concentrations of 0.02290 g g^{-1} and 0.02290 g g^{-1}, respectively, corresponding to a Ni concentration of

0.0046 g g^{-1} and a P/Ni molar ratio of 3.00. The solution also contained nitric acid, at a concentration of 0.5 M, to ensure full dissolution of the nickel phosphate precipitate.

The impregnation solution was mixed for a minimum duration of 8 hours, followed by overnight drying at 120 °C. The exact nickel loading for each sample was calculated from the recovered sample weight and the weight and concentration of the impregnation solution.

8.4.4 CATALYST REDUCTION

The catalysts were reduced in a 12 mm quartz tube reactor, heated inside a tubular furnace. The impregnated catalyst precursors were placed on a quartz wool plug in the centre of the tube, and the temperature was monitored using a thermocouple and data-logging software.

Prior to reduction, the catalyst precursors were dried at 120 °C overnight, under flowing nitrogen (250 mL min^{-1}). Subsequently, the temperature was ramped to 400 °C, and the materials were calcined for 4 hours. Following calcination, the temperature was increased further to 550 °C (or 650 °C), and the gas flow was switched to hydrogen (120 mL min^{-1}). At the same time, the nitrogen flow was re-directed to the reactor outlet to dilute the reaction gases prior to discharge to the fumehood vents. After 4 hour reduction, flow was switched back to nitrogen, and the reactor was left to cool overnight, before passivating the catalyst by flowing 250 mL min^{-1} of 1 % O_2/N_2 for a period of 4 hours.

The catalysts were weighed directly after recovery from the reactor, to determine the weight loss and calculate the final Ni loading.

8.4.5 SULPHIDING OF TRANSITION METAL CATALYSTS

The two transition metal catalysts $NiCoMo/Al_2O_3$ and $NiMo/CeO_2$ were pre-sulphided using a modified version of the catalyst reduction rig, by bubbling the hydrogen feed through a heated DMSO solution and scrubbing the reactor outlet in a 0.5 M NaOH solution.

For each reaction, 2 g of the catalyst precursor was loaded onto a quartz wool plug in the centre of the quartz tube and dried at 120 °C overnight, under flowing nitrogen (250 mL min^{-1}). After drying, the furnace temperature was increased to 200 °C, flow was switched to hydrogen and the DMSO solution was heated to 80 °C, with the nitrogen purge realigned to the reactor outlet. The reaction temperature was increased in 2 hour intervals to 250 °C, 300 °C and 400 °C. After 4 hours of reaction at the final temperature, flow was switched back to nitrogen, and the reactor was left to cool overnight, before passivating the catalyst in 1 % O_2/N_2 for a period of 4 hours. This procedure was chosen in line with a catalyst sulfiding guide published by Gaylord Chemical Company.[214]

The vapour pressure of DMSO at 80 °C was estimated to be 0.01993 bar using the vapour pressure correlation:

$$\ln P = C1 + C2/T + C3 \ln T + C4\, T^{C5}$$

with the following constants, as obtained from Perry's Chemical Engineers' Handbook:[215]

C1 = 56.273

C2 = -7620.6

C3 = -4.6279

C4 = 4.3819E-07

C5 = 2

As the reaction pressure was kept close to atmospheric, the volumetric DMSO concentration in the reaction gas was just below 2.0 %. Based on a hydrogen flowrate of 150 mL min^{-1}, and a maximum metal site concentration on the catalyst of 0.003 mol g^{-1}, the time required to sulphide 1 g of catalyst was estimated as 59 min. Therefore, the selected reaction time of 4 hours provided a 100 % margin for the 2 g catalyst samples.

8.4.6 CATALYST CHARACTERIZATION

8.4.6.1 X-ray diffraction

PXRD data was collected on a BRUKER D8 Advance diffractometer with a Cu Kα X-ray source (λ = 1.540619 Å) in flat plate mode using a rotation speed of 15 rpm, a scan range of 3 < 2Θ < 80, and a step size of 0.05 with a time step of 1 s, giving a total scan time of 30 min. Prior to analysis the samples were finely ground using a pestle and mortar.

The obtained data was processed (background extraction, peak search, FWHM) using the Bruker EVA XRD software.

Cubic cell parameters

The cubic cell parameters were determined using the *Unit Cell* leastsquares refinement program,[216] and the simulated XRD powder pattern for faujasite.[217]

Scherrer particle size

The Scherrer particle size was calculated using the Scherrer-calc. spreadsheet obtained from Newcastle University,[218] using the FWHMs of the strongest metal peaks, corresponding to the dominant Ni phase ([2 -1 1], [2 0 1] and [3 -1 0] for Ni_2P; [1 1 1], [2 0 0] and [2 2 0] for Ni and [1 1 2], [4 0 0] and [3 1 2] for $Ni_{12}P_5$).

8.4.6.2 BET surface area

BET surface areas were determined by nitrogen adsorption at 77 K on a Micromeritics 3Flex analyser. Each analysis was conducted with a minimum sample of 200 mg. Samples were pre-dried at 120 °C under vacuum, before drying on the analyser at 300 °C for 720 min under dynamic high vacuum (10^{-7} mbar).

Analysis was conducted in the P/P_0 range of 0.01 to 0.3, with a step size of 0.01 up to a P/P_0 ratio of 0.1, and steps of 0.05 thereafter. Due to the microporous nature of the samples, the P/P_0 range was adjusted for the BET analysis to achieve a positive gradient on the Rouqerol correction, in accordance to British Standard Guidelines.[219]

8.4.6.3 TPR

TPR analysis was conducted by Dr Laura Torrente Murciano at the University of Cambridge, UK, on a AutoChem II 2920 analyser, using a sample mass between 0.079 g and 0.194 g, with a ramp rate of 10 °C min^{-1} to a temperature of 1000 °C, under the flow of 50 mL min^{-1} of a 5 % H_2/Ar gas mixture. Hydrogen adsorption was determined using differences of thermoconductivity between the feed gas and the reactor outlet.

8.4.6.4 SEM-EDX

SEM-EDX analysis was conducted on a JEOL IT-300 Scanning Electron Miscroscope fitted with an Aztec X-Max^N 80 T analyser, and processes using the Oxford instruments Aztec software.

Ground catalyst samples were mounted on 12 mm aluminium stubs, using double-sided carbon sticky tape.

The working distance was 10 mm with an accelerating voltage of 20 keV. EDX spectra were determined using area scans with an acquisition time of 150 s and an accelerating voltage of 20 keV. For each sample, at least three scans of separate areas were conducted, normalized to exclude carbon and averaged to determine the Ni loading, Ni/P ratios, Si/Al ratios and the counter-ion to aluminium ratios.

8.4.6.5 TEM

TEM analysis was conducted by Dr Sean Davis, at the University of Bristol, on a JEM-2100F Field Emission Electron Microscope.

Samples were supported over carbon-covered 200 mesh copper grids and dried in air overnight.

The accelerating voltage was 200 kV, with a field emission current of 124 µA.

Elemental mapping through X-Ray energy dispersive spectroscopy was conducted using an Aztec X-Max^N 80 T analyser, using the Oxford instruments Aztec software. The picture resolution was 512 pixel, with a

beam diameter of 1.5 nm, an emission voltage of 20 keV and using a minimum of 20 frame counts for each analysis.

TEM images were analysed and processed using the ImageJ open source image processing software. Particle sizes were determined by manually outlining each particle using the oval shape selector tool and applying the measuring tool (Figure 8.2).

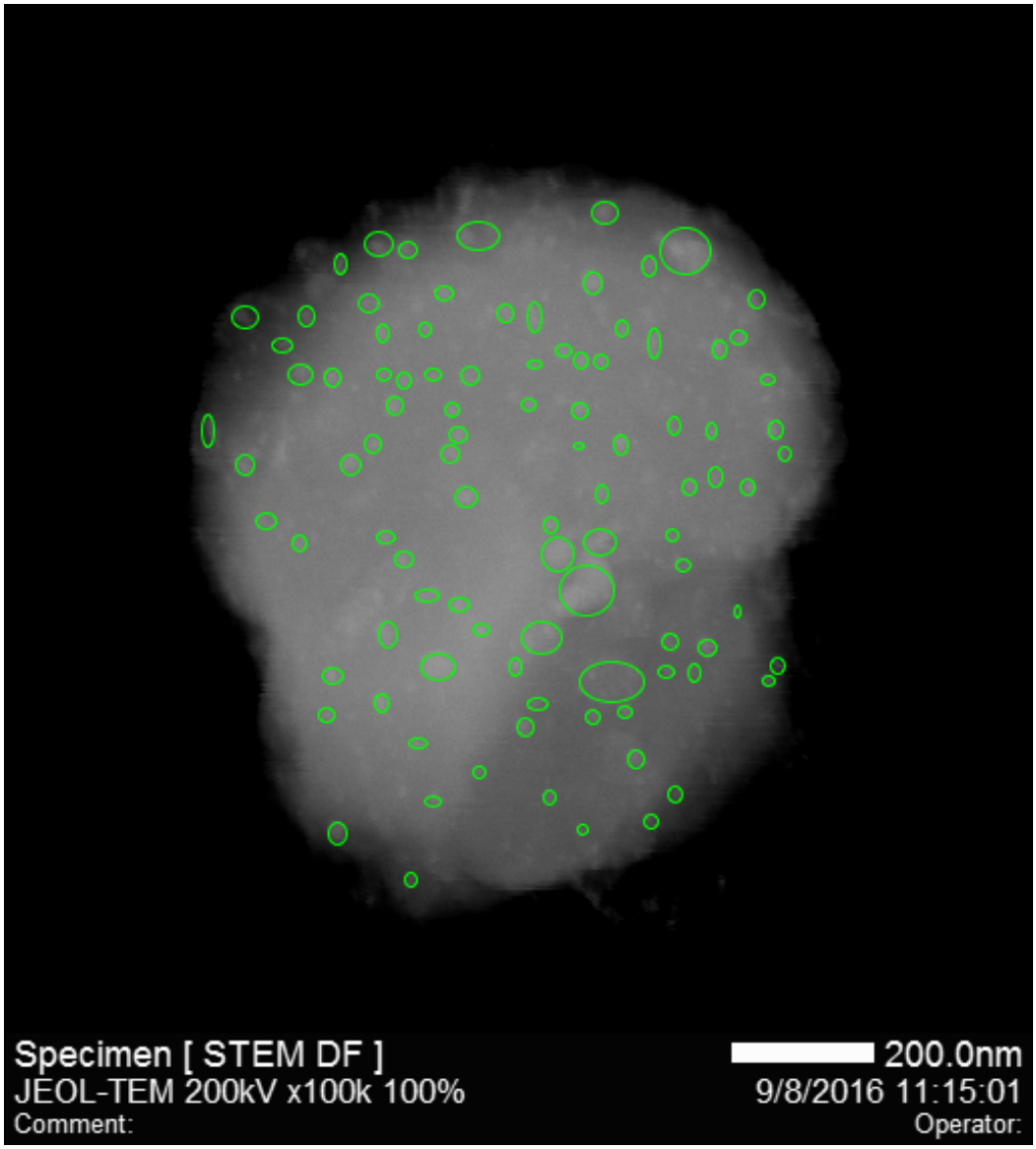

Figure 8.2: TEM image processed on ImageJ to outline nanoparticles and measure their size distribution

8.4.7 UPGRADING REACTIONS

Upgrading reactions were conducted in stainless steel batch reactors, made from 1/2 " Swagelok® tubing and with an internal volume of 6 mL. The top of each reactor was connected to a pressure gauge (0 – 100 bar) and a vent valve, and a thermocouple connected to data-logging software was inserted into each reactor. The reactors were heated inside a Micromeritics FlowPrep 060 furnace, containing 6 separate heating ports. The reactors were designed to fit tightly within the heating sleeves of the furnace to ensure good heat transfer. All reactions were conducted at the maximum furnace temperature of 400 °C, resulting in an average reaction temperature of 364.7 °C (± 4.2 °C) and an average heating time of 20.26 min (± 1.4 min) to reach 95 % of the maximum reaction temperature (Figure 8.3).

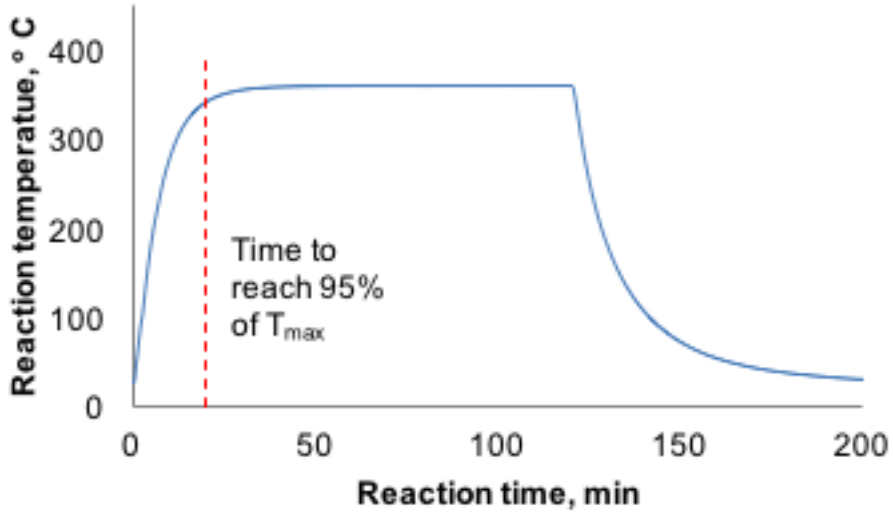

Figure 8.3: Temperature profile for typical upgrading reaction

8.4.7.1 Model compound conversion

The quinoline conversion studies were conducted using 50 mg of catalyst and 1 mL of a quinoline stock solution, containing 10 vol% (14.1 wt%) quinoline in dodecane. Dodecane acted both as a solvent as well as an internal standard for analysis.

Prior to reaction, the catalysts were dried at 120 °C overnight. The reactors were loaded with 1 g of silica, followed by the addition of the

catalyst, and the two materials were mixed by manually shaking the reactor. Silica was added to achieve a better catalyst distribution within the reactor and improve its contact with the reagents and compared to test reactions without silica, this resulted in a much higher degree of repeatability. Subsequently the reagent solution was added using a micropipette and the reactor was tightly sealed. The reactor was weighed after the addition of each reagent (silica, catalyst and quinoline solution) to determine the exact quantities of materials used.

The sealed reactors were purged two times with 40 bar nitrogen (using the vent connection at the top) before they were pressurised up to 80 bar for leak testing. After successful tests, the reactors were twice purged with 40 bar hydrogen before they were re-pressured to the reaction pressure of 40 bar.

The reactions were started by inserting up to three reactors into the furnace and commencing temperature datalogging. After 120 minutes, the reactors were removed and allowed to cool in the cooling ports of the furnace, until the temperatures fell below 40 °C. The reactor temperatures and pressures were recorded at the end of reaction (when the reactors were removed) and after the reactors had cooled back to room temperature, to allow the evaluation of the hydrogen consumption. Once the reactors were cool, the pressure was vented and the reactors were opened for extraction.

All reactions were conducted in triplicate, to allow calculation of the experimental variation (standard deviation), with exception of the reactions over the blank zeolites, which were based on single reaction runs only.

8.4.7.2 Oil Upgrading

The oil upgrading reactions employed the same reactor configuration as used for the model compound conversion, however in this case, the bio-oil was upgraded directly without reaction solvent. The rationale behind this decision was to allow more precise analysis of the reaction product

with CHN elemental analysis, even though the lack of solvents reduced the dispersion of bio-oil over the catalyst phase.

All reactions were conducted with the same batch of bio-oil, combined together from the individual light oil samples obtained from the continuous HTL of the wastewater algae. Prior to reactor loading, the oil was heated to 60 °C, to reduce its viscosity and facilitate the loading procedure.

The oil was allowed to drip directly onto the catalyst/silica bed, and care was taken to prevent contact with the reactor walls. After each drop the reactor was weighed, until a minimum oil loading of 100 mg was achieved. Whilst loading the reactors, three samples of bio-oil were taken on different days, to allow analysis of its elemental composition.

All oil upgrading reactions were conducted in triplicate and the standard deviation was determined.

8.4.7.3 Product recovery

The reactor contents were decanted through pre-weighed filter paper and the reactor was thoroughly rinsed with chloroform, until the solvent remained clear. Chloroform was removed from the filtrate by vacuum evaporation at 40 °C, and the weight of the liquid products was determined after allowing them to breathe at room temperature overnight. The filter paper containing the catalyst/silica phase and any solid reaction products was dried at 60 °C overnight, and the solid yields were calculated by difference.

8.4.8 PRODUCT ANALYSIS

8.4.8.1 NMR

^{1}H NMR and ^{13}C NMR spectra were obtained on a 400 MHz Bruker Avance III spectrometer.

For the analysis, the entire product phase from the model compound reactions was dissolved in 4 mL of deuterated chloroform and a 0.7 mL aliquot was drawn for NMR analysis.

The ^{1}H NMR data was used to calculate the conversion of quinoline and the product yields of 1234THQ, 5678THQ and OPA. The remaining reaction products (DHQ, PB, PCHA and PCH) could not be quantified, due to overlap with the solvent and other product peaks, and consequently were grouped together as 'other' and calculated by difference.

Quinoline

The quinoline and dodecane integrals were assigned using the ^{1}H NMR spectrum of the reagent solution (10 vol% quinoline in dodecane), and verified against the quinoline spectrum deposited on the SDBS database[209] (Figure 8.4). The integral areas were normalized against the quinoline-A peak and showed good correlation to the expected number of protons for all other peaks associated with quinoline (Table 8-1). The actual molar ratio in the reagent solution between quinoline and the CH_3 protons of dodecane was 27.7, compared to a ratio of 29.5 obtained from the ^{1}H NMR analysis. The measured CH_2/CH_3 ratio for dodecane of 3.36 also compared well with the theoretical ratio of 3.33. Consequently the conversion of quinoline was calculated from the ratio of the quinoline-A peak (δ = 8.97 – 8.90 ppm) to the dodecane-CH_3 peak (δ = 0.94 – 0.81 ppm).

Table 8-1: ^{1}H NMR integral ranges for quinoline and dodecane

Assignment	Integral range, δ, ppm		Normalized area (Q-A peak)	Theoretical number of protons
	Max	Min		
Quinoline - A	8.97	8.90	1.00	1
Quinoline – B/C	8.21	8.09	2.01	2
Quinoline - D	7.86	7.80	1.01	1
Quinoline - E	7.78	7.67	1.06	1
Quinoline - F	7.60	7.51	1.03	1
Quinoline - G	7.45	7.36	1.04	1
Dodecane – CH_2	1.36	1.18	99.30	92.2
Dodecane – CH_3	0.94	0.81	29.51	27.7

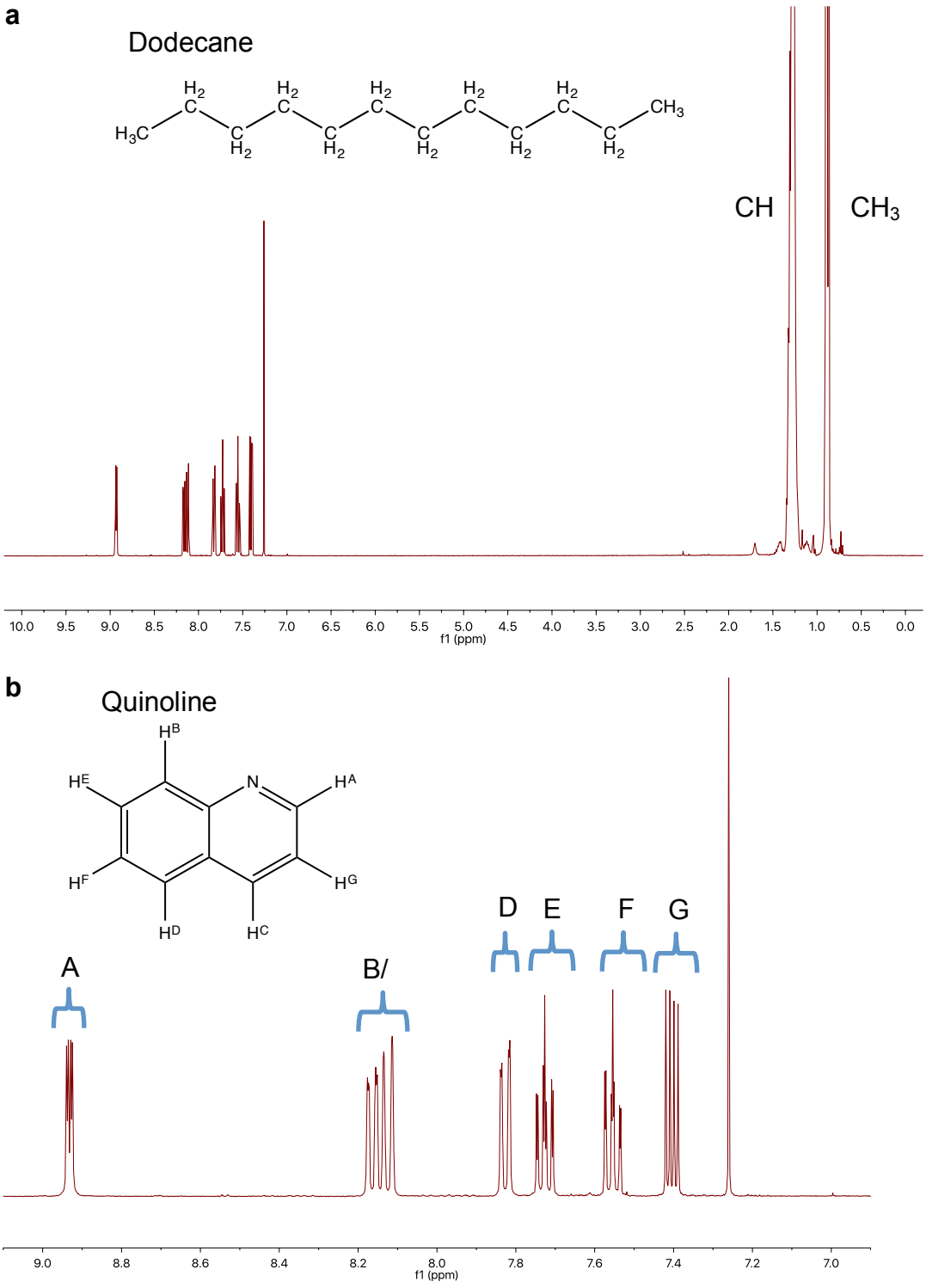

Figure 8.4: ^{1}H NMR spectrum for 10 vol% quinoline in dodecane. (a) whole spectrum, (b) downfield region containing quinoline peaks only

1234THQ and 5678THQ

In the absence of chemically pure calibration solutions, the integrals for the partial hydrogenation products 1234THQ and 5678THQ were assigned using the ^{1}H NMR spectrum of the reaction product from the

conversion of quinoline over Pd/C (Figure 8.5). This spectrum was chosen as Pd/C was the only catalyst that yielded sufficient amounts of 5678THQ to allow clear identification.

The assignment of the 1234THQ peaks was based on the spectrum deposited on the SDBS database[209] and all peaks except the 1234THQ-D peak, associated with the nitrogen-bound proton, could be identified. In contrast, the ^{1}H NMR spectrum for 5678THQ was not available online, and consequently the assignment was based on a spectrum predicted using Chemdraw®. Whilst this allowed clear identification of the 5678THQ-A peak, the identification of the 5678THQ-B peak and particular the 5678THQ-C peak was more ambiguous. Additional peaks at δ = 8.18 and 7.01 ppm could not be matched against any of the expected quinoline denitrogenation products, which suggests that they belong to products formed from undesired side reactions. The peak at δ = 7.01 ppm partially overlapped with the OPA-A peak (δ = 7.04 ppm), but consisted of a quadruplet, rather than the expected triplet.

Peaks at δ = 2.5ppm, δ = 1.67 ppm, δ = 1.58 ppm, δ = 1.14 ppm, δ = 1.04 ppm and δ = 0.72 ppm were associated with the two stereoisomers of the hydrogenation product DHQ and the denitrogenation product propylcyclohexane. However, due to the partial overlap with the solvent peaks and the stereoisomerism of DHQ, it was not possible to use these peak for quantitative analysis.

The normalized peak areas for 1234THQ (Table 8-2) and 5678THQ (Table 8-3) showed a lower correlation to the theoretical number of protons than those for quinoline, particularly within the upfield region. This could be the result of impurities and by-products introduced during the reaction process, increasing the level of noise, as well as a distortion across the whole spectrum, even after phase correction was applied.

As the clearest peaks were obtained in the downfield region, the yields of 1234THQ and 5678THQ were calculated from the respective ratios of the 1234THQ-A peak (δ = 7.01– 6.91ppm) and the 5678THQ-A peak (δ = 8.42 – 8.34 ppm) to the dodecane-CH_3 peak (δ = 0.94 – 0.81 ppm).

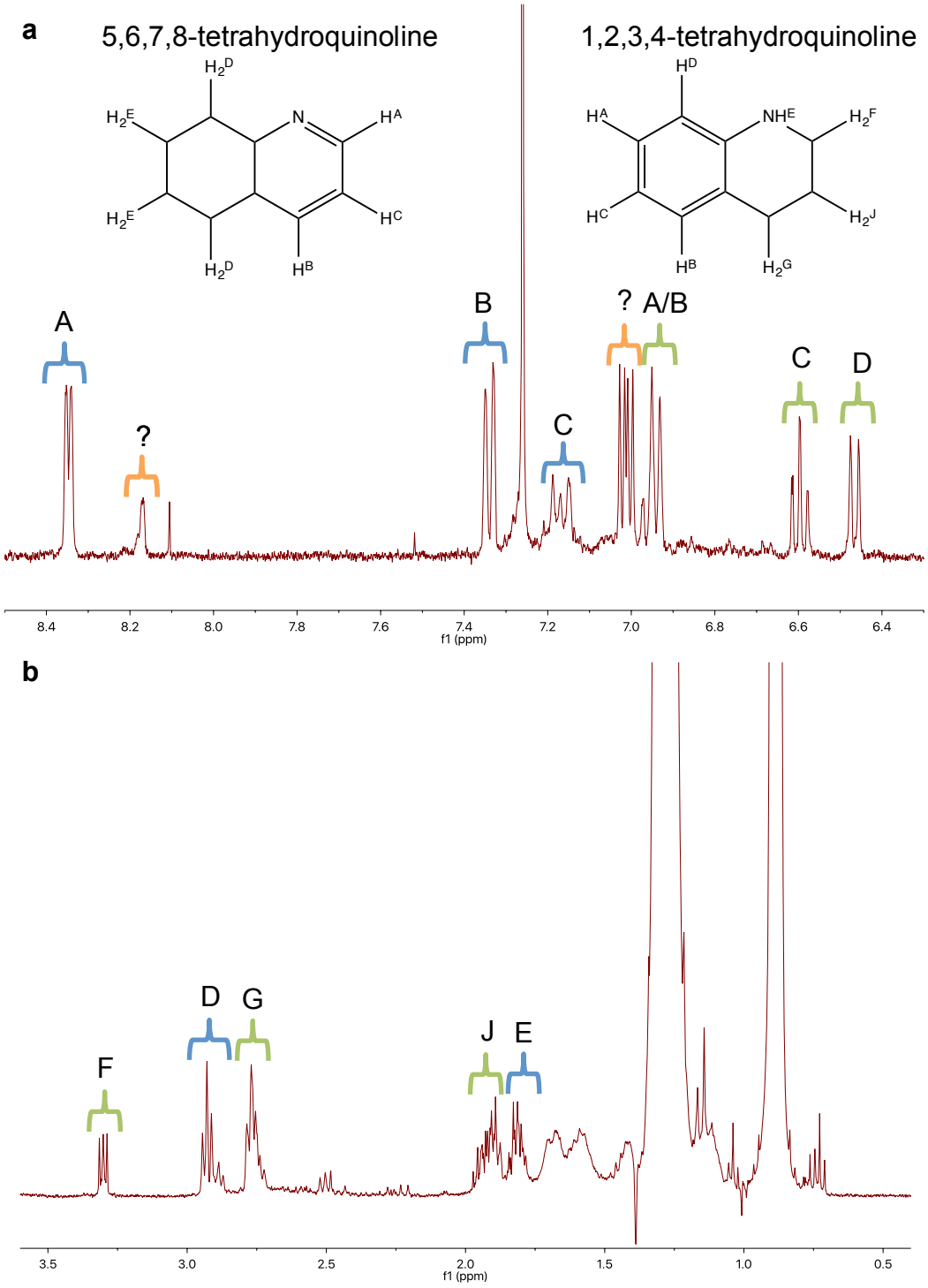

Figure 8.5: ^{1}H NMR spectrum for the product from the conversion of 10 vol% quinoline in dodecane over Pd/C catalyst used for the assignment of the integrals associated with 1234THQ (green) and 5678THQ (blue). (a) downfield region, (b) upfield region. The orange peaks denote unidentified products, which cannot be related to the quinoline denitrogenation pathway.

Table 8-2: ^{1}H NMR integral ranges for 1234THQ

Assignment	Integral range, δ, ppm		Normalized area (1234THQ-A peak)	Theoretical number of protons
	Max	Min		
1234THQ-A/B	7.01	6.91	2.00	2
1234THQ-C	6.65	6.57	0.77	1
1234THQ-D	6.53	6.40	0.88	1
1234THQ-F	3.37	3.24	1.66	2
1234THQ-G	2.85	2.70	5.15	2
1234THQ-J	2.02	1.88	4.76	2

Table 8-3: ^{1}H NMR integral ranges for 5678THQ

Assignment	Integral range, δ, ppm		Normalized area (1234THQ-A peak)	Theoretical number of protons
	Max	Min		
5678THQ-A	8.42	8.34	1.00	1
5678THQ-B	7.37	7.30	1.36	1
5678THQ-C	7.21	7.12	1.33	1
5678THQ-D	3.04	2.93	1.61	4
5678THQ-E	1.88	1.78	4.90	4

OPA

The OPA integrals were assigned using the ^{1}H NMR spectrum of a solution, containing 10 vol% OPA in dodecane, and verified against the OPA spectrum deposited on the SDBS database[209] (Figure 8.6). The integral areas were normalized against the OPA-A peak and showed good correlation to the expected number of protons for the OPA-B and OPA-C peaks (Table 8-4). The area of the OPA-D peak, corresponding to the -NH_2 protons, was slightly smaller than expected, however this can be attributed to the peak-broadening effect of the nitrogen-associated protons. Finally, the areas of the upfield OPA proton peaks (E, F and G) were slightly larger than expected, as a result of a distortion across the whole spectrum. The same was true for the protons associated with dodecane, which were slightly overestimated using the NMR data (131.3

and 39.1 vs actual values of 125.5 and 37.6). Nevertheless, the CH_2/CH_3 ratio of 3.35 showed a good match to the theoretical ratio of 3.33.

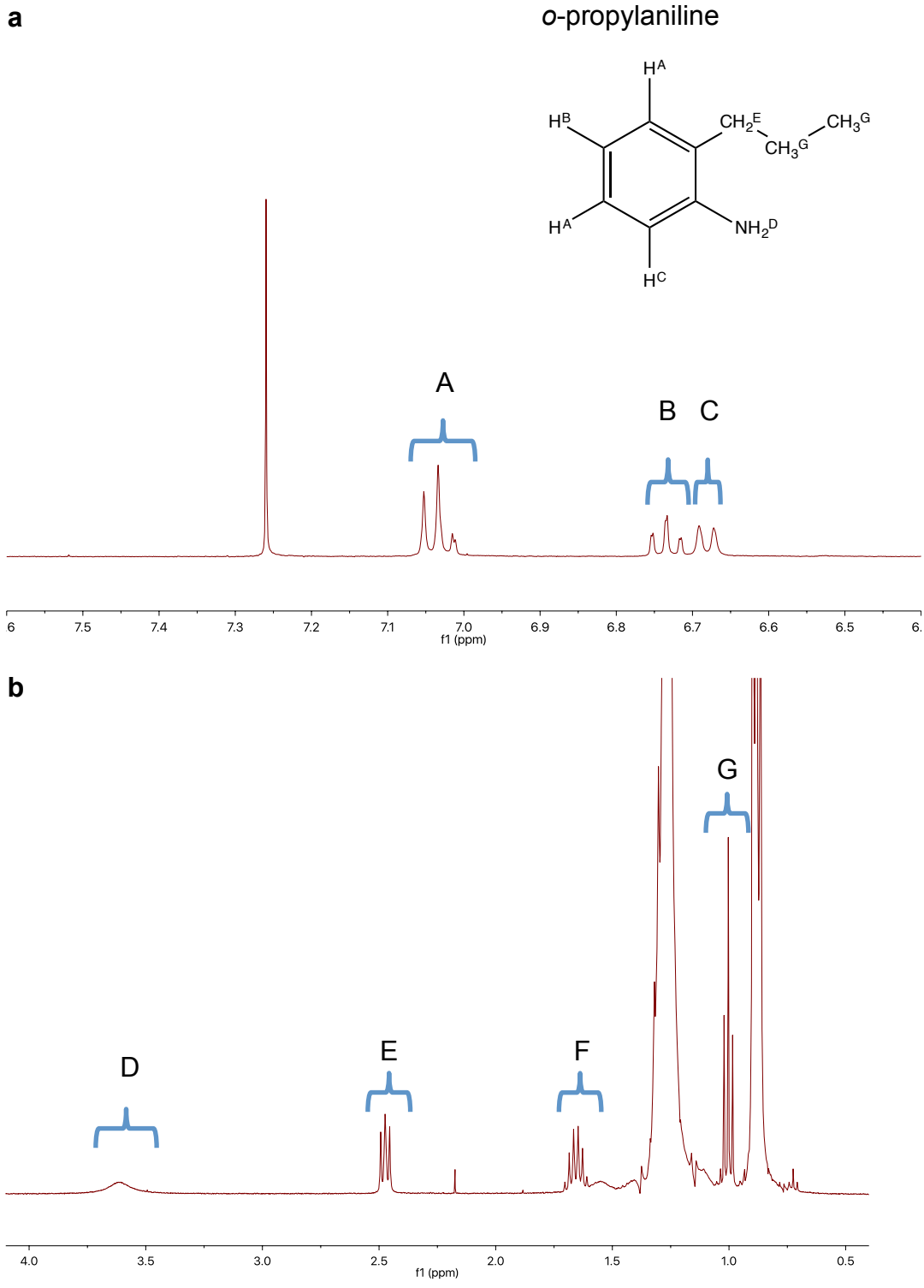

Figure 8.6: ^{1}H NMR spectrum for 10 vol% OPA in dodecane. (a) downfield region, (b) upfield region

As the OPA-A peak overlaps with the unidentified peak observed in the ^{1}H NMR spectrum obtained for the product from the reaction of quinoline over Pd/C, the OPA-C (δ = 6.71– 6.65 ppm) to dodecane-CH_3 (δ = 0.94 – 0.81 ppm) peak ratio was used for the quantification of OPA instead.

Table 8-4: ^{1}H NMR integral ranges for OPA and dodecane

Assignment	Integral range, δ, ppm		Normalized area (OPA-A peak)	Theoretical number of protons
	Max	Min		
OPA - A	7.08	7.00	2.00	2
OPA – B	6.77	6.71	0.99	1
OPA - C	6.71	6.65	1.04	1
OPA - D	3.71	3.49	1.75	2
OPA - E	2.53	2.42	2.16	2
OPA - F	1.73	1.58	2.74	2
OPA - G	1.05	0.97	3.58	3
Dodecane – CH_2	1.36	1.18	131.3	125.5
Dodecane – CH_3	0.94	0.81	39.1	37.6

8.4.8.2 GC-MS

GC-MS analysis was carried using an Agilent 7890B Gas Chromatograph on a DB-FFAP column (30 m, 0.25 mm x 0.25 µm) and analysed with internal FID and TCD detectors and an external Agilent 5977A MSD detector. The injection volume was 1 µL and samples were loaded at 40 °C, with a hold time of 1 min, followed by ramping at 10 °C min^{-1} to 60 °C, hold time of 4 min, and ramping at 10 °C min^{-1} to 250 °C, with a hold time of 4 min. The MS detector was turned off between 3.60 min and 5.50 min.

GC samples were prepared by dissolving the entire product phase in 4 mL deuterated chloroform and drawing a 0.5 mL aliquot. The solvent was evaporated at 50 °C, under vacuum, followed by the addition of 10 mL of GC-grade toluene. 0.4 mL of this solution was diluted further in 4 mL toluene to obtain a final sample concentration of approximately

1 mg mL^{-1}. As the quinoline concentration in dodecane was 10 vol%, the concentration of the reagents/products was approximately 100 µg mL^{-1}.

GC Calibration

The GC was calibrated with solutions of dodecane (62 µg mL^{-1} to 3.22 mg mL^{-1}), quinoline (40 µg mL^{-1} to 981 µg mL^{-1}), OPA (35 µg mL^{-1} to 850 µg mL^{-1}) and DHQ (52.1 µg mL^{-1} to 1.26 mg mL^{-1}) in toluene (Figure 8-7). Whilst the responses for dodecane and quinoline were highly linear and similar in magnitude, the signal for OPA and particularly DHQ was reduced at lower sample concentrations. The low signal for DHQ is related to very broad peaks, possibly as a result of the stereoisomerism of this compound. Therefore, it was not possible to quantify the DHQ yields using the GC-MS analysis.

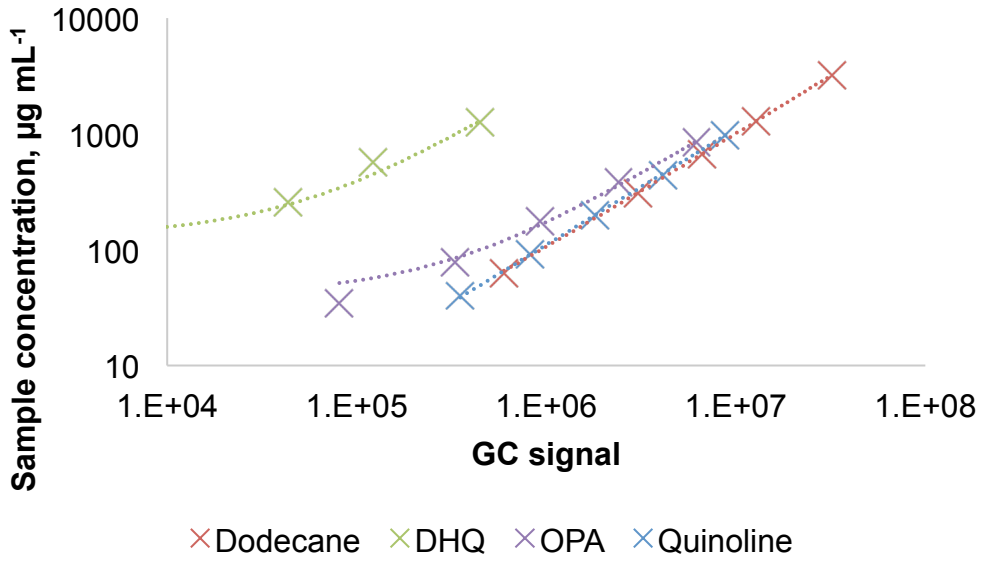

Figure 8-7: GC-MS calibration curves for dodecane (RT = 7.49 min), quinoline (RT = 18.90 min), OPA (RT = 18.15 min) and DHQ (RT = 16.89 min)

Due to the absence of calibration solutions for 1234THQ and 5678THQ, the GC response was assumed to be comparable to that of quinoline. Peaks associated with the fully denitrogenated reaction products PB and PCH overlapped with the solvent peak, and could not be determined. Consequently, these products were grouped together with DHQ as 'other' and calculated by difference.

8.4.8.3 Elemental analysis

Selected samples of the feed oil and upgraded crude bio-oil were analysed externally at London Metropolitan University on a Carlo Erba Flash 2000 Elemental Analyser to determine their CHN content.

REFERENCES

1. M. Billot, L. Coppens, V. Demkine, S. Diop, P. Gilruth, J. Jabbour, F. Keita-Ouane, J. N. Mwangi, B. Ohanga and N. Sharma, *GEO_5 - Environment for the future we want*, United Nations Environment Programme, 2012.
2. Airbus, *Sustainable Aviation - Aviation Environmental Roadmap*, 2013.
3. S. Bringezu, H. Schütz, M. O'Brien, L. Kauppi, R. W. Howarth and J. McNeely, *Towards sustainable production and use of resources: Assessing Biofuels*, UNEP, 2009.
4. Y. Chisti, *Journal of biotechnology*, 2013, **167**, 201-214.
5. L. Rodolfi, G. Chini Zittelli, N. Bassi, G. Padovani, N. Biondi, G. Bonini and M. R. Tredici, *Biotechnology and bioengineering*, 2009, **102**, 100-112.
6. M. McDermott, *World's first flight powered by 100% algae biofuels completed*, 2010, Available from: http://www.treehugger.com/aviation/worlds-first-flight-powered-by-100-algae-biofuels-completed.html [11 September 2016]
7. M. Y. Khan, R. L. Russell, W. A. Welch, D. R. Cocker and S. Ghosh, *Energy & Fuels*, 2012, **26**, 6137-6143.
8. *Sapphire Energy - FAQ*, 2015, Available from: http://www.sapphireenergy.com/green-crude/faq/ [11 September 2016]
9. *Algae Industry: Commercial Production*, Available from: allaboutalgae.com/commercial-production/ [11/09/2016]
10. P. E. Savage, *Science*, 2012, **338**, 1039-1040.
11. T. N. Kalnes, T. Marker, D. R. Shonnard and K. P. Koers, in *Biofuels Technology*, 2008, pp. 7-11.
12. S. Mikkonen, T. Hartikka, M. Kuronen and P. Saikkonen, *HVO, Hydrotreated Vegetable Oil - A Premium Renwable Biofuel for Diesel Engines*, Neste Oil Corporation, 2012.
13. H. A. Spoehr and H. W. Milner, *Plant Physiology*, 1949, **24**, 120-149.
14. D. López Barreiro, W. Prins, F. Ronsse and W. Brilman, *Biomass and Bioenergy*, 2013, **53**, 113-127.
15. C. Tian, B. Li, Z. Liu, Y. Zhang and H. Lu, *Renewable and Sustainable Energy Reviews*, 2014, **38**, 933-950.
16. N. Uduman, Y. Qi, M. K. Danquah, G. M. Forde and A. Hoadley, *Journal of Renewable and Sustainable Energy*, 2010, **2**, 012701.
17. L. Xu, D. W. Wim Brilman, J. A. Withag, G. Brem and S. Kersten, *Bioresource technology*, 2011, **102**, 5113-5122.
18. A. V. Bridgwater, D. Meier and D. Radlein, *Organic Geochemistry*, 1999, **30**, 1479-1493.
19. Y. Dote, S. Sawayama, S. Inoue, T. Minowa and S.-y. Yokoyama, *Fuel*, 1994, **73**, 1855-1857.

20. T. Minowa, S.-y. Yokoyama, M. Kishimoto and T. Okakura, *Fuel*, 1995, **74**, 1735-1738.
21. A. A. Peterson, F. Vogel, R. P. Lachance, M. Fröling, J. M. J. Antal and J. W. Tester, *Energy & Environmental Science*, 2008, **1**, 32.
22. S. S. Toor, L. Rosendahl and A. Rudolf, *Energy*, 2011, **36**, 2328-2342.
23. T. M. Yeh, J. G. Dickinson, A. Franck, S. Linic, L. T. Thompson and P. E. Savage, *Journal of Chemical Technology & Biotechnology*, 2013, **88**, 13-24.
24. C. J. Chuck, J. L. Wagner and R. W. Jenkins, in *Chemical Processes for a Sustainable Future*, eds. T. M. Letcher, J. L. Scott and D. A. Patterson, Royal Society of Chemistry, Cambridge, 2015, pp. 425-442.
25. S. Raikova, C. D. Le, J. L. Wagner, V. P. Ting and C. J. Chuck, in *Biofuels for Aviation - Feedstocks, Technology and Implementation*, ed. C. J. Chuck, Elsevier, London, 2016.
26. P. E. Savage, *Chemical Reviews*, 1999, **99**, 603-622.
27. L. Garcia Alba, C. Torri, C. Samorì, J. van der Spek, D. Fabbri, S. R. A. Kersten and D. W. F. Brilman, *Energy & Fuels*, 2012, **26**, 642-657.
28. H. Li, Z. Liu, Y. Zhang, B. Li, H. Lu, N. Duan, M. Liu, Z. Zhu and B. Si, *Bioresource technology*, 2014, **154**, 322-329.
29. P. J. Valdez, J. G. Dickinson and P. E. Savage, *Energy & Fuels*, 2011, **25**, 3235-3243.
30. D. Lopez Barreiro, C. Samori, G. Terranella, U. Hornung, A. Kruse and W. Prins, *Bioresource technology*, 2014, **174**, 256-265.
31. X. Cheng, M. D. Ooms and D. Sinton, *Lab Chip*, 2016, **16**, 256-260.
32. G. J. M. Versteegh and P. Blokker, *Phycological Research*, 2004, **52**, 325-339.
33. G. Markou and E. Nerantzis, *Biotechnology advances*, 2013, **31**, 1532-1542.
34. P. Duan and P. E. Savage, *Industrial & Engineering Chemistry Research*, 2011, **50**, 52-61.
35. A. B. Ross, P. Biller, M. L. Kubacki, H. Li, A. Lea-Langton and J. M. Jones, *Fuel*, 2010, **89**, 2234-2243.
36. P. Biller and A. B. Ross, *Bioresource technology*, 2011, **102**, 215-225.
37. G. Teri, L. Luo and P. E. Savage, *Energy & Fuels*, 2014, **28**, 7501-7509.
38. W. Yang, X. Li, Z. Li, C. Tong and L. Feng, *Bioresource technology*, 2015, **196**, 99-108.
39. C. Zhang, X. Tang, L. Sheng and X. Yang, *Green Chem.*, 2016, **18**, 2542-2553.
40. C. Torri, L. Garcia Alba, C. Samorì, D. Fabbri and D. W. F. Brilman, *Energy & Fuels*, 2012, **26**, 658-671.
41. D. Lopez Barreiro, C. Zamalloa, N. Boon, W. Vyverman, F. Ronsse, W. Brilman and W. Prins, *Bioresource technology*, 2013, **146**, 463-471.

42. S. S. Toor, H. Reddy, S. Deng, J. Hoffmann, D. Spangsmark, L. B. Madsen, J. B. Holm-Nielsen and L. A. Rosendahl, *Bioresource technology*, 2013, **131**, 413-419.
43. W. T. Chen, Y. Zhang, J. Zhang, G. Yu, L. C. Schideman, P. Zhang and M. Minarick, *Bioresource technology*, 2014, **152**, 130-139.
44. C. Jazrawi, P. Biller, A. B. Ross, A. Montoya, T. Maschmeyer and B. S. Haynes, *Algal Research*, 2013, **2**, 268-277.
45. U. Jena, K. C. Das and J. R. Kastner, *Bioresource technology*, 2011, **102**, 6221-6229.
46. D. Xu and P. E. Savage, *Algal Research*, 2015, **12**, 60-67.
47. J. L. Faeth, P. J. Valdez and P. E. Savage, *Energy & Fuels*, 2013, **27**, 1391-1398.
48. J. L. Faeth and P. E. Savage, *Bioresource technology*, 2016, **206**, 290-293.
49. J. L. Faeth, P. E. Savage, J. M. Jarvis, A. M. McKenna and P. E. Savage, *AIChE Journal*, 2016, **62**, 815-828.
50. Y. F. Yang, C. P. Feng, Y. Inamori and T. Maekawa, *Resources, Conservation and Recycling*, 2004, **43**, 21-33.
51. L. Yang, Y. Li and P. E. Savage, *Industrial & Engineering Chemistry Research*, 2014, **53**, 11939-11944.
52. Y. Chen, Y. Wu, R. Ding, P. Zhang, J. Liu, M. Yang and P. Zhang, *AIChE Journal*, 2015, **61**, 1118-1128.
53. D. López Barreiro, S. Riede, U. Hornung, A. Kruse and W. Prins, *Algal Research*, 2015, **12**, 206-212.
54. A. Cole, Y. Dinburg, B. S. Haynes, Y. He, M. Herskowitz, C. Jazrawi, M. Landau, X. Liang, M. Magnusson, T. Maschmeyer, A. F. Masters, N. Meiri, N. Neveux, R. de Nys, N. Paul, M. Rabaev, R. Vidruk-Nehemya and A. K. L. Yuen, *Energy Environ. Sci.*, 2016, **9**, 1828-1840.
55. S. B. Jones, Y. Zhu, D. B. Anderson, R. T. Hallen, D. C. Elliott, A. J. Schmidt, K. O. Albrecht, T. R. Hart, M. G. Butcher, C. Drennan, L. J. Snowden-Swan, R. Davis and C. Kinchin, *Process designs and economics for the conversion of algal biomass to hydrocarbons: whole algae hydrothermal liquefaction and upgrading* PNNL-23227, Pacific Northwest National Laboratory, Richland, Washington, USA, 2014.
56. X. Yuan, J. Wang, G. Zeng, H. Huang, X. Pei, H. Li, Z. Liu and M. Cong, *Energy*, 2011, **36**, 6406-6412.
57. H. Huang, X. Yuan, G. Zeng, J. Wang, H. Li, C. Zhou, X. Pei, Q. You and L. Chen, *Fuel Processing Technology*, 2011, **92**, 147-153.
58. R. Singh, T. Bhaskar and B. Balagurumurthy, *Process Safety and Environmental Protection*, 2015, **93**, 154-160.
59. P. Duan, B. Wang and Y. Xu, *Bioresource technology*, 2015, **186**, 58-66.
60. H.-j. Huang, X.-z. Yuan, H.-n. Zhu, H. Li, Y. Liu, X.-l. Wang and G.-m. Zeng, *Energy*, 2013, **56**, 52-60.
61. P. Duan, B. Jin, Y. Xu, Y. Yang, X. Bai, F. Wang, L. Zhang and J. Miao, *Bioresource technology*, 2013, **133**, 197-205.

62. B. Jin, P. Duan, C. Zhang, Y. Xu, L. Zhang and F. Wang, *Chemical Engineering Journal*, 2014, **254**, 384-392.
63. Y. Chen, Y. Wu, P. Zhang, D. Hua, M. Yang, C. Li, Z. Chen and J. Liu, *Bioresource technology*, 2012, **124**, 190-198.
64. M. P. Caporgno, J. Pruvost, J. Legrand, O. Lepine, M. Tazerout and C. Bengoa, *Bioresource technology*, 2016, **214**, 404-410.
65. D. L. Barreiro, B. R. Gómez, U. Hornung, A. Kruse and W. Prins, *Energy & Fuels*, 2015, **29**, 6422-6432.
66. D. C. Elliott, T. R. Hart, A. J. Schmidt, G. G. Neuenschwander, L. J. Rotness, M. V. Olarte, A. H. Zacher, K. O. Albrecht, R. T. Hallen and J. E. Holladay, *Algal Research*, 2013.
67. Y. Guo, T. Yeh, W. Song, D. Xu and S. Wang, *Renewable and Sustainable Energy Reviews*, 2015, **48**, 776-790.
68. B. Patel and K. Hellgardt, *Bioresource technology*, 2015, **191**, 460-468.
69. P. Biller, B. K. Sharma, B. Kunwar and A. B. Ross, *Fuel*, 2015, **159**, 197-205.
70. J. Jechura, *Refinery Feedstocks & Products - Properties & Specifications*, 2016, Available from: http://inside.mines.edu/~jjechura/Refining/02_Feedstocks_&_Products.pdf [30 August 2016]
71. M. Chakraborty, C. Miao, A. McDonald and S. Chen, *Fuel*, 2012, **95**, 63-70.
72. M. Lavanya, A. Meenakshisundaram, S. Renganathan, S. Chinnasamy, D. M. Lewis, J. Nallasivam and S. Bhaskar, *Bioresource technology*, 2016, **203**, 228-235.
73. P. Biller, C. Friedman and A. B. Ross, *Bioresource technology*, 2013, **136**, 188-195.
74. I. Sereewatthanawut, S. Prapintip, K. Watchiraruji, M. Goto, M. Sasaki and A. Shotipruk, *Bioresource technology*, 2008, **99**, 555-561.
75. J. L. Garcia-Moscoso, W. Obeid, S. Kumar and P. G. Hatcher, *The Journal of Supercritical Fluids*, 2013, **82**, 183-190.
76. W. Costanzo, U. Jena, R. Hilten, K. C. Das and J. R. Kastner, *Algal Research*, 2015, **12**, 377-387.
77. W. Costanzo, R. Hilten, U. Jena, K. C. Das and J. R. Kastner, *Algal Research*, 2016, **13**, 53-68.
78. C. Jazrawi, P. Biller, Y. He, A. Montoya, A. B. Ross, T. Maschmeyer and B. S. Haynes, *Algal Research*, 2015, **8**, 15-22.
79. C. Miao, M. Chakraborty and S. Chen, *Bioresource technology*, 2012, **110**, 617-627.
80. C. Yang, R. Li, C. Cui, S. Liu, Q. Qiu, Y. Ding, Y. Wu and B. Zhang, *Green Chem.*, 2016, **18**, 3684-3699.
81. D. López Barreiro, B. R. Gómez, F. Ronsse, U. Hornung, A. Kruse and W. Prins, *Fuel Processing Technology*, 2016, **148**, 117-127.
82. Y. Elkasabi, B. M. E. Chagas, C. A. Mullen and A. A. Boateng, *Energy & Fuels*, 2016, **30**, 4925-4932.
83. C. Zhang, P. Duan, Y. Xu, B. Wang, F. Wang and L. Zhang, *Bioresource technology*, 2014, **166**, 37-44.

84. P. Duan and P. E. Savage, *Energy & Environmental Science*, 2011, **4**, 1447.
85. C. Torri, D. Fabbri, L. Garcia-Alba and D. W. F. Brilman, *Journal of Analytical and Applied Pyrolysis*, 2013, **101**, 28-34.
86. Z. Li and P. E. Savage, *Algal Research*, 2013, **2**, 154-163.
87. P. Duan and P. E. Savage, *Applied Catalysis B: Environmental*, 2011, **104**, 136-143.
88. Y. Xu, P. Duan and B. Wang, *Algal Research*, 2015, **9**, 186-193.
89. P. Duan, X. Bai, Y. Xu, A. Zhang, F. Wang, L. Zhang and J. Miao, *Fuel*, 2013, **109**, 225-233.
90. P. Duan and P. E. Savage, *Bioresource technology*, 2011, **102**, 1899-1906.
91. Z. Wang, S. Adhikari, P. Valdez, R. Shakya and C. Laird, *Fuel Processing Technology*, 2016, **142**, 147-156.
92. S. G. Roussis, R. Cranford and N. Sytkovetskiy, *Energy & Fuels*, 2012, **26**, 5294-5299.
93. S. Shin, H. Yang, K. Sakanishi, I. Mochida, D. A. Grudoski and J. H. Shinn, *Applied Catalysis A: General*, 2001, **205**, 101-108.
94. G. Das and R. Hughes, in *Petroleum Refining and Petrochemical Based Industries in Eastern India.*, eds. R. K. Saha, B. R. Maity, D. Bhattacharyya, S. Ray, S. Ganguly and S. L. Chakraborty, Sunil Sachdev, New Delhi, 2000.
95. E. Furimsky and F. E. Massoth, *Catalysis Reviews*, 2005, **47**, 297-489.
96. G. Perot, *Catalysis Today*, 1991, **10**, 447-472.
97. R. Prins, 2001, **46**, 399-464.
98. S. S. Katti, B. C. Gates and L. Petrakis, *Industrial & Engineering Chemistry Process Design and Development*, 1986, **25**, 618-626.
99. C. Moreau, J. Joffre, C. Saenz and P. Geneste, *Journal of Catalysis*, 1990, **122**, 448-451.
100. J. van Gestel, C. Dujardin, F. Maugé and J. C. Duchet, *Journal of Catalysis*, 2001, **202**, 78-88.
101. M. Jian and R. Prins, *Catalysis Today*, 1996, **30**, 127-134.
102. P. L. Jokuty and M. R. Gray, *Industrial & Engineering Chemistry Research*, 1992, **31**, 1445-1449.
103. R. M. Laine, *Journal of Molecular Catalysis*, 1983, **21**, 119-132.
104. N. Nelson, *Journal of Catalysis*, 1979, **58**, 485-488.
105. S. Oyama, *Journal of Catalysis*, 2002, **210**, 207-217.
106. C. N. Satterfield, M. Modell, R. A. Hites and C. J. Declerck, *Industrial & Engineering Chemistry Process Design and Development*, 1978, **17**, 141-148.
107. C. N. Satterfield and J. F. Cocchetto, *Industrial & Engineering Chemistry Process Design and Development*, 1981, **20**, 53-62.
108. R. Prins and M. E. Bussell, *Catalysis Letters*, 2012, **142**, 1413-1436.
109. Z. Vit and M. Zrdažil, *Journal of Catalysis*, 1989, **119**, 1-7.
110. J. Shabtai, Q. Guohe, K. Balusami, N. K. Nag and F. E. Massoth, *Journal of Catalysis*, 1988, **113**, 206-219.
111. M. Ledoux and B. Djellouli, *Journal of Catalysis*, 1989, **115**, 580-590.

112. S. Eijsbouts, V. H. J. De Beer and R. Prins, *Journal of Catalysis*, 1988, **109**, 217-220.
113. H. Toulhoat, P. Raybaud, S. Kasztelan, G. Kresse and J. Hafner, *Catalysis Today*, 1999, **50**, 629-636.
114. M. Lacroix, C. Dumonteil, M. Breysse and S. Kasztelan, *Journal of Catalysis*, 1999, **185**, 219-222.
115. G. Berhault, M. Lacroix, M. Breysse, F. Maugé, J.-C. Lavalley, H. Nie and L. Qu, *Journal of Catalysis*, 1998, **178**, 555-565.
116. L. Zhang, G. Karakas and U. S. Ozkan, *Journal of Catalysis*, 1998, **178**, 457-465.
117. S. C. Kim and F. E. Massoth, *Journal of Catalysis*, 2000, **189**, 70-78.
118. G. Marroquin-Sanchez, J. Ancheyta, A. Ramirez-Zuniga and E. Farfan-Torres, *Energy & Fuels*, 2001, **15**, 1213-1219.
119. C. K. Groot, V. H. J. De Beer, R. Prins, M. Stolarski and W. S. Niedzwiedz, *Industrial & Engineering Chemistry Product Research and Development*, 1986, **25**, 522-530.
120. T. G. Harvey and T. W. Matheson, *Journal of Catalysis*, 1986, **101**, 253-261.
121. P. Leyrit, T. Cseri, N. Marchal, J. Lynch and S. Kasztelan, *Catalysis Today*, 2001, **65**, 249-256.
122. V. Kougionas, M. Cattenot, J. L. Zotin, J. L. Portefaix and M. Breysse, *Applied Catalysis A: General*, 1995, **124**, 153-164.
123. C. Suresh, D. Santhanaraj, M. Gurulakshmi, G. Deepa, M. Selvaraj, N. R. Sasi Rekha and K. Shanthi, *ACS Catalysis*, 2012, **2**, 127-134.
124. L. Qu and R. Prins, *Applied Catalysis A: General*, 2003, **250**, 105-115.
125. T. I. Korányi, Z. Vít and J. B. Nagy, *Catalysis Today*, 2008, **130**, 80-85.
126. S. T. Oyama, P. Clark, X. Wang, T. Shido, Y. Iwasawa, S. Hayashi, J. M. Ramallo-López and F. G. Requejo, *The Journal of Physical Chemistry B*, 2002, **106**, 1913-1920.
127. M. Lu, A. Wang, X. Li, X. Duan, Y. Teng, Y. Wang, C. Song and Y. Hu, *Energy & Fuels*, 2007, **21**, 554-560.
128. S. Oyama, *Journal of Catalysis*, 2003, **216**, 343-352.
129. Y.-K. Lee, Y. Shu and S. T. Oyama, *Applied Catalysis A: General*, 2007, **322**, 191-204.
130. S. T. Oyama, T. Gott, H. Zhao and Y.-K. Lee, *Catalysis Today*, 2009, **143**, 94-107.
131. C. Stinner, R. Prins and T. Weber, *Journal of Catalysis*, 2001, **202**, 187-194.
132. W. Robinson, J. N. M. vanGestel, T. I. Koranyi, S. Eijsbouts, A. M. vanderKraan, J. A. R. vanVeen and V. H. J. deBeer, *Journal of Catalysis*, 1996, **161**, 539-550.
133. H. Y. Zhao, D. Li, P. Bui and S. T. Oyama, *Applied Catalysis A: General*, 2011, **391**, 305-310.
134. N. Koike, S. Hosokai, A. Takagaki, S. Nishimura, R. Kikuchi, K. Ebitani, Y. Suzuki and S. T. Oyama, *Journal of Catalysis*, 2016, **333**, 115-126.

135. Y. Kanda, C. Temma, K. Nakata, T. Kobayashi, M. Sugioka and Y. Uemichi, *Applied Catalysis A: General*, 2010, **386**, 171-178.
136. A. Sawada, Y. Kanda, M. Sugioka and Y. Uemichi, *Catalysis Communications*, 2014, **56**, 60-64.
137. A. Infantes-Molina, J. A. Cecilia, B. Pawelec, J. L. G. Fierro, E. Rodríguez-Castellón and A. Jiménez-López, *Applied Catalysis A: General*, 2010, **390**, 253-263.
138. F. Sun, W. Wu, Z. Wu, J. Guo, Z. Wei, Y. Yang, Z. Jiang, F. Tian and C. Li, *Journal of Catalysis*, 2004, **228**, 298-310.
139. V. Zuzaniuk and R. Prins, *Journal of Catalysis*, 2003, **219**, 85-96.
140. J. Chen, H. Shi, L. Li and K. Li, *Applied Catalysis B: Environmental*, 2014, **144**, 870-884.
141. A. F. Gaudette, A. W. Burns, J. R. Hayes, M. C. Smith, R. H. Bowker, T. Seda and M. E. Bussell, *Journal of Catalysis*, 2010, **272**, 18-27.
142. I. Abu and K. Smith, *Journal of Catalysis*, 2006, **241**, 356-366.
143. I. I. Abu and K. J. Smith, *Catalysis Today*, 2007, **125**, 248-255.
144. L. Song, S. Zhang and Q. Wei, *Catalysis Communications*, 2011, **12**, 1157-1160.
145. Y.-S. Kim, G.-N. Yun and Y.-K. Lee, *Catalysis Communications*, 2014, **45**, 133-138.
146. H. Song, M. Dai, H. Song, X. Wan and X. Xu, *Applied Catalysis A: General*, 2013, **462-463**, 247-255.
147. Q. Guan, F. Wan, F. Han, Z. Liu and W. Li, *Catalysis Today*, 2016, **259**, 467-473.
148. H. Song, J. Gong, H. Song and F. Li, *Applied Catalysis A: General*, 2015, **505**, 267-275.
149. Z. Zhang, M. Tang and J. Chen, *Applied Surface Science*, 2016, **360**, 353-364.
150. P. Clark, *Journal of Catalysis*, 2003, **218**, 78-87.
151. Y. Shu, Y. Lee and S. Oyama, *Journal of Catalysis*, 2005, **236**, 112-121.
152. S. Oyama and Y. Lee, *Journal of Catalysis*, 2008, **258**, 393-400.
153. S. Yang and R. Prins, *Chem Commun (Camb)*, 2005, 4178-4180.
154. S. Yang, C. Liang and R. Prins, *Journal of Catalysis*, 2006, **237**, 118-130.
155. D. Liu, A. Wang, C. Liu and R. Prins, *Catalysis Communications*, 2016, **77**, 13-17.
156. T. Lundquist, I. Woertz, N. Quinn and J. Benemann, *A Realistic Technology and Engineering Assessment of Algae Biofuel Production*, Energy Biosciences Institute, University of California, Berkeley, California, 2010.
157. R. Davis, A. Aden and P. T. Pienkos, *Applied Energy*, 2011, **88**, 3524-3531.
158. J. W. Richardson, M. D. Johnson and J. L. Outlaw, *Algal Research*, 2012, **1**, 93-100.
159. N. H. Norsker, M. J. Barbosa, M. H. Vermue and R. H. Wijffels, *Biotechnology advances*, 2011, **29**, 24-27.
160. N. D. Orfield, PhD Thesis, University of Michigan, 2013.

161. C. M. Beal, L. N. Gerber, D. L. Sills, M. E. Huntley, S. C. Machesky, M. J. Walsh, J. W. Tester, I. Archibald, J. Granados and C. H. Greene, *Algal Research*, 2015, **10**, 266-279.
162. M. A. Borowitzka, *Journal of Applied Phycology*, 2013, **25**, 743-756.
163. R. Sayre, *BioScience*, 2010, **60**, 722-727.
164. M. K. Lam and K. T. Lee, *Biotechnology advances*, 2012, **30**, 673-690.
165. M. K. Lam, K. T. Lee and A. R. Mohamed, *International Journal of Greenhouse Gas Control*, 2012, **10**, 456-469.
166. R. J. Craggs, S. Heubeck, T. J. Lundquist and J. R. Benemann, *Water Sci Technol*, 2011, **63**, 660-665.
167. J. K. Pittman, A. P. Dean and O. Osundeko, *Bioresource technology*, 2011, **102**, 17-25.
168. L. Christenson and R. Sims, *Biotechnology advances*, 2011, **29**, 686-702.
169. L. Wang, M. Min, Y. Li, P. Chen, Y. Chen, Y. Liu, Y. Wang and R. Ruan, *Applied biochemistry and biotechnology*, 2010, **162**, 1174-1186.
170. A. F. Clarens, E. P. Resurreccion, M. A. White and L. M. Colosi, *Environ Sci Technol*, 2010, **44**, 1813-1819.
171. A. Kumar, S. Ergas, X. Yuan, A. Sahu, Q. Zhang, J. Dewulf, F. X. Malcata and H. van Langenhove, *Trends Biotechnol*, 2010, **28**, 371-380.
172. aquastat, Food and Agriculture Organization of the United Nations, 2014.
173. M. N. Somleva, O. P. Peoples and K. D. Snell, *Plant biotechnology journal*, 2013, **11**, 233-252.
174. G. F. Wu, Q. Y. Wu and Z. Y. Shen, *Bioresour Technology*, 2001, **76**, 85-90.
175. B. Panda, P. Jain, L. Sharma and N. Mallick, *Bioresource technology*, 2006, **97**, 1296-1301.
176. B. Panda and N. Mallick, *Letters in Applied Microbiology*, 2007, **44**, 194-198.
177. L. Sharma and N. Mallick, *Biotechnology Letters*, 2005, **27**, 59-62.
178. D. Cordell, J.-O. Drangert and S. White, *Global Environmental Change*, 2009, **19**, 292-305.
179. L. Lardon, A. Hélias, B. Sialve, J.-P. Steyer and O. Bernard, *Environmental Science & Technology*, 2009, **43**, 6475-6481.
180. M. Nelson, L. Zhu, A. Thiel, Y. Wu, M. Guan, J. Minty, H. Y. Wang and X. N. Lin, *Bioresource technology*, 2013, **136**, 522-528.
181. P. Biller, A. B. Ross, S. C. Skill, A. Lea-Langton, B. Balasundaram, C. Hall, R. Riley and C. A. Llewellyn, *Algal Research*, 2012, **1**, 70-76.
182. U. Jena, N. Vaidyanathan, S. Chinnasamy and K. C. Das, *Bioresource technology*, 2011, **102**, 3380-3387.
183. L. Garcia Alba, C. Torri, D. Fabbri, S. R. A. Kersten and D. W. F. Brilman, *Chemical Engineering Journal*, 2013, **228**, 214-223.
184. Z. Du, M. Mohr, X. Ma, Y. Cheng, X. Lin, Y. Liu, W. Zhou, P. Chen and R. Ruan, *Bioresource technology*, 2012, **120**, 13-18.

185. P. Duan, X. Bai, Y. Xu, A. Zhang, F. Wang, L. Zhang and J. Miao, *Bioresource technology*, 2013, **136**, 626-634.
186. R. Maurya, C. Paliwal, T. Ghosh, I. Pancha, K. Chokshi, M. Mitra, A. Ghosh and S. Mishra, *Bioresource technology*, 2016, **214**, 787-796.
187. M. A. Filho, *Um biodiesel de microalga*, 2015, Available from: http://www.unicamp.br/unicamp/noticias/2015/07/01/um-biodiesel-de-microalga [25 September 2016]
188. X. Wang and R. Rinaldi, *Energy & Environmental Science*, 2012, **5**, 8244.
189. X. Wang and R. Rinaldi, *Angew Chem Int Ed Engl*, 2013, **52**, 11499-11503.
190. R. O. Fournier and J. J. Rowe, *American Mineralogist*, 1977, **62**, 1052-1056.
191. M. F. Bouchard, S. Sauve, B. Barbeau, M. Legrand, M. E. Brodeur, T. Bouffard, E. Limoges, D. C. Bellinger and D. Mergler, *Environ Health Perspect*, 2011, **119**, 138-143.
192. W. F. DeGroot and F. Shafizadeh, *Preprints of Papers - American Cheical Society, Division of Fuel Chemistry*, 1984, **29**, 146-153.
193. P. T. Williams and P. A. Horne, *Renewable Energy*, 1994, **4**, 1-13.
194. C. A. Zaror, I. S. Hutchings, D. L. Pyle, H. N. Stiles and R. Kandiyoti, *Fuel*, 1985, **64**, 990-994.
195. F. Mariotti, D. Tome and P. P. Mirand, *Crit Rev Food Sci Nutr*, 2008, **48**, 177-184.
196. M. Saber, B. Nakhshiniev and K. Yoshikawa, *Renewable and Sustainable Energy Reviews*, 2016, **58**, 918-930.
197. S. Zhang, S. Zhang, L. Song and Q. Wei, *Powder Technology*, 2014, **253**, 509-513.
198. C. Stinner, R. Prins and T. Weber, *Journal of Catalysis*, 2000, **191**, 438-444.
199. S. Sawhill, K. Layman, D. Vanwyk, M. Engelhard, C. Wang and M. Bussell, *Journal of Catalysis*, 2005, **231**, 300-313.
200. E. R. Jones, University of Bath, 2016.
201. J. L. Wagner, University of Bath, 2013.
202. M. Ogura, S.-y. Shinomiya, J. Tateno, Y. Nara, M. Nomura, E. Kikuchi and M. Matsukata, *Applied Catalysis A: General*, 2001, **219**, 33-43.
203. A. I. d'Aquino, S. J. Danforth, T. R. Clinkingbeard, B. Ilic, L. Pullan, M. A. Reynolds, B. D. Murray and M. E. Bussell, *Journal of Catalysis*, 2016, **335**, 204-214.
204. H. Song, F. Zhang, H. Song, X. Xu and F. Li, *Catalysis Communications*, 2015, **69**, 59-62.
205. W. Wang, X. Li, Z. Sun, A. Wang, Y. Liu, Y. Chen and X. Duan, *Applied Catalysis A: General*, 2016, **509**, 45-51.
206. B. M. Q. Phan, Q. L. M. Ha, N. P. Le, P. T. Ngo, T. H. Nguyen, T. T. Dang, L. H. Nguyen, D. A. Nguyen and L. C. Luu, *Catalysis Letters*, 2014, **145**, 662-667.
207. C. D. Le, ed. J. L. Wagner, 2015.
208. D. J. Collins, E. C. Lloyd and R. Miranda, *Applied Catalysis*, 1988, **41**, 81-88.

209. SDBSWeb, *Spectral Database for Organic Compounds SDBS*, Available from: http://sdbs.db.aist.go.jp [22 July 2016]
210. L. Zhang, W. Fu, Q. Yu, T. Tang, Y. Zhao, H. Zhao and Y. Li, *Journal of Catalysis*, 2016, **338**, 210-221.
211. R. S. Coelho, A. D. S. Vidotti, É. M. Reis and T. T. Franco, *Chemical Engineering Transactions*, 2014, **38**, 313-318.
212. K. A. C. C. Taylor, *Applied biochemistry and biotechnology*, 1995, **53**, 207-214.
213. E. T. Kostas, D. A. White, C. Du and D. J. Cook, *J Appl Phycol*, 2016, **28**, 1427-1441.
214. Gaylord Chemical Company, *Catalyst Sulfiding Overview*, 2015, Available from: http://www.gaylordchemical.com/wp-content/uploads/2015/09/Literature205.pdf [19 September 2016]
215. *Perry's Chemical Engineers' Handbook*, 8th edn., McGraw-Hill, New York, 2007.
216. T. J. B. Holland, *Mineralogical Magazine*, 1997, **61**, 65-77.
217. M. M. J. Treacy and J. B. Higgins, *Collection of Simulated XRD Powder Patterns for Zeolites*, 4th edn., Elsevier, Amsterdam, 2001.
218. Newcastle University, *Scherrer-calc*, 2013, Available from: http://www.ncl.ac.uk/acma/resources/documents/Scherrer-calc_v3_2013.xlsx [24 September 2016]
219. International Organization for Standardization, *Determination of the specific surface area of solids by gas adsorption - BET method* ISO/DIS 9277, Geneva, 2008.